

Inaugural - Dissertation
for
obtaining the doctoral degree
of the
Combined Faculty of Mathematics, Engineering and Natural Sciences
of the
Ruprecht – Karls – University
Heidelberg

Presented by

Master of Science (M.Sc.) - Lars Christoph Beedgen

Born in Heidelberg (Baden-Württemberg)

Oral examination: November 9th, 2022

Mevalonate Kinase Deficiency and its pathophysiological relevance in metabolism

Referees:

Prof. Dr. Britta Brügger

PD. Dr. Christian Thiel

Für meine Eltern und Oma Maria

Table of Contents

| | |
|---|------|
| Table of Contents | I |
| List of Figures | IV |
| List of Tables | VII |
| Abbreviations | VIII |
| 1 Abstract | 1 |
| 2 Zusammenfassung | 2 |
| 3 Theory | 3 |
| 3.1 Mevalonate (Isoprenoid) Pathway | 3 |
| 3.2 Overview on Glycosylation | 6 |
| 3.3 Protein Glycosylation and Glycoprotein Synthesis | 6 |
| 3.4 N-Glycosylation | 6 |
| 3.5 O-Glycosylation | 11 |
| 3.6 O-Mannosylation | 12 |
| 3.7 C-Mannosylation | 13 |
| 3.8 Glycosphingolipids | 14 |
| 3.9 Congenital Disorders of Glycosylation (CDG) | 16 |
| 3.10 Mevalonate Kinase Deficiency / Mevalonate Aciduria | 18 |
| 4 Objective and experimental outline | 20 |
| 5 Material | 21 |
| 5.1 Patient-derived material | 21 |
| 5.2 Chemicals | 21 |
| 5.3 Kits, standards and enzymes | 23 |
| 5.4 Restriction enzymes and buffers | 24 |
| 5.5 Consumables | 24 |
| 5.6 Equipment | 26 |
| 5.7 Buffer, solutions and cell-culture media | 28 |
| 5.8 Oligonucleotides | 31 |
| 5.9 Radioactive compounds | 31 |
| 5.10 Antibodies, lectins and streptavidin-conjugate | 32 |
| 5.11 Plasmids | 34 |
| 5.12 Bacterial strains for plasmid transformation | 34 |

| | | |
|------|---|-----|
| 5.13 | Culture media and plates for bacteria | 35 |
| 5.14 | Culture media and solutions for mammalian cells | 35 |
| 5.15 | Cell-lines | 36 |
| 5.16 | Software, databanks and computer-aided resources | 37 |
| 6 | Methods | 38 |
| 6.1 | Mammalian cell culture | 38 |
| 6.2 | Biochemical methods | 41 |
| 6.3 | Molecular biological methods | 47 |
| 6.4 | Production and application of retroviral particles for transfer of nucleic acids into primary fibroblasts | 57 |
| 6.5 | Statistic | 58 |
| 7 | Results | 59 |
| 7.1 | Patient anamnesis and genetic characterization | 59 |
| 7.2 | MVK expression analysis in every patient | 64 |
| 7.3 | Changes in cell proliferation of MVK patients | 69 |
| 7.4 | Analysis of glycans by lectin blots | 71 |
| 7.5 | Analysis of glycosylation markers | 79 |
| 7.6 | Total N-glycan analysis by xCGE-LIF technology | 83 |
| 7.7 | Glycosphingolipid analysis by xCGE-LIF | 88 |
| 7.8 | nCounter expression analysis of patients' fibroblasts | 89 |
| 7.9 | Analysis of nCounter hits on protein level | 104 |
| 7.10 | LLO analysis | 109 |
| 7.11 | Prime PCR analysis | 111 |
| 7.12 | Energy metabolite analysis | 115 |
| 7.13 | Measurement of amino acids in cell lysates | 117 |
| 7.14 | Lipid analysis | 120 |
| 7.15 | Proteomics analysis | 127 |
| 7.16 | Complementation of fibroblasts with the MVK-wildtype gene | 131 |
| 8 | Discussion | 133 |
| 8.1 | Disease causing mutations in the MVK gene | 133 |
| 8.2 | MVK expression analysis | 134 |
| 8.3 | Impaired cellular proliferation | 135 |
| 8.4 | Impaired glycosylation status in MVA and the connection to CDG | 135 |

| | | |
|------|--|-----|
| 8.5 | nCounter expression analysis revealed dysregulation of multiple glycosylation pathways | 138 |
| 8.6 | LLO analysis | 142 |
| 8.7 | PrimePCR analysis revealed impact on the metabolism | 142 |
| 8.8 | Energy metabolites homeostasis is impaired | 144 |
| 8.9 | Amino acid profile indicates abnormalities | 144 |
| 8.10 | Impaired lipid homeostasis | 144 |
| 8.11 | Proteomics measurement | 147 |
| 8.12 | Conclusion | 149 |
| 8.13 | Future perspective | 149 |
| 9 | Literature | 151 |
| 10 | Appendix | 163 |
| 10.1 | Nucleotide- and protein sequence | 163 |
| 10.2 | Vector maps | 165 |
| 10.3 | ΔC_t -values of gene expression | 166 |
| 10.4 | nCounter ratios | 168 |
| 10.5 | PrimePCR ΔC_t -values | 169 |
| 10.6 | Proteomics measurement | 171 |
| 10.7 | Publications | 172 |
| 10.8 | Conference attendance | 173 |
| 11 | Declaration | 174 |
| 12 | Acknowledgment | 175 |

List of Figures

| | |
|--|----|
| Figure 1 - Mevalonate pathway. | 3 |
| Figure 2 - Continuation of the mevalonate pathway. | 5 |
| Figure 3 - The three main types of N-glycans. | 7 |
| Figure 4 - N-glycosylation pathway. | 10 |
| Figure 5 - Biosynthesis of O-linked mucin type glycans. | 11 |
| Figure 6 - Types of O-mannose glycans. | 12 |
| Figure 7 - Pathway of Dol-P-Man as a mannosyl donor for C-, O-mannosylation and N-glycosylation in the ER. | 13 |
| Figure 8 - Structure of GalCer and seven common tetrasaccharide neutral sugar core sequences. | 14 |
| Figure 9 - Synthesis of GSLs. | 15 |
| Figure 10 - Congenital Disorders of Glycosylation and their year of discovery. | 17 |
| Figure 11 - Clinical synopsis of MVA/MKD. | 18 |
| Figure 12 - Growth curve example determined by RTCA and exponential fit of the log-phase. | 40 |
| Figure 13 - nCounter workflow for gene expression. | 56 |
| Figure 14 - Sonographic findings in patient 9. “ | 59 |
| Figure 15 - Sanger sequence of patient 9 and control of <i>MVK</i> | 60 |
| Figure 16 - DynaMut prediction outcome of mutation Ile268Thr in the <i>MVK</i> protein. | 62 |
| Figure 17 - Western blot analysis and quantification of <i>MVK</i> protein expression in patients and controls. | 64 |
| Figure 18 - Quantification of mRNA expression of the <i>MVK</i> -gene. | 65 |
| Figure 19 - Quantification of mRNA expression of <i>HMGCR</i> and <i>PMVK</i> | 66 |
| Figure 20 - Immunofluorescence staining of the <i>MVK</i> patients fibroblast and controls. | 67 |
| Figure 21 - Continuation of immunofluorescence staining of fibroblast of the <i>MVK</i> patients and controls. | 68 |
| Figure 22 - Growth curves, specific growth rates and doubling times for 1000 cells per well. | 69 |
| Figure 23 - Growth curves, specific growth rate and doubling time for 2000 cells per well. | 70 |
| Figure 24 - NPA lectin blot and quantification. | 71 |
| Figure 25 - ConA lectin blot and quantification. | 72 |
| Figure 26 - GNA and LCH lectin blots and quantification. | 73 |
| Figure 27 - PHA-L and DSL lectin blots and quantification. | 74 |
| Figure 28 - AAL lectin blot and quantification. | 75 |
| Figure 29 - MAL I lectin blot and quantification. | 76 |
| Figure 30 - SNA and WGA lectin blots and quantification. | 77 |
| Figure 31 - ECL lectin blot and quantification. | 78 |
| Figure 32 - ICAM1 western blots and quantification of glycoforms. | 79 |

| | |
|---|-----|
| Figure 33 - ICAM1 ratio..... | 80 |
| Figure 34 - LAMP1 western blot and quantification..... | 81 |
| Figure 35 - LAMP2 western blot and quantification..... | 82 |
| Figure 36 - xCGE-LIF electropherograms of MVK2, 8 and 9 compared to controls. ... | 85 |
| Figure 37 - Glycan type distribution in MVK2, 8, 9 and controls..... | 86 |
| Figure 38 - N-glycan analysis of MVK patients and controls from fibroblasts by xCGE-LIF..... | 87 |
| Figure 39 - GSL analysis by xCGE-LIF..... | 88 |
| Figure 40 - Boxplot nCounter hits of all MVK patients together..... | 92 |
| Figure 41 - Boxplot MVK1 nCounter hits..... | 93 |
| Figure 42 - Boxplot MVK2 nCounter hits..... | 94 |
| Figure 43 - Boxplot MVK3 nCounter hits..... | 95 |
| Figure 44 - Boxplot MVK4 nCounter hits..... | 96 |
| Figure 45 - Boxplot MVK5 nCounter hits..... | 97 |
| Figure 46 - Boxplot MVK6 nCounter hits..... | 98 |
| Figure 47 - Boxplot MVK7 nCounter hits..... | 99 |
| Figure 48 - Boxplot MVK8 nCounter hits..... | 100 |
| Figure 49 - Boxplot MVK9 nCounter hits..... | 101 |
| Figure 50 - Boxplot MVK10 nCounter hits..... | 102 |
| Figure 51 - Boxplot MVK11 nCounter hits..... | 103 |
| Figure 52 - Western blots of DHDDS and SRD5A3..... | 104 |
| Figure 53 - Western blot of OGT..... | 104 |
| Figure 54 - Western blots of FUT8, FUT9 and SLC35C1..... | 105 |
| Figure 55 - Western blots of DPY19L1 and DPY19L3..... | 105 |
| Figure 56 - Western blots of GMPPA, PMM2, PGM2, ALG5 and GALE..... | 106 |
| Figure 57 - Western blots of DPAGT1, ALG13, ALG9, ALG12, ALG10, MAN1B1, MAN1A1, MAN2A1 and MGAT2..... | 107 |
| Figure 58 - Western blot of POMT2..... | 108 |
| Figure 59 - Short LLO profiles of MVK patients and control..... | 110 |
| Figure 60 - PrimePCR glycolysis and gluconeogenesis results..... | 111 |
| Figure 61 - Regulation of lipid metabolism Tier1 results of MVK2..... | 112 |
| Figure 62 - Regulation of lipid metabolism Tier1 results of MVK8..... | 113 |
| Figure 63 - Regulation of lipid metabolism Tier1 results of MVK9..... | 113 |
| Figure 64 - Energy metabolite measurement in MVK patient fibroblast and control cells..... | 115 |
| Figure 65 - Energy metabolites measurement in MVK patient fibroblast and control cells..... | 116 |
| Figure 66 - Determination of amino acid levels in MVK patient fibroblast and control cells..... | 117 |
| Figure 67 - Continuation of AA determination..... | 118 |
| Figure 68 - Continuation of AA determination..... | 119 |
| Figure 69 - Quantification of Oil Red O staining in MVK patients normalized to the control..... | 120 |

| | |
|---|-----|
| Figure 70 - Dolichyl phosphate levels in MVK patients' fibroblasts and controls. ... | 121 |
| Figure 71 - DolP species distribution in MVK patients and control. | 122 |
| Figure 72 - Continuation of DolP species distribution. | 123 |
| Figure 73 - Cholesterol and cholesterol ester measurement. | 124 |
| Figure 74 - Ceramide and sphingomyelin measurement. | 125 |
| Figure 75 - Phosphatidylethanolamines and phosphatidylserines measurement. .. | 125 |
| Figure 76 – Alkyl-phosphatidylcholines and alkyl-phosphatidylserines measurement. | 126 |
| Figure 77 – Alkyl-phosphatidylinositols and diacylglycerol measurement. | 126 |
| Figure 78 - Clustering in groups and PCA. | 127 |
| Figure 79 - New groups after clustering and PCA. | 128 |
| Figure 80 - KEGG pathway analysis of MVK affected. | 129 |
| Figure 81 - KEGG pathway analysis of mildly affected. | 130 |
| Figure 82 - Detection of MVK Myc-tag construct in lysates by anti-Myc of transfected cells. | 131 |
| Figure 83 - Detection of MVK Myc-tag by construct anti-MVK in lysates of transfected cells. | 132 |

List of Tables

| | |
|--|-----|
| Table 1 - List of chemicals and respective companies. | 21 |
| Table 2 - List of kits, standards and enzymes with respective companies. | 23 |
| Table 3 - List of restriction enzymes, corresponding recognition sides and buffer.... | 24 |
| Table 4 - List of consumables and respective companies..... | 24 |
| Table 5 - List of used equipment and corresponding companies. | 26 |
| Table 6 - List of buffer/solutions and their components. | 28 |
| Table 7 - List of used oligonucleotides with application and sequence. | 31 |
| Table 8 - List of radioactive compounds | 31 |
| Table 9 - List of primary antibodies..... | 32 |
| Table 10 - List of secondary antibodies..... | 33 |
| Table 11 - List of lectins and their specificity | 33 |
| Table 12 - List of plasmids..... | 34 |
| Table 13 - List of bacterial strains | 34 |
| Table 14 - List of culture media and plates for bacteria | 35 |
| Table 15 - List of culture media and solutions for mammalian cells | 35 |
| Table 16 - List of cell lines | 36 |
| Table 17 - List of software..... | 37 |
| Table 18 - List of databanks | 37 |
| Table 19 - List of computer-aided resources and tools | 37 |
| Table 20 - Composition of polyacrylamide gels for SDS-PAGE | 42 |
| Table 21 - Pipetting scheme for cDNA-synthesis with RevertAid First Strand Kit. | 49 |
| Table 22 - Pipetting scheme for cDNA-synthesis with <i>Omniscript Reverse Transcriptase</i> | 50 |
| Table 23 - Pipetting scheme for cDNA-synthesis with <i>iScript Advanced cDNA Synthesis Kit</i> | 50 |
| Table 24 - General scheme of the composition of a PCR-reaction. | 51 |
| Table 25 - Temperature-program for PCR-reactions. | 51 |
| Table 26 - Pipetting scheme for restriction digest..... | 53 |
| Table 27 - Pipetting scheme for ligation reaction..... | 53 |
| Table 28 - General scheme of the composition of a qRT-PCR reaction..... | 54 |
| Table 29 - Temperature program for qRT-PCR | 54 |
| Table 30 - PrimePCR reaction mixture | 55 |
| Table 31 - Prime PCR temperature protocol..... | 55 |
| Table 32 - Conservation of the mutated amino acid in the <i>MVK</i> gene in different species..... | 61 |
| Table 33 - Annotated pathogenicity scores | 61 |
| Table 34 - <i>MVK</i> patients and laboratory test results. | 63 |
| Table 35 - Peak assignment for electropherograms | 83 |
| Table 36 - nCounter genes | 89 |
| Table 37 - Regulation trends in all <i>MVK</i> patients..... | 91 |
| Table 38 - KEGG pathway analysis of severely affected. | 129 |

Abbreviations

| | |
|----------|--|
| % | Percent |
| ~ | Approximately |
| ± | Plus/Minus |
| °C | Degree Celsius |
| 3OMD | 3-O-Methyl-Dopa |
| AAL | Aleuria Aurantia |
| ACACB | Acetyl-CoA Carboxylase Beta |
| ACADL | Acyl-CoA Dehydrogenase Long Chain |
| ACLY | ATP Citrate Lyase |
| ACN | Acetonitrile |
| ACOX3 | Acyl-CoA Oxidase 3, Pristanoyl |
| ACTB | Actin Beta |
| ADP | Nadadenosine Diphosphate |
| ADRB2 | Adrenoceptor Beta 2 |
| AEBSF | 4-(2-Aminoethyl)Benzolsulfonylfluorid |
| AGTR1 | Angiotensin li Receptor Type 1 |
| AKT1 | AKT Serine/Threonine Kinase 1 |
| AKT2 | AKT Serine/Threonine Kinase 2 |
| AKT3 | AKT Serine/Threonine Kinase 3 |
| ALDOA | Aldolase, Fructose-Bisphosphate A |
| ALG | Asparagine Linked Glycosylation |
| AMP | Adenosine Monophosphate |
| Amp | Ampicillin |
| ANGPTL4 | Angiopoietin Like 4 |
| Apo-CIII | Apolipoprotein CIII |
| APOE | Apolipoprotein E |
| APS | Ammonium Peroxide Disulfate |
| ARG1 | Arginase |
| ARSA | Arylsulfatase A |
| ASAH1 | N-Acylsphingosine Amidohydrolase 1 |
| ATP | Adenosine Triphosphate |
| ATP6AP1 | ATPase H+ Transporting Accessory Protein 1 |
| ATP6V0D1 | ATPase H+ Transporting V0 Subunit D1 |
| ATP6V1C | ATPase H+ Transporting V1 Subunit C1 |
| B2M | Beta-2-Microglobulin |
| B3GALNT2 | B 1 3 N Acetylgalactosaminyltransferase 2 |

| | |
|-----------------|---|
| B4GALT1 | Beta-1,4-Galactosyltransferase 1 |
| B4GALT1 | Beta-1,4-Galactosyltransferase 1 |
| BMP2 | Bone Morphogenetic Protein 2 |
| Bp | Base pairs |
| BSA | Bovine Serum Albumine |
| C1orf43 | Chromosome 1 Open Reading Frame 43 |
| C3 | Complement C3 |
| CAV1 | Caveolin 1 |
| CD63 | Cd63 Molecule |
| CDG | Congenital Disorders of Glycosylation |
| CDG-I | Early Glycosylation Defect |
| CDG-II | Late Glycosylation Defect |
| cDNA | Complementary Desoxyribonucleic Acid |
| CDS | Coding Sequence |
| CHRM3 | Cholinergic Receptor Muscarinic 3 |
| CI | Cell Index |
| cm | Centimeter |
| cm ² | Square Centimeter |
| CMP | Cytidine Monophosphate |
| CMP-NeuAc | Cytidine-5'-Monophospho-N-Acetylneuraminic Acid |
| COG | Component Of Oligomeric Golgi Complex |
| ConA | Concanavalin A |
| CoQ10 | Coenzyme Q10 |
| Core-1-GalT | Core-1 Galactosyl Transferase |
| CPT1A | Carnitine Palmitoyltransferase 1a |
| CREB1 | Camp Responsive Element Binding Protein 1 |
| Ct | Cycle Threshold |
| CTP | Cytidine Diphosphate |
| Ctrl | Control |
| CTSD | Cathepsin D |
| CZE | Capillary Zone Electrophoresis |
| DHDDS | Dehydrodolichyl Diphosphate Synthase Subunit |
| DMAPP | Dimethylallyl Pyrophosphate |
| DMEM | Dulbecco's Modified Eagle's Medium |
| DMSO | Dimethyl Sulfoxide |
| DNA | Desoxyribonucleic Acid |
| DNASE2 | Deoxyribonuclease 2, Lysosomal |
| dNTP | Desoxy Nucleotide Triphosphate |

| | |
|--------------|--|
| DOLK | Dolichol Kinase |
| DolP | Dolichol-Phosphate |
| Dol-P | Dolichol-Phosphate |
| Dol-P-Glc | Dolichol-Phosphate-Glucose |
| Dol-P-GlcNAc | Dolichol-Phosphate-N-Acetylglucosamine |
| Dol-P-Man | Dolichol-Phosphate-Mannose |
| DOLPP1 | Dolichyldiphosphatase 1 |
| DPAGT1 | UDP-N-Acetylglucosamine--Dolichyl-Phosphate Acetylglucosaminophosphotransferase |
| DPBS | Dulbecco's Phosphate-Buffered Saline |
| DPM | Dolichol-Phosphate Mannosyltransferase Subunit 1 |
| DPM1-3 | Dolichyl-Phosphate Mannosyltransferase Subunit |
| DPY19L | DPY-19 Like C-Mannosyltransferase |
| dsDNA | Doublestranded DNA |
| DSL | Datura Stramonium |
| DTT | Dithiothreitol |
| ECL | Erythrina Cristagalli |
| ECL | Enhanced Chemiluminescence |
| EDTA | Ethylenediaminetetraacetic Acid |
| ENO1 | Enolase 1 |
| ENO3 | Enolase 3 |
| ER | Endoplasmic Reticulum |
| ESI | Electrospray Ionisation |
| Ex | Exon |
| FABP1 | Fatty Acid Binding Protein 1 |
| FBP1 | Fructose-Bisphosphatase 1 |
| FCS | Fetal Calf Serum |
| FGF2 | Fibroblast Growth Factor 2 |
| FLT1 | FMS Related Receptor Tyrosine Kinase 1 |
| FPP | Farnesyl Pyrophosphate |
| FPTase | Farnesyl Protein Transferase |
| Fuc | Fucose |
| FUT8 | Fucosyltransferase 8 |
| FUT9 | Fucosyltransferase 9 |
| g | Gram |
| G418 | Genitacin |
| GA | Golgi Apparatus |
| Gal | Galactose |

| | |
|-----------|--|
| GALE | Udp-Galactose-4-Epimerase |
| GalNAcT | Galnac Transferase |
| GANAB | Glucosidase Ii Alpha Subunit |
| GAPDH | Glyceraldehyde 3-Phosphate Dehydrogenase |
| GBA | Glucosylceramidase Beta |
| gDNA | Genomic Desoxyribonucleic Acid |
| GDP | Guanosine Diphosphate |
| GDP-Fuc | Guanosine Diphosphate Fucose |
| GDP-Man | Guanosine Diphosphate Mannose |
| GFP | Green Fluorescent Protein |
| GGPTase | Geranylgeranyl Protein Transferase |
| GLB1 | Galactosidase Beta 1 |
| Glc | Glucose |
| Glcase | A-Glucosidase |
| GlcNAc | N-Acetylglucosamine |
| GlcNAcT | N-Acetylglucosamine Transferase |
| GlutMRM | Glutamine Multiple Reaction Monitoring |
| GMPPA | GDP-Mannose Pyrophosphorylase A |
| GMPPB | GDP-Mannose Pyrophosphorylase B |
| GNA | Galanthus Nivalis |
| GNE | UDP-GlcNAc-2-Epimerase |
| GOI | Gene Of Interest |
| GOT2 | Glutamic-Oxaloacetic Transaminase 2 |
| GPI | Glucose-6-Phosphate-Isomerase |
| GPP | Geranyl Pyrophosphate |
| GSL | Glycosphingolipid |
| h | Hours |
| HB | Homogenization Buffer |
| HEXA | Hexosaminidase Subunit Alpha |
| HEXB | Hexosaminidase Subunit Beta |
| HIDS | Hyperimmunoglobulinemia D Syndrome |
| HiF1alpha | Hypoxia Inducible Factor 1 Subunit Alpha |
| HK2 | Hexokinase 2 |
| HLA-A | Major Histocompatibility Complex, Class I, A |
| HLA-B | Major Histocompatibility Complex, Class I, B |
| HMG-CoA | 3-Hydroxy-3-Methyl-Glutaryl-Coenzyme A |
| HMGCR | 3-Hydroxy-3-Methylglutaryl-Coa Reductase |
| HPLC | High Performance Liquid Chromatography |

| | |
|---------|--|
| HPRT1 | Hypoxanthine Phosphoribosyltransferase 1 |
| HRP | Horseradish Peroxidase |
| HSD17B4 | Hydroxysteroid 17-Beta Dehydrogenase 4 |
| HSPA5 | Heat Shock Protein Family A (Hsp70) Member 5 |
| ICAM1 | Intercellular Adhesion Molecule 1 |
| IDH1 | Isocitrate Dehydrogenase (Nadp(+)) 1 |
| IDH3B | Isocitrate Dehydrogenase (Nad(+)) 3 Non-Catalytic Subunit Beta |
| IEF | Isoelectric Focusing |
| IGF1R | Insulin Like Growth Factor 1 Receptor |
| IGF2 | Insulin Like Growth Factor 2 |
| IL1A | Interleukin 1 Alpha |
| IL1B | Interleukin 1 Beta |
| IP | Isopentyl Phosphate |
| IPP | Isopentyl Pyrophosphate |
| ITGAV | Integrin Subunit Alpha V |
| kDa | Kilo Dalton |
| l | Liter |
| LAMP | Lysosomal-Associated Membrane Protein |
| LB | Lysogeny Broth |
| LCH | Lens Culinaris |
| LDLR | Low Density Lipoprotein Receptor |
| LDs | Lipid Droplets |
| LLO | Short Lipid Linked Oligosaccharide |
| LLO | Lipid-Linked-Oligosaccharide |
| M | Molar (Mol/Litre) |
| mA | Milliampere |
| MAL I | Maackia Amurensis Leukoagglutinin I |
| MALII | Maackia Amurensis Lectin II |
| Man | Mannose |
| MAN1A1 | A-1-2-Mannosidase IA |
| MAN1A1 | Mannosidase Alpha Class 1a Member 1 |
| MAN1A2 | Mannosidase Alpha Class 1a Member 2 |
| MAN1B1 | A Mannosidase I |
| MAN1B1 | Mannosidase Alpha Class 1b Member 1 |
| MAN1C1 | Mannosidase Alpha Class 1c Member 1 |
| MAN2A1 | Mannosidase Alpha Class 2a Member 1 |
| MAPK8 | Mitogen-Activated Protein Kinase 8 |

| | |
|--------|--|
| MDH1 | Malate Dehydrogenase 1 |
| mg | Milligram |
| MGAT1 | Alpha-1,3-Mannosyl-Glycoprotein 2-Beta-N-Acetylglucosaminyltransferase |
| MGAT2 | Alpha-1,6-Mannosyl-Glycoprotein 2-Beta-N-Acetylglucosaminyltransferase |
| min | Minutes |
| mio | Million |
| MKD | Mevalonate Kinase Deficiency |
| ml | Milliliter |
| mm | Millimeter |
| mM | Millimolar |
| MOGS | Mannosyl-Oligosaccharide Glucosidase |
| MPDU | Mannose-P-Dolichol Utilization Defect 1 Protein |
| MPDU1 | Mannose-P-Dolichol Utilization Defect 1 |
| MPI | Mannose-Phosphate-Isomerase |
| mRNA | Messenger RNA |
| MS | Mass Spectrometry |
| MTA | Methylthioadenosine |
| mTOR | Mechanistic Target of Rapamycin Kinase |
| MVA | Mevalonic Aciduria |
| MVK | Mevalonate Kinase |
| NaAc | Sodium Acetate |
| NADH | Nicotinamide Adenine Dinucleotide |
| NAGK | N-Acetylglucosamine Kinase |
| NANS | N-Acetylneuraminase Synthase |
| Neu5Ac | N-Acetylneuraminic Acid |
| NFKB1 | Nuclear Factor Kappa B Subunit 1 |
| ng | Nanogram |
| nm | Nanometers |
| nm | Nanometer |
| nM | Nanomolar |
| NPA | Narcissus Pseudonarcissus |
| NPC2 | NPC Intracellular Cholesterol Transporter 2 |
| NR1H3 | Nuclear Receptor Subfamily 1 Group H Member 3 |
| NR3C1 | Nuclear Receptor Subfamily 3 Group C Member 1 |
| NST | Nucleotide Sugar Transporter |
| NUS1 | NUS1 Dehydrodolichyl Diphosphate Synthase Subunit |

| | |
|----------|--|
| OGT | O-Linked N-Acetylglucosamine (GlcNAc) Transferase |
| OST | Oligosaccharyl-Transferase-Complex |
| p | P-Value |
| P-5-C | Δ 1 Pyrrolin-5-Carboxylat |
| PAPSS1 | 3'-Phosphoadenosine 5'-Phosphosulfate Synthase 1 |
| PBS | Phosphate Buffered Saline |
| PBST | Phosphate Buffered Saline Tween |
| PCA | Principal Component Analysis |
| PCK2 | Phosphoenolpyruvate Carboxykinase 2, Mitochondrial |
| PCR | Polymerase Chain Reaction |
| PDK4 | Pyruvate Dehydrogenase Kinase 4 |
| PEP | Phosphoenolpyruvate |
| PFKM | Phosphofructokinase, Muscle |
| PFKP | Phosphofructokinase, Platelet |
| PGAM1 | Phosphoglycerate Mutase 1 |
| PGM | Phosphoglucomutase |
| PGM1 | Phosphoglucomutase 1 |
| PHA-L | Phaseolus Vulgaris Leucoagglutinin |
| PIK3R1 | Phosphoinositide-3-Kinase Regulatory Subunit 1 |
| PIM | Protease Inhibitor Mix |
| PKM2 | Pyruvate Kinase M1/2 |
| PLA2G4A | Phospholipase A2 Group Iva |
| PMM1 | Phosphomannomutase 1 |
| PMM2 | Phosphomannomutase 2 |
| pmol | Picomol |
| PMVK | Phosphomevalonate Kinase |
| POFUT | Protein O-Fucosyltransferase |
| POI | Protein Of Interest |
| POLR2A | Rna Polymerase Ii Subunit A |
| POMGNT1 | Protein O-Linked Mannose N-Acetylglucosaminyltransferase 1 (Beta 1,2-) |
| POMGNT2 | Protein O-Linked Mannose N-Acetylglucosaminyltransferase 2 (Beta 1,4-) |
| POMT1 | Protein O-Mannosyltransferase 1 |
| POMT2 | Protein O-Mannosyltransferase 2 |
| PPARA | Peroxisome Proliferator Activated Receptor Alpha |
| PPARG | Peroxisome Proliferator Activated Receptor Gamma |
| PPARGC1A | PPARG Coactivator 1 Alpha |

| | |
|----------|---|
| PRKAA1 | Protein Kinase Amp-Activated Catalytic Subunit Alpha 1 |
| PRKAA2 | Protein Kinase Amp-Activated Catalytic Subunit Alpha 2 |
| PRKAB1 | Protein Kinase Amp-Activated Non-Catalytic Subunit Beta 1 |
| PRKCA | Protein Kinase C Alpha |
| PRKCSH | Protein Kinase C Substrate 80k-H |
| PSME1 | Proteasome Activator Subunit 1 |
| PTGS1 | Prostaglandin-Endoperoxide Synthase 1 |
| PTM | Posttranslational Modification |
| qRT-PCR | Quantitative Real Time Polymerase Chain Reaction |
| RAB7A | Rab7a, Member Ras Oncogene Family |
| RARA | Retinoic Acid Receptor Alpha |
| RB1 | Rb Transcriptional Corepressor 1 |
| RFP | Tripartite Motif Containing 27 |
| RFT1 | Rft1 Homolog |
| RIPA | Radioimmunoprecipitation Assay Buffer |
| RISC | RNA-Induced Silencing Complex |
| RNA | Ribo Nucleic Acid |
| RNAse | Ribonuclease |
| rpm | Rounds Per Minute |
| RT | Room Temperature |
| RTCA | Real Time Cell Analyzer |
| RXRA | Retinoid X Receptor Alpha |
| SAHC | S-Adenosyl-L-Homocysteine |
| SAM | S-Adenosylmethionine |
| SAP | Shrimp Alkaline Phosphatase |
| SCARB2 | Scavenger Receptor Class B Member 2 |
| SCD | Stearoyl-Coa Desaturase |
| scRNA | Scrambled RNA |
| SDS-PAGE | Sodium Dodecyl Sulfate Polyacrylamide Gel Electrophoresis |
| sec | Second |
| SGK1 | Serum/Glucocorticoid Regulated Kinase 1 |
| Sia | Sialic Acid |
| siRNA | Small Interfering RNA |
| SIRT1 | Sirtuin 1 |
| SLC35A1 | CMP-Sialic Acid Transporter |

| | |
|---------|---|
| SLC35A1 | Solute Carrier Family 35 Member A1 |
| SLC35A2 | UDP-Galactose Transporter |
| SLC35A3 | UDP-N-Acetylglucosamine Transporter |
| SLC35C1 | GDP-Fucose Transporter 1 |
| SNA | Sambucus Nigra |
| SNA | Sambucus Nigra |
| SNRPD3 | Small Nuclear Ribonucleoprotein D3 Polypeptide |
| SOD1 | Superoxide Dismutase 1 |
| SRC | SRC Proto-Oncogene, Non-Receptor Tyrosine Kinase |
| SRD5A3 | Steroid 5 Alpha-Reductase 3 |
| SREBF1 | Sterol Regulatory Element Binding Transcription Factor 1 |
| ST3Gal3 | CMP-N-Acetylneuraminic-Beta-1,4-Galactoside Alpha-2,3-Sialyltransferase |
| ST6GAL1 | ST6 Beta-Galactoside Alpha-2,6-Sialyltransferase 1 |
| ST6GAL2 | ST6 Beta-Galactoside Alpha-2,6-Sialyltransferase 2 |
| STAT5A | Signal Transducer And Activator Of Transcription 5a |
| STK11 | Serine/Threonine Kinase 11 |
| STX7 | Syntaxin 7 |
| TAE | Tris Acetate EDTA |
| TAPBP | TAP Binding Protein |
| TBS | Tris Buffered Saline |
| TBST | Tris Buffered Saline Tween |
| TCEP | Thioredoxin |
| TEAB | Triethylammonium Bicarbonate |
| TEMED | Tetramethylethylenediamine |
| TF | Transferrin |
| TFA | Trifluoroacetic Acid |
| TGFB1 | Transforming Growth Factor Beta 1 |
| THRB | Thyroid Hormone Receptor Beta |
| TMD | Transmembrane Domains |
| TPI1 | Triosephosphate Isomerase 1 |
| TPP1 | Tripeptidyl Peptidase 1 |
| U | Unit |
| UAP1 | UDP-N-Acetylglucosamine Pyrophosphorylase 1 |
| UDP | Uridine Diphosphate |
| UDP-Gal | Uridine Diphosphate Galactose |
| UDP-Glc | Uridine Diphosphate Glucose |

| | |
|--------------|--|
| UDP-GlcNAc | Uridine Diphosphate-N-Acetylglucosamine |
| UGPase | UDP-Glucose-Pyrophosphorylase |
| UV | Ultraviolet |
| VAMP3 | Vesicle Associated Membrane Protein 3 |
| VIME | Vimentin |
| WB | Washing Buffer |
| WGA | Wheat Germ Agglutinin |
| WGA | Wheat Germ Agglutinin |
| WT | Wildtype |
| xCGE-LIF | High Performance Multiplexed Capillary Gel Electrophoresis with Laser-Induced Fluorescence Detection |
| α -DG | Alpha-Dystroglycan |
| μ g | Microgram |
| μ l | Microliter |
| μ M | Micromolar |
| μ m | Micrometer |










Abbreviation of nucleobases:

| | |
|---|----------|
| A | adenine |
| C | cytosine |
| G | guanine |
| T | thymine |
| N | any base |

Abbreviation of amino acids in one/three-letter-code:

| | | |
|-----|---|---------------|
| Ala | A | Alanine |
| Arg | R | Arginine |
| Asn | N | Asparagine |
| Asp | D | Aspartic acid |
| Cys | C | Cysteine |
| Gln | Q | Glutamine |
| Glu | E | Glutamic acid |
| Gly | G | Glycine |
| His | H | Histidine |
| Leu | L | Leucine |
| Ile | I | Isoleucine |
| Lys | K | Lysine |
| Met | M | Methionine |
| Phe | F | Phenylalanine |
| Pro | P | Proline |
| Thr | T | Threonine |
| Trp | W | Tryptophan |
| Tyr | Y | Tyrosine |
| Val | V | Valine |

Abbreviation and symbols of sugars:

| | | |
|--------|---|---------------------|
| Dol |  | Dolichol |
| Fru |  | Fructose |
| Fuc |  | Fucose |
| Gal |  | Galactose |
| GalNAc |  | N-Acetylglucosamine |
| Glc |  | Glucose |
| GlcNAc |  | N-Acetylglucosamine |
| Man |  | Mannose |
| Sia |  | Sialic acid |
| P | | Phosphate |
| PP | | Diphosphate |

Abbreviation for N-glycan analysis:

| | |
|--------|--|
| A | Antenna |
| B | Bisection |
| F | Fucose / fucosylation |
| G | Galactose / galactosylation |
| Ga | two connected galactoses |
| GalNAc | N-Acetyl-Galactosamine |
| GlcNAc | N-Acetyl-Glucosamine |
| (L) | Glycosidic link |
| Lac | Galactose linked with N-Acetyl-Galactosamine |
| M | Mannose |
| n | Number of monosaccharides |
| S / Sg | Sialic acid / sialylation |

Lipid nomenclature:

| | |
|-------|-----------------------------|
| CE | Cholesterol Ester |
| Cer | Ceramide |
| Chol | Cholesterol |
| DAG | Diacylglycerol |
| PC O- | Alkyl-Phosphatidylcholines |
| PE | Phosphatidylethanolamines |
| PI O- | Alkyl-Phosphatidylinositols |
| PS | Phosphatidylserines |
| PS O- | Alkyl-Phosphatidylserines |
| SM | Sphingomyelin |

1 Abstract

The mevalonate kinase deficiency (MKD) is an inherited disorder of the cholesterol biosynthesis. This early-onset disease is caused by mutations in the *MVK* gene and belongs to the ultra-rare diseases. Patients are divided into two groups, the mevalonate kinase deficiency (MKD)/ hyperimmunoglobulinemia D syndrome (HIDS) group and the mevalonic aciduria (MVA) group, which is the more severe end of the spectrum of symptoms. The clinical picture includes recurrent febrile crises, often accompanied by hepatosplenomegaly, lymphadenopathy, mental retardation, ocular symptoms, psychomotor retardation, skin rashes, cardiomyopathy, hypotonia and facial dysmorphism.

The new patient MVK9 displayed the typical symptoms of MVA patients and was initially diagnosed by the elevated mevalonate acid excretion in urine, which is the gold standard screening method for diagnosis. The patient died at day 11 due to cardiac arrest. Genetic analysis confirmed the *MVK* deficiency by identifying the homozygous mutation c.803T>C in exon 9 leading to amino acid change p.Ile268Thr. To get a better understanding of the pathophysiologic mechanism of the *MVK* deficiency, ten more *MVK* patients were included in this work. Sanger sequencing of these patients revealed two new mutations, c.782T>C in *MVK10* and c.790dupC in *MVK3*, which are not in the NCBI ClinVar database yet. All 11 patients belong to the MVA group, whereby also differences in the severity of the phenotype were present. *MVK* expression analysis revealed a diminished *MVK* protein expression in all *MVK* patients. Biochemical and genetic analyses used in this study comprised western blots, immunofluorescence studies, lectin blots, N-glycan analysis, nCounter expression analysis, qRT-PCR, lipid analysis and metabolite measurements.

Based on the results of this work it could be demonstrated for the first time that a *MVK* defect leads to a global N-glycosylation deficiency in patients caused by low levels of dolichol and dolichyl phosphate. In addition, hints to an impact on O-mannosylation and C-mannosylation have been found.

The *MVK* defect therefore belongs to the disease group of congenital disorders of glycosylation (CDG), and it is proposed to name this new defect 'MVK-CDG'.

2 Zusammenfassung

Der Mevalonat-Kinase-Mangel (MKD) ist eine vererbte Störung der Cholesterinbiosynthese. Diese früh auftretende Krankheit wird durch Mutationen im MVK-Gen verursacht und gehört zu den sehr seltenen Krankheiten. Die Patienten werden in zwei Gruppen unterteilt, die Mevalonatkina-Mangel (MKD)/Hyperimmunoglobulinämie-D-Syndrom (HIDS)-Gruppe und die Mevalonsäure Azidurie (MVA)-Gruppe, die das schwerere Ende des Symptomspektrums darstellt. Das klinische Bild umfasst wiederkehrende Fieberkrisen, die häufig von Hepatosplenomegalie, Lymphadenopathie, geistiger Retardierung, okulären Symptomen, psychomotorischer Retardierung, Hautausschlägen, Kardiomyopathie, Hypotonie und Gesichtsdysmorphismen begleitet werden.

Der neue Patient MVK9 wies die typischen Symptome von MVA-Patienten auf und wurde zunächst durch die erhöhte Mevalonsäureausscheidung im Urin diagnostiziert, die die Goldstandard-Screening Methode für die Diagnose darstellt. Der Patient starb am 11. Tag aufgrund eines Herzstillstands. Die genetische Analyse bestätigte den MVK-Mangel durch die Identifizierung der homozygoten Mutation c.803T>C im Exon 9, die zu einer Aminosäureveränderung p.Ile268Thr führt. Um ein besseres Verständnis des pathophysiologischen Mechanismus des MVK-Mangels zu erhalten, wurden zehn weitere MVK-Patienten in diese Arbeit einbezogen. Die Sanger-Sequenzierung dieser Patienten ergab zwei neue Mutationen, c.782T>C in MVK10 und c.790dupC in MVK3, die noch nicht in der NCBI ClinVar-Datenbank enthalten sind. Alle 11 Patienten gehören zur MVA-Gruppe, wobei auch Unterschiede im Schweregrad des Phänotyps vorhanden waren. Die MVK-Expressionsanalyse ergab eine verminderte MVK-Proteinexpression bei allen MVK-Patienten. Die in dieser Studie verwendeten biochemischen und genetischen Analysen umfassten Western Blots, Immunfluoreszenzstudien, Lektin-Blots, N-Glykan-Analysen, nCounter-Expressionsanalysen, qRT-PCR, Lipidanalysen und Metaboliten Messungen.

Anhand der Ergebnisse dieser Arbeit konnte erstmals gezeigt werden, dass ein MVK-Defekt bei Patienten zu einem globalen N-Glykosylierungsdefizienz führt, das durch niedrige Dolichol- und Dolicholphosphat Spiegel verursacht wird. Darüber hinaus wurden Hinweise auf einen Einfluss auf die O-Mannosylierung und die C-Mannosylierung gefunden.

Der MVK-Defekt gehört daher zur Krankheitsgruppe der angeborenen Störungen der Glykosylierung (CDG), und es wird vorgeschlagen, diesen neuen Defekt "MVK-CDG" zu nennen.

3 Theory

3.1 Mevalonate (Isoprenoid) Pathway

The mevalonate pathway is an important, highly conserved metabolic pathway that is responsible for the production of bioactive molecules for multiple vital cellular processes. The pathway is also known as the isoprenoid pathway or the HMG-CoA (3-hydroxy-3-methyl-glutaryl-coenzyme A) reductase pathway. It is essential and present in eukaryotes, archaea, and some bacteria [1], [2]. The two produced essential building blocks isopentyl pyrophosphate (IPP) and dimethylallyl pyrophosphate (DMAPP) are five-carbon structures, which are used to make a variety of isoprenoids. These are a diverse class of over 30,000 biomolecules which includes all steroid hormones, cholesterol, vitamin K and coenzyme Q10. The mevalonate pathway can be separated into two parts, the upper and lower one. For eukaryotes, archaea and eubacteria is the upper one the same. The starting substrates are two acetyl-CoA molecules that are condensed by the enzyme acetoacetyl-CoA thiolase to yield acetoacetyl-CoA (see Figure 1). The next step is a second condensation to form HMG-CoA (3-hydroxy-3-methyl-glutaryl-CoA) by HMG-CoA synthase followed by a reduction by HMG-CoA reductase to mevalonate.

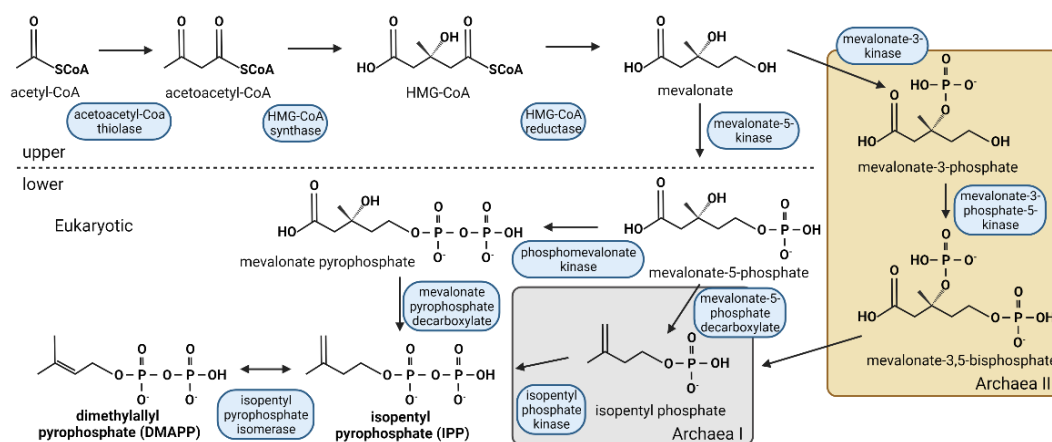


Figure 1 - Mevalonate pathway. The upper mevalonate pathway is the same for eukaryotes, archaea and eubacteria, starting from acetyl-CoA resulting in mevalonate. In eukaryotes mevalonate is two times phosphorylated to yield IPP and DMAPP, in the end. In archaea I (grey box) this is achieved over isopentyl phosphate. In archaea II (yellow box) mevalonate is phosphorylated at position 3 instead of 5 and the intermediate mevalonate-3,5-bisphosphate is only found here. (Created with BioRender.com.)

In eukaryotes, the lower pathway starts by the phosphorylation of mevalonate into mevalonate-5-phosphate followed by second phosphorylation to mevalonate pyrophosphate. This is performed by the mevalonate-5-kinase and phosphomevalonate kinase. The next step is a decarboxylation into isopentyl pyrophosphate (IPP) by the enzyme mevalonate pyrophosphate decarboxylase [3]. Another route (Archaeal Mevalonate Pathway) was found in some archaea (e.g. *Haloferax volcanii*) in which mevalonate is once phosphorylated in the 5-OH position and then decarboxylated by

mevalonate-5-phosphate decarboxylase to yield isopentyl phosphate (IP) [4]. IP is then phosphorylated a second time by isopentyl pyrophosphate kinase to IPP. In a third route (Archaeal Mevalonate Pathway II) found in *Thermoplasma acidophilum* mevalonate gets phosphorylated in the 3-OH position by mevalonate-3-kinase to mevalonate-3-phosphate. Then mevalonate-3-phosphate-5-kinase phosphorylates the resulting metabolite at the 5-OH position to mevalonate-3,5-bisphosphate which finally is decarboxylated to IP and phosphorylated to IPP [5], [6]. In the last step, IPP is converted into dimethylallyl pyrophosphate (DMAPP) by the isopentyl pyrophosphate isomerase. These two five-carbon compounds are the base for a huge variety of different metabolites.

IPP can be used for isopentenyl-tRNA whereby the amino group of the nucleoside adenosine with IPP to *N*⁶-isopentyladenosine converted is by the tRNA-isopentenyltransferase [7]. In the next step, IPP and DMAPP are condensed to form the 10-carbon compound geranyl pyrophosphate (GPP) followed by another addition of IPP to synthesize the 15-carbon farnesyl pyrophosphate (FPP). Both reactions are performed by farnesyl diphosphate synthase. FPP displays the branching point between sterols, longer-chain nonsterol synthesis and dolichol synthesis.

3.1.1 Cholesterol

For cholesterol and vitamin D, the enzyme squalene synthase condensate two FPP molecules head-to-head to form the sterol precursor squalene [8]. In mammals, this is the first and only step that leads to cholesterol biosynthesis. The reaction takes place in the endoplasmic reticulum (ER). Squalene is first activated and then cyclized into lanosterol by squalene monooxidase and epoxidase. In 19 following enzymatic reactions lanosterol is converted into cholesterol and the intermediate 7-dehydrocholesterol is used for vitamin D production. Cholesterol has an impact on steroid hormones, bile acid synthesis and hedgehog proteins [9].

3.1.2 Longer-chain Nonsterols

Another longer-chain nonsterol is the 20-carbon product geranylgeranyl pyrophosphate (GGPP) that is synthesized by GGPP synthase by fusing FPP with IPP [10]. GGPP and FPP can be used for the isoprenylation of proteins catalyzed by geranylgeranyl protein transferase (GGPTase) I and II, and farnesyl protein transferase (FPTase) [11], [12]. Another product of this branch is decaprenyl pyrophosphate synthesized by transprenyl transferase which is used as the sidechain of coenzyme Q10 [13].

3.1.3 Dolichol

One more important product of the mevalonate pathway is dolichol, which is needed in glycosylation (see chapter 3.4, 3.6, 3.7) [14]. Naturally occurring dolichol consists of a series of homologues containing 13 – 23 isoprene units which equals 65 –

110 carbon atoms [15]. Starting from IPP and FPP, the enzyme DHDDS in complex with NUS1 catalyzes the reaction to polyprenol pyrophosphate. After dephosphorylation by DOLPP1 to polyprenol dolichol is synthesized by SRDSA3. Dolichol is then activated by phosphorylation by DOLK using CTP as donor substrate. Dolichyl phosphate (DoLP) serves for dolichol-phosphate-mannose (Dol-P-Man), dolichol-phosphate-glucose (Dol-P-Glc), dolichol-phosphate-N-acetylglucosamine (Dol-P-GlcNAc) and as a lipid anchor for the oligosaccharide precursor in membranes during N-glycosylation [16].

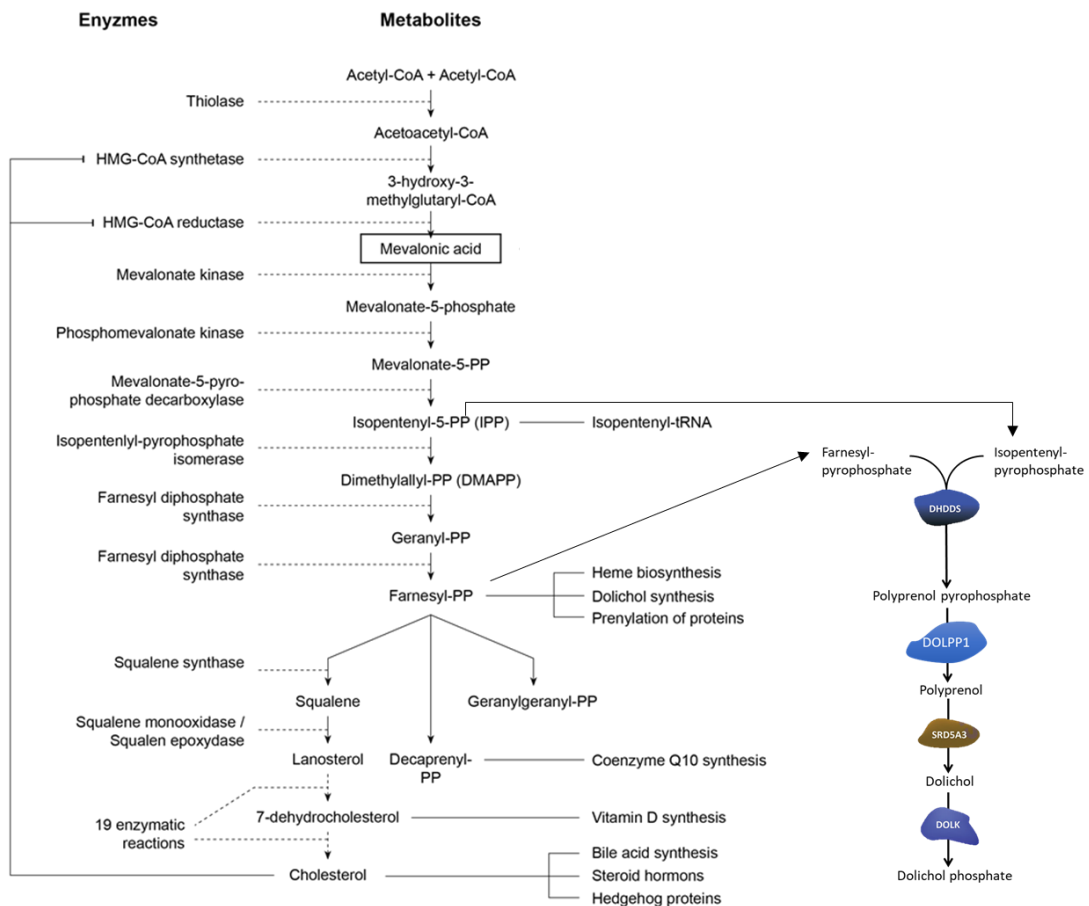


Figure 2 - Continuation of the mevalonate pathway. Depicted are intermediates of the mevalonate pathway and the involved enzymes. From the branching point farnesyl-PP (FPP) cholesterol or longer-chain nonsterols can be produced. Dolichol synthesis starts with FPP and IPP on the right side of the scheme. Adapted from [17].

3.2 Overview on Glycosylation

In nature carbohydrates are responsible for many important functions. The first, most widely known, function is the energy metabolism where glucose is converted to adenosine triphosphate (ATP). The other use of carbohydrates is the so-called glycosylation, the process where carbohydrates are attached to proteins or lipids, as a co- and posttranslational modification (PTM) and can be found in every organism from bacteria over plants to animals and humans [18]. The sugar structures of these glycoconjugates are termed glycans and are distinguished by length, type of monomers and type of linkage.

3.3 Protein Glycosylation and Glycoprotein Synthesis

Co- and post-translational modifications of proteins with glycans is called protein glycosylation. The main sites of glycosylation are the cytosolic and luminal leaflet of the endoplasmic reticulum (ER) and the Golgi-apparatus (GA) [19]. The covalently attached glycans are responsible for e.g., quality control, correct folding, function and localization of proteins. Glycosylation thereby displays an essential biological and physiological mechanism which is present in every prokaryotic and eukaryotic cell [20]. These glycoproteins are involved in processes like growth, differentiation, organ development, signal transduction, immune- and inflammation reactions and even in malignant transformations [21], [22]. They are distributed ubiquitously in the cell; from organelles to membranes and even the extracellular matrix. The property of proteins depends on these modifications and is one reason for the functional diversity and heterogeneity within molecules of the same protein. It is known that around 50 % of eukaryotic proteins have at least one type of glycosylation [23], [24]. Several types of protein glycosylation are acquainted like GPI-anchored proteins, proteoglycans and glycosaminoglycans. Especially important are the N- and O-glycosylation and the C-mannosylation that are defined by their glycosidic link to the elements nitrogen (N), oxygen (O) and carbon (C) [25]. The pathways are highly conserved within species and the biosynthesis involves glycosyltransferases, glycosidases, transporters, and associated pathways [26].

3.4 N-Glycosylation

N-glycosylation is the most abundant modification of membrane-bound- and secreted proteins and is also the best studied one. N-glycans are bound to the nitrogen of the amid group of the asparagine side chain in the consensus sequence Asn-X-Ser/Thr. X can be any amino acid except proline or aspartic acid [27]. In mammals all N-linked oligosaccharides are bound to the monosaccharide β -GlcNAc as the primary unit. Not every consensus sequence will be glycosylated, only around one third of them has a glycan attached, indicating that the protein's three-dimensional shape and location within the cell compartments also influence N-glycosylation [28], [29].

N-glycans have the same core structure which consist of five monosaccharides but a diverse terminal ending. On the first GlcNAc-unit another GlcNAc is attached, followed by three mannose (Man) residues attached in a branch setting, the outer ones in α 1,3 and α 1,6 glycosidic bond, named the 1,3 and 1,6 arm [30]. This is called the core structure $\text{Man}_3\text{GlcNAc}_2$. N-glycans can be divided into 3 main classes: The high-mannose type, the complex type and the hybrid type (see Figure 3). Glycans of the high-mannose type consist of the core with additional branched mannose residues. A complex type N-glycan has the core structure plus antennas with attached sugars like GlcNAc, galactose (Gal) and a terminal sialic acid (Sia). Some of them also carry a fucose residue either at the core or at the antenna. Glycans of the hybrid type carry one complex antenna while the second branch is composed of mannose.

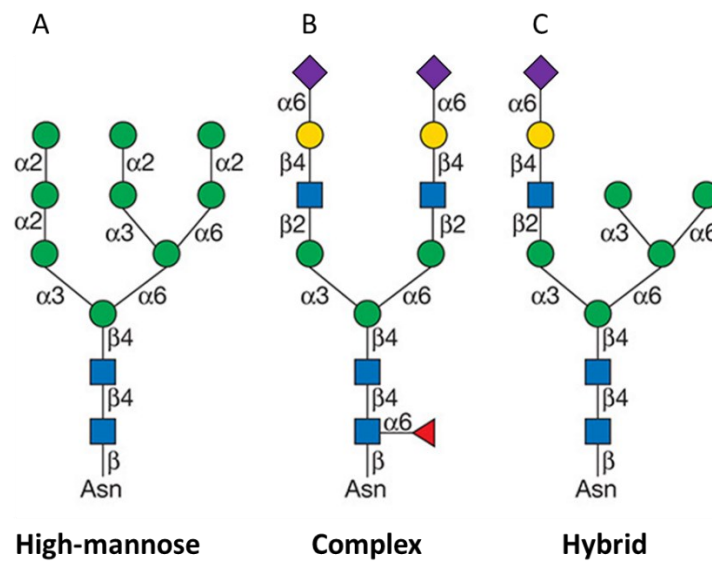


Figure 3 - The three main types of N-glycans. Depicted are examples of the high-mannose type (A), the complex (B) and hybrid (C) type. Also visible is the characteristic penta-saccharide core. Letter and number show the orientation of the glycosidic bond. Adapted from [31]. Legend of the sugar symbol code can be found in section *abbreviations*.

The synthesis of N-glycans can be divided into three steps: (1) synthesis of the lipid-linked-oligosaccharide precursor; (2) *en bloc* transfer of the precursor to the polypeptide with first modification processes and (3) more modifications and processing of the N-glycan in the Golgi apparatus. The first two steps occur in the ER.

3.4.1 Synthesis of the lipid-linked oligosaccharide precursor

The lipid dolichol is produced by intermediates of the mevalonic pathway and consists of 17 to 20 isoprenoid units which are responsible for the hydrophobic character. This chain is integrated into the double lipid layer of the ER membrane and serves as an anchor (see 3.1.3) [32]. The buildup of the oligosaccharide starts at the cytoplasmic side of the ER. Here the first GlcNAc and one phosphate residue are

attached to the lipid anchor dolichyl phosphate (DoIP) by DPAGT1 (ALG7) using UDP-GlcNAc. A second GlcNAc is added by ALG13/14 to form Dol-PP-GlcNAc₂. Then three mannose residues are attached by ALG1 and ALG2 whereby the bifunctional ALG2 is responsible for the branching adding them in an α 1,3 and α 1,6 orientation by using the donor GDP-Man. ALG11 attaches two more mannose units to form Dol-PP-GlcNAc₂Man₅ and then the LLO is flipped into the ER lumen with the help of RFT1. There, it is further processed by glycosyltransferases [33]. Inside the ER four more Man units are added by ALG3, ALG9 and ALG12 to form Dol-PP-GlcNAc₂Man₉ and further branching at the α 1,6 linked Man is conducted. The transfer of three Glc residues catalyzed by ALG6, ALG8 and ALG10 generates the mature N-glycan precursor Dol-PP-GlcNAc₂Man₉Glc₃. The donor sugar substrates needed inside the ER Dol-P-Man and Dol-P-Glc are produced by ALG5, DPM1-3 and MPDU1 from the corresponding nucleotide sugars GDP-Man and UDP-Glc together with DoIP.

3.4.2 *En bloc* transfer of glycan structure to nascent protein

The transfer of the mature lipid-linked N-glycan precursor Dol-PP-GlcNAc₂Man₉Glc₃ to the amine nitrogen atom of the asparagine-residue of a nascent protein is performed by the oligosaccharyl-transferase-complex (OST) [34]. OST is a multi-subunit complex that cleaves off the LLO at the GlcNAc-Dol-phosphate bond releasing Dol-PP. After the transfer the glycan is further processed in the ER lumen. The terminal α 1,2 linked Glc unit is removed by MOGS followed by the two α 1,3 linked Glc residues by PRKCSH and GANAB [35]. Before the glycosylated protein is sent to the Golgi apparatus the removal of the terminal α 1,2 linked Man unit from the central arm is performed by MAN1B1 and finally the protein undergoes the Calnexin/Calreticulin protein quality control [36]. Interestingly in man, MAN1B1 can also be present in the cis-Golgi compartment [37].

3.4.3 Processing of N-glycans in the Golgi apparatus

Depending on the type of N-glycan to be catalyzed, none, some or all of the α 1,2 linked Man residues are removed by mannosidases MAN1A, MAN1A2 or MAN1C1 in the *cis*-Golgi [38]. N-glycans of the high-mannose type are not trimmed and depart from the glycan biosynthesis very early [39]. In the *medial*-Golgi MGAT1 adds GlcNAc to the core α 1,3 linked Man and yields GlcNAcMan₅GlcNc₂-Asn, which can be used as precursor for the synthesis of a glycan of the hybrid type. After the exomanosidases MAN2A1 and MAN2A2 each remove one mannose residue, another GlcNAc unit is added to the second arm by MGAT2. The glycans which are further processed belong to the complex type and are based on the core structure of GlcNAc₂Man₃GlcNAc₂-Asn. The glycan is translocated to the *trans*-Golgi in which a huge variety of modifications and different terminal sugar decorations can be added to the core structure. The enzyme B4GALT1 elongates the carbohydrate chain by a β 1,4 linked galactose (Gal) to the distal GlcNAc residue. An important terminal modification is the capping of glycans with sialic acids (NeuAc) by ST6GAL1 or ST6GAL2 and is very common in humans [40]. Furthermore, a

fuco (Fuc) residue might be attached to the asparagine linked GlcNAc moiety by FUT 8 termed core fucosylation [41]. Fuco can also be linked to a terminal galactose (α 1,2) or GlcNAc (α 1,3/4) residue by other FUT enzymes and this is named terminal fucosylation [42]. Linkages can be seen in Figure 3. All necessary substrates (UDP-GlcNAc, GDP-Fuc, UDP-Gal and CMP-NeuAc) for modifications in the Golgi apparatus lumen are provided by specific nucleotide-sugar transporters of the SLC35 family [36], [43]. All described processes can be seen in detail in Figure 4.

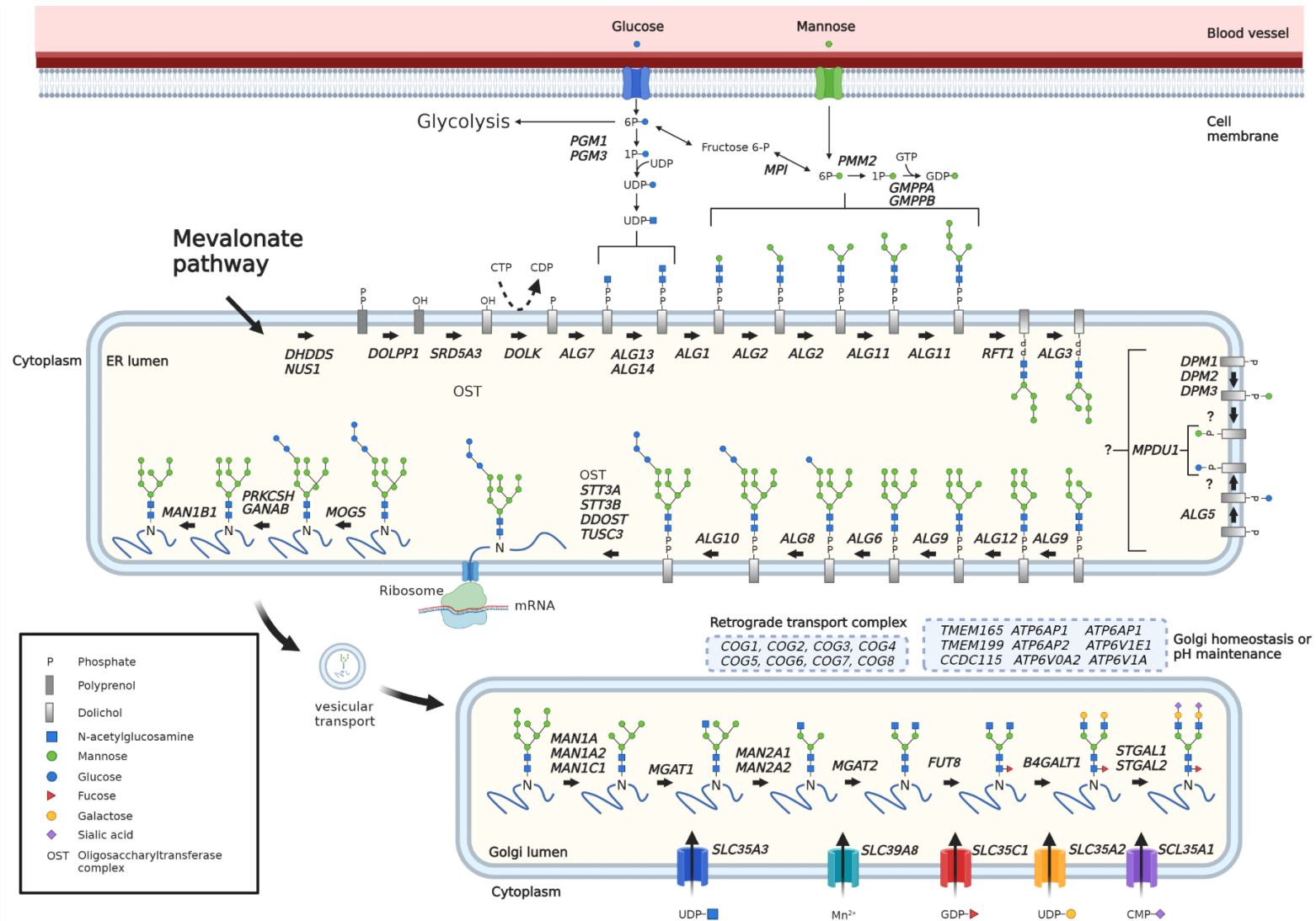


Figure 4 - N-glycosylation pathway. Depicted is the N-glycan synthesis starting at the cytosol until glycan is attached to the protein in the ER followed by trimming and processing in the Golgi. (Created with BioRender.com)

3.5 O-Glycosylation

O-glycosylation is carried out post-translationally in the Golgi apparatus as the main site of action. This group includes several types like O-GlcNAcylation, O-mannosylation, O-sialylation and O-fucosylation. It is a covalent attachment of sugar moieties to the hydroxy group of serine or threonine and is defined by steric exposure of these amino acids to the secondary and tertiary structure of the protein. In contrast to the N-glycosylation no *en bloc* transfer on the nascent protein of an O-glycan occurs. The assembly of the chain is step wise starting with a N-galactosamine (GalNAc) catalyzed by one of around 21 GalNAc transferases (GalNAcT) utilizing UDP-GalNAc. This is the most abundant O-glycosidic linkage and classified as mucin type glycan. Mucins are highly glycosylated proteins that provide the protective barrier of e.g. the intestinal mucosa and the respiratory tract by formation of a viscous mucus. O-glycans are responsible for over 50 % of the total mass in mucins, and the sialic acid residues and hydroxy groups of the polysaccharides with a polar character explain the high amount of water binding capacity. Four different core structures of mucin-type glycans can be distinguished. Based on the first attached GalNAc, Core-1 is synthesized by addition of galactose in β 1,3 orientation followed by Core-2 by the addition of GlcNAc in β 1,6 orientation. In Core-3 a GlcNAc unit is added to the initial GalNAc followed by another one in β 1,6 orientation for Core-4 (see Figure 5) [44]. Other terminal monosaccharides of O-GalNAc glycans can be fucose-, galactose, sialic acid and GlcNAc residues [45], [46].

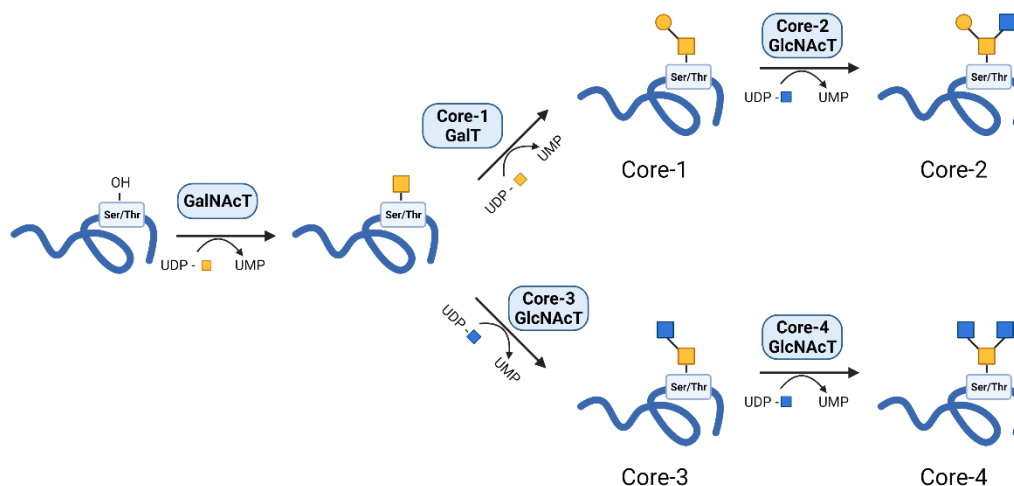


Figure 5 - Biosynthesis of O-linked mucin type glycans. Initial step is the attachment of GalNAc to serine or threonine of a polypeptide by the GalNAc transferase. From this base either Core-1 or Core-3 is synthesized by addition of Gal or GlcNAc in β 1,3 orientation, respectively. For Core-2 and Core-4 a GlcNAc in β 1,6 is added to Core-1 and Core-3, respectively. Legend of sugar symbol code can be found in section *abbreviations*. (Created with BioRender.com.)

3.6 O-Mannosylation

O-mannosylation is another important type of O-glycosylation and it is conserved among fungi, animals, and humans. It is initiated in the ER by POMT1 and POMT2 and starts with the transfer of a mannosyl residue from Dol-P-D-Man to serine or threonine residues of secretory and membrane proteins in α -D-mannosidic linkage [47]. Depending on the further modification of the first O-linked mannose residue, four types of core glycans M0, M1, M2 and M3 can be generated. The first O-linked mannose residue forms the M0 structure and is the base for all other three types. POMGNT1 adds a GlcNAc in β 1,2 orientation, called core M1 core. In a next step MGAT5 attaches another GlcNAc in β 1,6 linkage and this results in core M2. β 1,4 linkage of GlcNAc to the initial mannose unit by POMGNT2 yields the M3 core glycan [29].

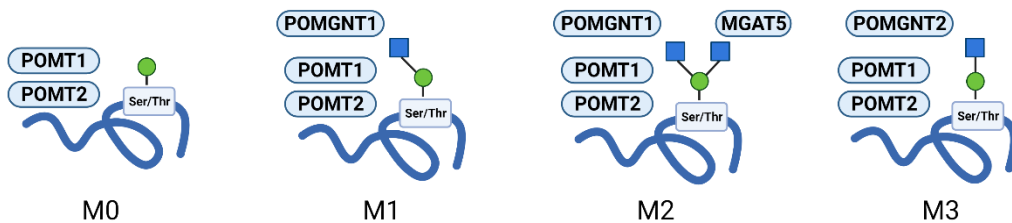


Figure 6 - Types of O-mannose glycans. The first covalent linkage of the mannose with serine or threonine is catalyzed by POMT1 and POMT2. The resulting structure is M0 as base for all other three types. POMGNT1 adds a GlcNAc in β 1,2 orientation forming core M1. In a next step MGAT5 attaches another GlcNAc in β 1,6 linkage resulting in core M2. β 1,4 linkage of GlcNAc to the initial mannose unit by POMGNT2 yields the M3 core glycan. Legend of sugar symbol code can be found in section *abbreviations*. (Created with BioRender.com.)

The substrate Dol-P-Man, which is also the substrate for C-mannosylation (see Figure 7) is produced by DPM1-3. DPM1 catalyzes the transfer of mannose from GDP-Man to Dol-P on the cytosolic side of the ER membrane. DPM2 and DPM3 stabilize DPM1 and most likely facilitate interactions with its substrate Dol-P. Then Dol-P-Man is flipped across the ER membrane with help of MPDU1, whereby this process still needs to be elucidated [49]. Defects in O-mannosylation lead to the disease spectrum of alpha-dystroglycanopathies as Walker Warburg Syndrome and Muscle Eye Brain Disease [50], [51].

3.7 C-Mannosylation

C-mannosylation is a carbon-carbon linkage between a mannose and a protein, and is performed by the C-mannosyltransferase enzymes of the DPY(dumpy)-19 family [52], [53]. The C1 atom of the α -mannose is thereby attached to the indole C2 atom of the tryptophan. This takes place in the ER and presumably co-translationally [54]. The consensus sequence is W-X-X-W/C and till today is one of the least well characterized glycosylation types [55]. It has been predicted that around 18 % of human secreted and transmembrane proteins like ADAMTS13 or properdin are C-mannosylated [56].

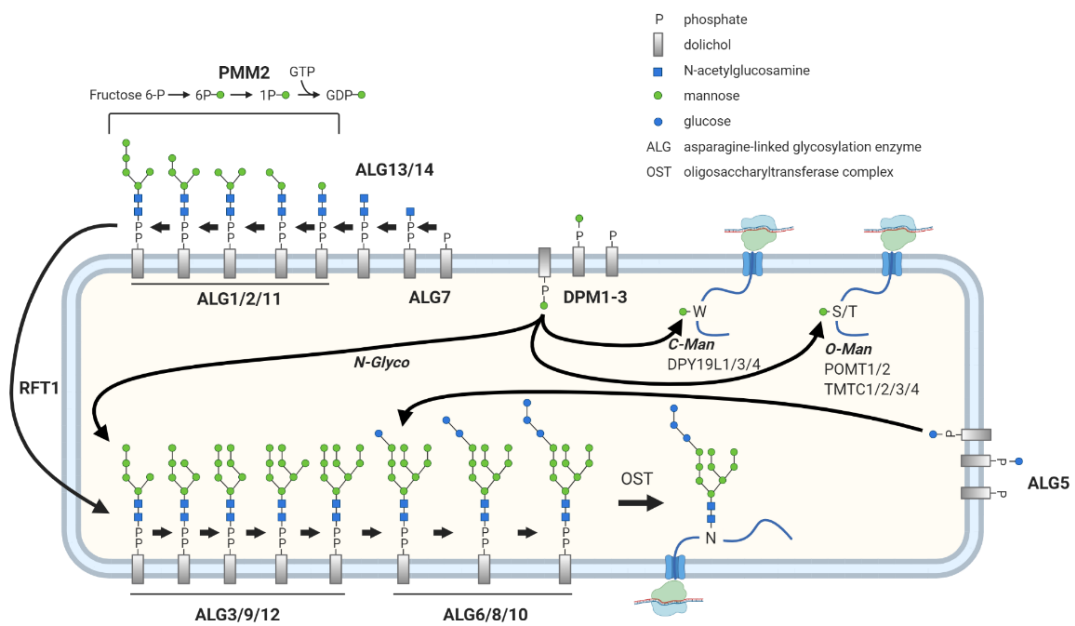


Figure 7 - Pathway of Dol-P-Man as a mannosyl donor for C-, O-mannosylation and N-glycosylation in the ER. DPM1-3 are responsible for the supply of Dol-P-Man in the ER cytosol as a mannosyl donor for glycan trees. (Created with BioRender.com)

3.8 Glycosphingolipids

The major glycolipids found in animals are glycosphingolipids (GSLs), which are found in cell membranes. GSLs have a biological impact on membrane structure, modulation of membrane protein function, host-pathogen interactions and cell-cell recognition [57]. One of the simplest and the first characterized GSL is galactosylceramide (GalCer, see Figure 8 A), which is also the most abundant molecule in vertebrate brain. GSLs belong to the larger family of sphingolipids (lipids built on sphingoid base) and nearly all glycolipids in vertebrates are GSLs.

The structure of GSLs is the following: a variety of glycans are attached to the lipid moiety ceramide, which is a long-chain amino alcohol (sphingosine) in C-2 amid linkage to a fatty acid, which has hydroxyls at the C-1 and C-3 carbons and a *trans* double bond between C-4 and C-5 (Figure 8 A). The attached fatty acid components of ceramides have lengths between C14 to C30 or greater, whereby the ceramide structures modulate functions of GSLs and membrane associations [58]. The major structural and functional classifications of GSLs are based on the glycans, where the first sugar is typically a β -linked galactose or glucose. Most GSL structures are classified based on seven common tetrasaccharide neutral sugar core sequences, which can be seen in Figure 8 B. The ganglio- (predominantly in the brain), globo- (most abundant in erythrocytes), and neolacto-series (certain hematopoietic cells including leukocytes) are the quantitatively major series in vertebrates.

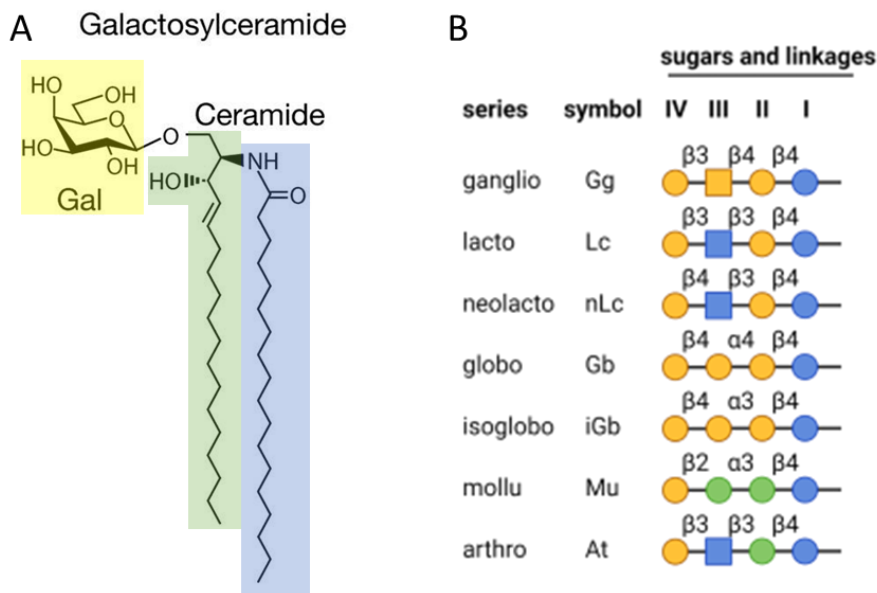


Figure 8 - Structure of GalCer and seven common tetrasaccharide neutral sugar core sequences. A Structure of GalCer. Yellow: galactose, green: fatty acid, blue: long-chain amino alcohol. **B** Sugar core sequences, names and linkages. (Created with BioRender.com)

GSLs are synthesized stepwise by the addition of the first sugar in β -linkage to ceramide and then to the growing glycans [59]. In Figure 9 can be seen the stepwise synthesis of major brain GSLs. The addition of UDP-Gal or UDP-Glc is performed by a β -galactosyltransferase or β -glucosyltransferase respectively. The extension of GlcCer with Gal-UDP by the UDP-Gal:GlcCer β 1-4 galactosyltransferase creates lactosylceramide (LacCer), which is the precursor of a variety of gangliosides. The addition of CMP-Neu5A or UDP-GalNAc is performed by several sialyltransferases or N-acetylgalactosaminyltransferase respectively.

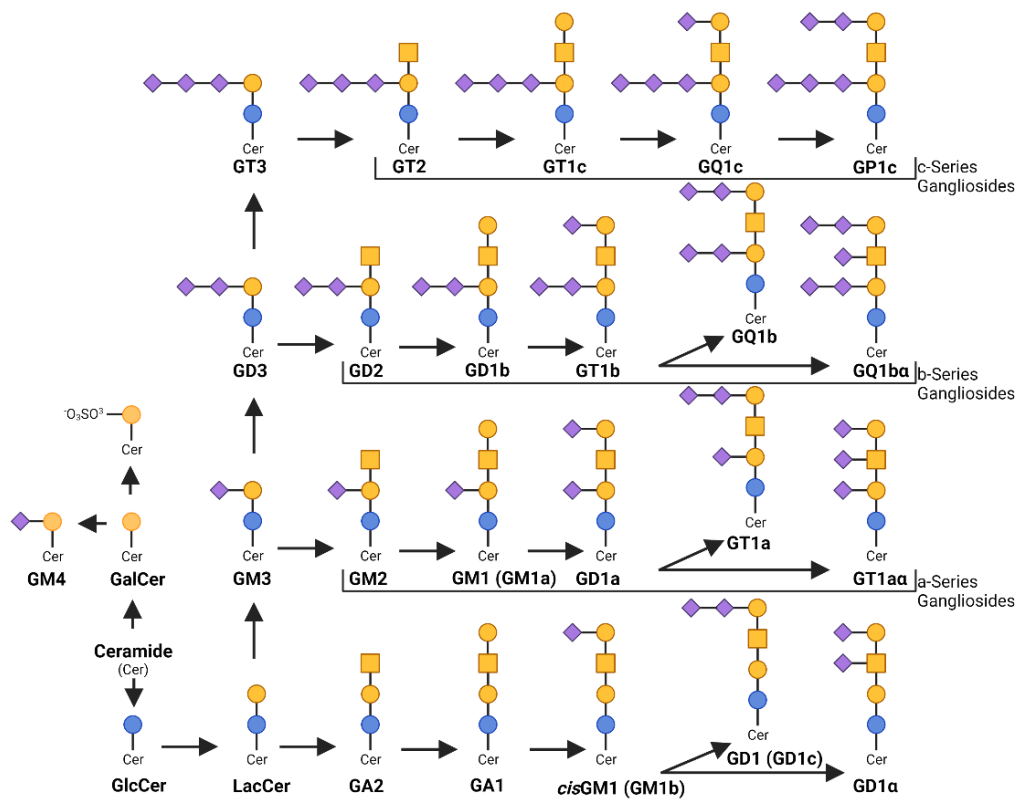


Figure 9 - Synthesis of GSLs. Major brain GSLs are shown as examples. Adapted from [31] and Created with BioRender.com.

The metabolic pathway of GSLs is embedded in the endomembrane system [60]. The synthesis is initiated in the ER. The common precursors GlcCer and GalCer are synthesized in the Golgi complex by the Golgi glycosyltransferases. GSL degradation is catabolized in lysosomes [61].

3.9 Congenital Disorders of Glycosylation (CDG)

Congenital Disorders of Glycosylation (CDG) are a group of rare inherited diseases caused by defects in the glycoconjugate biosynthesis. The genetic defects, that affect key players of protein- and lipid glycosylation are mostly monogenetic mutations, following an autosomal recessive transmission. Glycosylation of proteins or lipids is essential for numerous biological processes in the body, therefore patients affected by CDG often present with a multisystemic phenotype. This feature is the reason that many patients do not receive their diagnosis from the beginning on, which also leads to a huge number of undiagnosed CDG patients. The spectrum of symptoms is broad and comprise several dysmorphias, delocalized fat pads, strabismus, hepato-splenomegaly, enteropathy, blood coagulation abnormalities and neurological deficits like mental retardation, psychomotor retardation, epilepsy, and microcephaly. The severity ranges from almost unaffected patients over severe to premature death. In 1980 Jeaken et al. was the first pediatrician, who clinically described CDG disease [62]. He revealed a defect in the *Pmm2* gene, which is to date the most frequent CDG-syndrome with around 62 % of all CDG cases in Europe [63]. Till now more than 160 CDG diseases have been identified which cover several glycosylation pathways including N-linked, glycosaminoglycan (GAG), dystroglycanopathy, O-linked (O-mannose, O-glucose, O-fucose, O-GlcNAc, O-GalNAc) glycoposphatidylinositol (GPI) and glycolipids (see Figure 10) [64]. The nomenclature introduced in 2009 names CDG types according to the affected protein in connection with CDG. So, for example a defect in the *Pmm2* gene leads to the name PMM2-CDG [65].

Therapies for CDG-defects are rare and only available for a couple of CDG-types in which therapies with monosaccharides like mannose, fucose and galactose are performed in MPI-CDG, PGM1-CDG, GFUS-CDG, SLC35C1-CDG, SLC35A2-CDG and TMEM165 or with manganese in SLC39A8-CDG [66]–[74]. Usually, only symptoms can be treated.

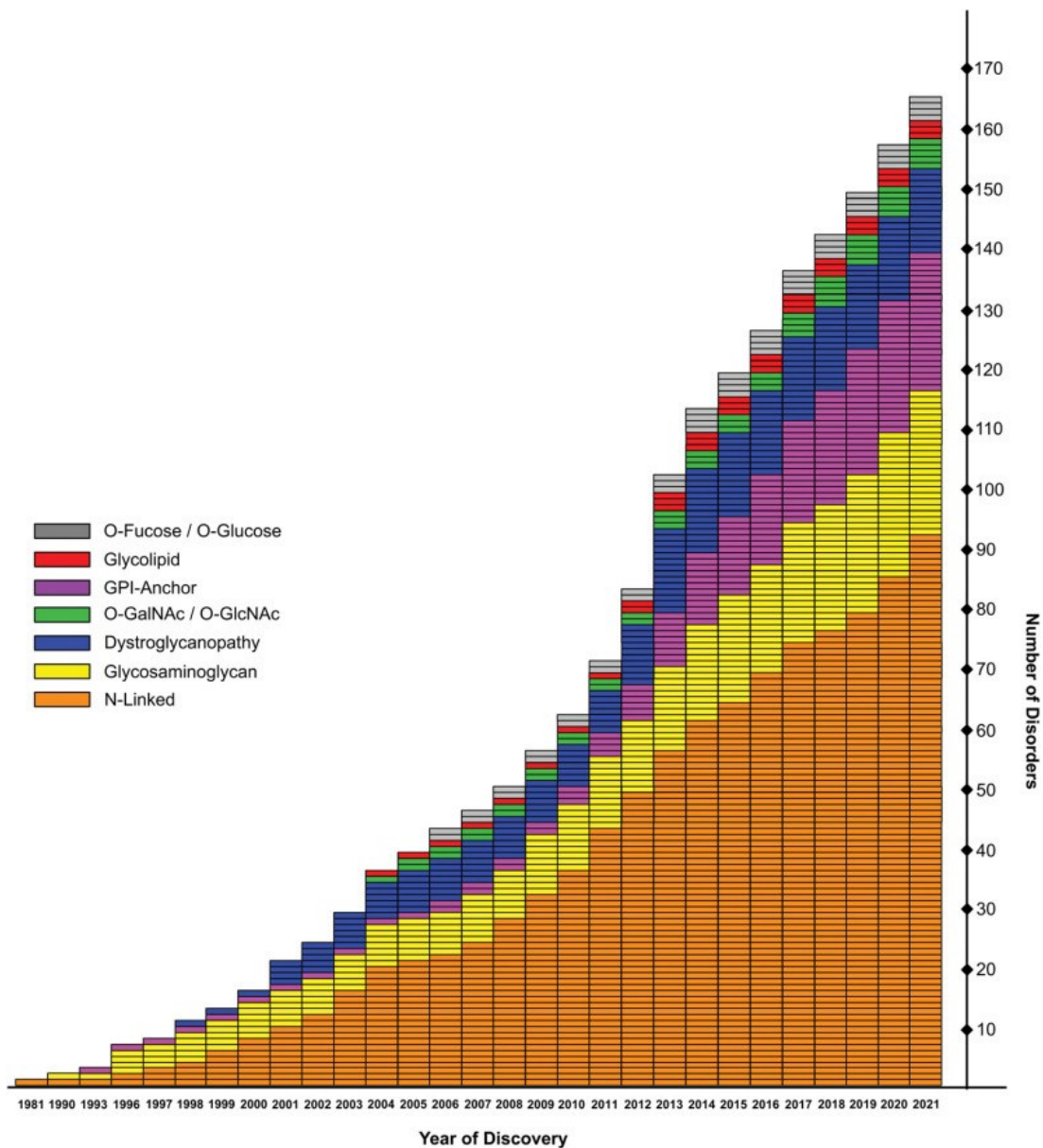


Figure 10 - Congenital Disorders of Glycosylation and their year of discovery. Overview of the discovered CDG-defects between 1981 and 2021 separated by the different types of glycosylation disorder. Taken from [64]

The routine diagnostic for N-glycosylation disorders is performed by isoelectric focusing (IEF) of serum transferrin. This glycoprotein serves as a biomarker as it has two biantennary complex type sialylated oligosaccharides which are negative charged. Two groups of N-glycosylation defects, CDG-I and CDG-II can be distinguished with this diagnostic tool [75]. CDG-I defects are early defects in the glycoconjugate synthesis until the transfer of the LLO to the polypeptide. CDG-II defects occur within the glycan processing in the Golgi apparatus. A change in in the charge of transferrin resulted from missing glycans lead to different band pattern in the IEF.

3.10 Mevalonate Kinase Deficiency / Mevalonate Aciduria

Mevalonate kinase deficiency (MDK) is a rare inherited metabolic disorder in which the mevalonate pathway is affected. It is an early-onset disease that is caused by mutations in the MVK gene coding for mevalonate kinase (MVK; E.C. 2.7.1.36) that facilitates the phosphorylation of mevalonate to mevalonate-5-phosphate (see Figure 1). The MVK gene spans over 11 exons, with a total of 10 coding exons and is located on the long arm of chromosome 12 (12q24.11, chr12[hg19] 109,573,255-109,598,125) [76]. It is a cytosolic protein with 42 kDa and 396 amino acids encoded by the transcript with a length of 2833 base pairs (ENST00000228510.8) [77].

Hoffman *et al.* made the first clinical description in the 1980s [78], [79]. Patients with pathogenic MVK variants are divided into two groups: Mevalonate kinase deficiency/ hyperimmunoglobulinemia D syndrome (MKD/HIDS, OMIM #260920) and mevalonic aciduria (MVA, OMIM #610377) [80]. They share the same genetic background of pathogenic compound heterozygous or homozygous missense MVK variants. The spectrum of symptoms includes early-onset recurrent febrile crises, often accompanied by hepatosplenomegaly, lymphadenopathy, arthralgia, and skin rashes. A full list of the clinical picture can be found in Figure 11.

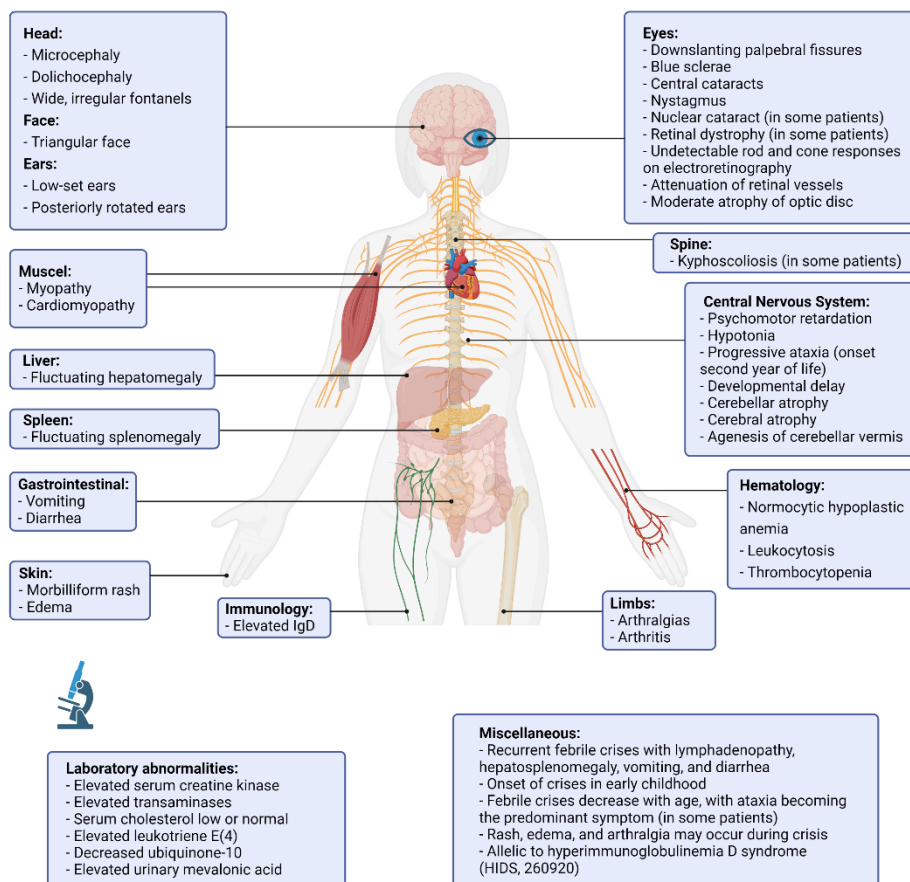


Figure 11 - Clinical synopsis of MVA/MKD. (Created with BioRender.com.)

MVA patients typically find themselves at the severe end of the phenotypic spectrum and the phenotype of HIDS patients is milder without neurological impairment [81], [82]. Around 300 patients with MKD have been identified and have been reported to literature, whereby most of them have been found in Western Europe [83], [84]. From these approximately 10 % (n=30) are classified as MVA patients [80].

As seen in other organic acidurias, episodes of metabolic decompensation are absent in MVA. Patients have a massive permanent increase of mevalonic acid excretion in urine that is also considered as pathognomonic as this leads to a hyperinflammatory state (based on in vitro data). One of the key laboratory findings is elevated urinary mevalonic acid which is also independent from febrile crisis. The gold standard analysis is stable isotope dilution chromatographic-mass spectrometric analysis [85]. MVK is like glutathione synthetase deficiency (OMIM #266130) a defect in the synthetic pathway and feedback inhibition is lacking because the final product is underproduced [86]. Other laboratory findings are high urinary excretion of leukotriene E₄ as well as high plasma concentrations of immunoglobulin A and D. The prognosis for patients with early onset multisystemic MVA is poor and half of them die in infancy or early childhood [83].

Up to date there is no established therapeutic regime for patients affected by MVA. In the past a combination treatment of Coenzyme Q₁₀ (CoQ₁₀, 5-10 mg/kg/d), vitamin C (50-60 mg/kg/d), and E (25 mg/kg/d) has shown to temporarily stabilize the disease course and even the psychomotor development was affected positively in some cases. For shortening and decreasing the febrile crisis steroids (2 mg prednisone/kg/d), Anakinra and canakinumab have been successfully used.

4 Objective and experimental outline

Inborn genetic defects in the glycoprotein biosynthesis belong to the group of Congenital disorders of glycosylation. The mevalonate kinase deficiency is a defect in the isoprenoid pathway and products, especially dolichyl phosphate, are important substrates for the glycosylation machinery. Goal of this dissertation was whether a defect in MVK would have an influence on the allocation of dolichol and would subsequently lead to a glycosylation deficiency. Up to know, no connection between MKD and CDG was made in literature. For this goal fibroblast of 11 MVK patients were used to conduct a broad range of analyses.

5 Material

5.1 Patient-derived material

Primary skin fibroblasts of 11 MVK patient were kindly provided by the University Hospital Heidelberg. Primary skin fibroblasts were obtained by skin biopsy in the course of a surgery. The study was performed in accordance with the Declaration of Helsinki. Written informed consent was obtained from the parents of the patient for performing biochemical, -genetic and cell biological analyses.

5.2 Chemicals

Table 1 - List of chemicals and respective companies.

| Chemicals | Company |
|---|-------------------------------|
| 2-mercaptoethanol | Merck, Darmstadt |
| Acetic acid, 100 %, p.a. | Roth, Karlsruhe |
| AEBSF | Sigma-Aldrich, St. Louis, USA |
| Ammonium persulfate ≥ 98 %, p.a., ACS | Roth, Karlsruhe |
| Benzamidine | Roth, Karlsruhe |
| Bromophenol blue, ACS, Reag. Ph Eur | Merck, Darmstadt |
| Calcium chloride, dehydrated, powdered, pure 95 % | Merck, Darmstadt |
| Dimethyl sulfoxide, dried | Merck, Darmstadt |
| Di-sodium hydrogen phosphate dodecahydrate | Merck, Darmstadt |
| Dodecylsulfat, Na-salt in pellets | Serva, Heidelberg |
| EDTA, ≥ 99 %, p.a., ACS | Roth, Karlsruhe |
| Ethidium bromide - solution 1 % | Applichem, Darmstadt |
| Ferric(III)-citrat | Sigma-Aldrich, St. Louis, USA |
| Formaldehyde 4 % | Merck Darmstadt |
| Glutardialdehyde | Merck Darmstadt |
| Glycerine, anhydrous | neoLab, Heidelberg |
| Glycine, ≥ 99 % | Roth, Karlsruhe |
| H ₂ O, HPLC-grade | Roth, Karlsruhe |
| Imidazole | Roth, Karlsruhe |
| Isopropanol | Roth, Karlsruhe |

Material

| | |
|---|-------------------------------|
| Potassium chloride | Merck, Darmstadt |
| Potassium dihydrogen phosphate, p.a. | Merck, Darmstadt |
| Magnesium chloride hexahydrate | Merck, Darmstadt |
| Milkpowder, blotting grade | Roth, Karlsruhe |
| Sodium acetate, crystalline, p.a. | Merck, Darmstadt |
| Sodium azide | Merck, Darmstadt |
| Sodium carbonate | Merck, Darmstadt |
| Dimethyl sulfoxide | Merck, Darmstadt |
| Di-sodium hydrogen phosphate | Roth, Karlsruhe |
| Paraformaldehyde, pure, DAC | Roth, Karlsruhe |
| Phosphoric acid, ACS reagent, ≥ 85 wt. % in H ₂ O | Sigma-Aldrich, St. Louis, USA |
| Pyridine | Sigma-Aldrich, St. Louis, USA |
| Hydrochloric acid, smoking 37 %, p.a. | Roth, Karlsruhe |
| Sucrose | Roth, Karlsruhe |
| TEMED, 99 %, p.a. | Roth, Karlsruhe |
| Trichloromethane/ chloroform, ≥ 99 %, p.a. | Roth, Karlsruhe |
| Tris-(hydroxymethyl)-aminomethane ≥ 99.9 %, p.a. | Roth, Karlsruhe |
| Triton X-100 | Serva, Heidelberg |
| Trypan Blue Solution | Fluka, Buchs, Switzerland |
| Tween 20, Ph.Eur. | Roth, Karlsruhe |
| UltraPure Agarose | ThermoFisher, Waltham, USA |
| Urea | Applichem, Darmstadt |
| Ultima Gold liquid scintillation cocktail | PerkinElmer, Waltham, USA |
| NucBlue | ThermoFisher, Waltham, USA |
| Trichloroacetic acid ≥ 99.2 % | Sigma-Aldrich, St. Louis, USA |
| HEPES ≥ 99.5 %, BioScience-Grade | Roth, Karlsruhe |
| MOPS Pufferan ≥ 99.5 % | Roth, Karlsruhe |
| Sodium chloride ≥ 99.5 %, p.a. | Roth, Karlsruhe |
| Ethanol ≥ 99.8 %, p.a. | Roth, Karlsruhe |
| Methanol ≥ 99.9 %, p.a., ACS | Roth, Karlsruhe |
| Albumin bovine Fraction V, pH 7.0 | Serva, Heidelberg |

| | |
|--------------------------------------|-------------------|
| 30 % acrylamide /0.8 % bisacrylamide | Roth, Karlsruhe |
| Rotiphorese Gel 30 (37, 5:1) | Roth, Karlsruhe |
| Servalyte pH 3-5 / pH 4.2-4.9 | Serva, Heidelberg |

5.3 Kits, standards and enzymes

Table 2 - List of kits, standards and enzymes with respective companies.

| Component | Company |
|---|--------------------------------|
| Adenosintriphosphat (ATP) | Merck, Darmstadt |
| Ampicillin (Amp.) | Calbiochem, Frankfurt |
| Bovine Serum Albumin (BSA) | Serva, Heidelberg |
| DC™ Protein Assay Kit | Bio-Rad, München |
| Dimethyl sulfoxide (DMSO) | Merck, Darmstadt |
| DNA-Loading Dye | Fermentas, St. Leon Rot |
| DNase I, RNase-free (1 U/μl) | ThermoFisher, Waltham, USA |
| dNTP Mix, 10 mM | ThermoFisher, Waltham, USA |
| DTT | ThermoFisher, Waltham, USA |
| ECL Plus Western Blotting Substrate | Pierce Biotechnology, Rockford |
| Fluoromount-G™ Mounting Medium | ThermoFisher, Waltham, USA |
| FuGENE® HD Transfection Reagent | Promega, Madison, USA |
| GeneRuler 1 kb/100 bp DNA Ladder | ThermoFisher, Waltham, USA |
| Geneticin (G418) | Life Technologies, Darmstadt |
| iScript™ Reverse Transcription Supermix | Biorad, München |
| MgCl ₂ , 25 mM | ThermoFisher, Waltham, USA |
| Omniscript RT Kit (50) | Qiagen, Hilden |
| PageRuler Prestained Protein Ladder | ThermoFisher, Waltham, USA |
| peqGOLD Gel Extraction Kit | Peqlab, Erlangen |
| peqGOLD Plasmid Miniprep Kit I | Peqlab, Erlangen |
| peqGold Xchange Plasmid Midi Kit | Peqlab, Erlangen |
| PerfeCTa® SYBR® Green FastMix® | Quantbio, Beverly, USA |
| PrimePCR | Biorad, München |
| Protease Inhibitor Mix complete | Roche, Heidelberg |
| Proteinase K | Roth, Karlsruhe |

| | |
|--|-------------------------------|
| QIAshredder | Qiagen, Hilden |
| Revert Aid First Strand cDNA Synthesis Kit | ThermoFisher, Waltham, USA |
| RiboLock RNase Inhibitor | Fermentas, St. Leon Rot |
| RIPA-buffer Pierce™ | ThermoFisher, Waltham, USA |
| RNase-Free DNase Set | Qiagen, Hilden |
| Rneasy® Mini Kit | Qiagen, Hilden |
| Sequa-brene | Sigma-Aldrich, St. Louis, USA |
| Shrimp Alkaline Phosphatase | Fermentas, St. Leon Rot |
| T4-DNA-Ligase | ThermoFisher, Waltham, USA |
| T4-DNA-Ligase 10x buffer | ThermoFisher, Waltham, USA |
| Taq DNA-Polymerase (5 U/μl) | ThermoFisher, Waltham, USA |
| Taq Puffer (10x) with potassium chloride | ThermoFisher, Waltham, USA |

5.4 Restriction enzymes and buffers

Table 3 - List of restriction enzymes, corresponding recognition sites and buffer.

| Enzyme/ buffer | Restriction site | Company |
|----------------|------------------------------|------------------------------------|
| <i>XhoI</i> | 5'-C [↓] TCGAG-3' | ThermoFisher, Waltham, USA |
| <i>NotI</i> | 5'-GC [↓] GGCCGC-3' | New England Biolabs®, Ipswich, USA |
| 10x buffer O | / | ThermoFisher, Waltham, USA |

5.5 Consumables

Table 4 - List of consumables and respective companies.

| Consumables | Company |
|--------------------------------------|------------------------------------|
| 4-, 6-, 24-well Cell culture plates | Greiner, Nürtingen |
| Blotting paper 330 g/cm ² | neoLab, Heidelberg |
| Cell culture dishes 150 mm | Sarstedt, Nümbrecht |
| Cell culture flask T25, T75, T125 | Sarstedt, Nümbrecht |
| Cell Scraper | Sarstedt, Nümbrecht |
| Cover slips No. 1 round 12 mm | Paul Marienfeld, Lauda Königshofen |
| Cryovial | Nunc, Wiesbaden |
| Dialysis membrane | Herma |

Material

| | |
|--|-----------------------------------|
| Disposable hypodermic needle Sterican (sterile), 20G, 22G, 23G | Braun, Melsungen |
| Dual-chamber cell counting slides | Bio-Rad, München |
| Erlenmeyer-flask 100 ml, 250 ml | Schott, Mainz |
| Falcon Tubes 15 ml, 50 ml | Sarstedt, Nümbrecht |
| Glass bottles, 100 ml, 250 ml, 1000 ml | Schott, Mainz |
| Hyperfilm ECL | GE Healthcare, München |
| Immersion oil 518c | Zeiss, Oberkochen |
| Leukotape classic | BSN medical, Hamburg |
| Microplate, 96-Well, flat bottom | Greiner Bio-One, Kremsmünster |
| Microscope slides with double sided frosted ends | LaborService Brenzinger, Walldorf |
| Mini-PROTEAN®TGXTM gradient Gels 4-15 % | Bio-Rad, München |
| Needle Sterican (sterile) 22G | Braun, Melsungen |
| Nitrocellulose membrane Hybond ECL | GE Healthcare, München |
| Parafilm | American National, Neenah, USA |
| Pasteur pipette | Schütt, Göttingen |
| PCR plate sealing foil | Star Lab, Hamburg |
| PCR-vials Multiply-Pro, 0.2 ml | Sarstedt, Nümbrecht |
| Pipette tips | Sarstedt, Nümbrecht |
| Plastic Petri dishes 10 cm | Sarstedt, Nümbrecht |
| Plastic pipettes, steril 5 ml, 10 ml, 25 ml | Sarstedt, Nümbrecht |
| Reaction vials 0.5 ml; 1.5 ml; 2.0 ml | Sarstedt, Nümbrecht |
| Scalpel, sterile | Braun, Melsungen |
| Single-use syringe 1 ml, 5 ml, 25 ml | Braun, Melsungen |
| Sterile filter 0.2 µm, 0.45 µm | Sartorius AG, Göttingen |
| Super Polyethylene Vial, 20 ml | PerkinElmer, Waltham, USA |
| SW-40 Polyallomer vials | Beckmann-Coulter, Brea USA |
| Thermo Fast 96-well PCR Plates | Applied Biosystems |
| Whatman-paper (3 mm) | Whatman-distribution, Göttingen |
| xCelligence RTCA E-plate 16 | ACEA Bioscience, San Diego, USA |

5.6 Equipment

Table 5 - List of used equipment and corresponding companies.

| Component | Company |
|---|-----------------------------------|
| Autoclave VX-95 | Systec, Linden |
| Balance PH204L Mettler | Mettler Toledo, Greifensee, CH |
| Balance XP56 | Mettler Toledo, Greifensee, CH |
| Binocular Stemi 2000-C | Zeiss, Jena |
| Blotting chamber PerfectBlue Semi-Dry SEDECM | Peqlab, Erlangen |
| Cell proliferation xCELLigence® RTCA DP | ACEA Biosciences, San Diego, USA |
| Cell-counter TC20 | Biorad, München |
| Centrifuge 5415D | Eppendorf, Hamburg |
| Centrifuge 5804 R | Eppendorf, Hamburg |
| Centrifuge Avanti J-26S XP | Beckman Coulter, Brea, USA |
| Centrifuge Optima TLX120 | Beckman Coulter, Brea, USA |
| Centrifuge Rotina 48 R | Hettich, Tuttlingen, |
| CO ₂ Incubator MCO-20AIC | Sanyo, Loughborough, UK |
| Dishwasher G7883CD | Miele, Gütersloh |
| Dounce homogenizer | Roth, Karlsruhe |
| Electrophoresis chamber (EtBr) self-made | Universitätsklinikum, Heidelberg |
| Electrophoresis chamber (SDS) Mini-PROTEAN 3 Cell | Biorad, München |
| Freezer, diverse -20 °C | Liebherr Bulle, CH |
| Freezer, diverse -80 °C | Liebherr Bulle, CH |
| GeneAmp® PCR-System 2700 | Applied Biosystems, Waltham, USA |
| Icemachine | Ziegra, Isernhagen |
| Incubator MCO-20A/C | Panasonic Biomedical, Kadoma, JPN |
| Magnetic stirrer MR 3001 | Heidolph, Schwabach |
| Mastercycler GeneAmpPCR System 2700 | Applied Biosystems, Waltham, USA |
| Microwave R-233 (W) | Sharp, Osaka, Japan |
| Milipore GenPure Pro UV-TOC/UF | ThermoFisher, Waltham, USA |
| NanoDrop™ Lite Spectrophotometer | ThermoFisher, Waltham, USA |
| nCounter® SPRINT profiler | Nanostring, Seattle, USA |

| | |
|--|-------------------------------------|
| pH-Meter inoLab pH Level 1 | WTW, Weilheim |
| Photometer Spectra max Plus 384 | Molecular Devices, Sunnyvale, USA |
| Pipettes | Eppendorf Hamburg |
| Power supplies for electrophoresis E835 | Consort, Turnhout, BEL |
| Power supplies for electrophoresis EPS601 | Bioscience, Amersham, UK |
| Quattro Ultima triple quadrupole mass spectrometer | Micromass, Manchester, UK |
| Real-Time PCR System StepOnePlus | Applied Biosystems, Waltham, USA |
| Refrigerated centrifuge Biofuge fresco | Heraeus, Hanau |
| Refrigerator, diverse 4 °C | Liebherr Bulle, Schweiz |
| Rocker Rocky 1100 | Labortechnik Fröbe, Lindau |
| Rotorhead SW 40 Ti | Beckman Coulter, Brea, USA |
| Rotorhead TLA100.3 | Beckman Coulter, Brea, USA |
| Rotorhead Type 45 Ti | Beckman Coulter, Brea, USA |
| Safety workbench class 2 SterilGard III Advance | The Baker Company, Sanford, USA |
| Shaking incubator HTMR-133 HLC Haep | Labor Consult, Bovenden |
| Shaking incubator Thermomixer | Eppendorf, Hamburg |
| Tabletop centrifuge Biofuge Pico | ThermoFisher, Waltham, USA |
| Tri-Carb 2800TR liquid scintillation analyzer | PerkinElmer, Waltham, USA |
| Ultrasonic bath Sonorex Super RK 255 H | Brandelin, Berlin |
| UV-hand lamp VL-4.LC | Vilber, Eberhardzell |
| UV-Transilluminator CN-TFX | Vilber, Eberhardzell |
| Vortexer Vortex-Genie 2 | Scientific Industries, Bohemia, USA |
| Water bath1092 | GFL, Burgwedel |
| Westernblot documentation Fusion SL4 | Peqlab, Erlangen |

5.7 Buffer, solutions and cell-culture media

Table 6 - List of buffer/solutions and their components.

| Buffer /Solution | Components |
|---|--|
| Blocking solution for WB (antibodies) | 5 % (w/v) BSA or milk powder 0.1 % (v/v) Tween-20 in 1x PBS |
| Blocking solution for WB (lectins) | 0.5 % (v/v) Tween-20 in 1x TBS |
| Hanks buffer | 8 g/l NaCl 0.4 g/l KCl 0.06 g/l KH_2PO_4 0.35 g/l NaHCO_3 1 g/l glucose pH 7.4 |
| Upper phase (+) buffer | 48 % methanol 47 % H_2O 3 % chloroform 1 M MgCl_2 |
| Upper phase (-) buffer | 48 % methanol 47 % H_2O 3 % chloroform |
| DNA-electrophoresis loading-buffer (6x) | 40 % saccharose (w/v) 0.25 % bromophenol blue (w/v) |
| Lysis buffer | 50 mM EDTA 50 mM NaCl 100 mM SDS 0.5 % (w/v) Tris/HCl pH 8.0 |

Material

| | |
|---------------------------------------|--|
| PBS buffer | 8.0 g/l NaCl 11.5 g/l Na ₂ HPO ₄ 0.2 g/l KCl 0.2 g/l KH ₂ PO ₄ Tris/HCl pH 7.4 |
| PBST-buffer | PBS-Puffer + 0,1 % Tween 20 (v/v) Tris/HCl pH 7,4 |
| PFA-solution | 4 % paraformaldehyde (w/v) 8,0 g/l NaCl 11,5 g/l Na ₂ HPO ₄ 0,2 g/l KCl 0,2 g/l KH ₂ PO ₄ Tris/HCl pH 8,0 |
| Mowiol | 6,0 g glycerin 2,4 g Mowiol 4-88 6,0 ml H ₂ O 0,2 M Tris/HCl pH 8,5 |
| Pierce™ RIPA buffer | 25 mM TRIS HCl pH 7.6 150 mM NaCl 1 % NP-40 1 % sodium deoxycholate 0.1 % sodium dodecyl sulfate |
| SDS-PAGE electrophoresis buffer (10x) | 151,1 g Tris 50 g SDS 720 g glycine |

Material

| | |
|------------------------------|---|
| SDS-PAGE loading buffer (6x) | 12 % SDS (w/v) 45 % glycerin (v/v) 12 % β -mercaptoethanol (v/v) 0,06 % Bromophenol blue (w/v) 480 mM Tris/HCl pH 6,8 |
| SDS-PAGE stacking gel buffer | 0,4 % SDS (w/v) 0,5 M Tris/HCl pH 8,8 |
| SDS-PAGE separation buffer | 0,4 % SDS (w/v) 1,5 M Tris/HCl pH 6,8 |
| Semidry-Blot anode buffer | 20 % methanol (v/v) 75 mM Tris/HCl pH 7,4 |
| Semidry-Blot cathode buffer | 40 mM 2-Aminocaproic acid 20 % methanol (v/v) 75 mM Tris/HCl pH 9,0 |
| TBS | 8 g/l NaCl 0.2 g/l KCl 3 g/l Tris/HCl pH8.0 |
| TBST | TBS (1x) 0.1/0.5 % Tween 20 (v/v) Tris/HCl pH 7.4 |

5.8 Oligonucleotides

All used oligonucleotides (Primer) were synthesized from Invitrogen (Karlsruhe) and Seqlab-Microsynth GmbH (Göttingen).

Table 7 - List of used oligonucleotides with application and sequence.

| Oligonucleotide | Application | Sequence (5'-3') |
|-------------------------|-------------|---|
| hMVK_F1 | cloning | gcaggattcccaggagccAT |
| hMVK_F2 | cloning | gccATGTTGTCAGAAGTCCTAC |
| hMVK_R1 | cloning | gactgcagagcttgctggc |
| hMVK_R2 | cloning | ctgcagtgtcgtgggctcc |
| hMVK_XhoI_ATG_F | cloning | TAAGCActcgagGCCACCATGTTGTC AGAAGTCCTACTGGTG |
| hMVK_-stop_MYC_NotI_R | cloning | TGCTTAgcggccgcTCACAGATCCTCT TCTGAGATGAGTTTTTGTTCgctgcc gccgccgccGAGGCCATCCAGGGCTT |
| hMVK_F3 | sequencing | GGGATTGCGTCAACAGGTGG |
| hMVK_R3 | sequencing | CTTGATGGTATCGGAGGGCTCC |
| hMVK_F4 | sequencing | GCGTCAGAAACAGGCTGCTC |
| hMVK_R4 | sequencing | GTAAAGAAAGGCCAGCACAGCC |
| hMVK_qPCR_F | RT-qPCR | TTCCCAGGAGCCATGTTGTC |
| hMVK_qPCR_R | RT-qPCR | TACAGCCAGTGCTACCTTGC |
| hHMGCRC_qPCR_F | RT-qPCR | CCGCGACTGCGTAACTGG |
| hHMGCRC_qPCR_R | RT-qPCR | CAGAATCCTTGGATCCTCCAGA |
| hPMVK_qPCR_F | RT-qPCR | GAAGGACATGATCCGCTGGG |
| hPMVK_qPCR_R | RT-qPCR | TGTCACTCACCAGCCAGATG |
| h β -Actin_qPCR_F | RT-qPCR | agagctacgagctgcctgac |
| h β -Actin_qPCR_R | RT-qPCR | agcactgtgtggcgtacag |

5.9 Radioactive compounds

Table 8 - List of radioactive compounds

| Radioactive compound | Company |
|----------------------------------|--------------------------------|
| D-[2- ³ H(N)]-Mannose | Perkin Elmer, Rodgau-Jügesheim |

5.10 Antibodies, lectins and streptavidin-conjugate

For western blotting applications primary antibodies from different species were diluted in PBST 0.1 % according to the manufacturer's recommendation. Secondary HRP-conjugated antibodies were diluted 1:10,000 in PBST 0.1 %.

5.10.1 Primary antibodies (1:1,000 in western blot; 1:400 in immunofluorescence)

Table 9 - List of primary antibodies

| Primary antibody | Host | Dilution | Company |
|-------------------------|-------------|-----------------|------------------------------------|
| Anti human ALG10 | rabbit | 1:1,000 | ThermoFisher, Waltham, USA |
| Anti human ALG12 | rabbit | 1:1,000 | Abcam, Cambridge, UK |
| Anti human ALG13 | rabbit | 1:1,000 | Sigma-Aldrich, St. Louis, USA |
| Anti human ALG5 | rabbit | 1:1,000 | Proteintech, Manchester, UK |
| Anti human ALG9 | rabbit | 1:1,000 | Aviva Systems Bio., San Diego, USA |
| Anti human beta-actin | mouse | 1:1,000 | Sigma-Aldrich, St. Louis, USA |
| Anti human DHDDS | rabbit | 1:1,000 | Proteintech, Manchester, UK |
| Anti human DPAGT1 | rabbit | 1:1,000 | ThermoFisher, Waltham, USA |
| Anti human DPY19L1 | rabbit | 1:1,000 | Novus Biological, Colorado, USA |
| Anti human DPY19L3 | rabbit | 1:1,000 | ThermoFisher, Waltham, USA |
| Anti human FUT8 | mouse | 1:500 | Proteintech, Manchester, UK |
| Anti human FUT9 | mouse | 1:1,500 | Proteintech, Manchester, UK |
| Anti human GALE | rabbit | 1:1,000 | Proteintech, Manchester, UK |
| Anti human GMPPA | rabbit | 1:1,000 | Proteintech, Manchester, UK |
| Anti human ICAM1 | rabbit | 1:1,000 | Sigma-Aldrich, St. Louis, USA |
| Anti human LAMP1 | rabbit | 1:1,000 | Abcam, Cambridge, UK |
| Anti human LAMP2 | mouse | 1:1,000 | ThermoFisher, Waltham, USA |
| Anti human MAN1A1 | rabbit | 1:1,000 | Abcam, Cambridge, UK |
| Anti human MAN1B1 | mouse | 1:1,000 | Novus Biological, Colorado, USA |
| Anti human MAN2A1 | rabbit | 1:1,000 | Santa Cruz, Dallasm USA |
| Anti human MGAT2 | rabbit | 1:1,000 | Proteintech, Manchester, UK |
| Anti human MVK | rabbit | 1:1,000 | Proteintech, Manchester, UK |
| Anti human OGT | rabbit | 1:1,000 | Proteintech, Manchester, UK |
| Anti human PGM2 | rabbit | 1:1,000 | Proteintech, Manchester, UK |
| Anti human PMM2 | rabbit | 1:1,000 | Proteintech, Manchester, UK |

Material

| | | | |
|--------------------|--------|---------|------------------------------------|
| Anti human PMM2 | mouse | 1:400 | Abnova, Taipei City, TWN |
| Anti human POMT2 | rabbit | 1:1,000 | ThermoFisher, Waltham, USA |
| Anti human SLC35C1 | rabbit | 1:1,000 | Sigma-Aldrich, St. Louis, USA |
| Anti human SRD5A3 | rabbit | 1:1,000 | Novus Biological, Colorado, USA |
| Anti MYC-tag | rabbit | 1:1,000 | Cell Signaling Tec., Cambridge, UK |

5.10.2 Secondary antibodies (1:10,000 in western blot; 1:700 in immunofluorescence)

Table 10 - List of secondary antibodies

| Secondary antibody | Host | Modification | Company |
|--------------------|------|-----------------|--|
| Anti-mouse | goat | HRP coupled | Santa Cruz Biotechnology, Heidelberg, DE |
| Anti-rabbit | goat | HRP coupled | Dianova, Hamburg, DE |
| Anti-rabbit | goat | Alexa Fluor 488 | ThermoFisher, Waltham, USA |
| Anti-mouse | Goat | Alexa Fluor 568 | ThermoFisher, Waltham, USA |
| Streptavidin | | HRP coupled | ThermoFisher, Waltham, USA |

5.10.3 Lectins and streptavidin-HRP-conjugates

All Lectins and HRP-streptavidin conjugates were obtained from Vector Laboratories (Burlingham, USA). Lectins for WB application were biotinylated and diluted 1:500 in TBST 0.1 %. Streptavidin-HRP-conjugates were diluted 1:10,000 in TBST 0.1 %.

Table 11 - List of lectins and their specificity

| Lectins | Abbr. | Modification | specificity |
|---|-------|--------------|--|
| <i>Aleuria aurantia</i> | AAL | biotinylated | α 1-2, α 1-3, α 1-4 and α 1-6 fucose |
| <i>Concanavalin A</i> | ConA | biotinylated | α -mannose, α -glucose |
| <i>Narcissus pseudonarcissus</i> | NPA | biotinylated | α -mannose |
| <i>Galanthus nivalis</i> | GNA | biotinylated | α 1-3 and α 1-6 mannose |
| <i>Lens culinaris</i> | LCH | biotinylated | α -mannose, α -glucose |
| <i>Phaseolus Vulgaris Leucoagglutinin</i> | PHA-L | biotinylated | β 1-2-mannose-GlcNAc |

Material

| | | | |
|--|------|--------------|--|
| <i>Datura stramonium</i> | DSL | biotinylated | β 1-6-mannose-GlcNAc, β 1-2-mannose-GlcNAc, GlcNAc |
| <i>Erythrina Cristagalli</i> | ECL | biotinylated | galactosyl(β -1-4)GalNAc |
| <i>Maackia amurensis</i> <i>Leukoagglutinin I</i> | MALI | biotinylated | Neu5Ac/Gca2-3Gal β 1-4GlcNAc β 1-R |
| <i>Sambucus Nigra</i> | SNA | biotinylated | Neu5Ac α 2-6GalNAc-R |
| <i>Wheat Germ</i> <i>Agglutinin</i> | WGA | biotinylated | GlcNAc, Neu5Ac |

5.11 Plasmids

Vector maps of listed plasmids can be found in the appendix section 10.2.

Table 12 - List of plasmids

| Plasmids | Company |
|-------------|----------------------------|
| pGEM-T Easy | Promega, Walldorf |
| pLNCX2 | Takara, Mountain View, USA |

5.12 Bacterial strains for plasmid transformation

Table 13 - List of bacterial strains

| Strain | Genotype |
|------------------------------|--|
| <i>E. coli</i> XL1-Blue | F- Tn10 proA+B+ lacI Δ (lacZ)M15/recAI endAI gyrA96(Nal) thi hsdR17 (rK-mk+) supE44 relAI lac |
| <i>E. coli</i> DH5- α | F- deoR recAI endAI hsdR1(rk-mk+) supE44 1-thi gyrA96 relAI |

5.13 Culture media and plates for bacteria

Table 14 - List of culture media and plates for bacteria

| Medium/ Plates | Components |
|----------------|---|
| LB-media | 1 % (w/v) Trypton/Pepton 1 % (v/v) NaCl 0.5 % (w/v) yeast extract |
| LB-Amp | LB-media 50 µg/ml ampicillin |
| LB-Amp plates | LB-Amp 1.5 % Agar |

5.14 Culture media and solutions for mammalian cells

Table 15 - List of culture media and solutions for mammalian cells

| Medium | Components |
|----------------------------|--|
| Normal cell culture medium | DMEM (high glucose 4.5 g/L) 10 % FCS (heat-inactivated) 1 % Penicillin /Streptomycin (10,000 U/ml) 1 % Fungizone Amphotericin B (250 µg/ml) |
| Selection medium | Normal cell culture medium 250 µg/ml Geneticin /Neomycin |
| Stable medium | Normal cell culture medium 25 µg/ml Geneticin /Neomycin |
| Cryo conservation medium | Normal cell culture medium 10 % DMSO |

Material

| | |
|---------------------|--|
| Hunger Medium | DMEM without glucose, glutamine, phenol red and pyruvate 10 % FCS 0.5 mM Glucose 2 mM L-Glutamine 1 % Penicillin /Streptomycin (10,000 U/ml) |
| Labeling Medium | DMEM without glucose, glutamine, phenol red and pyruvate 0.5 % dialyzed FCS 0.5 mM Glucose 2 mM L-Glutamine 20 μ Ci/ml 2-[³ H]-mannose |
| Trypsin-EDTA 0.25 % | 1X |
| DPBS | 1X |
| OPTI-MEM® | 1X |

5.15 Cell-lines

Primary fibroblasts were obtained by skin-biopsy. Besides the patient cell lines, the control cell lines N21, HDF and PCS were used. All cell lines were stored at -80 °C in liquid nitrogen and revitalized for cell culture.

Table 16 - List of cell lines

| Cell line | Characteristics |
|-------------------|---|
| N21 | Control-fibroblast cell line derived from primary foreskin-fibroblasts by skin-biopsy. |
| HDF (c12300) | Commercially available (PromoCell) Control-fibroblast cell line derived from primary human juvenile foreskin fibroblasts. |
| PCS (PCS-201-010) | Commercially available (ATCC) Control-fibroblast cell line derived from primary human foreskin fibroblasts. |
| Phoenix-eco | Retroviral packaging cell line derived from HEK 293T cells which was transformed with adenovirus E1a for subsequent generation of ecotropic and amphotropic retroviruses. |
| PT67 | Retroviral packaging cell line derived from NIH 3T3-cells which were transformed with Moloney murine leukemia virus. Designed to produce infectious, replication-incompetent virus. |

5.16 Software, databanks and computer-aided resources

5.16.1 Software

Table 17 - List of software

| Name | Company |
|------------------------|-----------------------------|
| ApE | M. Wayne Davis |
| BioRender | biorender.com |
| CFX Manager | Bio-Rad Laboratories, Inc. |
| Chromas 2 | Technelysium |
| GraphPad PRISM 9 | GraphPad Software, Inc. Ape |
| ImageJ | Wayne Rasband (NIH) |
| Mendeley | Elsevier Inc. |
| nSolver 4.0 | NanoString Technologies |
| Office | Microsoft |
| RTCA operator software | ACEA |

5.16.2 Databanks

Table 18 - List of databanks

| Name | Website |
|-------------|------------------|
| Ensembl | ensembl.org |
| NCBI | ncbi.nlm.nih.gov |
| OMIM | Omim.org |
| UniProt | uniprot.org |

5.16.3 Computer-aided resources and tools

Table 19 - List of computer-aided resources and tools

| Name | Website |
|-----------------------|--------------------------------------|
| CBS prediction Server | cbs.dtu.dk/services/ |
| Clustal Omega | ebi.ac.uk/Tools/msa/clustalo/ |
| dbNSFP database v4.2A | sites.google.com/site/jpopgen/dbNSFP |
| DynaMut | biosig.unimelb.edu.au/dynamut |
| NCBI Blast | blast.ncbi.nlm.nih.gov/Blast.cgi |

6 Methods

6.1 Mammalian cell culture

6.1.1 Cultivation of mammalian cells

All cell lines used were adherent cells (Table 16). Cell cultivation was performed in either T25, T75 or T175-cell culture flasks using DMEM cell culture medium (high glucose 4.5 g/l) supplemented with 10 % FCS, 1 % penicillin / streptomycin and 1 % amphotericin B. Standard culturing conditions were 37 °C and 5 % CO₂. The medium was changed at least once a week to provide nutrients and remove dead cells.

6.1.2 Thawing and revitalization of cells

All cell-lines were stored in liquid nitrogen. For revitalization and subsequent culturing, cryo-vials were taken out and slightly opened up to release pressure. The outside of the vials was disinfected and thawed at RT under a sterile bench. 500 µl of prewarmed (37 °C) DMEM cell culture medium was added to the vial to transfer the cells into a prepared T25 cell culture flask already containing 5 ml of prewarmed cell culture medium. Residual cells inside the vial were flushed with 500 µl medium and transferred to the cell culture flask. The cell growth and health were visually checked after 24 hours, cells were washed with DPBS and medium was changed to remove remaining DMSO.

6.1.3 Trypsinization and cell harvest

Cells were grown until they were confluent and then passaged. For a T75 flask, cell culture medium was removed, and cells were washed with 5 ml prewarmed (37°C) DPBS. Detachment of the adherent cells was performed by addition of 2 ml Trypsin-EDTA 0.25 % and a five-minute incubation at 37 °C and 5 % CO₂. The reaction was stopped by addition of 8 ml prewarmed DMEM medium. Cell aggregates were separated by gentle pipetting and the cell suspension was seeded into new cell culture flasks with prewarmed DMEM medium to a final volume of 10 ml. In general, cells were splitted 1:2 to 1:5.

To collect cell material for biochemical, genetic and cell biological analyses, cells were grown to 80 – 90 % confluency and then harvested by scraping. For this, medium was removed, and cells were washed with DPBS (unsterile). Also, the cells were detached in DPBS with a cell scraper. The cell-suspension was transferred into a 15 ml Falcon-tube and centrifuged at 2,000 rpm for 5 min. The supernatant was removed and the tube containing the cell pellet was flash frozen in liquid nitrogen. Pellets were stored at -80 °C until further analysis.

6.1.4 Cell count

The cell count was determined with an automated *Cell Counter T20* of BioRad. Cells were incubated with Trypsin-EDTA and resuspended in 7 or 10 ml cell medium. 10 µl of the suspension was mixed with 10 µl trypan blue and filled into the counting chamber. The count was performed automated.

6.1.5 Cryo conservation of cells

Cells grown in a T75 cell culture flask were detached with trypsin like described before. The cell suspension was centrifuged at 2,000 rpm for 5 min and the cell pellet was resuspended in 3 ml ice cold cryo conservation medium containing 10 % DMSO. Aliquots of 1 ml cell suspension were transferred into cryo vials and frozen at -20 °C for 12 hours. Afterwards, the cryo-vials were stored in -80 °C for short-term or in liquid nitrogen for long-term.

6.1.6 Investigation of cell proliferation

The *xCELLigence® Real-Time Cell Analyzer* (ACEA Bioscience, USA) was used to investigate the proliferation status of patient- and control-fibroblasts. The corresponding protocol was used, and the specific growth rate and doubling time was determined. The principle of the proliferation measurement is based on impedance. Cells grow in a well which is equipped with gold microelectrodes fused to its bottom. After application of an electric potential, electrons migrate from the negative electrodes to the positive electrodes through the conductive growth media. The electron flow is impeded by cells growing in the media or covering the electrode surface. The measured impedance is reported as the unitless parameter cellindex (CI) and corresponds to the number of cells in the well.

First, the 16-well E-plate and *the xCELLigence® RTCA DP-instrument* were prepared. 100 µl of normal DMEM-cell culture medium was added to each well and incubated at RT for equilibration. To measure the background impedance for each well, the E-plate was inserted into the RTCA-instrument inside the incubator. Patient- and control-fibroblasts were harvested by trypsinization and the viable cell-concentration inside the suspension was determined by trypan-blue staining using the *Cell-Counter TC20* (Biorad). The cell suspensions were adjusted with cell culture medium to obtain 1000 or 2000 cells per well which were seeded in duplicates into the E-plate. Prior to insertion of the E-plate into the RTCA-instrument, a 30-minute incubation at RT was carried out to ensure homogenous distribution of the cells inside the wells. The RTCA-instrument containing the E-plate was incubated at 37 °C and 5 % CO₂. The impedance for each well was measured automatically over a period of 200 hours in intervals of 30 minutes. The impedance was converted into the CI and recorded via a computer with *xCelligence*

RTCA operator software. To ensure constant conditions during the measurements, the incubator remained closed for the whole experiment period.

For the evaluation of the results the CI was plotted against the time. The resulting growth curves were used to determine the exponential growth phase (log-phase) of the cells. An exponential fit was applied to the data in the log-phase including CI (y), starting CI (A), specific growth rate (k) and time (x). An example is shown in Figure 12. The exponential equation of the fit was used to derive growth parameters as follows:

$$y = A \cdot e^{kx}$$

Rearranging of the equation yields:

$$x = \frac{\ln \frac{y}{A}}{k} \quad y = 1 \quad x_1 = \frac{\ln \frac{1}{A}}{k} \quad y = 2 \quad x_2 = \frac{\ln \frac{2}{A}}{k}$$

As the doubling time T_d is the difference between x_1 and x_2 it can be postulated:

$$T_d = \left(\frac{\ln \frac{2}{A}}{k} \right) - \left(\frac{\ln \frac{1}{A}}{k} \right) = \left(\frac{\ln(2) - \ln(A)}{k} \right) - \left(\frac{\ln(1) - \ln(A)}{k} \right)$$

$$T_d = \frac{\ln(2)}{k} - \frac{\ln(A)}{k} - \left(-\frac{\ln(A)}{k} \right) = \frac{\ln(2)}{k}$$

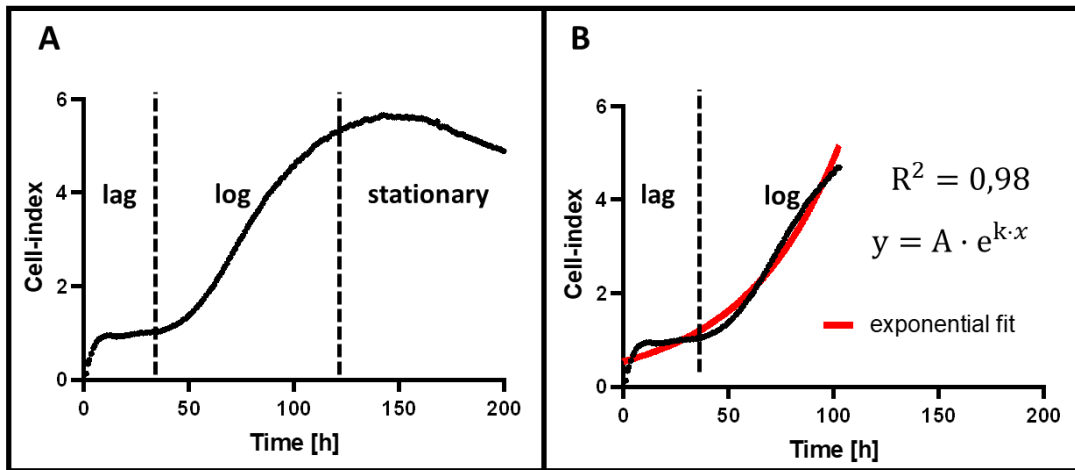


Figure 12 - Growth curve example determined by RTCA and exponential fit of the log-phase. (A) Blotted cell-index over a time period of 200 hours. The resulting growth curve can be divided into lag-, log- and stationary-phase. (B) The log-phase is estimated by an exponential fit (red line). The correlation of the fit with the data points is given by R^2 . Data displays growth curve of control.

Doubling time (T_d) and specific growth rate (k) were determined for each well. Mean and standard deviation for each cell number condition of control and patients were calculated.

6.1.7 Immunofluorescent staining of human fibroblasts

The staining was performed in a 24-well plate. Round glass cover-slips were placed in the wells and 30,000 fibroblasts were seeded one day before analysis. All steps were performed at RT. All solutions were diluted in DPBS buffer, if not stated differently. At first, the medium was removed from the wells and the adherent cells were washed 3x with PBS. Then, cells were fixed with 4 % PFA solution for 20 min. Permeabilization was performed with 0.5 % Triton X-100 for 10 min. To block unspecific antibody binding, cells were incubated in 5 % BSA solution. Primary antibodies were diluted 1:200 in 1 % BSA and incubated at 37 °C for one hour. After three washing steps with DPBS the secondary antibody coupled with a fluorophore (1:700 dilution in 1% BSA) was incubated for 30 min at 37 °C. After three washing steps the nucleus was stained by NucBlue. The cover-slips with stained cells were then mounted on a glass slide with Fluoromount™.

6.1.8 Lipid Oil red O analysis

To analyze the lipid droplets (LDs) in fibroblast, control and patient cells were stained with the Lipid (Oil Red O) Staining Kit (Sigma-Aldrich). Cells were seeded into a 24-well plate (3.5×10^4 cells/well) one day prior staining. Fixation with 10 % Formalin and staining with Hematoxylin was performed according to the manufacturer. Pictures were taken under a light microscope at 20x magnification whereby LDs appeared red and nuclei appeared blue. For quantification, the stain was extracted with isopropanol and extracted solutions were measured at 492 nm in a plate reader.

6.2 Biochemical methods

6.2.1 Protein preparation from fibroblasts

Cell pellets of fibroblasts were obtained as mentioned in section 6.1.3. All steps were performed on ice. Pellets were resuspended in 100 µl ice cold RIPA-buffer containing 1X protease inhibitor mix and transferred into a 1,5 ml tube. The solution was incubated for 30 minutes on ice. Afterwards, for cell disruption the sample was passed 20 times through a ø22G needle with a 1 ml syringe. The homogenized solution was centrifuged at 13,000 rpm and 4 °C for 30 minutes to remove cell debris. The supernatant was transferred into a new 1.5 ml tube and stored at -20 °C for short-term or at -80 °C for long-term.

6.2.2 Determination of protein concentration with Lowry-assay

The DC™ Protein Assay Kit was used to determine the protein concentration in cell-lysate, which is based on a modified Lowry assay [87]. BSA diluted in the same buffer system as the sample was used as a standard. The standard curve was generated with eight different BSA concentrations ranging from 0 to 2 mg/ml. Protein concentration of

an unknown sample was derived from calibration with a protein standard curve via absorbance at 750 nm. For the measurement, the instructions in the provided protocol were followed. Every sample was measured in duplicates. Absorbance was measured at 750 nm. The protein concentration of the sample was calculated from absorbance of the sample with the slope and y-intercept of the standard curve.

6.2.3 SDS-PAGE

Sodium dodecyl sulfate polyacrylamide gel electrophoresis (SDS-PAGE) was performed for the electrophoretic separation of proteins by their molecular weight [88]. Gels with separation- and stacking-zone were self-casted with mini protean tetra cell system from Bio-rad. For some applications precast Mini-PROTEAN®TGXTM gradient Gels (4-15 % acrylamide) were obtained from Bio-Rad.

Separation gels with an area of 46 cm² were prepared with either 10 % or 12.5 % polyacrylamide, HPLC water, separation gel buffer, TEMED and APS. The gel-mixture was transferred in a gel casting form and layered with isopropanol for smoothing the border, resulting in a 5.6 mm high stacking-gel. After polymerization of the separation gel, isopropanol was removed with Whatman-paper, and the stacking gel was casted on top. Depending on the number of samples a 10-well- or 15-well-comb was inserted. The gel was used directly after polymerization or was stored in wet tissues at 4 °C for few a days. Table 20 shows the mixture of each gel. Composition of separation- and stacking-gel-buffers can be found in the material section in Table 6.

Table 20 - Composition of polyacrylamide gels for SDS-PAGE

| Component | Separation gel | | Stacking gel |
|---------------------------------|----------------|-----------|--------------|
| | 10 % PA | 12,5 % PA | |
| 30 % polyacrylamide | 2010 µl | 2505 µl | 338 µl |
| Separation-/ stacking-buffer | 1500 µl | 1500 µl | 338 µl |
| 10 % APS in H ₂ O | 60 µl | 60 µl | 30 µl |
| TEMED | 6 µl | 6 µl | 3 µl |
| H ₂ O | 2475 µl | 1965 µl | 1500 µl |

Two gels were placed in the electrophoresis chamber and combs were removed. The buffer tank and the space between the gels was filled with 1X SDS-PAGE electrophoresis-buffer. The sample pockets of the gel were rinsed to remove gel-residuals.

To prepare samples for the electrophoretic separation, equal amounts of protein from cell lysate were diluted in H₂O and SDS-PAGE loading buffer (1x) to a protein concentration of 0.5 µg/µl. The samples were then incubated for 5 minutes at 95 °C. After preparation, 20 µl of each protein sample was loaded into the gel pockets. One lane was loaded with 10 µl of PageRuler prestained Protein Ladder. Electrophoretic separation of the proteins was carried out at 100 V for 10 minutes followed by 150 V till the running front reached the end of the SDS-PAGE gel.

6.2.4 Western- and lectin blotting

The separated proteins were transferred to a nitrocellulose membrane for further detection with antibodies or lectins. Transfer was carried out by semi-dry-blotting. Three pieces of 1 mm Whatman-paper cut to the size of the separation gel were soaked in anode buffer and another three in cathode buffer. Composition of the buffers can be found in the material section (Table 6). Papers soaked in anode buffer were stacked on the anode and a nitrocellulose membrane of the same size previously incubated in anode buffer was layered on top. After electrophoresis, the stacking gel was carefully removed. The separation gel was transferred into cathode buffer and precisely positioned on the nitrocellulose on top of the stack. Three Whatman-papers soaked in cathode buffer were layered above the gel and the cathode plate was positioned on top of the stack. Protein transfer was performed at 1 mA/cm² for 45 minutes. By applying an electric current, proteins coated in negatively charged SDS migrate out of the polyacrylamide gel to the direction of the anode and thus are transferred to the nitrocellulose membrane.

6.2.5 Protein detection via chemiluminescence

To detect specific proteins and glycan structures on the nitrocellulose membrane, primary antibodies and biotinylated lectins were utilized. The solutions for washing and blocking of the membrane differ according to application of lectins or primary antibodies. For detection with a primary antibody, blocking was carried out with 5 % BSA in PBST 0.1 % and washing with PBST 0.1 %. For lectin applications the membrane was blocked with 0.5 % TBST and washed with TBST 0.1 % (see Table 6).

In the first step membranes were incubated in the corresponding blocking solutions for one hour while shaking. The blocking solution was removed, and the membrane was slightly washed with the corresponding washing solution. Incubation of the membrane with biotinylated lectins or primary antibodies was carried out at 4 °C overnight. The dilutions can be found in the material section (5.10.1, 5.10.3). Next, three washing steps of 5 min each with PBST 0.1 % or TBST 0.1 % were carried out. To detect the primary antibody or biotinylated lectin, the membrane was incubated for 45 min at RT with an HRP-conjugated secondary antibody in PBST 0.1 % or HRP-conjugated streptavidin in TBST 0.1 %, both diluted 1:10,000. After three washing steps and prior to detection, ECL

reagent (Pierce Biotechnology, Rockford) was freshly prepared in accordance to the manufacturer's specifications. The membrane was incubated in ECL reagent for 5 min at RT while shaking. Detection of the emitted light signal was performed with the Fusion SL4 Western Blot documentation system.

Depending on the samples, different loading controls were used. For cell lysate of fibroblasts β -actin or GAPDH served as loading controls. To remove the primary antibody the membrane was incubated in 10 % acetic acid and washed until no acidic acid could be smelled anymore (3-4 times). Now the membrane could be reused starting with blocking and was carried out as described before. In lectin applications the loading control was detected first.

6.2.6 Total N-glycan analysis by high performance multiplexed capillary gel electrophoresis with laser-induced fluorescence detection (xCGE-LIF) technology

For further analysis the total N-glycan fingerprint of fibroblast samples were measured in cooperation with the MPI Magdeburg (Erdmann Rapp). Cell pellets were collected as described in 6.1.3. N-glycans were dissected by PNGase F from glycoproteins and fluorescently labeled with 8-Aminopyrene-1,3,6-trisulfonic acid trisodium salt (APTS). Separation was conducted by a capillary gel electrophoresis and detection was performed by laser-induced fluorescence detection. Glycans have different characteristic retention times dependent on their structure. Some glycans show signal overlay which can be solved by using glycosidases to cut certain sugar structures. [89]

6.2.7 Glycosphingolipids measurement by xCGE-LIF

The analysis of glycosphingolipids was performed in cooperation with the Hannover Medical School (Falk Büttner). Cell pellets were collected as described in 6.1.3. The method is described in the supplement information in Rossdam et al. [90]. In short, glycolipids were extracted by liquid-liquid extraction, desalted and dried. The glycan head group was released from the ceramide moiety by either LudgerZyme Ceramide Glycanase (CGase) or Endoglycoceramidase I (EGCase I). Glycans were labeled and detected as described above.

6.2.8 Short lipid linked oligosaccharide (LLO) analysis

Metabolic labeling of human fibroblast for analysis of lipid-linked (dolichol-linked) oligosaccharides was performed using media containing 2- ^3H -Man and is based on the reported protocol by Körner et al. [91]–[93] MVK patient fibroblast and control fibroblast were used. 1×10^6 cells were seeded into 6-cm culture plates and grown for 18 – 24 hours until approximately 75 % confluency. Plates were washed three times with 2 ml DPBS and incubated in hunger medium overnight at 37 °C and 5 % CO_2 . Hunger medium was removed and plates were washed three times with 2 ml DPBS. Metabolic

labeling was performed for 30 min at 37 °C, 5 % CO₂ with 2.5 ml LLO labeling medium, which contained 50 µCi/ml 2-[³H]-mannose. The plate was washed after the labeling period 3 x 5 min with 2 ml ice-cold Hanks Buffer and cells were scraped in 1 ml ice-cold methanol using a rubber cell scraper. The methanol was transferred to a 15 ml conical falcon tube, the plate was washed again with 1 ml ice-cold methanol with additional scrapping and combined with the first collection. In the next step the samples were briefly vortexed and sonicated for 3 x 5 pulses. Then four ml of ice-cold chloroform was added to each sample and sonicated again 3 x 5 pulses. Until further analysis chloroform/methanol (2:1) extracts were stored on ice at 4 °C.

The extracts were sonicated and centrifuged at 4,000 rpm at 4 °C. The upper phase was carefully removed and the pellets were extracted two more times with chloroform/methanol (3:2). The combined upper phases containing Dol-P-Man and LLOs of small size were dried under a gently stream of nitrogen and dissolved in 3 ml chloroform/methanol (3:2) and 600 µl 4 mM MgCl₂ in H₂O. Samples were sonicated five times one pulse, briefly vortexed and centrifuged for 3 min at 4,000 rpm. The upper phase was removed and discarded. 2 ml of upper phase (+) buffer were added and samples were sonicated, vortexed and centrifuged as bevor. After discarding the upper phase, 2 ml of upper phase (-) buffer was added and samples were sonicated, vortexed and centrifuged as bevor. This was repeated twice. In the last step the lower phase was dried under nitrogen and dissolved in 0.1 ml chloroform/methanol (3:2). Samples were analyzed by thin layer chromatography on Silica gel60 aluminum sheets in a running buffer containing chloroform/methanol/water (65:25:4) as described previously by Lehle et. al [94].

6.2.9 Measurement of amino acids in cell lysates

Amino acids were analyzed by electrospray ionization tandem mass spectrometry (ESI-MS/MS). Cell pellets of an 80 % confluent T75 flask were harvested and extracted in 50 µl H₂O. For cell disruption, the sample was passed 20 times through a ø22G needle with a 1 ml syringe. The homogenized solution was centrifuged at 13,000 rpm and 4 °C for 30 minutes to remove cell debris. The supernatant was transferred into a new 1.5 ml tube and stored at -20 °C. Protein content of the sample was determined as described in section 6.2.2. To prepare the samples, 5 µl of extract was dried at room temperature overnight on a 4.7 mm filter paper punch. The paper was extracted for 20 minutes with a deuterium labeled standard solution in methanol. After centrifugation the extract was dried and absorbed in 60 µl of 3 N HCl/butanol and transferred into a sealed microtiter plate. The plate was incubated for 15 minutes at 65 °C. Afterwards, samples were dried and the residue in each well was reconstituted in 100 µl of acetonitrile-water-formic acid solution (50:50:0.025). Samples were measured by ESI-MS/MS in technical triplicates and normalized to protein content [95].

6.2.10 Metabolite measurement

The measurement was performed in cooperation with the metabolomics core technology facility of the University Heidelberg (Gernot Poschet). Energy metabolites were extracted from 1×10^6 cells with 0.2 ml of 0.1 M HCl in an ultrasonic ice-bath for 10 min. The resulting extracts were centrifuged for 10 min at 4 °C and 16.400 g to remove cell debris. For determination of nucleotide concentrations, the extracts were derivatized with chloroacetaldehyde as described in Bürstenbinder et al. [96] and separated by reversed phase chromatography on an Acquity HSS T3 column (100 mm x 2.1 mm, 1.7 μ m, Waters) connected to an Acquity H-class UPLC system. Prior separation, the column was heated to 43 °C and equilibrated with 5 column volumes of buffer A (5.7 mM TBAS, 30.5 mM KH₂PO₄ pH 5.8) at a flow rate of 0.6 ml min⁻¹. Separation of adenosine derivatives was achieved by increasing the concentration of buffer B (2/3 acetonitrile in 1/3 buffer A) in buffer A as follows: 1 min 1 % B, 2 min 8 % B, 3.2 min 14 % B, 9.5 min 50 % B, and return to 1 % B in 1.5 min. The separated derivatives were detected by fluorescence (Acquity FLR detector, Waters, excitation: 280 nm, emission: 410 nm) and quantified using ultrapure standards (Sigma). Data acquisition and processing was performed with the Empower3 software suite (Waters) [97].

6.2.11 Lipid measurement

Lipidomic analysis was performed in collaboration with Britta Brügger (BZH, Heidelberg) by nano-electrospray ionization tandem mass spectrometry. Full methods for different lipid classes can be found in [98], [99].

Dolichyl phosphate measurement was also performed in collaboration with Britta Brügger by reverse-phase liquid chromatography-mass spectrometry (RPLC-MS) and method can be found in Analytical Chemistry - Manuscript ID ac-2022-03623a and [100].

6.2.12 Proteomics measurement

Proteome profiling was supported by the Core Facility for Mass Spectrometry & Proteomics (CFMP) at the Center for Molecular Biology at University of Heidelberg (ZMBH) in cooperation with Thomas Ruppert. 100 μ g of protein of MVK fibroblast and controls was precipitated using Wessel-Flügge chloroform/methanol method and protein pellet was dissolved in 8M Urea buffer [101]. After reduction and alkylation for 30 minutes at RT using 10 mM TCEP and 40 mM CAA, Lys-C was added at 1:100 enzyme:protein ratio and incubated for 4h at 37 °C. Mixture was diluted 1:4 with 50 mM TEAB pH 8.5 and trypsin was added in ratio 1:100. After overnight incubation at 37 °C, samples were acidified. In case of a spike in (medium labeled) control, 500 μ g of protein was precipitated. The remaining steps were adjusted accordingly.

Desalting and dimethyl labeling of the peptides was performed using self-made C18 Empore® extraction discs (3M) StageTips [102]. Briefly, each StageTip was conditioned

with 20 μ l MeOH followed by 20 μ l 80 % ACN/0.1 % TFA. Next, they were equilibrated with 20 μ l 0.1 % TFA and 20 μ g of acidified peptides were loaded on each StageTip. Immobilized peptides were flushed with 300 μ l of light labeling reagent (270 μ l 100 mM TEAB pH 8.0, 15 μ l 4 % Formaldehyde, 15 μ l 0.6 M Cyanoborohydride) for 10 minutes. Toxic flow through was discarded and StageTip was transferred into a fresh microtube. Peptides were eluted using 20 μ l of 80 % ACN/0.1 % TFA. Elution step was repeated once. Medium labeling of the spike in standard was performed on SepPak C18 columns by flushing the column five times with 500 μ l of the labeling reagent (2.25 mL 100 mM TEAB pH 8.0, 125 μ l 4 % deuterated Formaldehyde, 125 μ l 0.6 M Cyanoborohydride). Volume of the conditioning, equilibrating and eluting solutions were adjusted accordingly. 20 μ g of medium labeled control was mixed with 20 μ g of light labeled samples, concentrated in a SpeedVac and stored at -20 °C until measured.

Samples were suspended in 0.1 % TFA and an equivalent to 1 μ g of peptides was analyzed using Ultimate 3000 liquid chromatography system coupled to an Orbitrap QE HF (Thermo Fisher). An in-house packed analytical column (75 μ m x 200 mm, 1.9 μ m ReprosilPur-AQ 120 C18 material Dr. Maisch, Germany) was used. Mobile phase solutions were prepared as follows, solvent A: 0.1 % formic acid / 1 % acetonitrile, solvent B: 0.1 % formic acid, 89.9 % acetonitrile.

Peptides were separated in a 120 min linear gradient starting from 3 % B and increased to 23 % B over 100 min and to 38 % B over 20 min, followed by washout with 95 % B. The mass spectrometer was operated in data-dependent acquisition mode, automatically switching between MS and MS2. MS spectra (m/z 400–1600) were acquired in the Orbitrap at 60,000 (m/z 400) resolution and MS2 spectra were generated for up to 15 precursors with normalized collision energy of 27 and isolation width of 1.4 m/z.

6.3 Molecular biological methods

6.3.1 Isolation of genomic DNA

Preparation of genomic DNA (gDNA) was carried out for primary human fibroblasts of the MVK patients and control cell lines to detect mutations in the *MVK*-gene on the genomic level. Fibroblasts were grown and harvested as described in section 6.1.3. Each pellet was resuspended in 500 μ l lysis buffer and 50 μ l of proteinase K (10 mg/ml) was added. The pellet was digested for 2 ½ hours at 56 °C shaking at 250 rpm. To the precipitate gDNA, 550 μ l ethanol (100%) was added and the tube was carefully inverted a couple of times. The precipitated gDNA was either fished with a sharpened Pasteur pipette or pelleted by centrifugation (13,000 rpm; 10 min) followed by a washing step with 70 % ethanol. Any residual liquid was removed from the gDNA precipitate which was dried at RT. Finally, gDNA was resuspended in 500 μ l H₂O and stored at 4 °C.

6.3.2 Isolation of total RNA

Total RNA was isolated from control- and patient-fibroblast cells with the *Rneasy® Mini Plus Kit* (Qiagen, Hilden) for multiple applications. Isolation was carried out following the manufacturer's protocol. Prior to isolation the workspace and pipettes were carefully wiped and disinfected to prevent contamination with RNase. Cells were harvested and pelleted according to section 6.1.3. Pellets were resuspended in 600 µl RLT plus buffer containing 1 % β-mercaptoethanol. Cell disruption was performed with a QIAshredder spin column. A gDNA eliminator column was used to remove gDNA. The homogenate was mixed with 1 volume of 70 % ethanol and transferred to a silica membrane column for RNA purification. After multiple washing steps RNA was eluted in 35 µl RNase-free H₂O. RNA quality was controlled by photometric measurement and agarose-gel electrophoresis. Total RNA was stored at -80 °C.

6.3.3 Photometric determination of nucleic acid concentration

To determine the concentration of DNA and RNA in a sample, absorption was measured at 260 nm and 280 nm with the NanoDrop™ Lite Spectrophotometer (ThermoFisher, Waltham, USA). The concentration was calculated by modification of the Beer-Lambert law with an absorption at a wavelength of 260 nm (A_{260nm}):

$$A_{260nm} = \varepsilon \cdot c \cdot d \qquad c = \frac{A_{260nm}}{\varepsilon \cdot d}$$

ε is the extinction coefficient which is 0.20 (µg/ml)⁻¹cm⁻¹ for double stranded DNA (dsDNA) and 0.025 for single stranded RNA (µg/ml)⁻¹cm⁻¹. C is the concentration of the nucleic acid and d the layer thickness of the radiated body. Purity can be derived from the ratio of A_{260nm} / A_{280nm} . DNA values around 1.8 are generally accepted as pure and RNA at around 2.0.

6.3.4 Primer design

Primers for two different applications qRT-PCR and the traditional PCR were used in this work. The traditional PCR primers were also utilized in reverse transcription and Sanger-sequencing. Primers can be found in 5.8. For qRT-PCR a maximum length of 22 base pairs (bp) and a melting temperature (T_m) of between 50 °C and 65 °C was chosen. It was also considered that the oligonucleotides span an exon-exon junction to reduce contamination through gDNA and the amplicon did not exceed 400 bp. The primers for the traditional PCR were designed between 18 and 27 bp with a G/C content between 40 % and 60 %. Furthermore, it was tried to achieve a T_m of around 55 °C. For designing and to verify T_m the program ApE was used.

6.3.5 Reverse transcription

To synthesize cDNA from RNA transcripts of total RNA samples, the enzyme reverse transcriptase was used. Various reverse transcription kits for different applications were used.

Synthesis of cDNA for qPCR-applications was carried out with *Revert Aid First Strand Kit* (ThermoFisher, Waltham, USA) according to manufacturer and with random hexamer primers. Depending on the concentration, 1-5 µg of total RNA was transcribed with RevertAid RT in 20 µl reaction volume for 60 minutes at 42 °C. The reaction was terminated by incubation at 70 °C for 5 min. The pipetting scheme is shown in Table 21. After reverse transcription cDNA was diluted to 25 ng/µl with H₂O and stored at -20 °C.

Table 21 - Pipetting scheme for cDNA-synthesis with RevertAid First Strand Kit.

| Component | Volume |
|------------------------------------|---------------------------|
| Total RNA | X (1-5 µg) |
| Random hexamer primers (100 µM) | 1 µl |
| Reaction buffer (5X) | 4 µl |
| Ribolock RNase inhibitor (20 U/µl) | 1 µl |
| dNTP Mix (10 mM) | 2 µl |
| RevertAid RT (200 U/µl) | 1 µl |
| H ₂ O | Add up to volume of 20 µl |
| Total volume | 20 µl |

For cDNA-synthesis of a specific transcript or nCounter application, *Omniscript Reverse Transcription Kit* (Qiagen) in combination with a gene specific antisense-primer (R1-primer) was used. 100-1000 ng total RNA was transcribed with *Omniscript RT* for 52 min at 37 °C. Afterwards, PCR-reactions were carried out with the cDNA-template to amplify the desired gene. cDNA was stored at -20 °C. The pipetting scheme for cDNA-synthesis with the *Omniscript RT* is shown in Table 22.

Table 22 - Pipetting scheme for cDNA-synthesis with *Omniscript Reverse Transcriptase*

| Component | Volume [μl] |
|---|--------------------------------------|
| Total RNA | X (0.1-1 μ g) |
| R1-primer (10 μ M) | 2 |
| Reaction buffer (10X) | 2 |
| <i>Ribolock RNase inhibitor</i> (20 U/ μ l) | 0.5 |
| dNTP Mix (5 mM) | 2 |
| <i>Omniscript RT</i> (200 U/ μ l) | 1 |
| H ₂ O | Add up to total volume of 20 μ l |
| Total volume | 20 μl |

Synthesis of cDNA for the PrimePCR was carried out with the *iScript Advanced cDNA Synthesis Kit* (Biorad). Reaction was incubated for 20 minutes at 46 °C followed by heat inactivation at 95 °C for 1 minute. See Table 23.

Table 23 - Pipetting scheme for cDNA-synthesis with *iScript Advanced cDNA Synthesis Kit*

| Component | Volume [μl] |
|---|--------------------------------------|
| Total RNA | X (2000 ng) |
| 5x <i>iScript Advanced Reaction Mix</i> | 4 |
| <i>iScript Advanced RT</i> | 1 |
| RT Control Assay Template | 1 |
| H ₂ O | Add up to total volume of 20 μ l |
| Total volume | 20 μl |

6.3.6 Polymerase chain reaction

To amplify specific sequences from various DNA templates, Polymerase chain reaction (PCR) was used [68]. The desired sequence was amplified by application of a specific forward primer (F) and reverse primer (R) that flank the target sequence and serve as starting point for a DNA polymerase that synthesizes a complementary DNA strand under consumption of dNTP's. For PCR, the enzyme Taq DNA Polymerase (ThermoFisher, Waltham, USA) from *Thermus aquaticus* was used. PCR was either performed in 25 μ l or 50 μ l reaction volume. Depending on the template (cDNA, gDNA, PCR-product) different DNA-amounts were used in the reactions. The general composition of a PCR-reaction is shown in Table 24. The PCR-temperature program is

shown in Table 25. The elongation-phase was adjusted depending on the length of the template (1000 bp/minute).

Table 24 - General scheme of the composition of a PCR-reaction.

| Component | Concentration/ Amount |
|---|------------------------------|
| Template (cDNA/gDNA/PCR-product) | 100 ng |
| MgCl ₂ | 2 mM |
| Taq buffer with (NH ₄) ₂ SO ₄ | 1X |
| DMSO | 2 % |
| dNTP's | 0.2 mM |
| Forward primer | 250 nM |
| Reverse primer | 250 nM |
| <i>Taq-DNA polymerase</i> | 1 U |
| H ₂ O | X |
| Total volume | 20 µl |

Table 25 - Temperature-program for PCR-reactions.

| Cycle-step | Temperature [°C] | Duration [sec.] | |
|-------------------|-------------------------|------------------------|-----|
| Pre-incubation | 94 | 60 | |
| Denaturation | 94 | 30 | 35X |
| Primer annealing | 55 | 30 | |
| Elongation | 72 | 60 sec / 1 kbp | |
| Final elongation | 72 | 180 | |
| Termination | 4 | ∞ | |

The coding sequence (CDS) of the *MVK*-transcript from the patient and a control cell line were amplified by a nested PCR. In a nested PCR a sequence is successively amplified with two primer pairs that flank the CDS to increase selectivity. The product of the first PCR-reaction with primers F1 and R1 is used for second amplification with primers F2 and R2. F2 and R2 bind closer to the CDS than F1 and R1. cDNA was used to amplify *hMVK*-CDS with primers *hMVK_F1* and *hMVK_R1*. 1 µl of the first PCR-product was used for a second PCR with *hMVK_F2* and *hMVK_R2*.

6.3.7 Agarose Gel-electrophoresis and gel-extraction of DNA

The PCR-products were separated and purified by agarose gel-electrophoresis. Depending on the size of the fragments different percentages of the gel were used. As a standard, 1 % agarose gels with ethidium bromide (1:10,000 (w/v)) in 1x TAE buffer were used. DNA samples were mixed with 6x loading buffer. A current of 130 V for 1-2 h was applied. The intercalating ethidium bromide with the nucleotides was excited with 354 nm wavelength and captured in a gel documentation system. The DNA-fragments for some experiments were isolated. To do so, they were cut out by a scalpel under UV light. For DNA extraction the pegGOLD Gel Extraction kit was used according to the manufacturer's protocol. DNA was eluted in ddH₂O.

6.3.8 Sanger-sequencing

DNA was sequenced by the service provider Seqlab Microsynth AG (Göttingen, DE). Samples were worked up according to the provider. 3 µl of 20 µM sequence primer were added to 900 ng DNA in 12 µl ddH₂O. Nested PCR was used for gene sequencing to reduce background to a minimum. For plasmid sequencing the standard primer list of Seqlab was used.

6.3.9 Restriction digest of DNA

The enzymatic cleavage on specific sites of the DNA was performed with restriction endonucleases. These enzymes have a high specificity and use a certain base recognition site. Molecular cloning relies on DNA (PCR fragments) and plasmid digestion with specific restriction enzymes. After linearization of the plasmid a subsequent ligation with the digested insert (PCR fragment) into the multiple cloning site is achieved. For directed insertion two different cleavage sites are needed.

For the cloning process of the MVK gene the restriction enzymes XhoI (ThermoFisher, USA) in combination with NotI (New England Biolabs®, USA) were used. Restriction sites of the enzymes are shown in Table 3. Double-digest was carried out with 1.5 µg of recipient plasmid and whole PCR-reactions (0.2-1 µg) in suitable buffer and total volume of 20 µl. Shrimp Alkaline Phosphatase (SAP) (Fermentas, DE) was added to the reaction to prevent re-ligation. Reactions were incubated at 37 °C for one hour. Termination of the reaction was achieved by incubation at 80 °C for 5 minutes. Pipetting schemes for the double digestions are shown in Table 26.

Table 26 - Pipetting scheme for restriction digest

| Component | <i>XhoI-NotI</i> |
|-----------------------|--|
| Template | 1.5 µg plasmid / 0.2-1 µg PCR-fragment |
| <i>XhoI</i> (10 U/µl) | 1 µl |
| <i>NotI</i> (10 U/µl) | 1 µl |
| SAP (1U/µl) | 1 µl |
| O-buffer (10X) | 2 µl |
| H2O | Add up to 20 µl |
| Total Volume | 20 µl |

Reaction-aliquots were mixed with a loading buffer and subjected to agarose gel electrophoresis to separate undigested plasmid and insert. Digested insert and linearized plasmid were isolated by gel extraction and DNA-concentrations were determined.

6.3.10 Ligation with T4 DNA-Ligase

For the ligation of cleaned up DNA-fragments into the linearized plasmids the T4 DNA-ligase (ThermoFisher, USA) was used. The complementary overhangs, created by restriction digestion, are ligated and a molar-ratio of vector to insert of 1:3 was used. Reaction mix can be seen in Table 27.

Table 27 - Pipetting scheme for ligation reaction

| Component | Volume/Amount |
|----------------------------|------------------------------|
| Linearized Plasmid | 50 ng |
| Digested Insert | 1:3 molar ratio over plasmid |
| T4 DNA-Ligase buffer (10x) | 2 µl |
| T4-DNA-Ligase | 1 µl |
| H2O | Add up to 20 µl |
| Total volume | 20 µl |

6.3.11 Transformation into competent E. coli cells

The non-viral transformation into competent E. coli cells was performed via heat shock. 5 µl of ligation mixture or 1 µl of pure plasmid-solution were transferred into a fresh 1.5 ml reaction tube. 50 µl of competent E. coli cells (see Table 13) were thawed

on ice and added to the reaction tube. Cells were incubated for 20 minutes on ice before heat shocked at 42 °C for 60 seconds. The tube was incubated on ice for two minutes prior to addition of 950 µl LB-medium, followed by incubation for 30 minutes at 37 °C with shaking at 200 rpm. The bacteria were pelleted by centrifugation at 6000 rpm for 3 minutes. The pellet was resuspended in 100 µl LB-Amp (50 µg/ml ampicillin) and spread out on a LB-Amp-plate. The transformed plasmids carried an ampicillin resistance for selection. Bacteria were grown over-night at 37 °C and stored short term the next day at 4 °C. Colonies were picked to expand the clones in LB-medium and to extract plasmid DNA via “miniprep” or “midiprep”. LB volumes if the “miniprep” were 2 ml and for the “midiprep” 50 ml. Cleaned up DNA was stored at -20 °C.

6.3.12 Quantitative Real-Time Polymerase Chain Reaction

The transcript level of genes based on their mRNA amount can be determined by quantitative real-time polymerase chain reaction (qRT-PCR). For this work, PerfeCTa® SYBR® Green FastMix® (Quantbio) was used. The qPCR was setup in triplicates in a reaction volume of 10 µl with 50 ng cDNA. The pipetting scheme for the qRT-PCR reaction is shown in Table 28. qRT-PCR was performed with cDNA synthesized from total RNA to access information about the transcript levels of specific genes.

Table 28 - General scheme of the composition of a qRT-PCR reaction.

| Component | Volume |
|-----------------------------|-----------------|
| 2XSensiFAST® No-ROX Mix | 5 µl (1X) |
| qPCR-forward primer (10 µM) | 0.4 µl (400 nM) |
| qPCR-reverse primer (10 µM) | 0.4 µl (400 nM) |
| cDNA (25 ng/µl) | 2 µl (50 ng) |
| H ₂ O | Add up to 10 µl |
| Total volume | 10 µl |

qRT-PCR was performed with the CFX Connect Real-Time PCR Detection System (Biorad). The temperature program was designed as a three-step-cycling (Table 29).

Table 29 - Temperature program for qRT-PCR

| Cycle-step | Temperature [°C] | Duration [sec.] |
|-------------------|-------------------------|------------------------|
| Pre-incubation | 95 | 30 |
| Denaturation | 95 | 4 |
| Primer annealing | 55 | 15 |
| Elongation | 70 | 10 |

40X

qRT-PCR was carried out for a gene of interest (GOI) and housekeeping gene (HKG) which functions as reference. To evaluate the mRNA-transcript level relative to the housekeeping gene, the $\Delta\Delta C_t$ Method was used. The fold change was calculated as followed:

$$\Delta\Delta C_t = (C_{t(GOI)} - C_{t(HKG)})_{patient} - (C_{t(GOI)} - C_{t(HKG)})_{control}$$

and

$$Fold\ change = 2^{-\Delta\Delta C_t}$$

The C_t value (cycle threshold) describes the number of replication cycles that are necessary till an exponential increase of the fluorescence signal is detected.

6.3.13 PrimePCR

cDNA synthesized by iScript Advanced cDNA Synthesis Kit (see 6.3.5) was diluted in H₂O to an end volume of 100 μ l. A 96-well format of predesigned PrimePCR assay was used. Primers for the different targets are lyophilized in each well. In each reaction well 20 μ l reaction mixture (Table 30) was added.

Table 30 - PrimePCR reaction mixture

| Component | Volume [μ l] |
|---|-------------------|
| 20x PrimePCR | Dried in well |
| 2x SsoAdvanced Universal SYBR [®] Green Supermix | 10 |
| cDNA Sample | 1 |
| Nuclease-Free water | 9 |
| Total volume | 20 μ l |

qRT-PCR was performed with the CFX Connect Real-Time PCR Detection System (Biorad). The temperature program can be found in Table 31.

Table 31 - Prime PCR temperature protocol.

| Cycle-step | Temperature [°C] | Duration [sec.] | |
|---------------------|---------------------------------|-----------------|-----|
| Activation | 95 | 120 | |
| Denaturation | 95 | 5 | 40X |
| Annealing/extension | 60 | 30 | |
| Melt curve | 65-95 °C (0.5 °C increments) | 5 sec / step | |

Reference genes for normalization were used according to the manufacturer's protocol. Quality control was checked in the CFX connect manager software and data analysis was performed as described in 6.3.12.

6.3.14 nCounter analysis

The nCounter expression system was developed in collaboration with the Core Facility of the Institute of Human Genetics at the University Hospital Heidelberg. In this course, the nCounter-analysis was used to examine the expression profile of genes of which most are relevant for glycosylation. The list of measured genes can be found in the appendix (Table 46). nCounter (nanosttring technology, USA) is a hybridization-assay to quantify specific RNA transcripts in a sample without requiring any enzymatic reaction like cDNA synthesis.

The RNA sample is incubated with two DNA-oligo-probes, a capture-probe and reporter probe for hybridization. The reporter probe carries a fluorescent barcode consisting of 5 fluorophores that are unique for each target. The capture probe is biotinylated for immobilization and excessive probes are removed. Both probes hybridize specifically with a unique RNA-transcript over a length of 50 base pairs each. As the RNA-molecule is hybridized to the biotin coupled capture-probe, it will be immobilized on a streptavidin coated cartridge and aligned to the imaging surface by a laminar flow and an applied electric current. Each target can be specifically detected due to hybridization with the reporter probe carrying a gene specific barcode that encodes for the identity of the hybridized transcript. In the last step, the number of barcodes corresponding to a specific transcript are counted. These counts are equivalent to the number of RNA-transcripts in this specific sample. The principle of the method is shown in Figure 13.

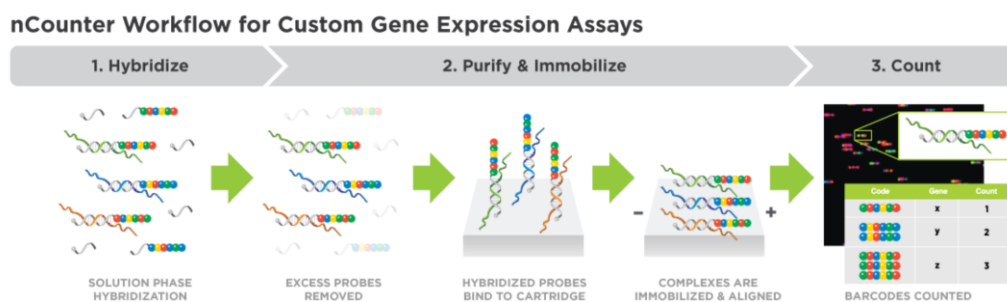


Figure 13 - nCounter workflow for gene expression. The target RNA hybridizes with a reporter probe carrying a fluorescent barcode and a biotin-labeled capture probe. (2) Purification and immobilization on the cartridge of the target-probe complex. Laminar flow and application of an electric current align the complexes to the surface of the cartridge. (3) Individual RNA molecules in the sample are counted by the barcodes in the image. RNA counts were normalized to housekeeping genes and compared to controls. Figures were taken and adapted from nanosttring website (www.nanotstring.com).

Total RNA was extracted from approx. 8×10^5 cells from patients and control cells with the RNeasy mini kit (Qiagen) in combination with the QIAshredder system (Qiagen) according to the manufacturer's protocol. RNA was eluted in 30 μ l nuclease-free H₂O. RNA quantity and quality were assessed using NanoDrop 2000 (Thermo Fisher Scientific), the Agilent Bioanalyzer 2100 (TotalRNA Nanokit) and the Qubit™ Fluorometer (Qubit RNA HS Kit; Invitrogen). 50 ng of total RNA were used per hybridization reaction. Transcript abundance of 72 genes including control genes were determined using an nCounter® SPRINT Profiler (NanoString Technologies). For each patient and control fibroblast cell line, 3 replicates were analyzed. The acquired data was normalized according to manufacturer's guidelines in multiple steps. For normalization three RNA control samples from primary fibroblasts were used. First, the transcript counts for every gene of every control were separately normalized to the housekeeping genes *ACTB*, *GAPDH*, *C1orf43*, *RAB7A*, *SNRPD3*. From this normalization an average value for every gene for every control was calculated. The averages of all three controls were used to calculate an average for every gene. This mean value was used to evaluate the data of the patients. The data of the patients was acquired in triplicates.

Data were analyzed according to the manufacturer's guidelines using nSolver Analysis Software 4.0. Housekeeping genes *ACTB*, *C1orf43*, *GAPDH*, *RAB7A* and *SNRPD3* were used for normalization. All results were plotted with nSolver Analysis Software 4.0.

6.4 Production and application of retroviral particles for transfer of nucleic acids into primary fibroblasts

6.4.1 Preliminary work

The wildtype MVK gene was isolated from control cells by reverse transcriptase followed by PCR. A 5'-*XhoI* and a 3'-*NotI* restriction site was appended to the *hMVK-CDS* by PCR using the primers *hMVK_XhoI_ATG_F* and *hMVK_-stop_MYC_NotI_R*. The PCR product was site-directed inserted into the pLNCX2 mammalian expression vector by double digestion with *XhoI* and *NotI* and subsequent ligation according to section 6.3.9 and 6.3.10. After transformation in *E. coli*, selection of positive clones was done by colony PCR. Positive clones were picked and verified after purification by restriction digest and Sanger-sequencing.

6.4.2 Production of retroviral particles

For transfection of the plasmid in mammalian cells the FUGENE®HD Transfection Reagent Kit was used. The mock vector (empty vector) and the vector with the MVK construct were transfected into Phoenix-eco cells according to the manufacturer. Transfection mix was incubated for 48 h at 37 °C. For production of retroviral particles, transfected cells were washed and incubated overnight at 33 °C with fresh medium. As

the produced retroviral particles are not able to efficiently infect primary fibroblast, another cell line, PT 67, was infected. In a 6-well plate 2,000 PT67 cells/well were seeded overnight. The supernatant of the Pheonix-eco cells, that contain the retroviral particles, were filtered and added to the PT67 cells. To increase the efficiency of the infection, 1 μ l/ml polybrene was added and incubated at 37 °C for 24h. This procedure was repeated one time on the next day. The infected PT67 cells were selected with neomycin (1 %) for 10 days. The infected PT76 cells were cryopreserved.

6.4.3 Retroviral infection of primary fibroblasts

The infection of primary fibroblast was performed in the same way as the infection of PT67 cells. Infection was performed in duplicates and also with mock vector. In a 6-well plate 5,000 fibroblast of each patient were seeded and cultivated over-night at 37 °C. The supernatants with the retroviral particles were filtered, polybrene was added and then added to the seeded fibroblast. Also, this infection was repeated two times and selection was performed with neomycin.

The stable fibroblast cell lines with the construct and with mock were cultivated after selection with 0.1 % neomycin to maintain a slight selection pressure. These cells were harvested and used for biochemical analysis. The infected cell lines were cryo conserved.

6.5 Statistic

All experiments were performed at least 3 times if not stated otherwise. Mean and standard deviation were determined and data was analyzed with student t-test. For more than one condition two-way ANOVA was performed. P-value of ≤ 0.05 (* $0.05 \geq p \geq 0.01$; ** $0.01 \geq p \geq 0.001$; *** $0.001 \geq p$) was considered as significant. Data is presented as mean \pm standard deviation.

7 Results

7.1 Patient anamnesis and genetic characterization

7.1.1 Anamnesis

“Patient MVK9 was the first child of consanguineous parents of North-African descent. She had been antenatally diagnosed with severe hypertrophic cardiomyopathy at 21 weeks of gestation and was delivered 8 weeks later by caesarean section due to abnormal cardiotocography. Immediately after birth, she developed severe respiratory distress and hypoxemia, as well as metabolic acidosis. Clinical examination revealed dysmorphic facial features, including prominent frontal bossing, hypertelorism, a triangular-shaped face with low-set ears, and macroglossia. Echocardiography revealed a left ventricular non-compaction pattern with severely impaired cardiac function with need of inotropic support. Cerebral ultrasound showed intraventricular and periventricular cysts (Figure 3). Ophthalmologic evaluation revealed bilateral cataracts and diffuse retinal hemorrhages. Upon suspicion of a mitochondrial disease, the patient was started on supportive therapy. Several days later, she developed an erythematous skin rash. A full metabolic screening revealed excessive excretion of mevalonic acid in urine (4,042 mmol/mol creatinine). Due to ongoing inflammation, the patient was started on an anti-inflammatory therapy with methylprednisolone (2 mg/kg/day) on day 10, but died 11 days later due to cardiac arrest [17].”

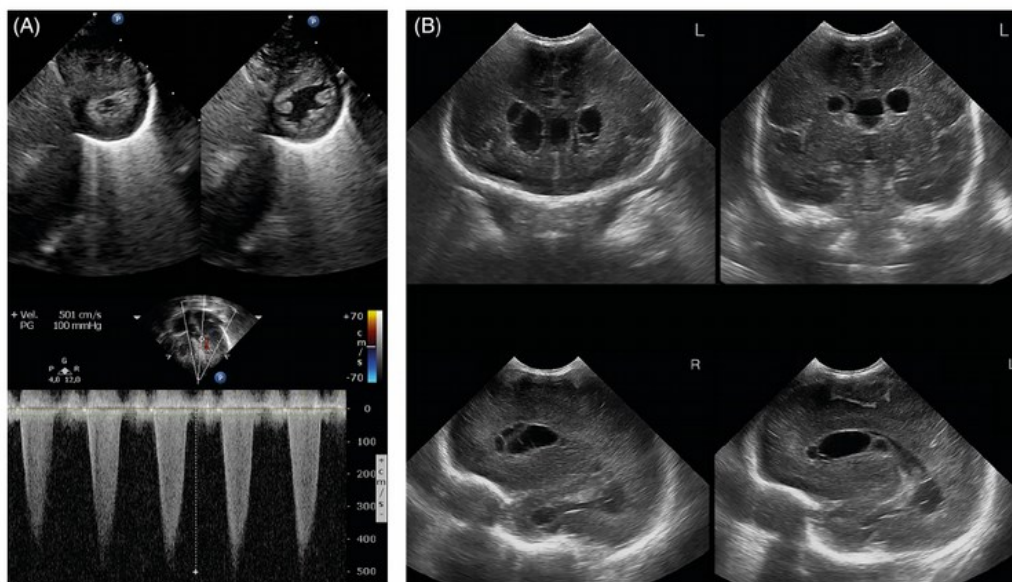


Figure 14 - Sonographic findings in patient 9. “(A) Echocardiography showing hypertrophic interventricular septum with left-ventricular noncompaction pattern (left, systole; right, diastole) and left ventricular output tract pressure gradient (PG). (B) Cerebral ultrasound showing multiple periventricular cysts, hyperechoic periventricular white matter and poor gyration. Top line: coronal views; bottom line: sagittal views. L: left, R: right. Picture and legend taken from [17].”

7.1.2 Genetic characterization

The excessive excretion of mevalonic acid in the urine was the indication to perform Sanger sequencing of the *MVK* gene. Genomic DNA (gDNA) and mRNA was isolated from patient MVK9 and control fibroblasts. mRNA was used to synthesize cDNA. The *MVK* gene was sequenced and a homozygous missense mutation of thymine to cystine (c.803T>C) on cDNA level was found which could also be confirmed in exon 9 in the gDNA (see Figure 15). This variant leads to an amino acid change from isoleucine to threonine at position 268 on protein level (p.Ile268Thr). To understand the importance of this region of the protein, a BLAST-search followed by a sequence alignment with Clustal Omega was conducted. The analysis revealed that I²⁶⁸ and adjacent amino acids (S²⁶⁷, D²⁶⁹, A²⁷⁰, I²⁷¹) are highly conserved throughout different species (see Table 32).

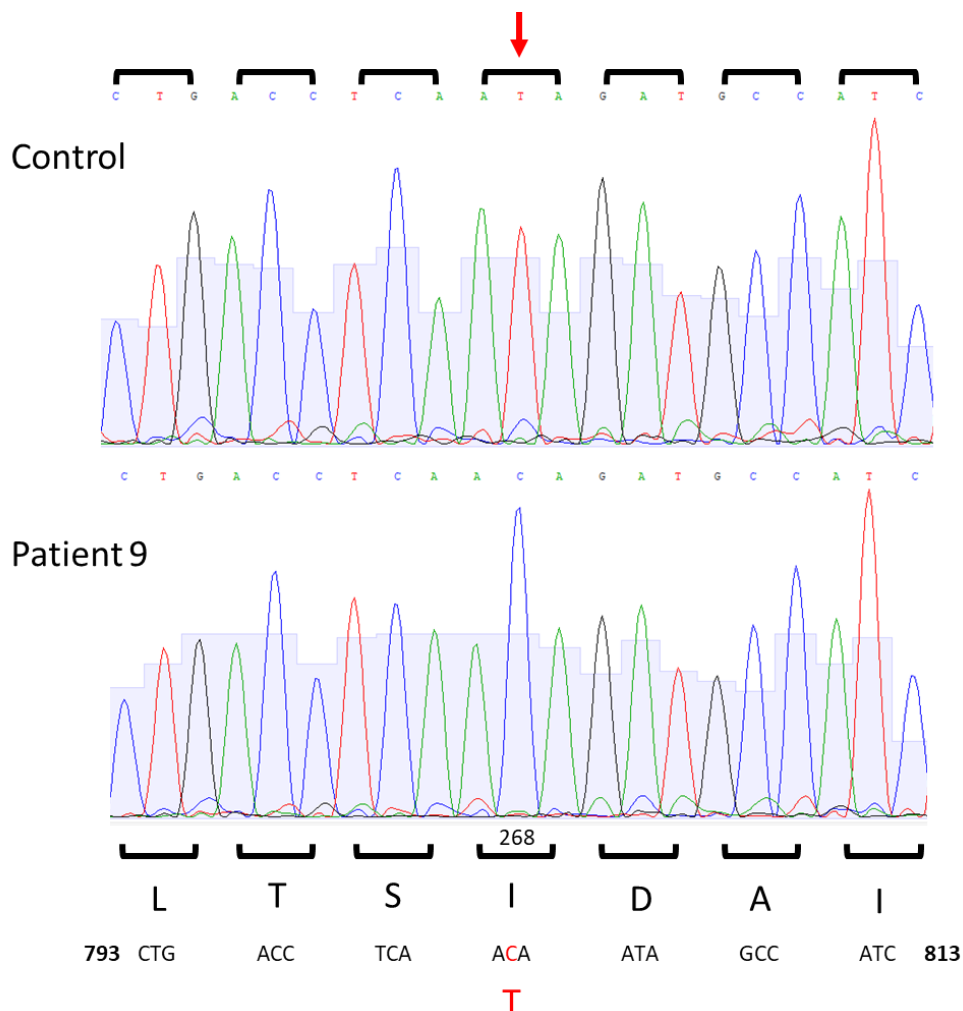


Figure 15 - Sanger sequence of patient 9 and control of *MVK*. The homozygous point mutation c.[803C>T] is shown in the lower electropherogram. This variant leads to an amino acid exchange from isoleucine to threonine at position 268 compared to control. Blue bars represent quality values.

Table 32 - Conservation of the mutated amino acid in the MVK gene in different species. ClustalW alignment. *=single, fully conserved, := conservation between groups of strongly similar properties, .= conservation between groups of weakly similar properties

| | | |
|-------------------------------|---|-----|
| <i>Homo_sapiens</i> | TRALVAGVRNRLKLFPEIVAPLLTSIDAI SLECE RVLGEM | 282 |
| <i>Patient_MVK9</i> | TRALVAGVRNRLKLFPEIVAPLLTS T DAI SLECE RVLGEM | 282 |
| <i>Chimpanzee_pan</i> | TRALVAGVRNRLKLFPEIVAPLLTSIDAI SLECE RVLGEM | 282 |
| <i>Mus_musculus</i> | TKALVA AVRSRLTKFPEIVAPLLTSIDAI SLECE RVLGEM | 282 |
| <i>Rattus_norvegicus</i> | LAASFAGHESEV GQFPEI MAPLLTSIDAI SLECE RVLGEM | 282 |
| <i>Gallus_domesticus</i> | TKVLVAGVKEKILKFP AIMPVLDSIDAI SQECQSVLEAM | 283 |
| <i>Camelus_dromedarius</i> | TKALVAGVRSRLKLFPEIVAPLLTSIDAI SLECE RVLGEM | 282 |
| <i>Monodon_monoceros</i> | TKALVAGVKSRLKLFPEI MAPLLTSIDAI SLECE RLLGEM | 282 |
| <i>Oryzias_melastigma</i> | TKALVARVKDKINKFPSIMNPVLESVD AISYTCEKVL TCE | 282 |
| <i>Xenopus_tropicalis</i> | TKVLVAGVKEKLLKFPDI EPVLS SIHAI SQECQ RVLKEM | 292 |
| <i>Caenorhabditis_elegans</i> | TARMVQTVKERLKKFPEVVDAMFGSIDAI SLDA AKILHRP | 418 |
| Consensus symbols | : **: :: :: *:.*** . :: | |

7.1.3 Pathogenic impact and structural changes of the MVK protein

To predict the impact of the missense mutation on the enzymatic activity and pathogenicity of the MVK protein, high-performance in-silico prediction meta scores were annotated using the dbNSFP database v4.2A[103], [104]. The following scores were used: CADD phred, MetaSVM, M-CAP, VEST4, Polyphen2 and REVEL. The results of this analysis can be seen in Table 33. All six prediction tools list the mutation of patient 9 as pathogenic.

Table 33 - Annotated pathogenicity scores

| HGVSc / HGVS _p | CADD phred | MetaSVM score | M-CAP score | VEST4 score | Polyphen2 score | REVEL score |
|---------------------------|------------|---------------|-------------|-------------|-----------------|-------------|
| c.803T>C / p.Ile268Thr | 23.7 | 1.061 | 0.484 | 0.811 | 0.888 | 0.885 |

Note: Interpretation as pathogenic variant: CADD phred ≥ 20 , MetaSVM score ≥ 0 , M-CAP-score ≥ 0.025 , VEST4 score ≥ 0.5 , Polyphen2 score ≥ 0.85 , and REVEL score ≥ 0.4 . Red means variant is interpreted as pathogenic by respective score.

To understand the effect of the mutation on the tertiary structure of the MVK protein (PDB: 2R3V), the DynaMut software was used. This simulation gives insights on the structural impact of the mutation. The prediction outcome shows a destabilizing effect of $\Delta\Delta G$: -3.162 kcal/mol. Also, the Δ Vibrational Entropy Energy between wildtype and mutant is predicted to $\Delta\Delta S_{\text{Vib}}$ ENCoM: 0.600 kcal·mol⁻¹·K⁻¹ which indicates an increase of flexibility of the molecule in this region (see Figure 16 D). As seen in Figure 16 B, the mutant protein loses some interatomic interactions, which is indicated by the colored dashed lines. The disappearing blue dashed line is a halogen bond and hydrogen bonds are getting lost or weakened (red/orange dashed lines). This all leads to a destabilized protein.

In the wildtype protein the active site of the MVK protein is at amino acid S 146 and D 204, the nucleotide binding region is from G 140 to S 146 and the metal binding site is supposed to be at S 146 and E 191.

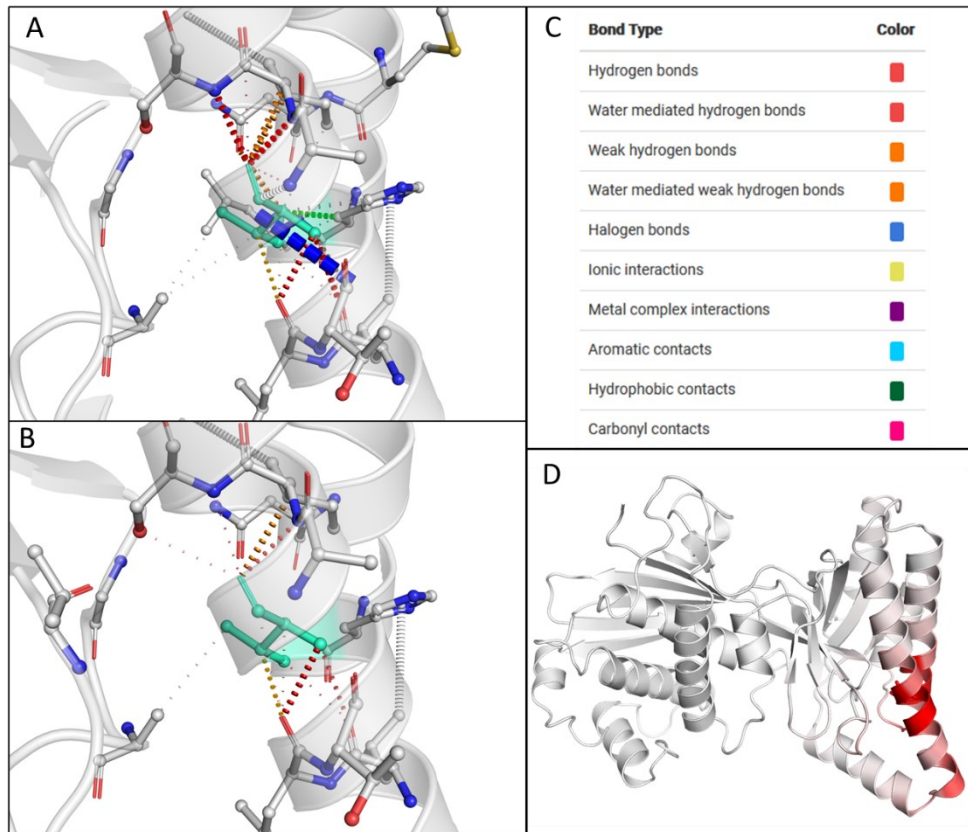


Figure 16 - DynaMut prediction outcome of mutation Ile268Thr in the MVK protein. (A) Interatomic interactions of wildtype protein (B) Changes of interatomic interactions of mutant protein Ile268Thr. Light green indicates wildtype and mutant residues as sticks alongside with the surrounding residues which are involved in any type of interaction. (C) Color of different bond types (D) Region of increased flexibility in the mutant protein.

7.1.4 Additional MVK patients

For this study, also 10 diagnosed MVK patients, kindly provided by the Children's Hospital Heidelberg, were included. Biochemical analysis previously showed excessive excretion of mevalonic acid in their urine but only for patients MVK1, 5 and 7 genetic data on MVK was available. Patients MVK2, 3, 4, 8 and 10 were analyzed by Sanger sequencing. Phenotypes were extracted from evaluated clinical reports. Two new mutations, which are not in the NCBI ClinVar database, were found. Mutation c.790dupC of patient MVK3 and mutation c.782T>C of patient MVK 10. The patients' mutations and the phenotype of all MVK patients from this study are depicted in Table 34.

Results

Table 34 - MVK patients and laboratory test results.

| MVK ID | Gender | Current age (years) | Phenotype | HGVS _c | | HGVS _p | | HGVS _g | | chromosomal position (GRCH38) | | ClinVar | | dbSNP | |
|--------|--------|---------------------|-------------|-------------------|-----------|-------------------|---------------|-------------------|-----------|-------------------------------|--------------|---------|-----|-------------|-------------|
| MVK 1 | male | 26 | mild | c.72dupT | c.1000G>A | p.(Gly25Trpfs) | p.(Ala334Thr) | g.166dupT | g.1094G>A | 12:109574893 | 12:109595142 | x | x | rs104895322 | rs104895317 |
| MVK 2 | female | decreased | severe | c.803T>C | c.803T>C | p.(Ile268Thr) | p.(Ile268Thr) | g.897T>C | g.897T>C | 12:109591275 | 12:109591275 | x | x | rs104895304 | rs104895304 |
| MVK 3 | male | decreased | severe | c.790dupC | c.928G>A | p.(Leu264fs) | p.(Val310Met) | g.884dupC | g.1022G>A | 12:109591262 | 12:109595070 | new | x | - | rs104895319 |
| MVK 4 | - | - | - | c.510C>T | c.803T>C | p.(Asp170=) | p.(Ile268Thr) | g.604T>A | g.897T>C | 12:109581533 | 12:109591275 | x | x | rs2287218 | rs104895304 |
| MVK 5 | female | 16 | mild | c.60T>A | c.60T>A | p.(His20Gln) | p.(His20Gln) | g.154T>A | g.154T>A | 12:109574882 | 12:109574882 | x | x | rs104895335 | rs104895335 |
| MVK 6* | female | 35 | mild | c.643C>T | c.1000G>A | p.(Arg215*) | p.(Ala334Thr) | g.737C>T | g.1094G>A | 12:109586765 | 12:109595142 | x | x | rs758026399 | rs104895317 |
| MVK 7* | male | decreased | mild | c.643C>T | c.1000G>A | p.(Arg215*) | p.(Ala334Thr) | g.737C>T | g.1094G>A | 12:109586765 | 12:109595142 | x | x | rs758026399 | rs104895317 |
| MVK 8 | male | decreased | severe | c.803T>C | c.902A>C | p.(Ile268Thr) | p.(Asn310Thr) | g.897T>C | g.996A>C | 12:109591275 | 12:109595044 | x | x | rs104895304 | rs121917789 |
| MVK 9 | female | decreased | severe | c.803T>C | c.803T>C | p.(Ile268Thr) | p.(Ile268Thr) | g.897T>C | g.897T>C | 12:109591275 | 12:109591275 | x | x | rs104895304 | rs104895304 |
| MVK 10 | female | - | mild-severe | c.728C>T | c.782T>C | p.(Thr243Ile) | p.(Val261Ala) | g.822C>T | g.876T>C | 12:109590821 | 12:109591254 | x | new | rs104895314 | - |
| MVK 11 | male | 43 | mild | c.59A>C | c.1000G>A | p.(His20Pro) | p.(Ala334Thr) | g.153A>C | g.1094G>A | 12:109574881 | 12:109574881 | x | x | rs104895295 | rs104895295 |

*Siblings

| MVK ID | Mevalonic acid (urine) | Total cholesterol | Aspartate aminotransferase | Immunoglobulin D | Leukotriene E ₄ | Ubiquinone 50 |
|--------|------------------------|-------------------|----------------------------|------------------|----------------------------|---------------|
| MVK 1 | 3190 | 1.4 | - | 21.2 | - | 2125 |
| MVK 5 | 318 | 2.5 | - | 12.6 | - | 2.1 |
| MVK 6* | 6286 | 4.2 | 16 | 508.2 | 272 | - |
| MVK 7* | 2687 | - | - | 1760 | 263.5 | - |
| MVK 9 | 4042 | 3.4 | 38.3 | - | - | - |
| MVK 11 | 2796 | - | - | 438 | - | - |

Note: Average concentrations are given, mevalonic acid (urine) in mmol/mol creatinine (ref. 0-0.49 mmol/mol creatinine), total cholesterol (ref. age-dependent 2.62-7.67 mmol/l), Aspartate aminotransferase in U/l (ref. < 37 U/l), immunoglobulin D in mg/l (ref. 1.3-152.7 mg/l), leukotriene E₄ in nmol/mol creatinine, ubiquinone-50 in μmol/l (ref. age-dependent <12 months 0.55-1.34 μmol/l; 1-6 years 0.56-1.67 μmol/l, >6 years 0.44-1.19 μmol/l)

7.2 MVK expression analysis in every patient

To investigate abnormalities in the MVK protein and MVK-mRNA expression, fibroblast of the MVK patients as well as control fibroblasts were analyzed by western blotting and qRT-PCR.

7.2.1 Western blot analysis showed reduced MVK protein amount

The protein level from fibroblast lysates was determined by SDS-PAGE followed by western blotting. The intensity of the immunodetected MVK-protein was normalized to β -actin (see Figure 17). The MVK protein was significantly reduced in all patients, ranging from 65.1 % \pm 28 % (MVK11) to 3.7 % \pm 2 % (MVK5) residual amount compared to controls.

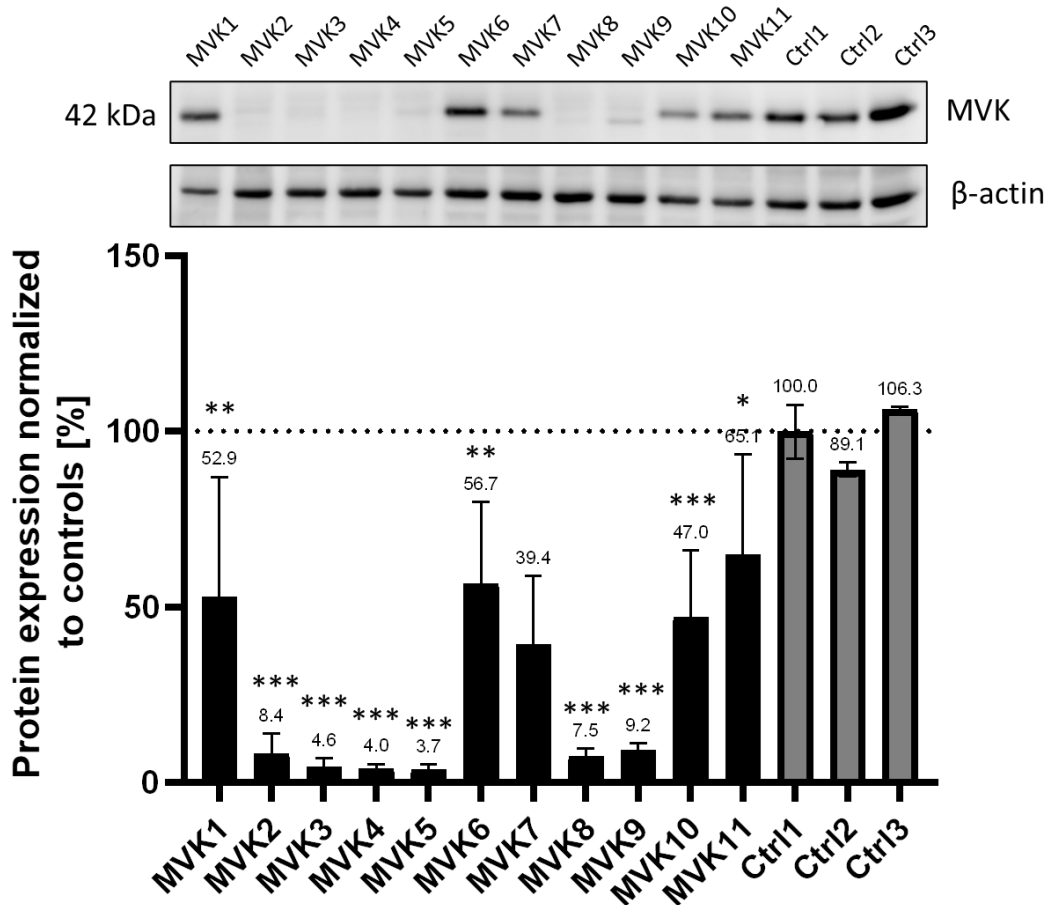


Figure 17 - Western blot analysis and quantification of MVK protein expression in patients and controls. MVK signal was normalized to β -actin (n=4) and mean of controls was set to 100 %. Data are presented as biological replicates' mean \pm SD (n=3). Protein expression was reduced in all MVK patients.

7.2.2 Increased expression of MVK transcript

To investigate the impact of the mutations on the transcript level, qRT-PCR for the MVK gene was performed. The measured C_t value (cycle threshold) was normalized to the reference gene β -actin and then compared to controls. The ΔC_t values can be found in the appendix 10.3. As seen in Figure 18, all patients showed significantly increased MVK mRNA levels except for patient MVK5, of which the mRNA is downregulated. MVK9 showed the highest transcript level of 4.11 ± 0.42 compared to controls.

MVK mRNA levels

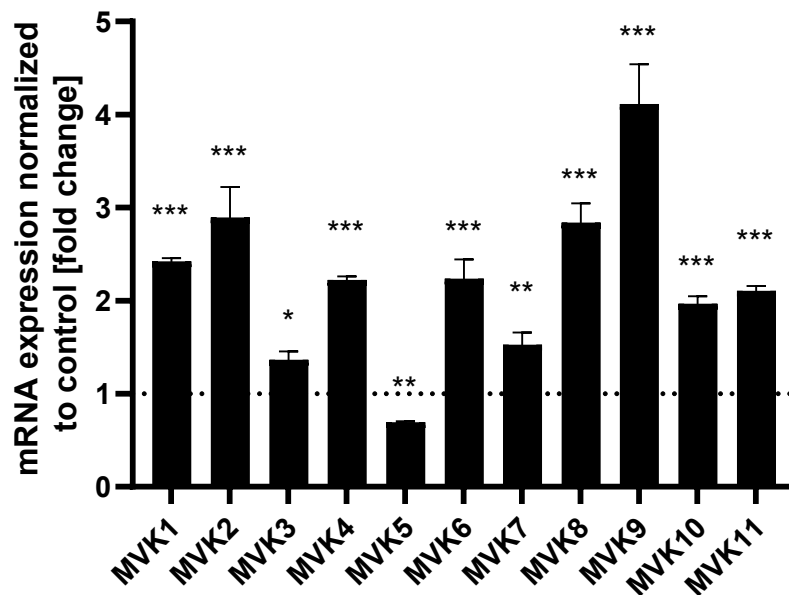


Figure 18 - Quantification of mRNA expression of the MVK-gene. Values were normalized to β -actin and compared to control. Data are presented as biological replicates' mean \pm SD (n=3).

7.2.3 *HMGR* and *PMVK* transcript expression

To analyze whether a mutated *MVK* gene might have an effect on the polyisoprene pathway before and after the mevalonate kinase, the genes *HMGR* and *PMVK* were additionally analyzed by qRT-PCR (Figure 19). The measured C_t value (cycle threshold) was normalized to the reference gene *β -actin* and then compared to controls. All *MVK* patients showed an increase in the *HMGR* transcript, which is the enzyme right before *MVK*. *MVK3* had a significant increase of 3.83 ± 1.58 . For *PMVK*, which acts right after *MVK*, no change on transcript level was found.

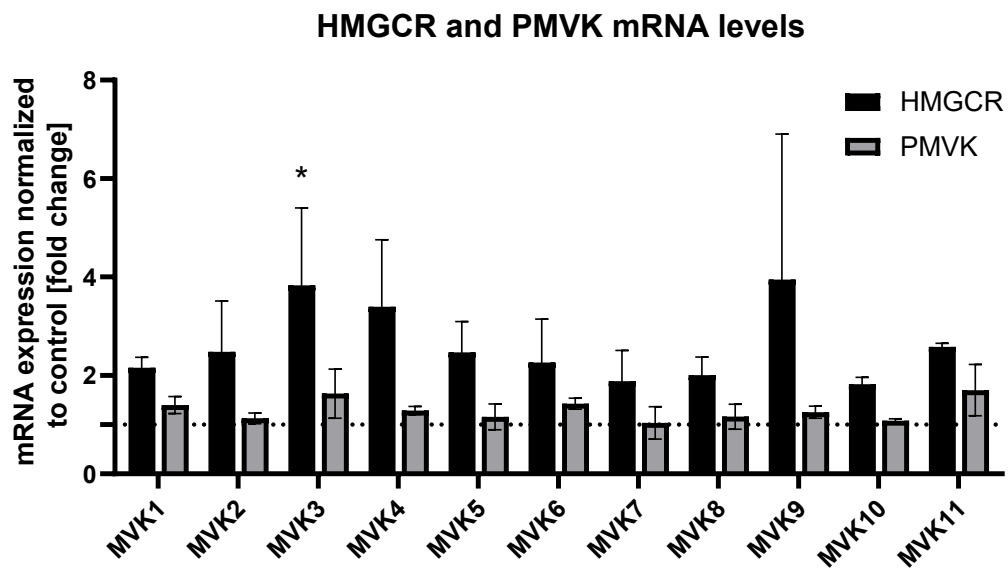


Figure 19 - Quantification of mRNA expression of *HMGR* and *PMVK*. Values were normalized to *β -actin* and compared to controls. Data are presented as biological replicates' mean \pm SD (n=2).

7.2.4 Localization and presence of the MVK protein in control and patient cells

For further analysis of the MVK protein and its localization, patient cells and control cells were analyzed by immunohistochemistry (6.1.7). Antibodies against MVK (green fluorescence signal) and cytosolic Pmm2 (red fluorescence signal) were used for staining. The cell nucleus was stained with NucBlue™ (blue fluorescence signal). The signal for MVK showed a cytosolic location and overlapped with the signal for Pmm2. Between the patients a difference in intensity for MVK was visible in comparison to control.

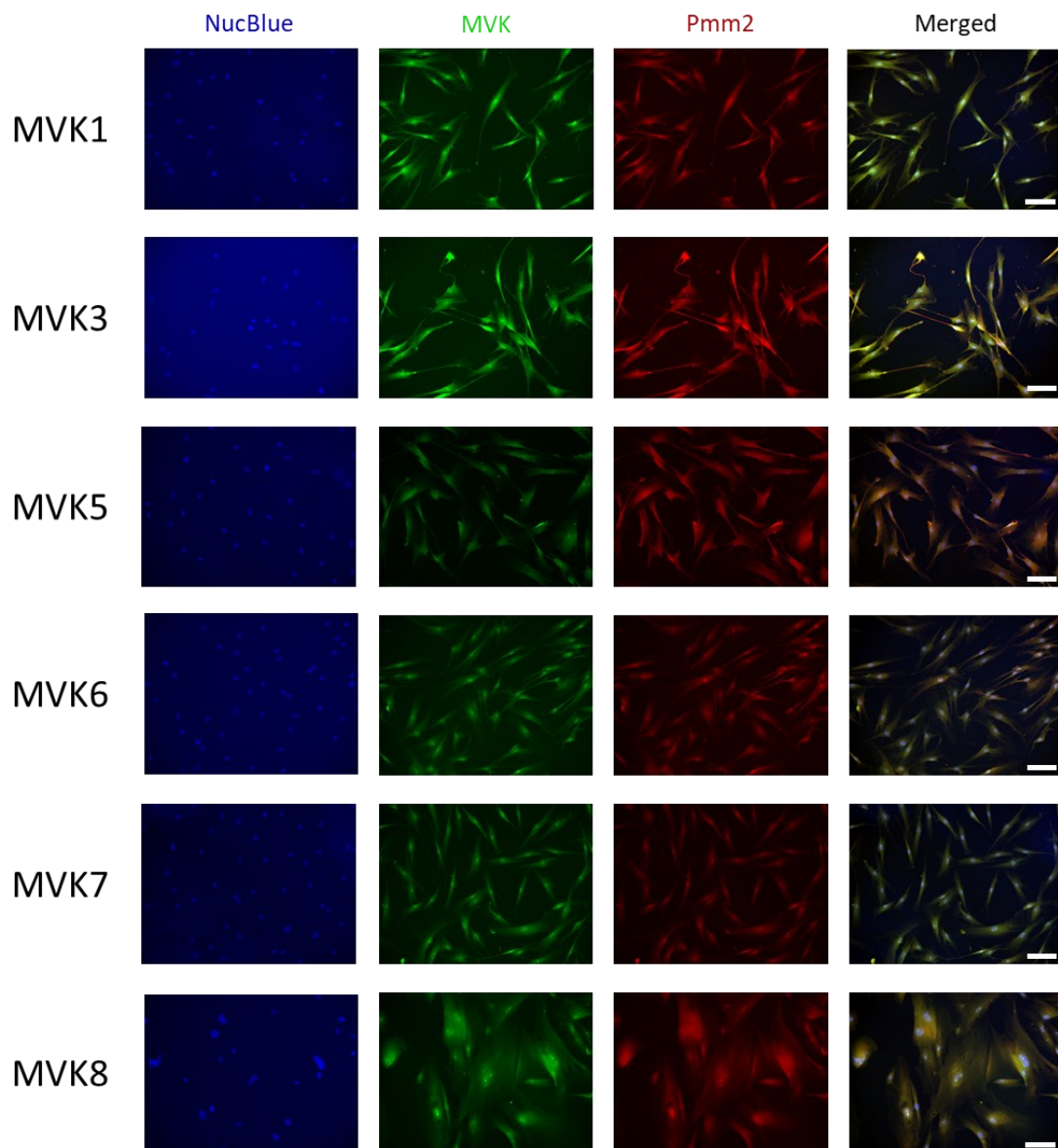


Figure 20 - Immunofluorescence staining of the MVK patients fibroblast and controls. Depicted are cells at 20x magnification. White bar equals 10 μm . MVK (green) was detected with the fluorophore GFP and Pmm2 (red) with RFP. MVK signals overlap (colocalization) with Pmm2 which indicates cytosolic localization. Signal intensity for MVK is decreased in patients, which can be seen in the merged photo by a more reddish color compared to controls. Continued in Figure 21.

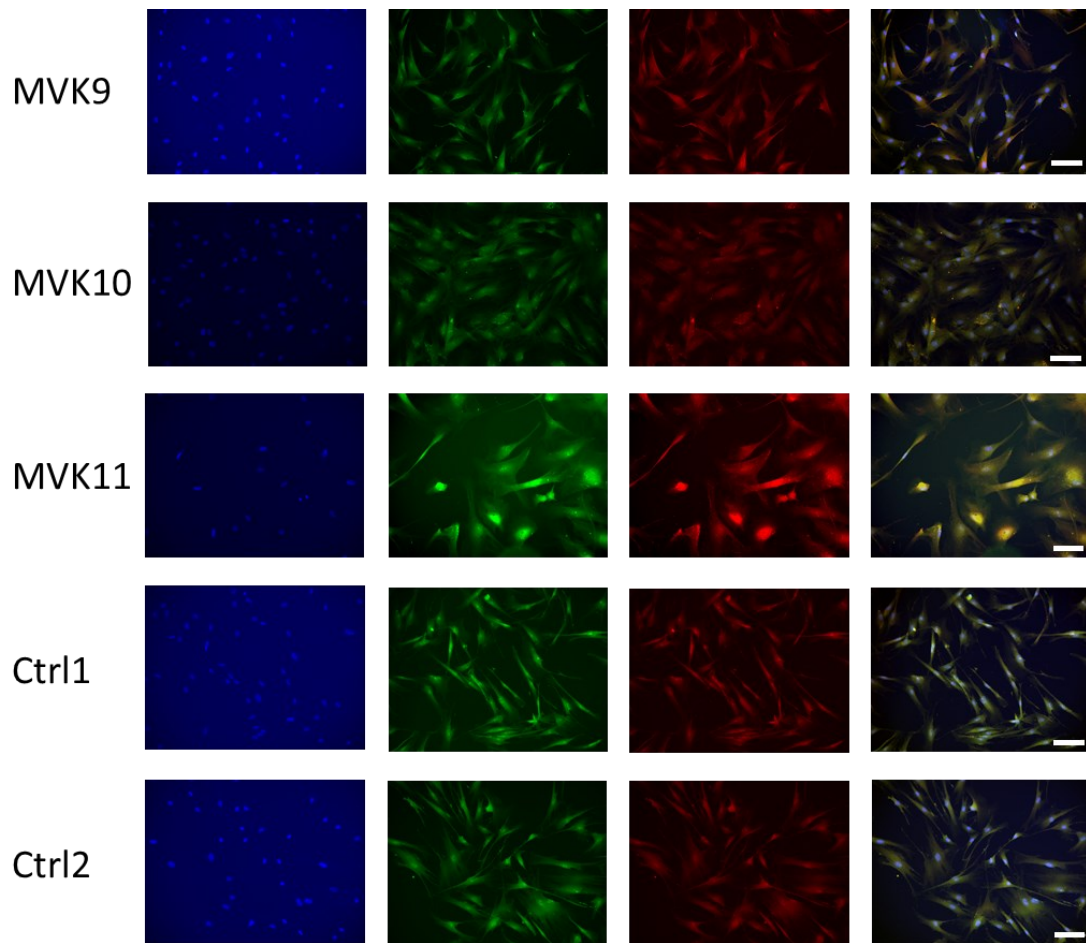


Figure 21 - Continuation of immunofluorescence staining of fibroblast of the MVK patients and controls.

In general, it can be seen that MVK patients showed a decreased signal for MVK (green) compared to controls. This leads to a more reddish overlap in the merged pictures compared to controls. Also, it is visible that the cell morphology of patients MVK8 and MVK11 was different compared to the other ones. Cells grow more spread out and the cytosolic area seems to be bigger.

7.3 Changes in cell proliferation of MVK patients

During this work, it was observed that some of the patient cells grew markedly slower than control fibroblasts. To characterize this observation cell growth and proliferation were measured with the “xCELLigence” device. For each MVK patient and control 1000 cells were seeded per well (0.32 cm²/well) and proliferation was measured over 200 hours in 30-minute intervals. For MVK1, 2, 6, 8 and 9 also 2000 cells were seeded. Specific growth rate and doubling time were derived from the individual growth curves in duplicates. The growth curves for seeding density 1000 can be seen in Figure 22. The control showed a specific growth rate of $0.0146 \text{ h}^{-1} \pm 0.0002 \text{ h}^{-1}$ and a doubling time of $30 \text{ h} \pm 0.064 \text{ h}$. The new patient MVK9 did show the lowest growth rate (0.0002 h^{-1}) and the highest doubling time ($333.7 \text{ h} \pm 24.3 \text{ h}$) compared to all other patients, followed by MVK8 (0.0006 h^{-1} and $120.5 \text{ h} \pm 3.8 \text{ h}$). Interestingly, MVK1 and MKV2 demonstrated slightly higher specific growth rate (0.017 h^{-1} and 0.180 h^{-1} respectively) than the control.

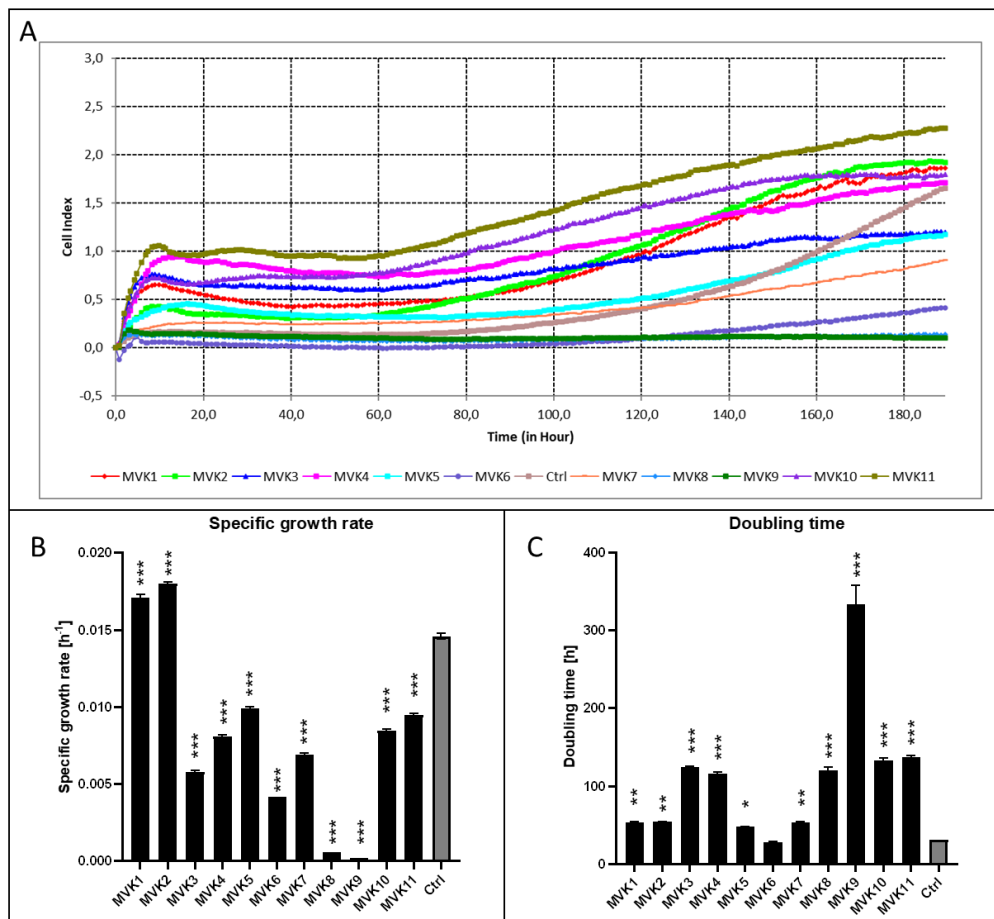


Figure 22 - Growth curves, specific growth rates and doubling times for 1000 cells per well. (A) Individual growth curves for MVK patients and control were acquired in duplicates with RTCA-proliferation assay over a period of 200 hours with measurement intervals of 30 minutes. Fibroblasts were seeded at 1000 cells per well and (B) specific growth rate and (C) doubling time were determined as noted in section 6.1.6.

For MVK1, 2, 6, 8, 9 and control also 2000 cells were seeded to see if the starting density changes the acquired parameters. Under this condition the control had a specific growth rate of $0.025 \text{ h}^{-1} \pm 0.0003 \text{ h}^{-1}$ and a doubling time $42 \text{ h} \pm 0.52 \text{ h}$. The selected MVK patients showed all a significantly decreased specific growth rate and a significantly elevated doubling time.

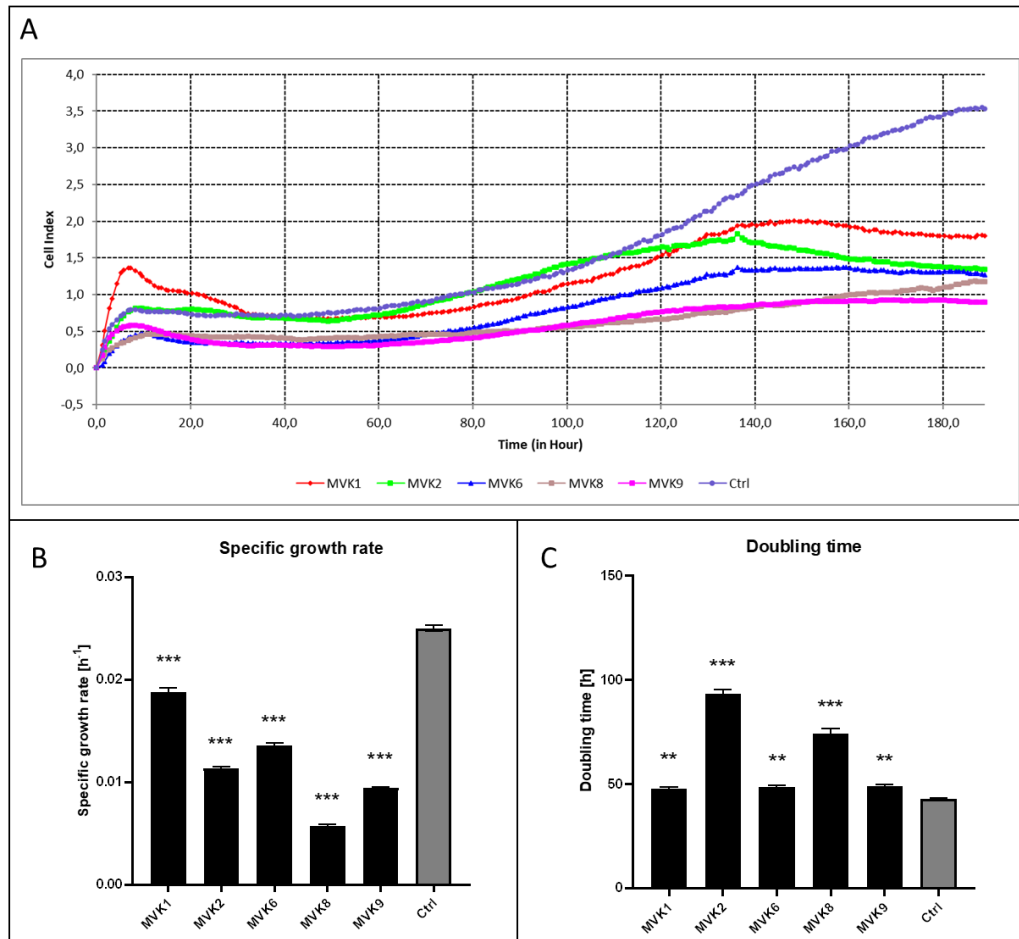


Figure 23 - Growth curves, specific growth rate and doubling time for 2000 cells per well. (A) Individual growth curves for MVK patients and control were acquired in duplicates with RTCA-proliferation assay over a period of 200 hours with measurement intervals of 30 minutes. Fibroblasts were seeded at 2000 cells per well and (B) specific growth rate and (C) doubling time were determined as noted in section 6.1.6.

7.4 Analysis of glycans by lectin blots

As the MVK defect is located within the isoprenoid pathway, which among other products also allocates dolichol, it was of interest to find out whether this deficiency might affect glycosylation. To address this question, lectin binding studies with protein extracts from patient fibroblasts were performed. Lectins are able to recognize various specific sugar structures and sugar linkages. As lectins do not bind to a specific protein size, quantification was performed for the entire lane of one patient's lysate on the SDS-PAGE compared to the loading control.

7.4.1 An increase of mannose/glucose residues

The lectin *Narcissus pseudonarcissus* (NPA) binds specific α -mannose residues. As seen in Figure 24, MVK patients showed a significantly increased signal ranging from 104 % \pm 3 % (MVK5) to 190 % \pm 46 % (MVK1) compared to controls (n=3). Taking all MVK patients together resulted in an increase to 140 % \pm 26 % compared to controls.

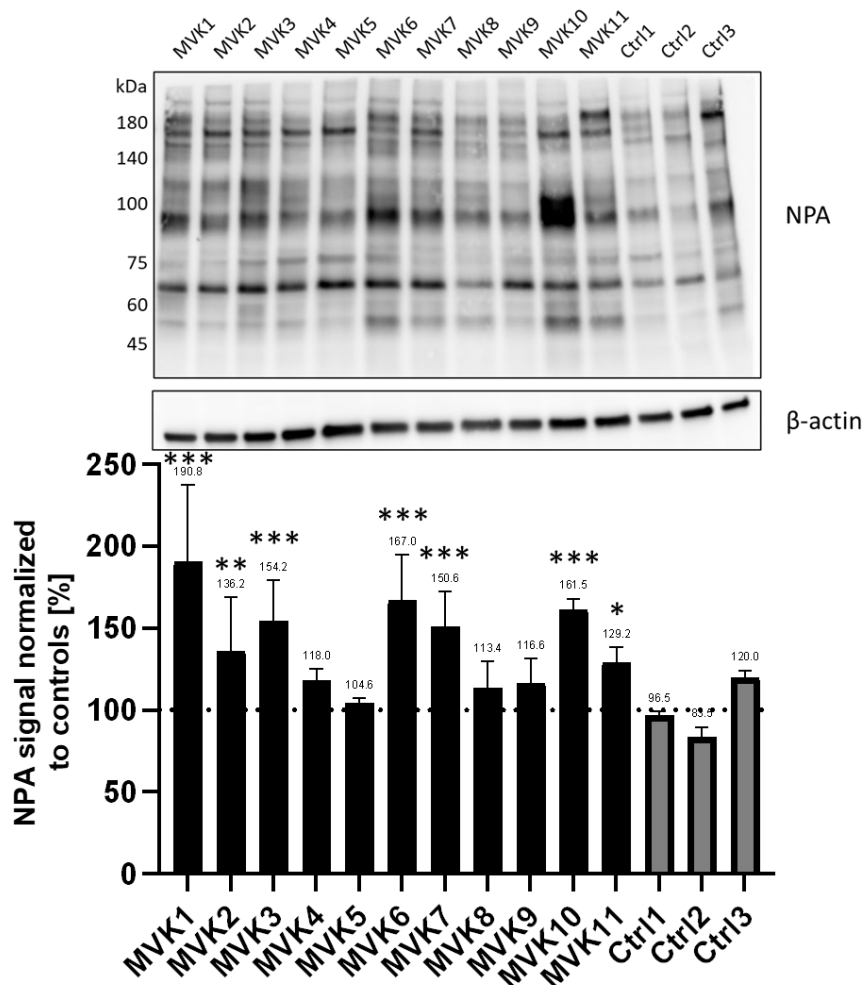


Figure 24 - NPA lectin blot and quantification. Depicted are the lectin blot and the quantification results to the β -actin loading control. Data are presented as biological replicates' mean \pm SD (n=3).

Another lectin that recognizes α -mannose and additional α -glucose residues is *Concanavalin A* (ConA). All MVK patients displayed (Figure 25) a significantly increased signal ranging from 123 % \pm 4 % (MVK4) to 380 % \pm 8% (MVK6) compared to controls (n=2). Taking all MVK patients together they presented an increase of up to 206 % \pm 75 % compared to controls.

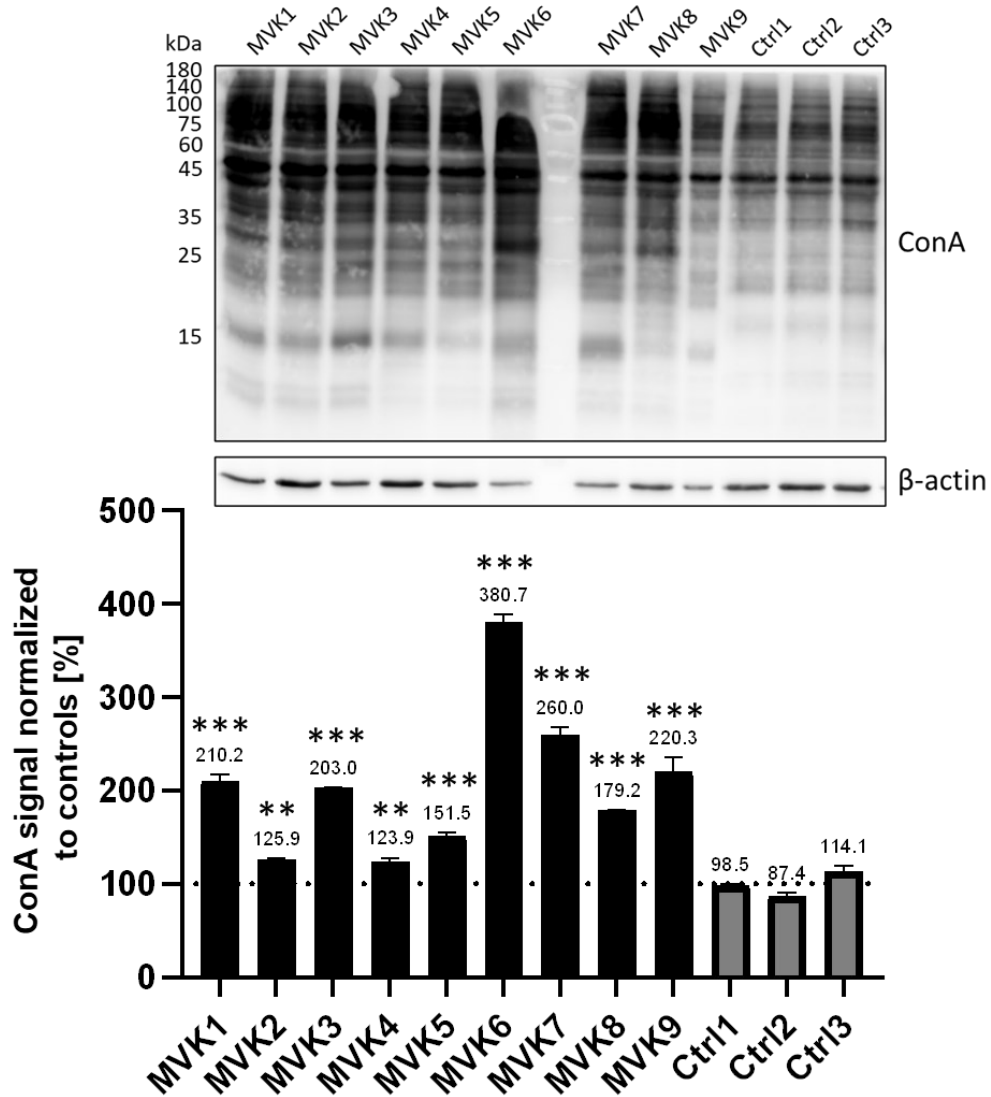


Figure 25 - ConA lectin blot and quantification. Depicted are the lectin blot and the quantification results to the β -actin loading control. Data are presented as biological replicates' mean \pm SD (n=2).

The lectins *Galanthus nivalis* (GNA) (n=2) and *Lens culinaris* (LCH) (n=1) recognize both mannose residues, LCH also additional glucose and core fucosylation. All MVK patients showed an increased signal for both lectins, except for MVK9. Taking all MVK patients together resulted in an increase of up to 155% ± 31 % for GNA and 173% ± 50 % for LCH compared to controls.

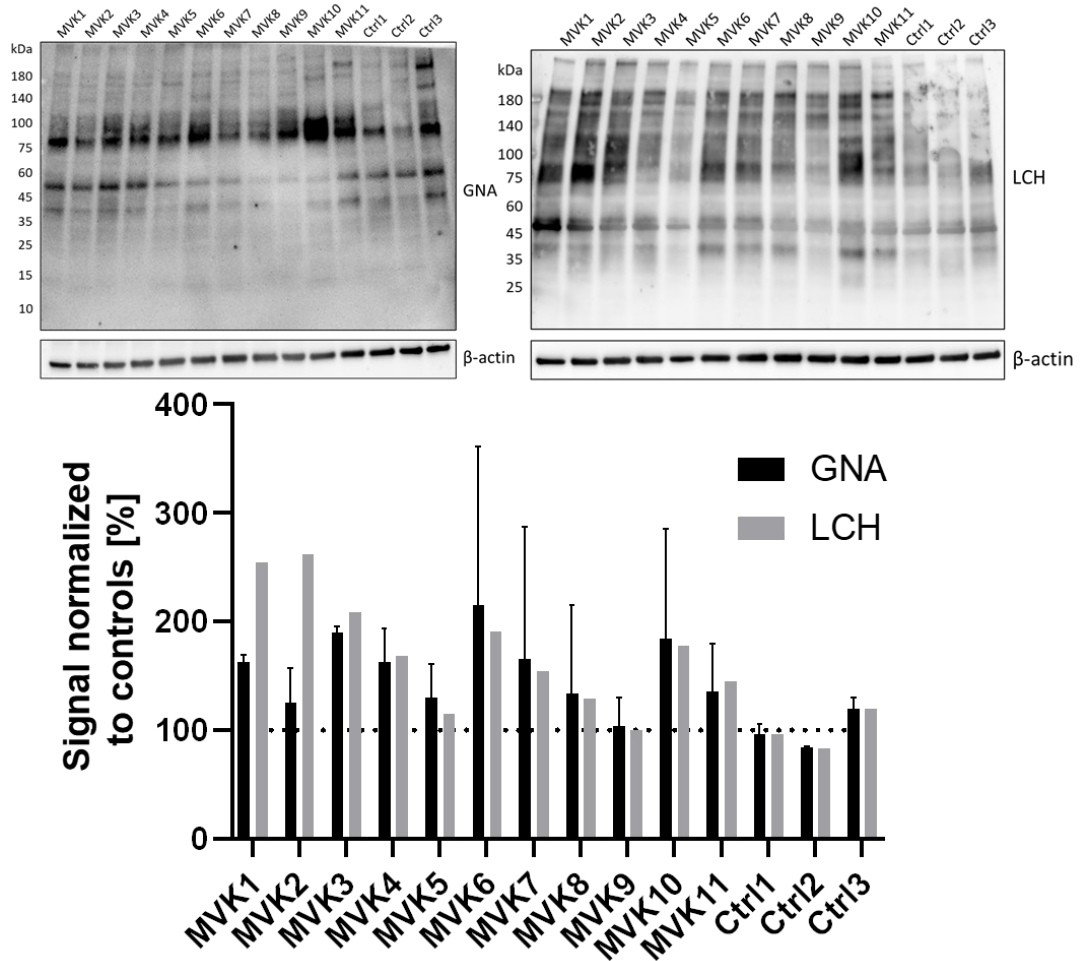


Figure 26 - GNA and LCH lectin blots and quantification. Depicted are the lectin blots and the quantification results to the β-actin loading control. Data are presented as biological replicates' mean ± SD (n=2).

For the recognition of β 1-2-mannose-GlcNAc residues the lectin *Phaseolus Vulgaris* *Leucoagglutinin* (PHA-L) (n=1) was used. MVK1 - 7 showed an increased signal, whereas MVK8 - 11 a decreased one. The lectin *Datura stramonium* (DSL) was used for the detection of β 1-6-mannose-GlcNAc, β 1-2-mannose-GlcNAc and GlcNAc residues. All MVK patients displayed an elevated signal compared to controls. MVK6 with 232 % had the highest increase followed by MVK2 (230 %) and MVK1 (229 %). Taking all MVK patients together resulted in a signal strength of $110\% \pm 33\%$ for PHA-L and $177\% \pm 46\%$ for DSL compared to controls.

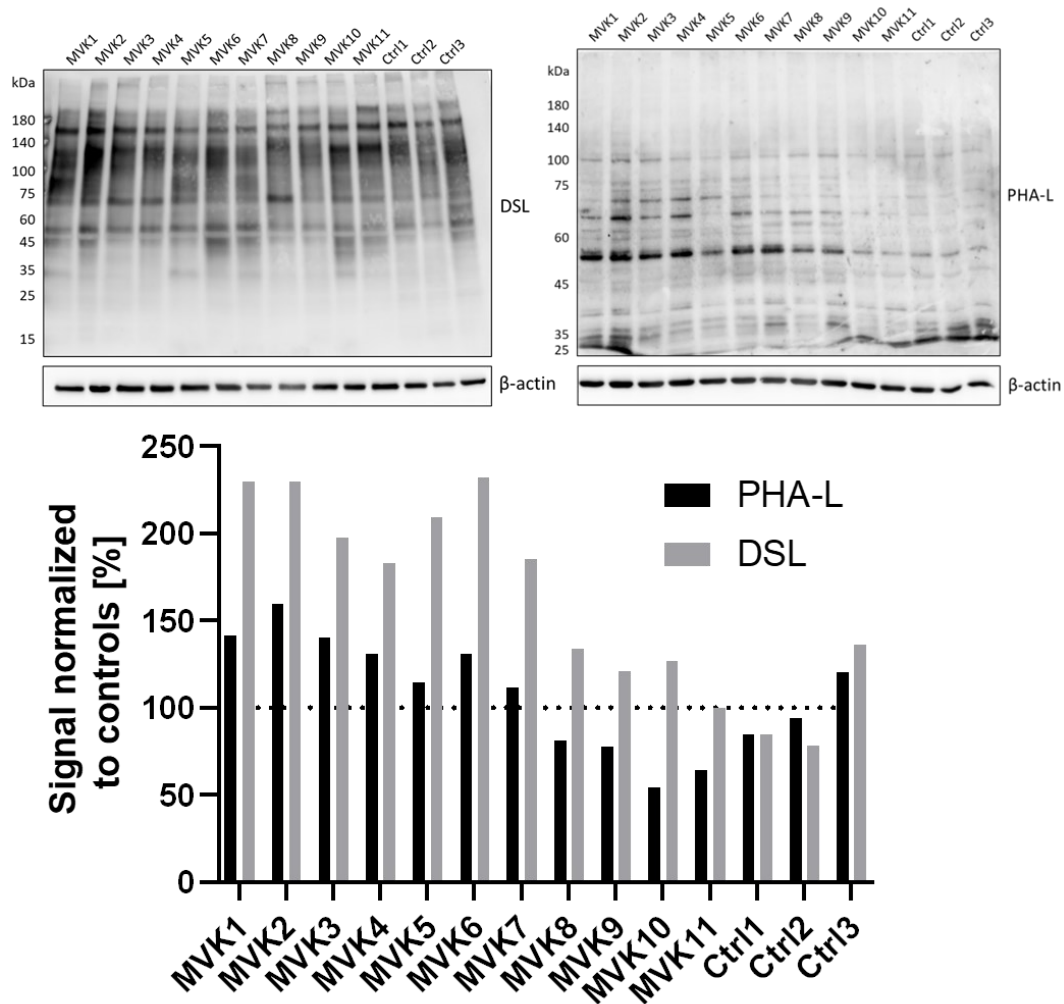


Figure 27 - PHA-L and DSL lectin blots and quantification. Depicted are the lectin blots and the quantification results to the β -actin loading control.

7.4.2 An increase of fucose residues

The lectin *Aleuria aurantia* (AAL) binds specifically to fucosylated structures. As seen in Figure 28, all MVK patients showed an increased signal ranging from 121.5 % (MVK2) to 213.3 % (MVK11) compared to controls. Taking all MVK patients together resulted in an increase to 155% ± 25 % compared to controls.

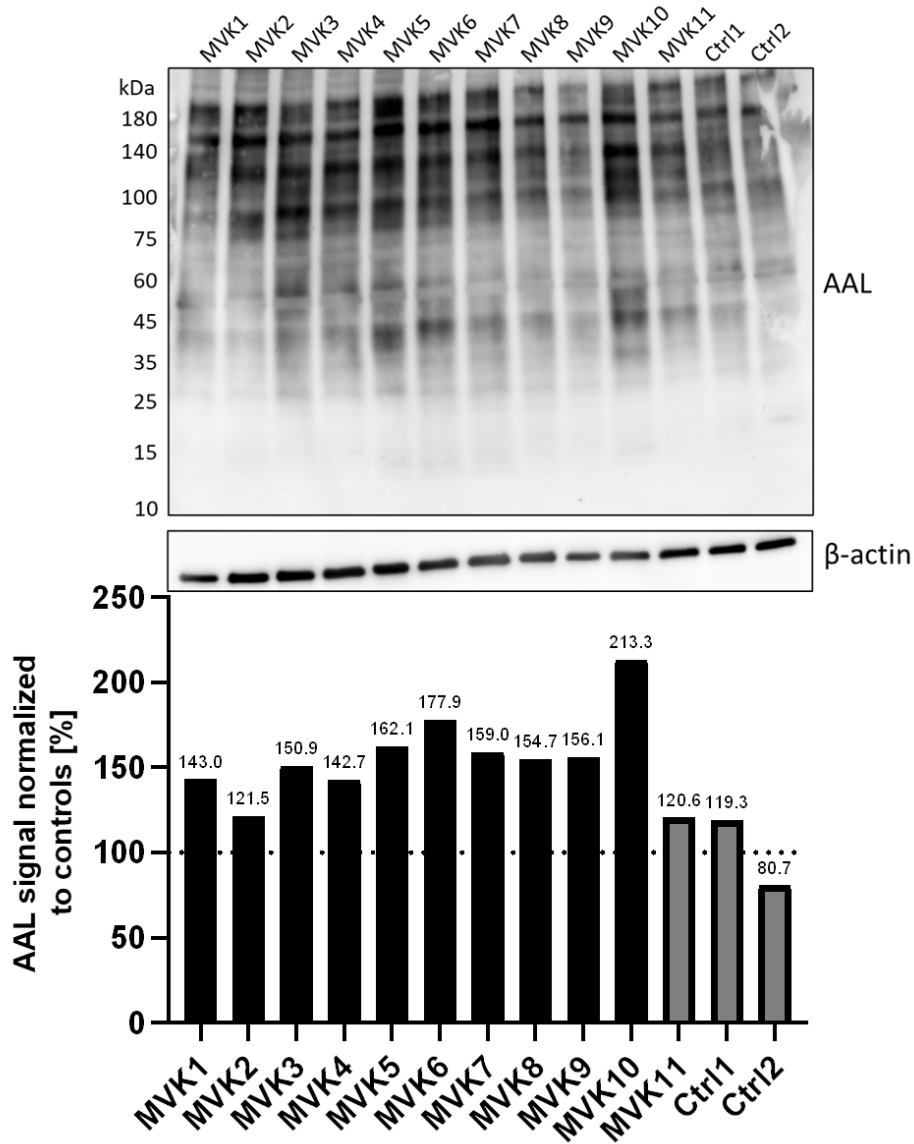


Figure 28 - AAL lectin blot and quantification. Depicted are the lectin blot and the quantification results to the β -actin loading control.

7.4.3 Sialic acid residues

For the recognition of sialic acid residues, the lectin *Maackia amurensis* *Leukoagglutinin I* (MAL I) (n=1) was used. MVK patients showed an increased sialylation status (except for MVK 11) ranging from 131.1 % (MVK3) to 218.5 % (MVK8) compared to controls. Taking all MVK patients together resulted in an increase to 169% \pm 40 % compared to controls.

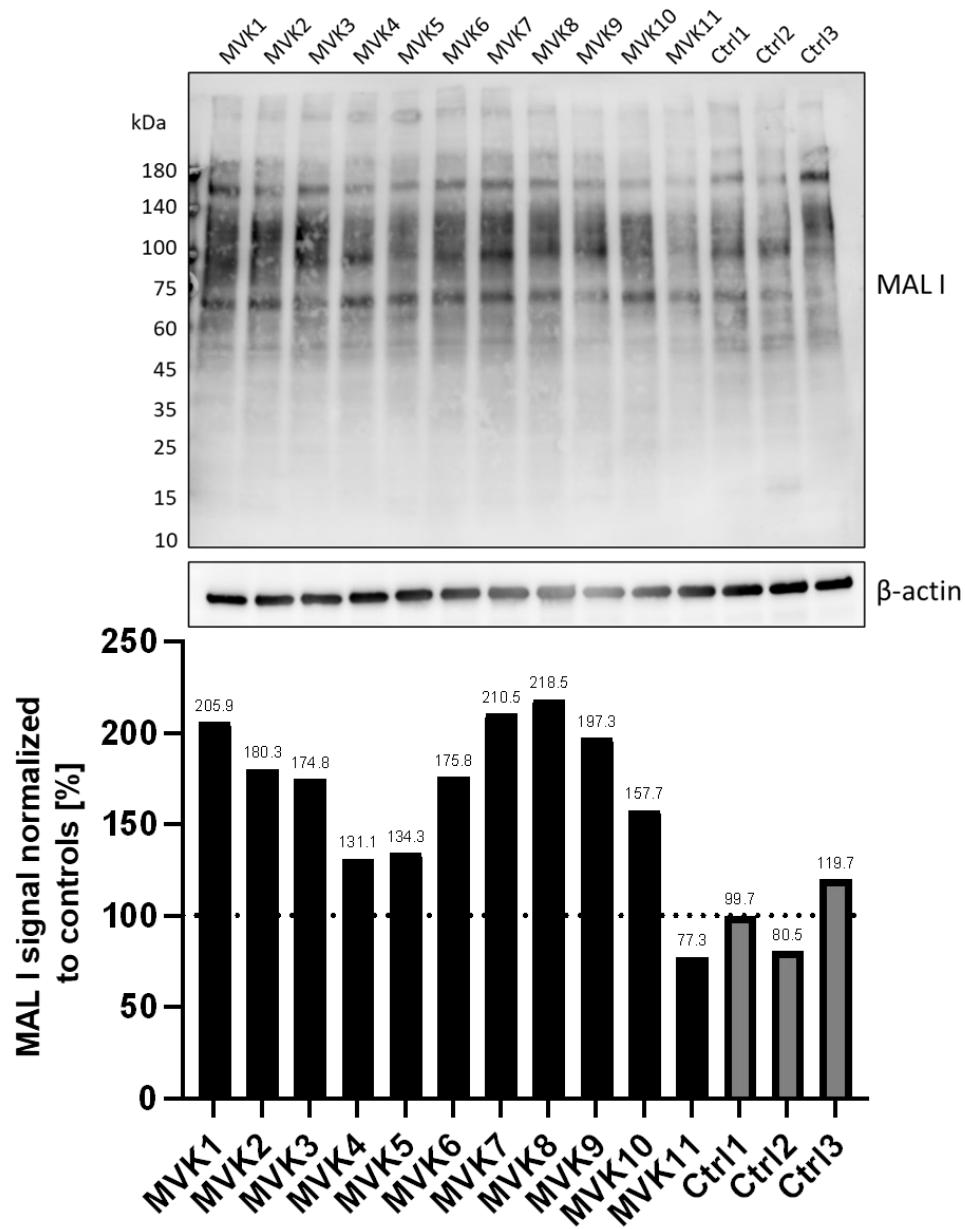


Figure 29 - MAL I lectin blot and quantification. Depicted are the lectin blot and the quantification results to the β -actin loading control.

The lectin *Sambucus nigra* (SNA) detects sialic acid residues attached to terminal galactose. The results are quite diverse. MVK1 (190 % ± 16 %), MVK3 (106 ± 2.5 %) and MVK 7 (157.2 ± 6 %) showed an increase. MVK6 was excluded from analysis, as some protein degradation was seen. The other MVK patients showed a slight decrease. The lectin *Wheat germ agglutinin* (WGA) recognizes N-acetyl-D-glucosamine and sialic acid residues. MVK 6 was excluded here as well. A slight increase for MVK patients was visible.

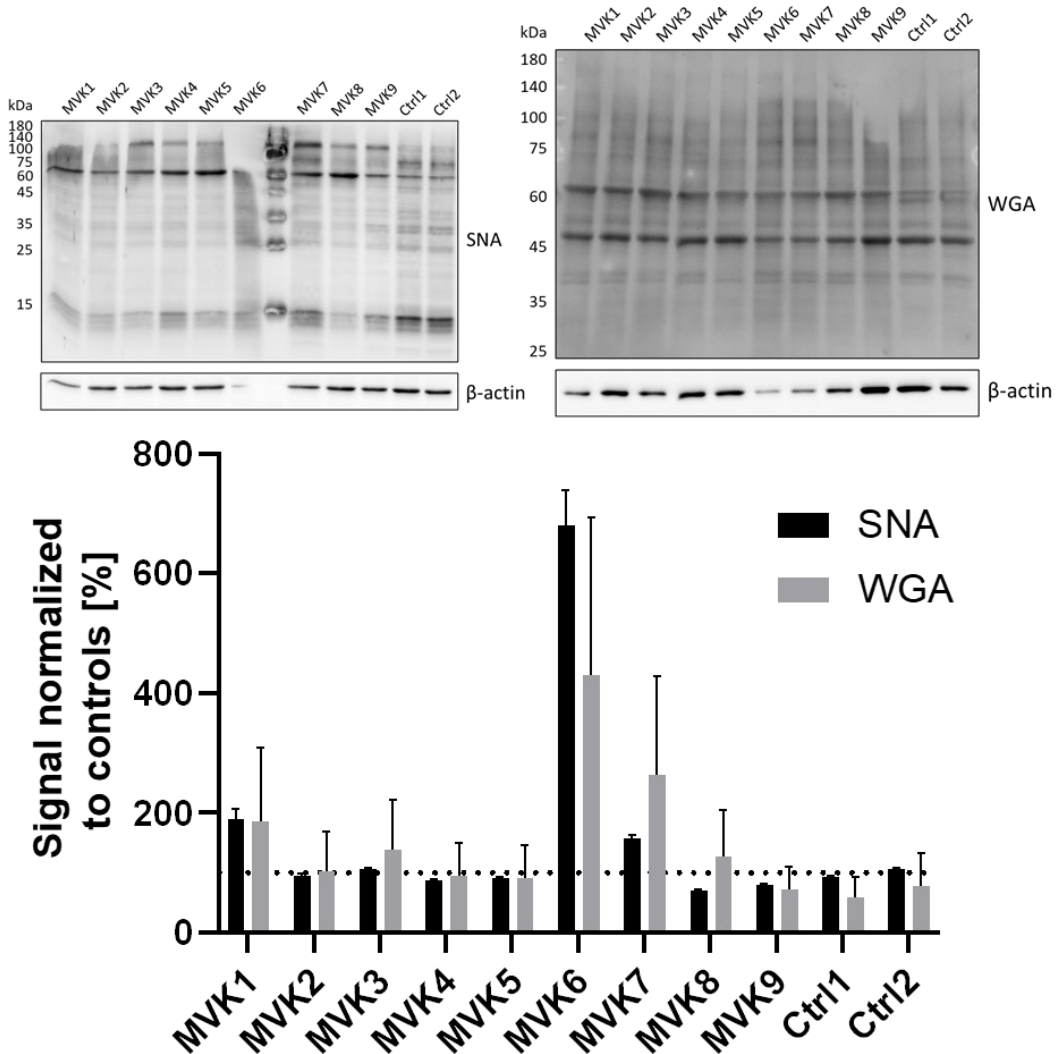


Figure 30 - SNA and WGA lectin blots and quantification. Depicted are the lectin blots and the quantification results to the β -actin loading control. Data are presented as biological replicates' mean \pm SD (n=2). MVK6 was excluded, as protein degradation was visible.

7.4.4 Galactose residues

The lectin *Erythrina Cristagalli* (ECL) binds preferable to galactose residues. Five of the MVK patients (MVK1, 2, 6, 10, 11) showed an increase while the other ones showed a decrease in signal.

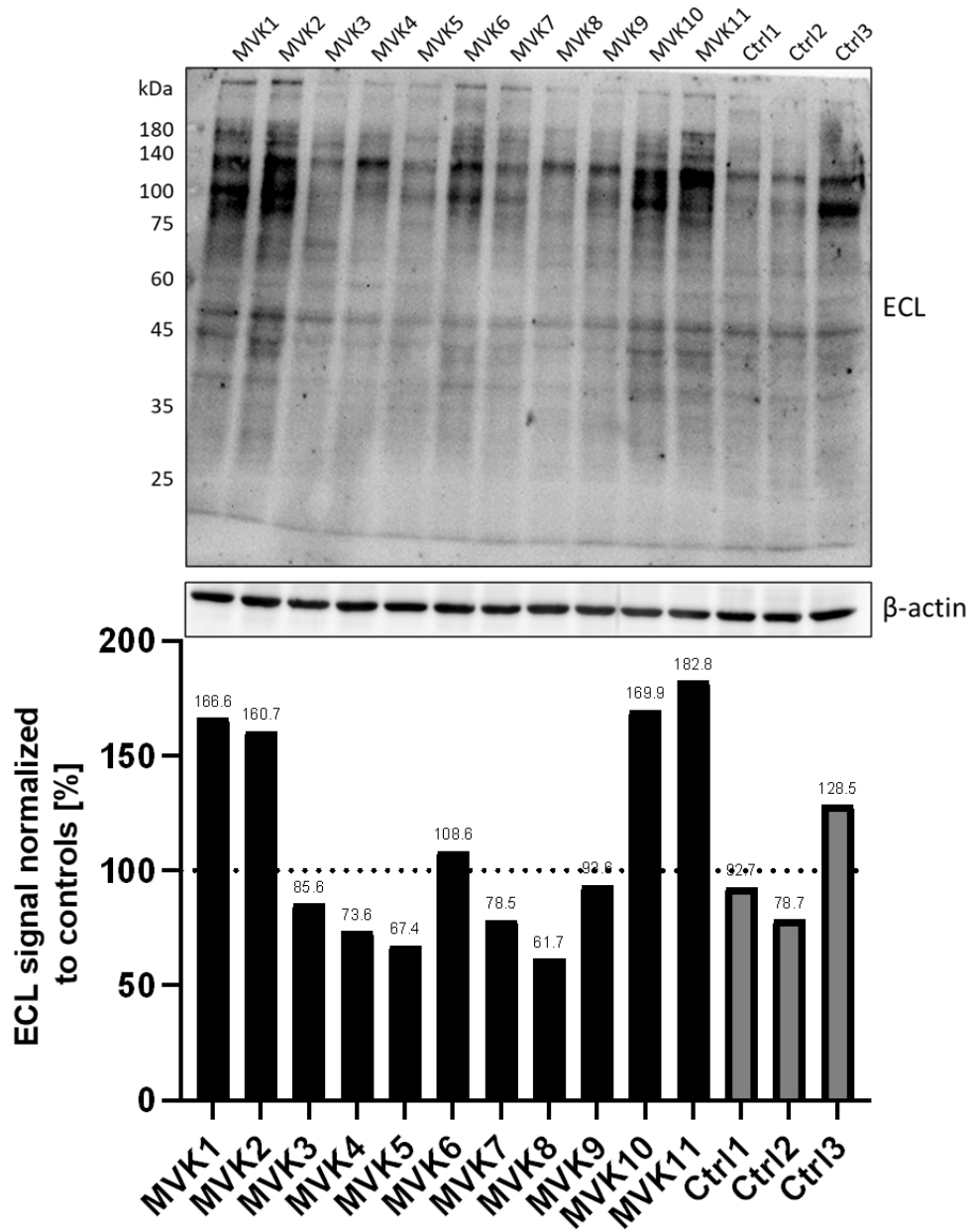


Figure 31 - ECL lectin blot and quantification. Depicted are the lectin blot and the quantification results to the β -actin loading control.

7.5 Analysis of glycosylation markers

Since the analysis of the lectin blots showed changes in the glycosylation status of the MVK patients, next the impact of MVK deficiency on glycoprotein markers was elucidated. In this course, the markers ICAM1 (intercellular adhesion molecule 1), LAMP1 (Lysosomal-associated membrane protein 1) and LAMP2 (Lysosomal-associated membrane protein 2) were analyzed by western blotting and quantification was performed. These proteins are highly glycosylated and therefore are suitable for the evaluation of the glycosylation status in the MVK patients.

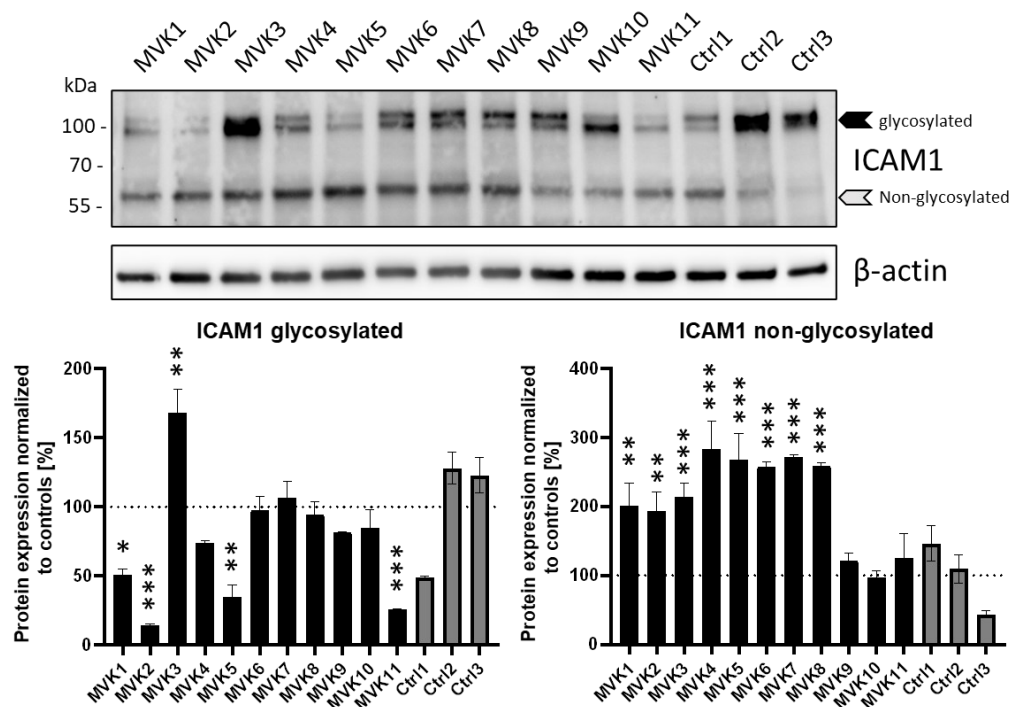


Figure 32 - ICAM1 western blots and quantification of glycoforms. Depicted are the western blot and the quantification results to the β -actin loading control for the glycosylated and non-glycosylated form. Data are presented as biological replicates' mean \pm SD (n=2).

The antibody for ICAM1 detects the glycosylated and non-glycosylated form of the respective protein. Glycosylated ICAM1 has a size of around 100 kDa and the non-glycosylated form of around 57 kDa as seen in the upper part in Figure 32. The ICAM1 signal was normalized to actin and compared to controls (n=2). The MVK patients showed a clearly reduced signal of the glycosylated ICAM1 (except MVK3, which showed an increased signal) and an increased signal of the non-glycosylated form. MVK10 had nearly normal non-glycosylated levels.

Ratios of glycosylated to non-glycosylated ICAM1 were also calculated and can be seen in Figure 33. All MVK patients demonstrated a significant reduction in the ratio compared to controls. MVK2 has the lowest ratio of 0.226 ± 0.001 ($p < 0.001$) followed by MVK 5 (0.389 ± 0.065 , $p < 0.001$) and MVK11 (0.627 ± 0.066 , $p < 0.001$), compared to

controls with 4.485 ± 1.628 . Patient MVK10 showed a normal level of non-glycosylated ICAM1, but when calculating the ratio, a clear reduction of 2.663 ± 0.667 ($p=0.003$) can be seen. The same applied for MVK3, which had an increased signal for the glycosylated form, but showed a significant decrease within the ratio (2.348 ± 0.506 , $p=0.001$).

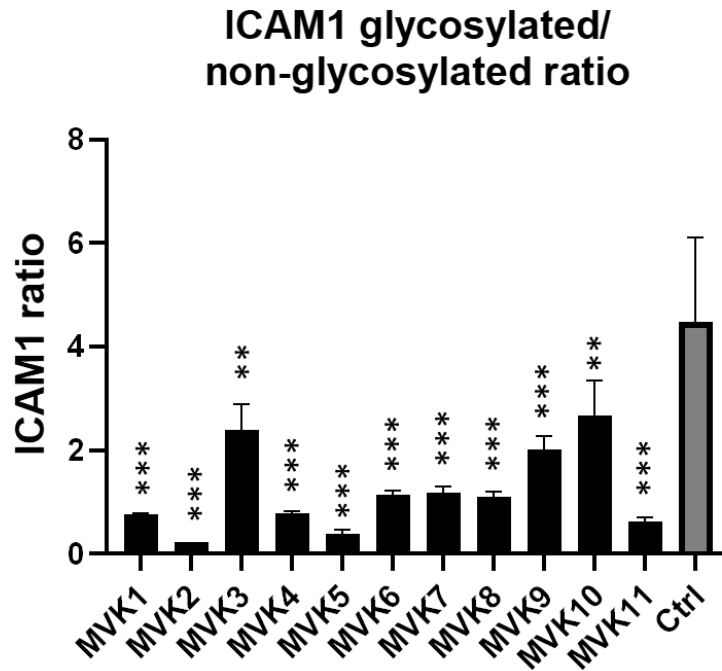


Figure 33 - ICAM1 ratio. Depicted are the calculated ICAM1 ratios of the glycosylated to non-glycosylated form. Data are presented as biological replicates' mean \pm SD ($n=2$).

Next, the glycoprotein markers LAMP1 and LAMP2 were analyzed. The western blots can be seen in Figure 34 and Figure 35. When analyzing LAMP1 especially MVK1, 2, 3, 7, 8, 9, 10 and 11 showed a significant overexpression and also a broader band compared to the controls, which indicates the presence of under-glycosylated protein. This was also seen for MVK4, 5 and 6 with comparable protein amounts to controls.

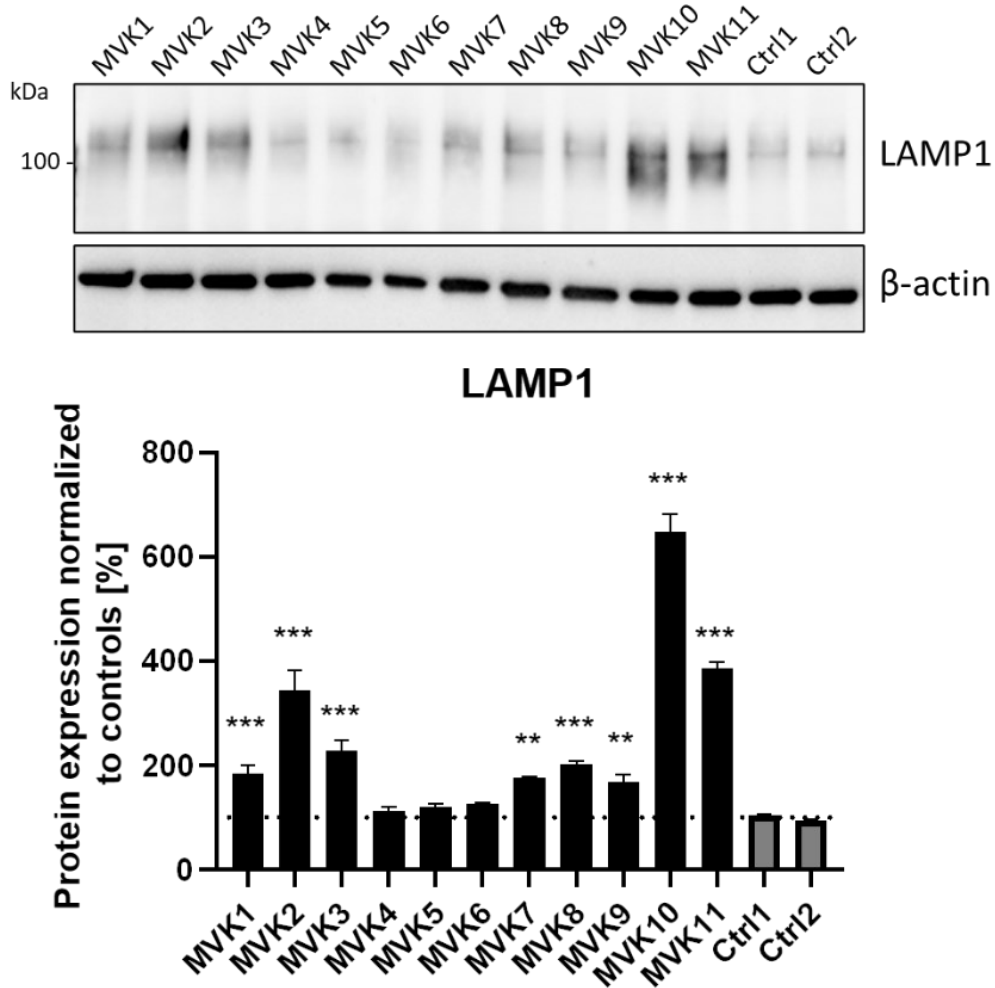


Figure 34 - LAMP1 western blot and quantification. Depicted are the western blot and the quantification results to the β -actin loading control. Data are presented as biological replicates' mean \pm SD (n=2).

When analyzing LAMP2, the effect of the broader protein band was even more dominant in MVK patients compared to controls. The controls also showed a slight smear of the band, whereas the smear of the MVK patients was even more prominent. For MVK1, 3, 5, 6 and 10 it appeared that LAMP2 is significantly more expressed compared to controls.

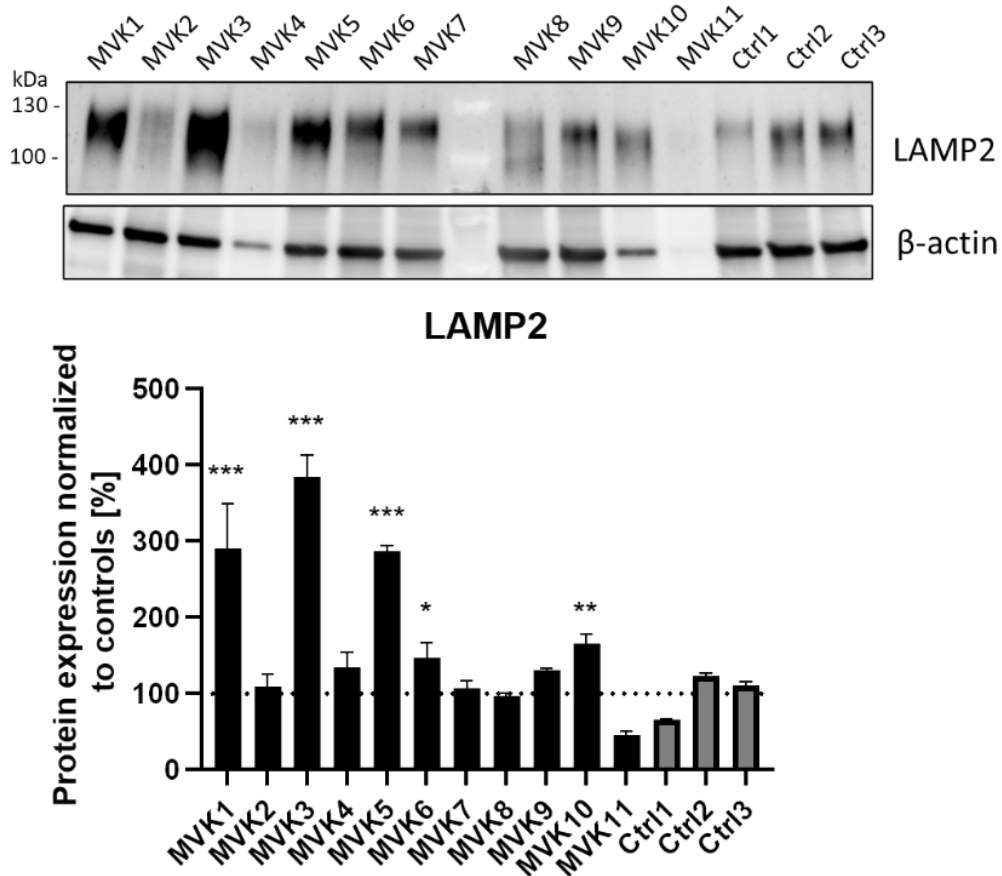


Figure 35 - LAMP2 western blot and quantification. Depicted are the western blot and the quantification results to the β -actin loading control. Data are presented as biological replicates' mean \pm SD (n=2). β -actin for MVK4 shows less protein amount compared to other samples. The western blot of patient MVK11 failed, as there is also no β -actin signal visible.

7.6 Total N-glycan analysis by xCGE-LIF technology

As the lectin binding studies revealed complex changes in glycosylation of the patients' fibroblasts, total N-glycans were subsequently determined by high performance multiplexed capillary gel electrophoresis with laser-induced fluorescence detection (xCGE-LIF) from patients MVK2, 8 and 9 and compared to three different controls. These patients were chosen as they presented the most severe phenotype. Measurement in biological triplicates (n=3) was performed in cooperation with the group of Erdmann Rapp (MPI Magdeburg). In total, 29 N-glycans have been measured and compared to the controls. Structures were determined in normalized peak height (TPH = total peak height).

Individual electropherograms of MVK2, 8 and 9 compared to controls can be seen in Figure 36. The corresponding peak assignment can be found in Table 35. A = Number of glycan antenna, F = fucose (F at the beginning depicts core connection), G = galactose, S = sialic acid, B = bisecting, and in brackets is the glycosidic bond; number behind the sugar is the amount.

Table 35 - Peak assignment for electropherograms.

| Peak # | Structural Assignment | Type | Sialylation | Fucosylation |
|--------|---|--------------|-----------------|----------------|
| 1 | Man2 | high-mannose | no | no |
| 2 | A3G3S1(2,3)[3,4] S2(2,6) | complex | tri-sialylated | no |
| 3 | A2G2S2(2,6) | complex | di-sialylated | no |
| 4 | A2G2S1(2,6)S1(2,3) | complex | di-sialylated | no |
| 5 | A2BG2S2(2,6) | complex | di-sialylated | no |
| 6 | A1G1S1(2,6)[3] | hybrid-type | mono-sialylated | no |
| 7 | Man3 | high-mannose | no | no |
| 8 | A2G2S2(2,3) | complex | di-sialylated | no |
| 9 | FA2BG2S2(2,6) | complex | di-sialylated | Core |
| 10 | FA2G2S2(2,3) | complex | di-sialylated | Core |
| 11 | A3[2,4]S1(2,6)G1(3) [3,4]G2(4)S1(2,6)[3,2] | complex | di-sialylated | No |
| 12 | FA2F1(1,3)G2S2(2,3) | complex | di-sialylated | antenna & core |
| 13 | FMan3 | hybrid | no | core |
| 14 | A3G3S1(2,3)S1(2,6) | complex | di-sialylated | no |
| 15 | A2G2S1(2,6) | complex | mono-sialylated | no |

Results

| | | | | |
|----|-----------------|--------------|-----------------|------|
| 16 | A2G2S1(2,3)[3] | complex | mono-sialylated | no |
| 17 | Man5 | high-mannose | no | no |
| 18 | FA2G2S1(2,3)[6] | complex | mono-sialylated | core |
| 19 | FA2G2S1(2,3)[3] | complex | mono-sialylated | core |
| 20 | Man6 | high-mannose | no | no |
| 21 | FA2BG0 | complex | no | core |
| 22 | Man7[D1] | high-mannose | no | no |
| 23 | Man7[D3] | high-mannose | no | no |
| 24 | A2G2 | complex | no | no |
| 25 | Man8 | high-mannose | no | no |
| 26 | Man9 | high-mannose | no | no |
| 27 | FA2G2 | complex | no | Core |
| 28 | Man9-Glc | high-mannose | no | No |
| 29 | FA3G3[2,6] | complex | no | Core |

Patient MVK2 had a significant increase of the high-mannose structures Man2 (+1.6 % TPH, $p=0.001$), Man3 (+1.0 % TPH, $p=0.004$), Man9 (+0.24 % TPH, $p=0.02$) and a significant decrease of the di-sialylated complex structures A2G2S1(2,6)S1(2,3) (-3.3 % TPH, $p=0.002$) and FA2BG2S2(2,6) (-2.1 % TPH, $p=0.03$). Core fucosylated structures FA2F1(1,3)G2S2(2,3) (+0.5 % TPH, $p=0.0002$), FA2G2S1(2,3)[6] (+0.54 % TPH, $p=0.0004$), FA2G2S1(2,3)[3] (+1.4 % TPH, $p=0.0003$) and FA2G2 (+4.2% TPH, $p=0.000001$) were all increased compared to controls.

Patient MVK8 had a significant decrease of the high-mannose structures Man8 (-2.1 % TPH, $p=0.0006$), Man9 (-1.1 % TPH, $p=0.000001$) Man9-Glc (-0.31 % TPH, $p=0.005$) and Man7[D3] (-0.48 % TPH, $p=0.04$). A markedly increase of the core fucosylated structures FMan3 (+6.9 % TPH, $p=0.00003$) was dominant in this patient whereby the other core fucosylated structures FA2G2S2(2,3) (-2.2 % TPH, $p=0.01$) and FA2F1(1,3)G2S2(2,3) (+0.27 % TPH, $p=0.008$) were decreased. Sialylated structures like A2G2S2(2,6) (+2.0 % TPH, $p=0.02$), A3G3S1(2,3)S1(2,6) (+0.81 % TPH, $p=0.0001$) and A3[2,4]S1(2,6)G1(3)[3,4]G2(4)S1(2,6)[3,2] (+0.41 % TPH, $p=0.001$) were slightly increased.

Patient MVK9 showed a significant elevation of the high-mannose structures Man2 (+2.4 % TPH, $p=0.0001$), Man3 (+1.2 % TPH, $p=0.001$) and Man5 (+1.5 % TPH, $p=0.02$), as patient MVK2. The glycan Man9 demonstrated a slight decrease of - 0.75 % TBH($p=0.00001$), whereas sialylated structures such as A2BG2S2(2,6) (+1.0 % TPH,

$p=0.00001$), A2G2S1(2,6) (+0.55 % TPH, $p=0.00001$) and A3G3S1(2,3)[3,4]S2(2,6) (+0.45 % TPH, $p=0.046$) were slightly increased.

All three MVK patients were increased in the core fucosylated structure FMan3.

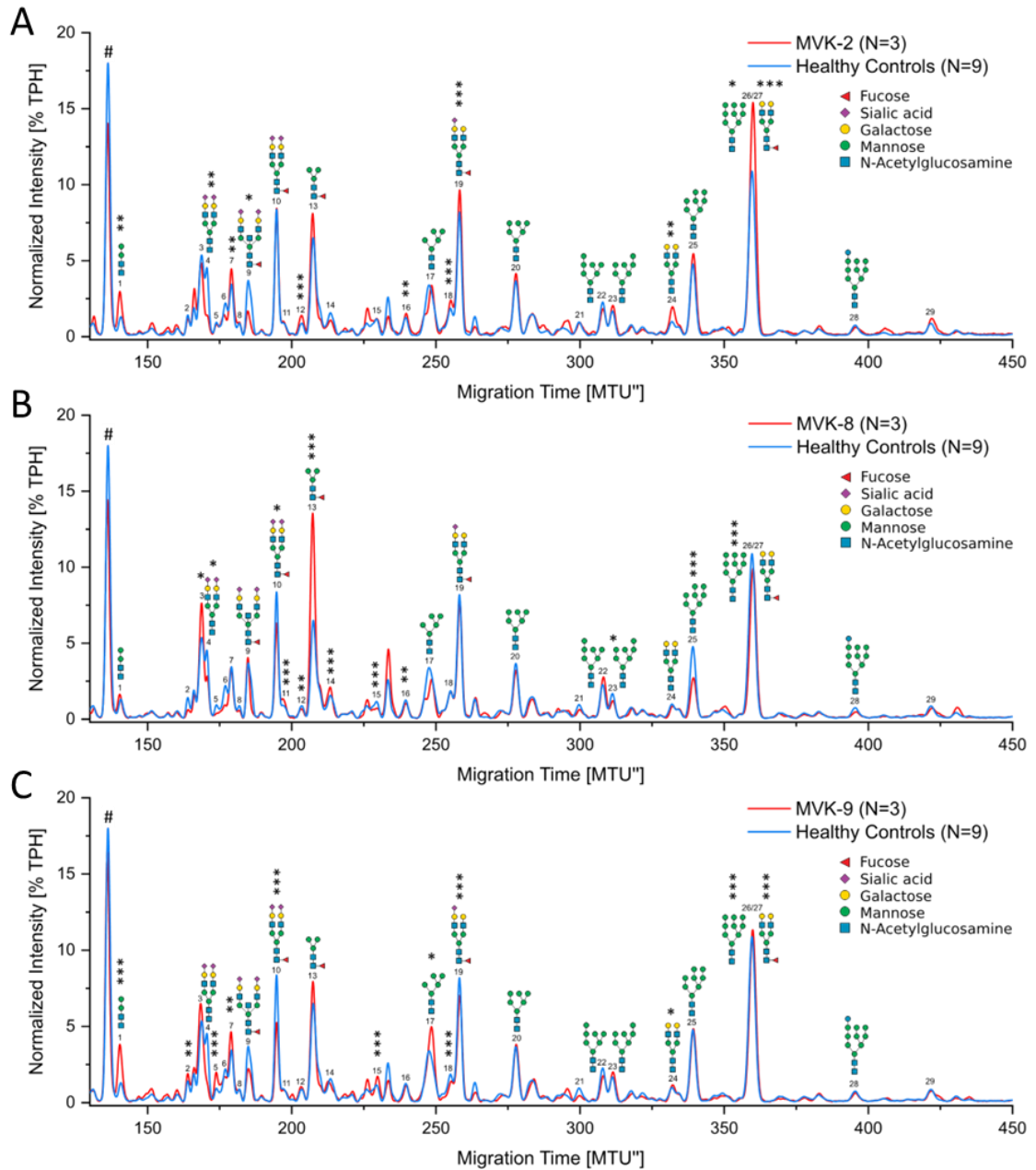


Figure 36 - xCGE-LIF electropherograms of MVK2, 8 and 9 compared to controls. (A) Electropherogram of MVK2 and controls **(B)** Electropherogram of MVK8 and controls **(C)** Electropherogram of MVK9 and controls. # is the internal standard. Figure created by Valerian Grote (MPI).

In general, N-glycans are distinguished in complex types, high mannose types and hybrid types. Quantification was done for these groups (see Figure 37). Normally, the

N-glycans of the complex type (control 60.6 % ± 7.1 %) are the most abundant followed by high mannose type (control 29 % ± 3.8 %) and hybrid type (control 10.5 % ± 2.9 %). This general pattern was also visible for the patients MVK2, 8 and 9 whereby small changes were visible. For the MVK patients, the complex type glycans were reduced with -2.5 % for MVK2, -3.2 % for MVK8 and 7.7 % for MVK9. MVK2 (+2.3 %) and MVK9 (+6.4 %) showed an increase in high mannose type glycans whereby MVK8 had a decrease of -3.1 %. All patients were elevated in hybrid type glycans. However, MVK8 showed the highest increase with 7.1 % followed by MVK9 (+1.2 %) and MVK2 (+0.1 %).

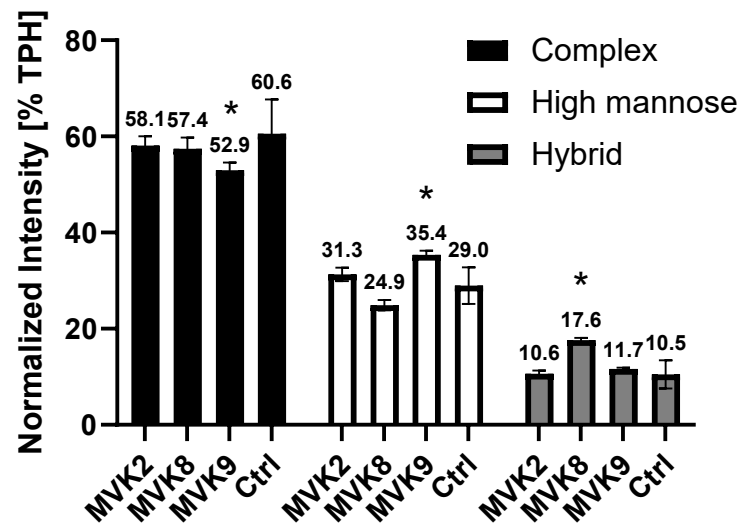


Figure 37 - Glycan type distribution in MVK2, 8, 9 and controls. The measured glycan peaks were divided into complex, high mannose, and hybrid types. Normalized intensities were added up.

The normalized peak height of the measured glycans of fibroblast lysates from MVK2, MVK8, MVK9 and controls can be seen in Figure 38.

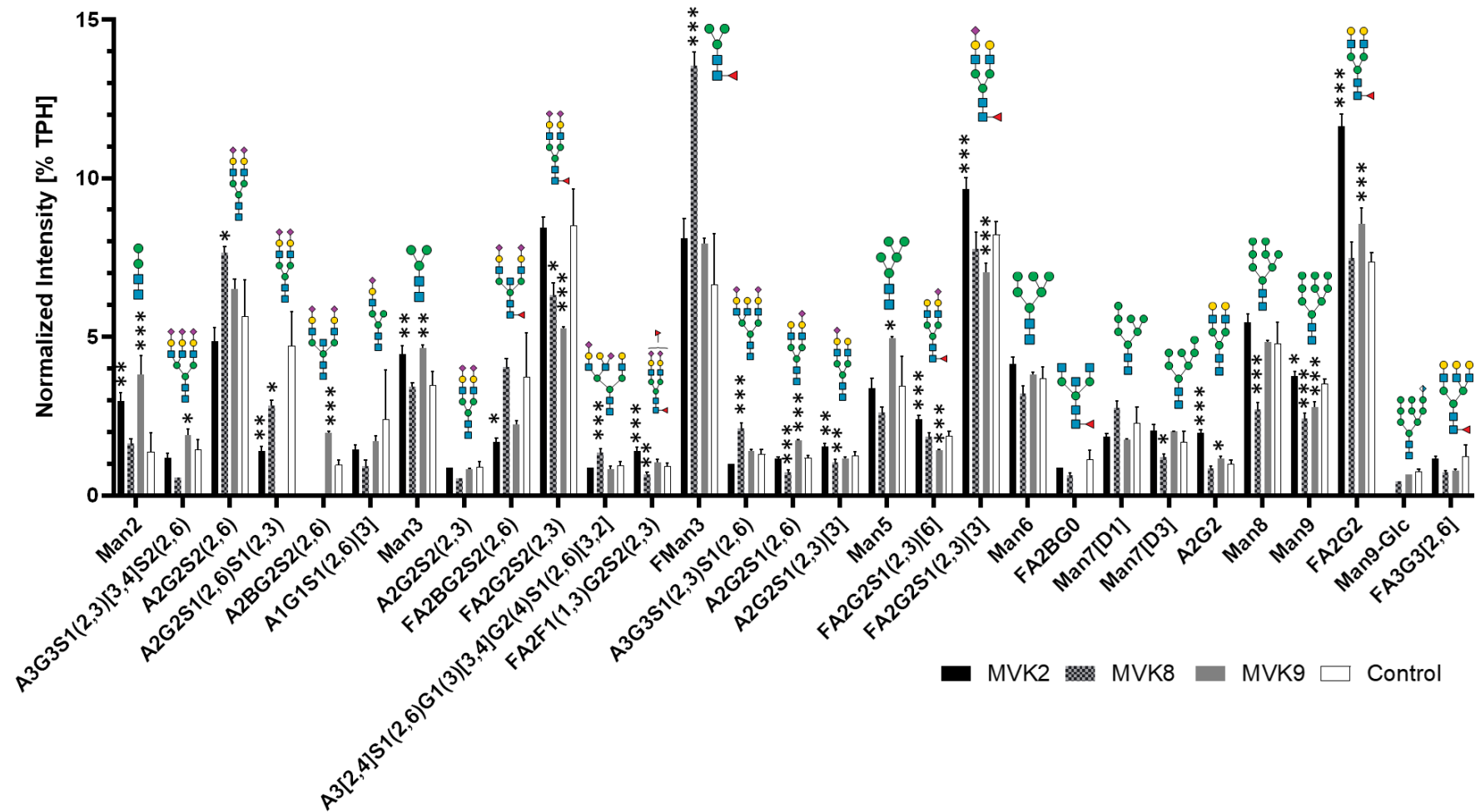


Figure 38 - N-glycan analysis of MVK patients and controls from fibroblasts by xCGE-LIF. Depicted are the 29 measured N-glycans from MVK2, 8,9 and controls. A = Number of glycan antenna, F = fucose (F at the beginning = core connection), G = galactose, S = sialic acid, B = bisecting and in brackets is the glycosidic bond; number behind the sugar is the amount.

7.7 Glycosphingolipid analysis by xCGE-LIF

Glycosphingolipid (GSL) measurement of patient MVK9 and a control in biological triplicates ($n=3$) was performed in cooperation with the group of Falk Büttner (Medical School Hannover). 17 glycan peaks were detected and analyzed. The normalized peak intensities can be seen in Figure 39.

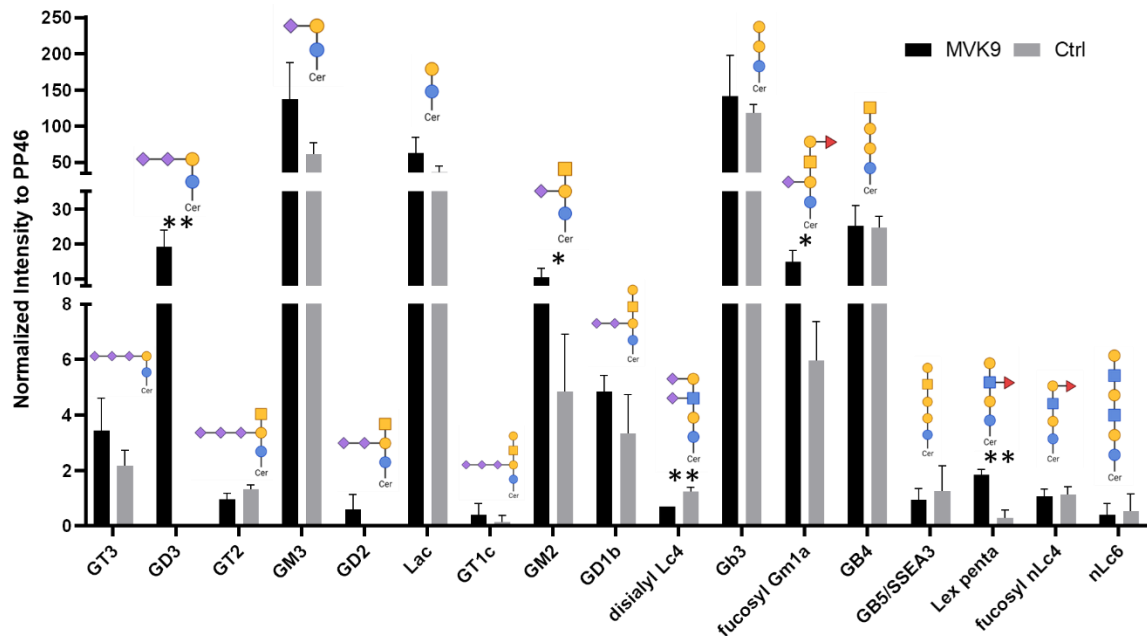


Figure 39 - GSL analysis by xCGE-LIF. 17 glycan peaks were detected and analyzed. Normalized peak intensities to PP46 (internal standard) of MVK9 and control are depicted.

The ganglioside GD3 was significantly ($p=0.002$) increased in MVK9 ($19.2 \% \pm 4.7 \%$) when compared to control, where it was completely absent. Also, GD2 was absent in the control compared to MVK9. GM2 was significantly ($p=0.04$) elevated in MVK9 with $10.4 \% \pm 2.6 \%$ to $4.8 \% \pm 2.1 \%$ in the controls. A significant decrease ($p=0.004$) in the ganglioside disialyl Lc4 from $1.3 \% \pm 0.2 \%$ in the controls to $0.7 \% \pm 0.0 \%$ in MVK9 could be determined. Further, the fucosylated GSL fucosyl Gm1a ($14.9 \% \pm 3.2 \%$, $p=0.01$) and Lex penta ($1.8 \% \pm 0.2 \%$, $p=0.001$) were both significantly elevated in MVK9 compared to controls.

7.8 nCounter expression analysis of patients' fibroblasts

nCounter analysis was used to examine the expression profile of 72 genes, most of them highly relevant for N-glycosylation as well as O- and C-mannosylation pathways. Transcript quantities were determined from total RNA of MVK patients and controls derived fibroblasts. In the following figures (Figure 41 - Figure 51), only significant results are depicted. Expression of all genes can be found in the supplementary part 10.4. Data was normalized to the housekeeping genes *ACTB*, *C1orf43*, *GAPDH*, *RAB7A* and *SNRPD3* and the log₂ ratio compared to controls can be seen. MVK patients were measured in biological triplicates (n=3) and compared to controls (n=3). The following genes were analyzed:

Table 36 - nCounter genes

| | | | | | |
|-------|------------|---------|-----------|---------|---------|
| ACADL | ALG6 | DPY19L1 | GNF | MPI | RFT1 |
| ACOX3 | ALG8 | DPY19L2 | HSPA5 | OGT | SGK1 |
| ACTB | ALG9 | DPY19L3 | HiF1alpha | PGM1 | SLC35A1 |
| ALG1 | B3GalNAcT2 | DPY19L4 | MAN1A1 | PGM2 | SLC35A2 |
| ALG10 | B4GALT1 | FUT8 | MAN1B1 | PMM1 | SLC35A3 |
| ALG11 | C1orf43 | FUT9 | MAN2A1 | PMM2 | SLC35C1 |
| ALG12 | DHDDS | GALE | MGAT1 | POLR2A | SNRPD3 |
| ALG13 | DOLK | GANAB | MGAT2 | POMGnT1 | SRD5A3 |
| ALG14 | DPAGT1 | GAPDH | MGAT3 | POMGnT2 | ST3GAL3 |
| ALG2 | DPM1 | GFPT1 | MGAT5 | POMT1 | ST6GAL1 |
| ALG3 | DPM2 | GMPPA | MOGS | POMT2 | UAP1 |
| ALG5 | DPM3 | GMPPB | MPDU1 | RAB7A | mTOR |

Color legend: Cellular stress; Housekeeping; N-glycosylation; Nucleotide activated sugars; O-glycosylation; Dolichol synthesis; C-mannosylation; O-mannosylation; Transporter

In the following section, nCounter-data of the MVK patients is summarized, focusing on the main important results. In Figure 40, the significant results of all MVK patients together are depicted. The cellular stress genes **ACOX3**, **HiF1alpha** and **SGK1** were upregulated in the MVK patients. In this group, **SGK1** had the highest upregulation of 1.5 order of logarithmic magnitude. The expression level of **mTOR** was downregulated. For the **N-glycosylation**, in general, an upregulation can be seen. A few genes were downregulated which are **ALG10** (counts are very low and must be considered with caution), **ALG3**, **MGAT1** and **ST3GAL3**. The highest increase was seen in **B4GALT1** (1 order of logarithmic magnitude), **MAN1A1** (1.5 order of logarithmic magnitude) and **MAN2A1** (1 order of logarithmic magnitude). The transcript levels of **MAN1A1**,

MAN1B1, **MAN2A1**, **MGAT2** and **MGAT3**, which are involved in the N-glycan processing and synthesis of complex type glycans in the Golgi apparatus, were all upregulated in the MVK patients. For **FUT9**, a slight upregulation in transcript levels was visible. **FUT9** catalyzes the transfer of fucose from GDP-fucose to GlcNAc-residues of a distal lactosamine unit of a glycoprotein. In the group for **nucleotide activated sugars**, a downregulation for **GALE** (-1.2 order of logarithmic magnitude), **GMPPA**, **PGM2** (-1.2 order of logarithmic magnitude) and **UAP1** was found. An upregulation in transcript levels for **GFPT1** and **PGM1** was present. The **O-glycosylation** transcripts **B3GalNAcT2** and **OGT** were both increased in MVK patients. Interestingly, in the group of **dolichol synthesis**, which includes six genes, only **DPM2** was significantly affected and showed a slight downregulation. The next group is involved in **C-mannosylation** and includes **DPY19L1** to **DPY19L4**. An upregulation for **DPY19L1**, **DPY19L3** and **DPY19L4** was found, while **DPY19L2** was downregulated. The **O-mannosylation** transcripts **POMT1** and **POMT2** were both increased in MVK patients. The last group is the **transporter** group in which the transporters provide the sugar substrates for N-glycan processing in the Golgi apparatus. The two transporters **SLC35A2** (UDP-galactose translocator) and **SLC35C1** (GDP-fucose transporter 1) were both downregulated. **SLC35A1**, which is responsible for CMP-sialic acid transport, was decreased in transcript levels.

In Figure 41 - Figure 51 the results for the individual MVK patients can be found. Results equal or larger than 1 order of logarithmic magnitude were only considered in the following description. Results for **ALG10** were not considered, as counts are very low and must be considered with caution. Patient MVK1 has 32 genes in total, which were significantly deregulated. Together with MVK10 and MVK11, these showed the highest number of deregulated transcripts within all MVK patients. Increased transcription levels were found for **B4GALT1**, **MAN1A1**, **MAN2A1**, **PGM1**, **POMT2** and **SGK1** and decreased ones for **DPY19L2**, **GALE** and **PGM2**. In MVK2 a total of 21 genes were markedly deregulated. Upregulation can be seen for **MAN1A1** and **MAN2A1** while downregulation for the transcripts **GALE** and **PGM2** was found. Patient MVK3 had the lowest significant transcript hits of 13. A significant increase was present for **MAN1A1** and **SGK1**. 25 genes were deregulated in MVK4 and an increase for **B4GALT1**, **MAN1A1**, **PGM1** and **SGK1** was seen. The decreased genes were the same as in MVK1 (**DPY19L2**, **GALE**, **PGM2**). MVK5 and MVK6 had the same number (24) of genes that were significantly different compared to the control. Both had an upregulation in **B4GALT1**, **MAN1A1** and **SGK1**. **GALE** was downregulated in both patients while in MVK5 this was also found for **PGM2**. MVK7 had 26 markedly deregulated transcripts and this was the second highest number in MVK patients. Upregulation was seen for **HiF1alpha**, **MAN1A1**, **MAN2A1** and **SGK1**. The downregulated transcripts are the same as in MVK5 (**GALE**, **PGM2**). Patient MVK8 had 24 hits and only one gene that was upregulated with equal or larger than 1 order of logarithmic magnitude which was **MAN1A1**. Downregulation was found for **GALE**, **PGM2** and **UAP1**. The new patient MVK9 had in total 25 deregulated transcripts. Transcript levels for **B4GALT1**, **HiF1alpha**, **MAN1A1**

and **MAN2A1** were increased and decreased for **DPY19L2**, **GALE** and **PGM2**. In MVK11 upregulation was seen for **B4GALT1**, **HiF1alpha**, **MAN1A1**, **PGM1** and **SGK1**. Downregulation was the same as in MVK9 (**DPY19L2**, **GALE**, **PGM2**). In MVK11, the transcript levels for **MAN1A1** and **MAN2A1** were increased. A decrease was seen for **PGM2** as in a lot of the MVK patients. Additionally, a downregulation of -3.5 orders of logarithmic magnitude in **ST3GAL3** was present which was not seen in any other patient. In Table 37, genes which showed the same regulation trend in all MVK patients are depicted. This means that the gene is either up- or downregulated in all patients.

Table 37 - Regulation trends in all MVK patients.

| Upregulation | Downregulation |
|---|---|
| ALG12 B3GalNAcT2 B4GALT1 DPY19L1 DPY19L4 GANAB HiF1alpha MAN1A1 MAN1B1 MAN2A1 MGAT2 OGT PGM1 POMT2 | ALG3 GALE GMPPA PGM2 SLC35A2 SLC35C1 |

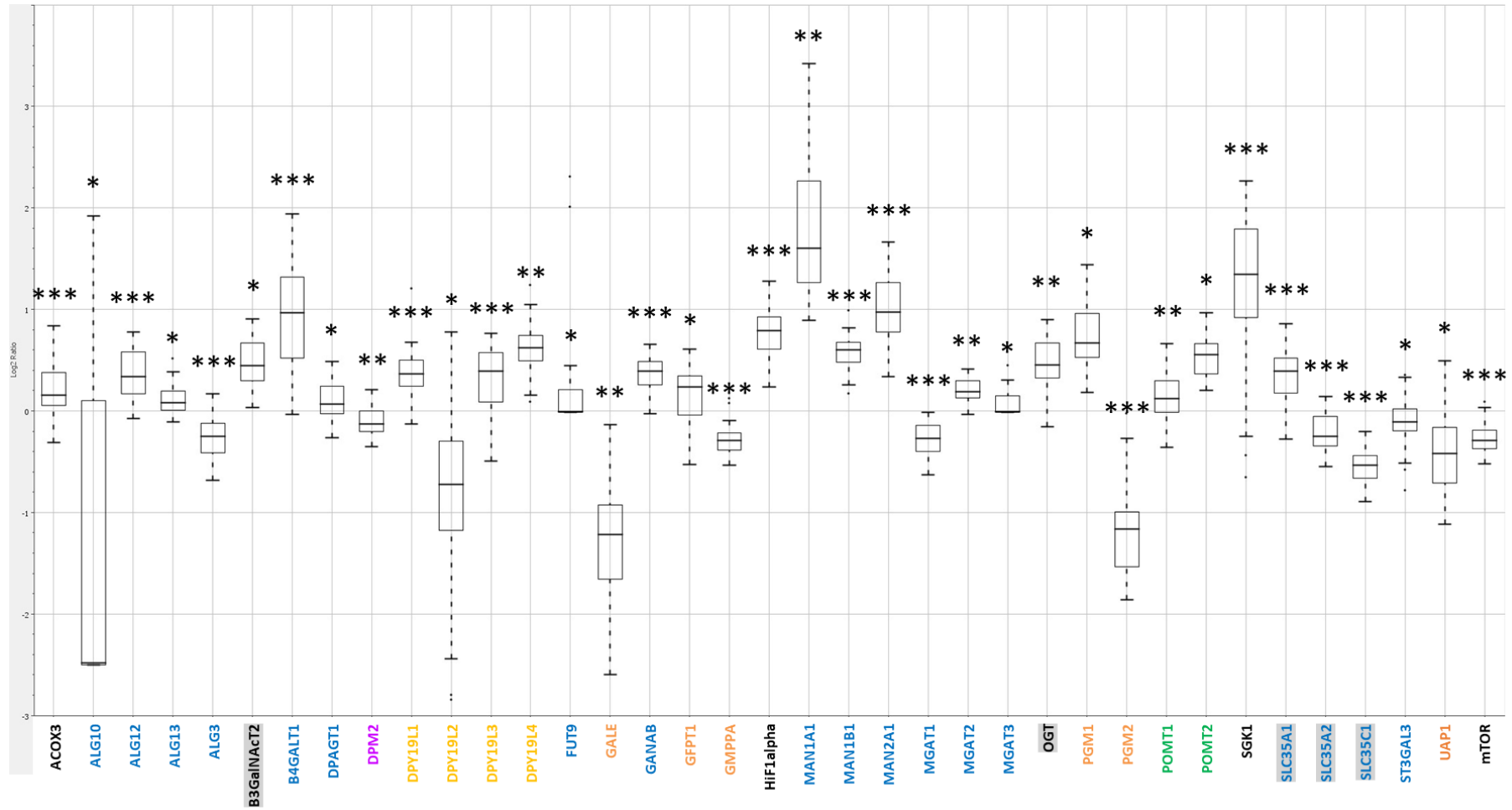


Figure 40 - Boxplot nCounter hits of all MVK patients together. Depicted are the significant results of all MVK patient together in log₂ ratio to the controls.

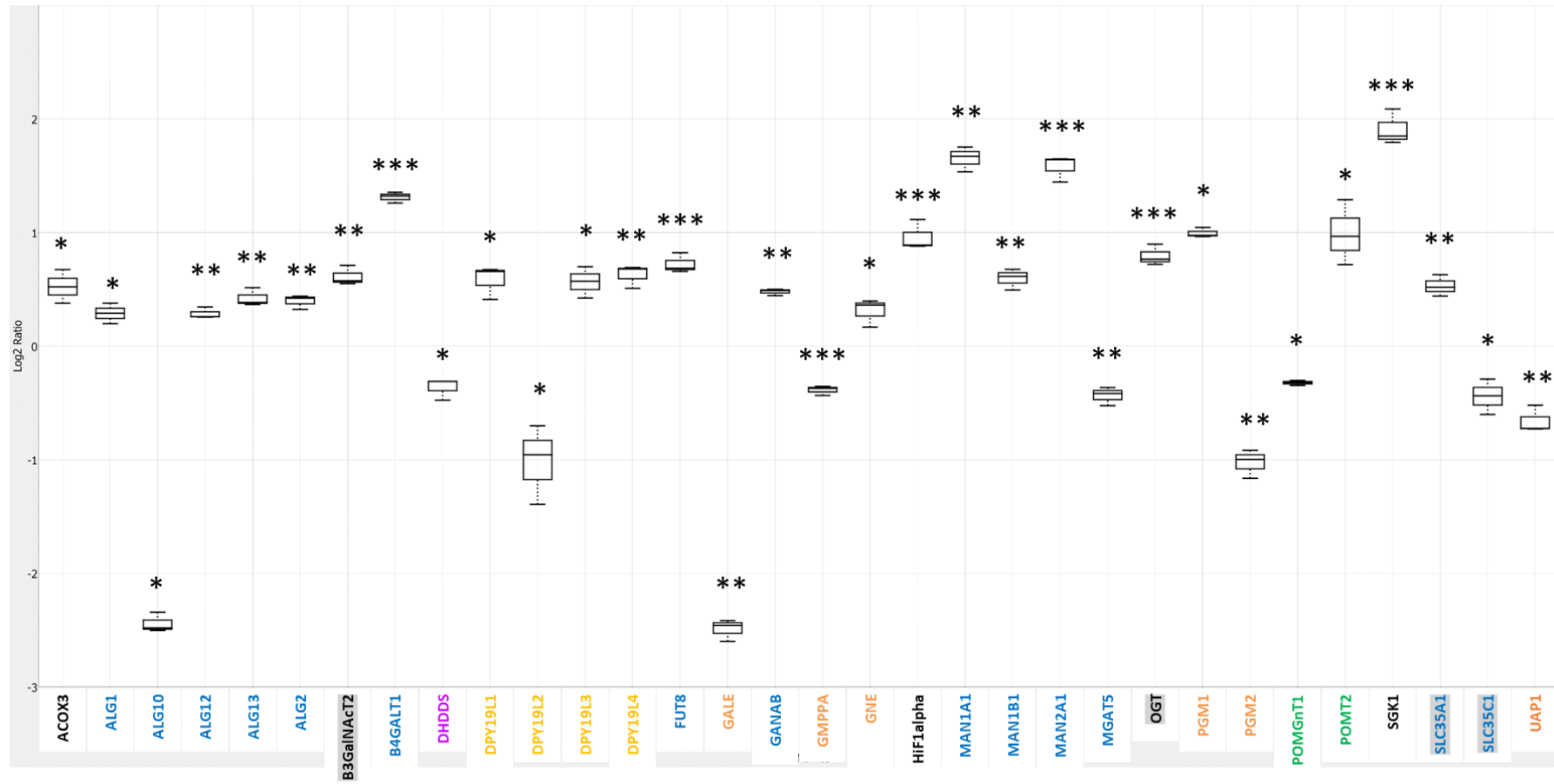


Figure 41 - Boxplot MVK1 nCounter hits. Depicted are the significant results of the corresponding MVK patient in log₂ ratio to the controls. Data are presented as biological replicates' mean ± SD (n=3).

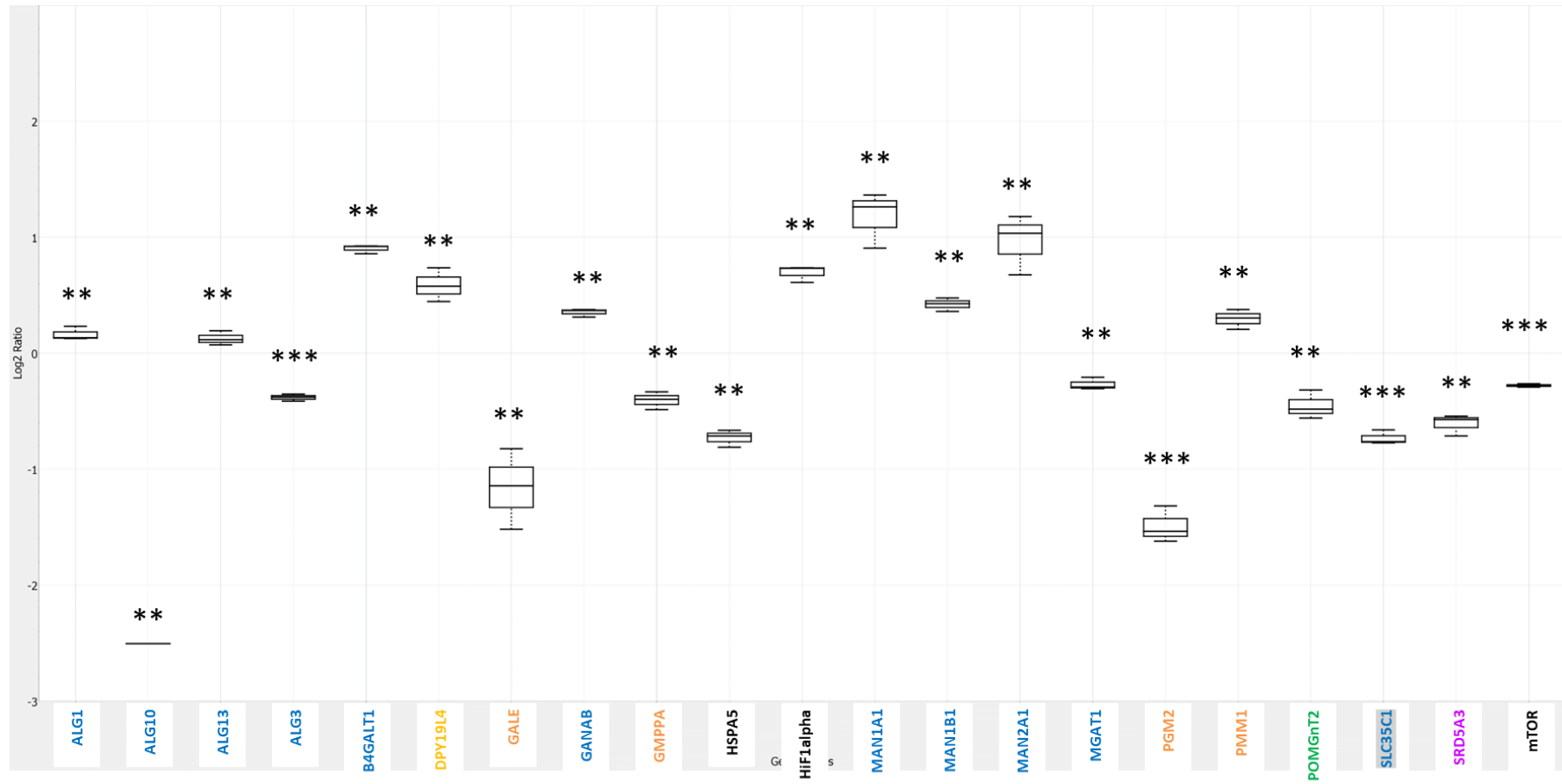


Figure 42 - Boxplot MVK nCounter hits. Depicted are the significant results of the corresponding MVK patient in log₂ ratio to the controls. Data are presented as biological replicates' mean \pm SD (n=3).

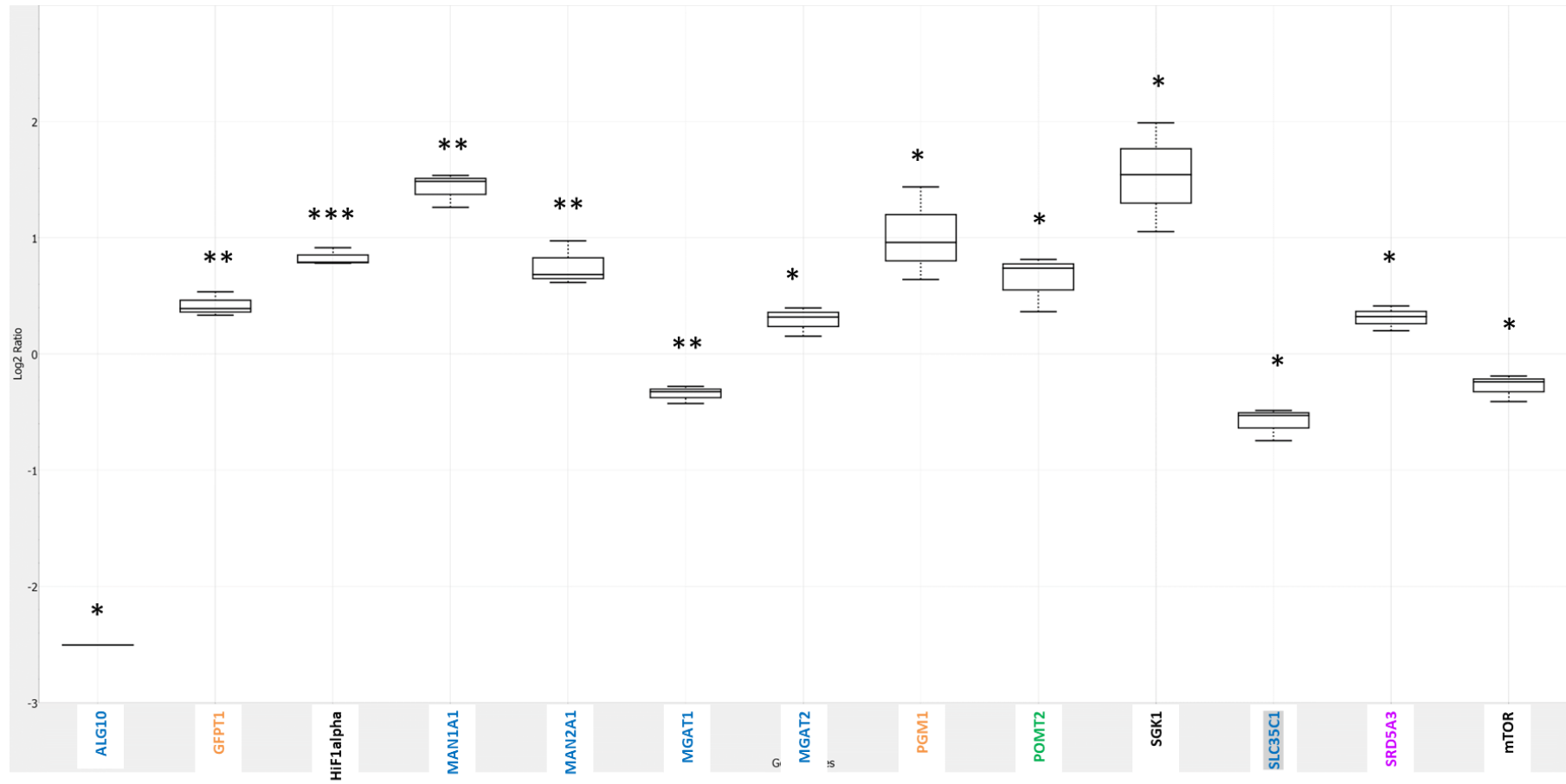


Figure 43 - Boxplot MVK3 nCounter hits. Depicted are the significant results of the corresponding MVK patient in log₂ ratio to the controls. Data are presented as biological replicates' mean ± SD (n=3).

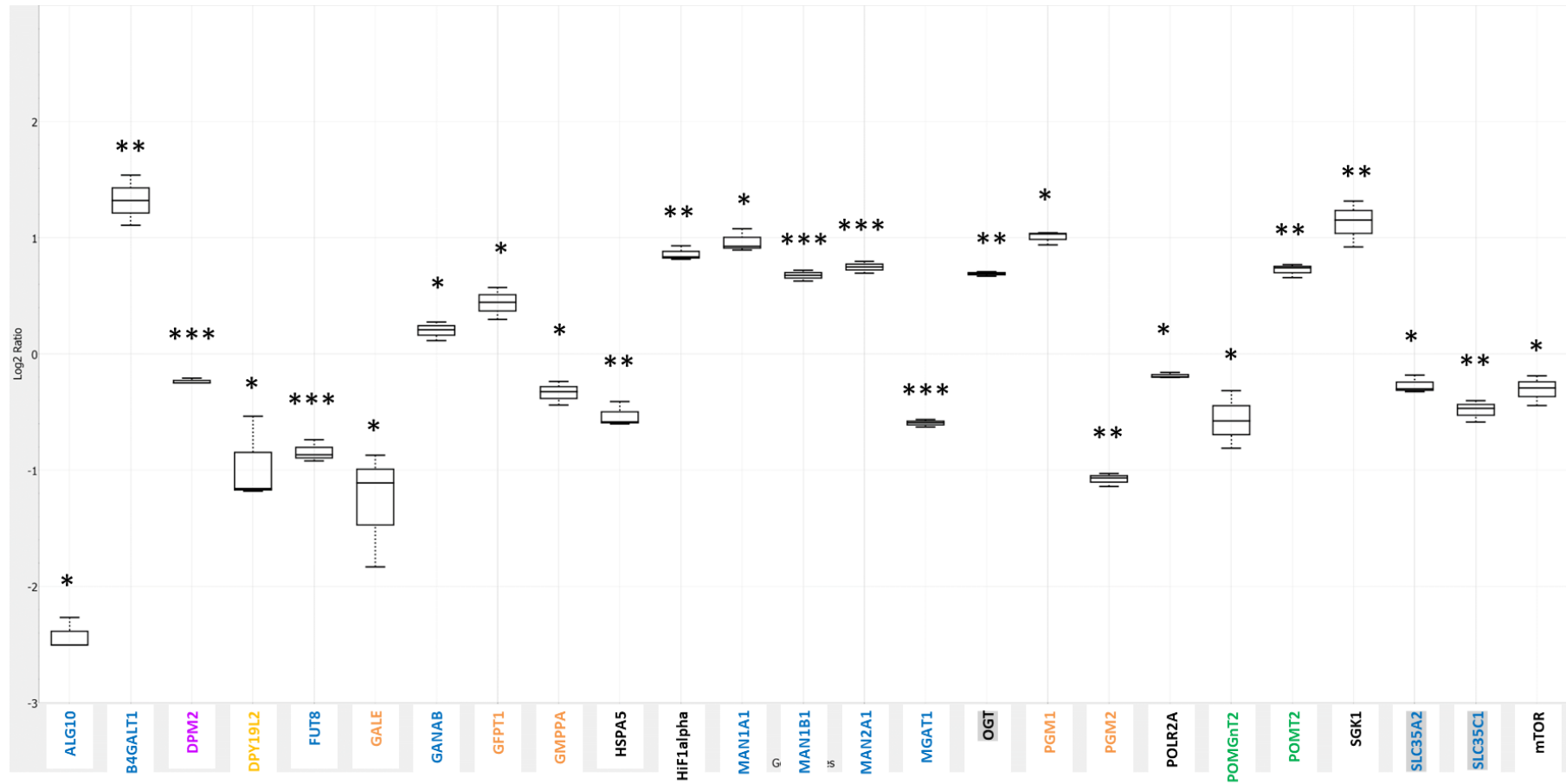


Figure 44 - Boxplot MVK4 nCounter hits. Depicted are the significant results of the corresponding MVK patient in log₂ ratio to the controls. Data are presented as biological replicates' mean ± SD (n=3).

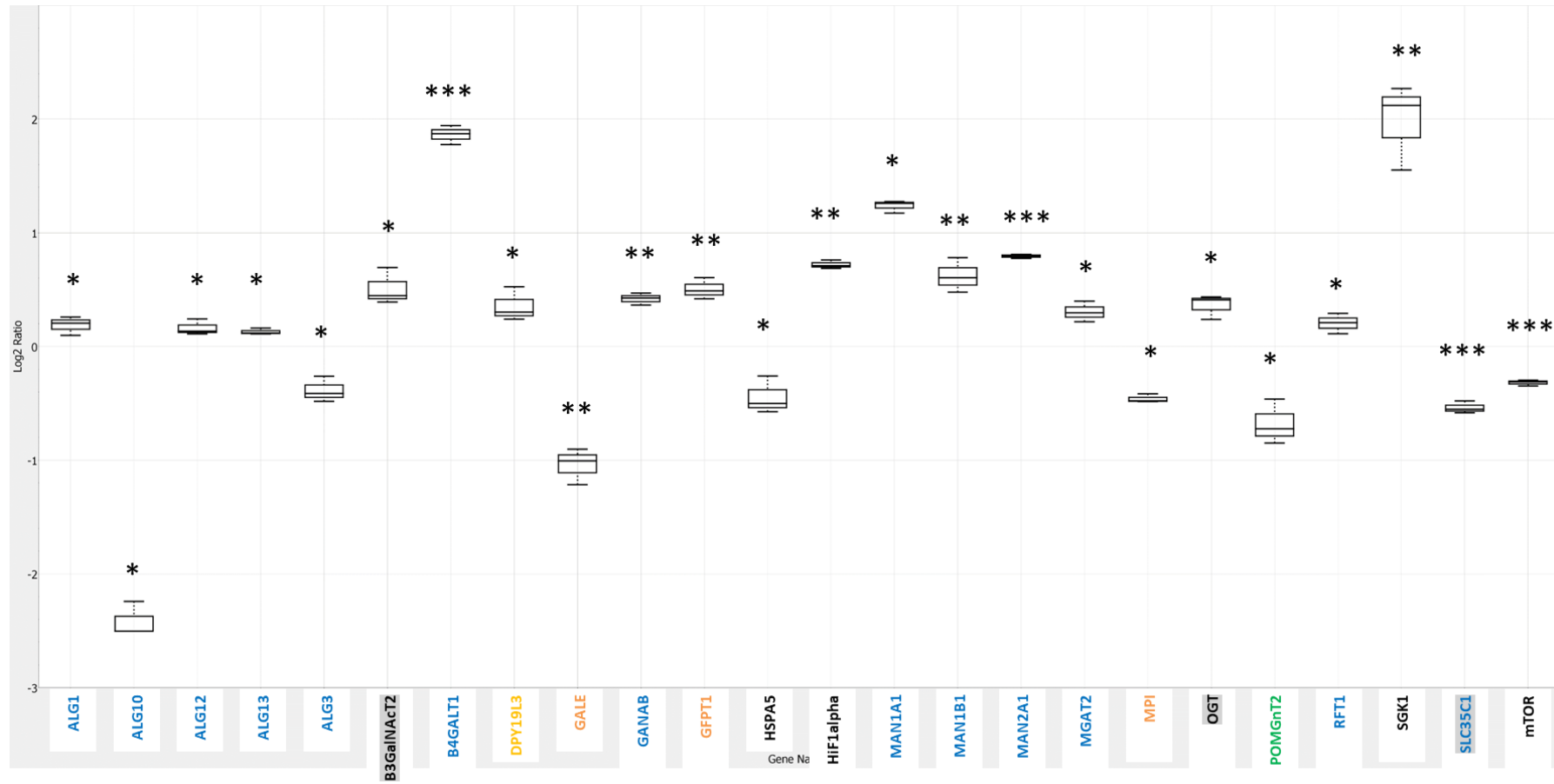


Figure 45 - Boxplot MVK5 nCounter hits. Depicted are the significant results of the corresponding MVK patient in log₂ ratio to the controls. Data are presented as biological replicates' mean ± SD (n=3).

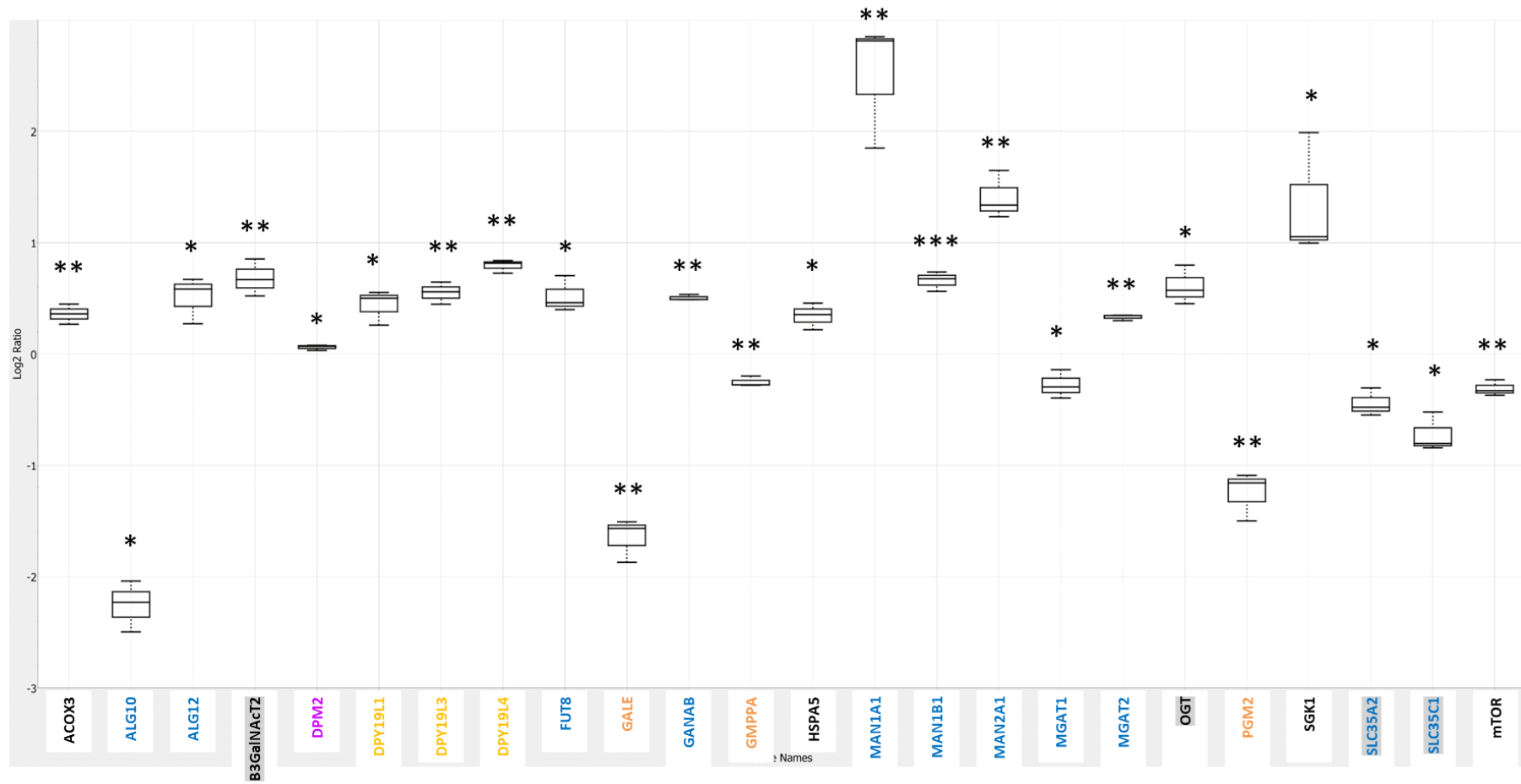


Figure 46 - Boxplot MVK nCounter hits. Depicted are the significant results of the corresponding MVK patient in log₂ ratio to the controls. Data are presented as biological replicates' mean ± SD (n=3).

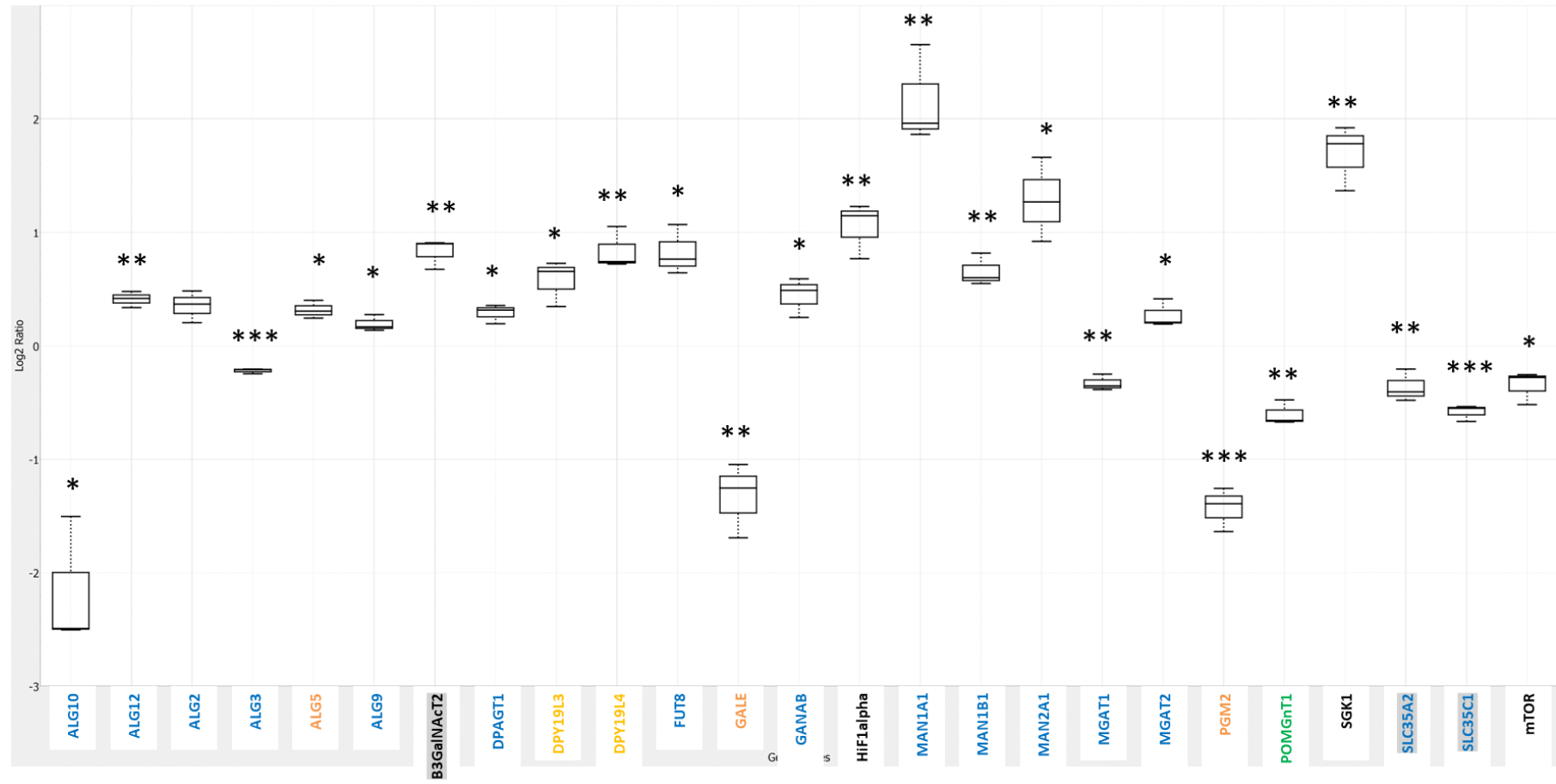


Figure 47 - Boxplot MVK7 nCounter hits. Depicted are the significant results of the corresponding MVK patient in log₂ ratio to the controls. Data are presented as biological replicates' mean ± SD (n=3).

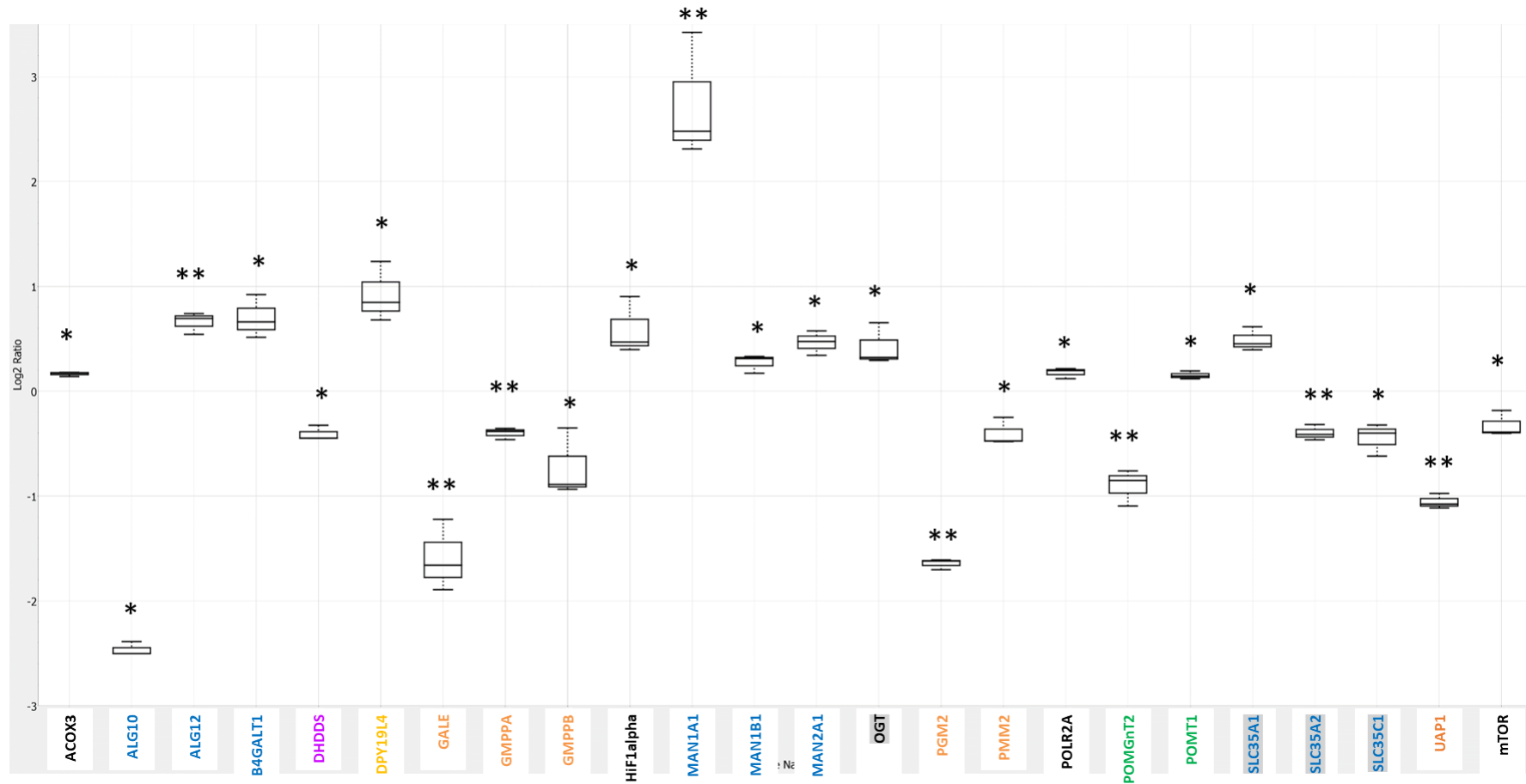


Figure 48 - Boxplot MVK nCounter hits. Depicted are the significant results of the corresponding MVK patient in log₂ ratio to the controls. Data are presented as biological replicates' mean ± SD (n=3).

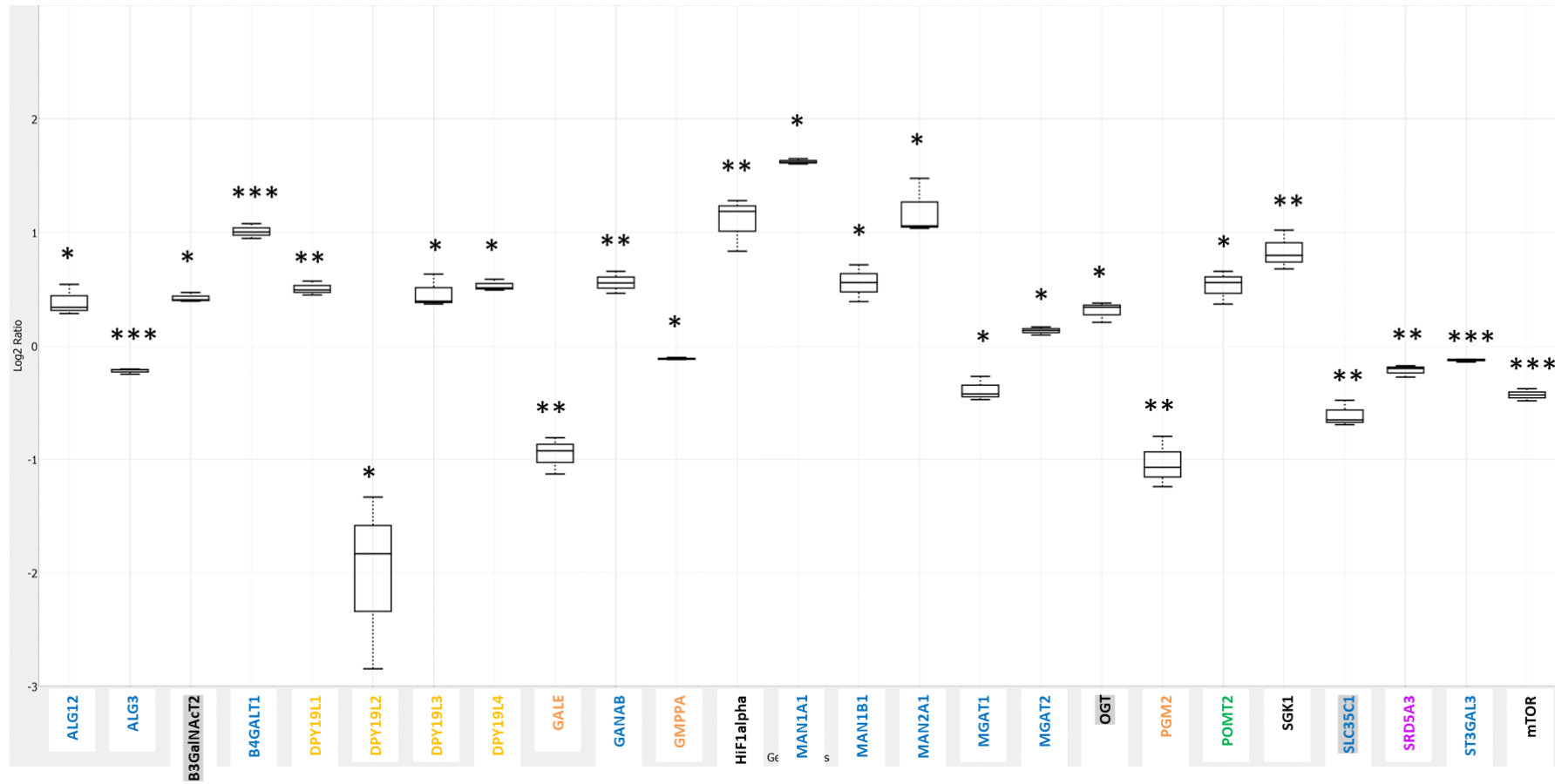


Figure 49 - Boxplot MVK9 nCounter hits. Depicted are the significant results of the corresponding MVK patient in log₂ ratio to the controls. Data are presented as biological replicates' mean \pm SD (n=3).

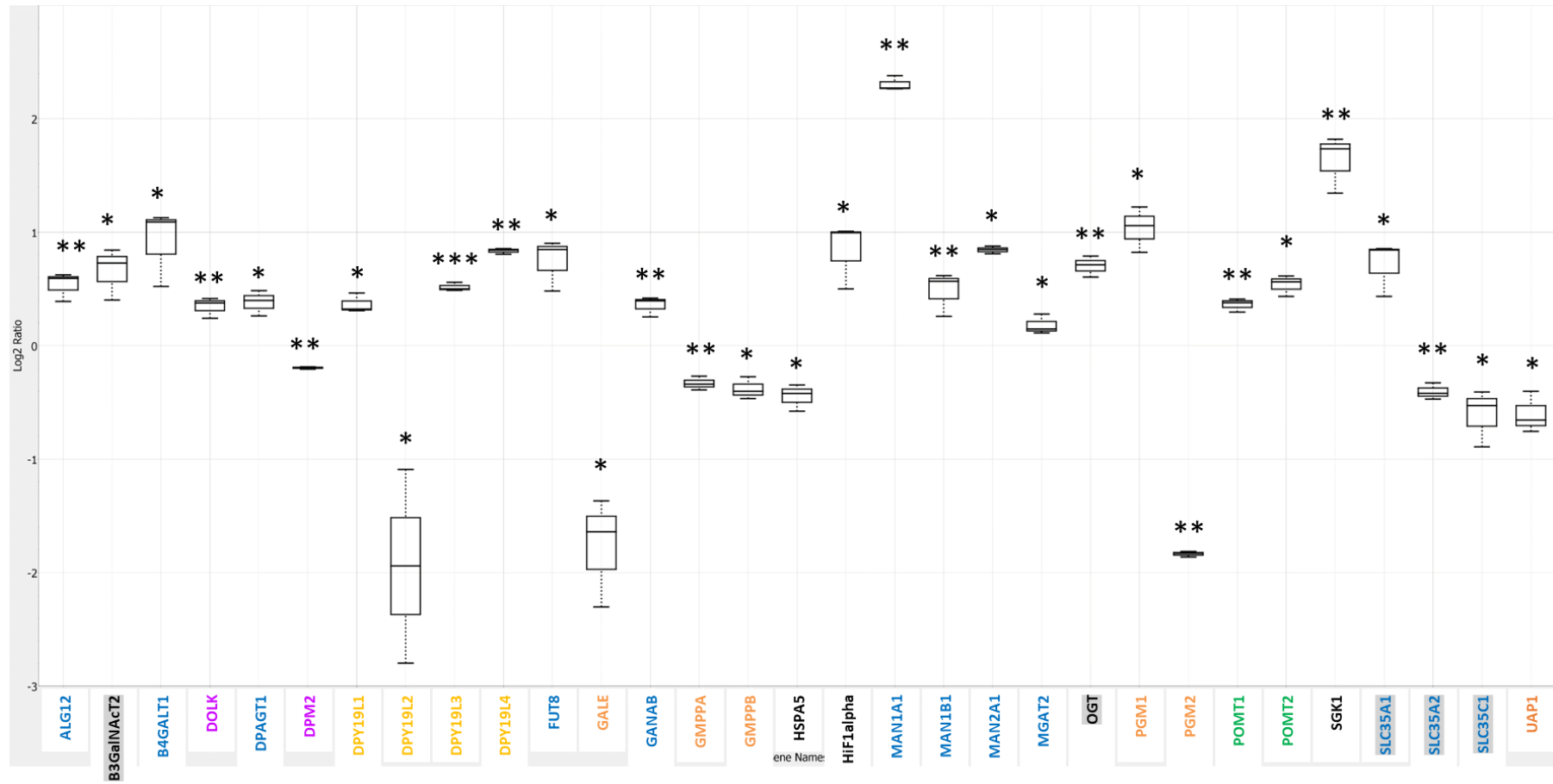


Figure 50 - Boxplot MVK10 nCounter hits. Depicted are the significant results of the corresponding MVK patient in log₂ ratio to the controls. Data are presented as biological replicates' mean \pm SD (n=3).

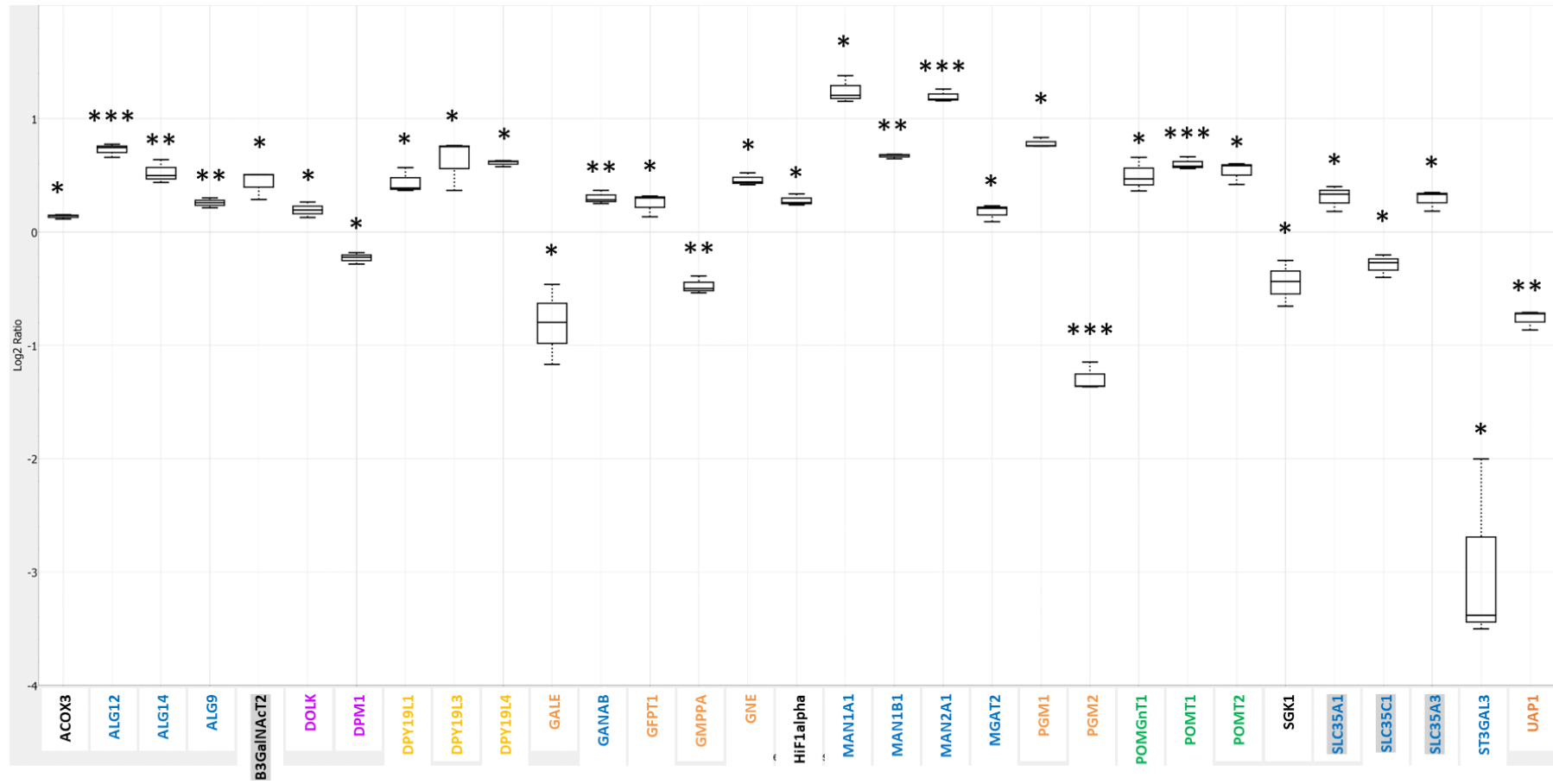


Figure 51 - Boxplot MVK11 nCounter hits. Depicted are the significant results of the corresponding MVK patient in log₂ ratio to the controls. Data are presented as biological replicates' mean ± SD (n=3).

7.9 Analysis of nCounter hits on protein level

Several transcripts were found by the nCounter to be deregulated in MVK patients compared to controls. To see the effect on protein level of these hits, several western blots were performed.

The enzymes DHDDS and SRD5A3 are important for dolichol synthesis. DHDDS levels were decreased in all MVK patients except for MVK1. Also, SRD5A3 was downregulated in most MVK patients, except for MVK6, 7 and 9. Results can be seen in Figure 52.

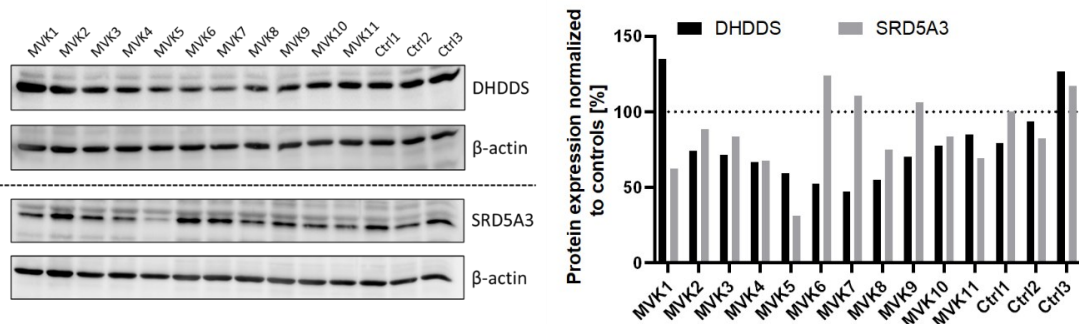


Figure 52 - Western blots of DHDDS and SRD5A3. Depicted are the western blots and the quantification results to the corresponding loading control.

The OGT enzyme is responsible for the addition of a single N-acetylglucosamine for O-glycosylation. As seen in Figure 53, the protein amount of OGT was in most MVK patients comparable to controls (n=1). MVK1 showed a slight increase while MVK10 and 11 depicted a slight decrease.

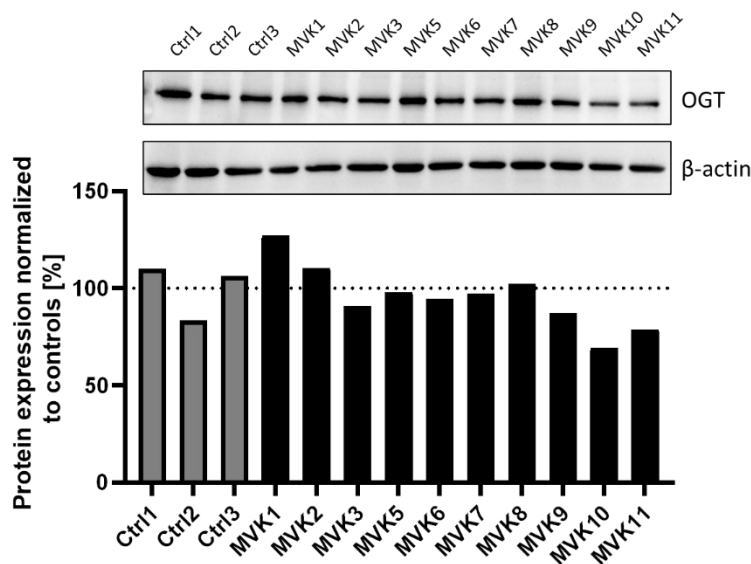


Figure 53 - Western blot of OGT. Depicted are the western blot and the quantification results to the corresponding loading control.

To cover the fucosylation pathway the enzymes FUT8, FUT9 and SLC35C1 were analyzed (n=1). Results are depicted in Figure 54. MVK patients showed a large increase from 107 % (MVK2) to 426 % (MVK5) in FUT8 protein amount. Only MVK1 (46 %) showed a decrease, but this might be an artifact and needs to be reevaluated. The overall amount of FUT9 seemed to have decreased, while MVK2 (169 %), MVK4 (115%) and MVK11 (166 %) showed an increase. The SCL35C1 expression in most MVK patients was decreased. MVK7, 8 and 11 had the same level as controls.

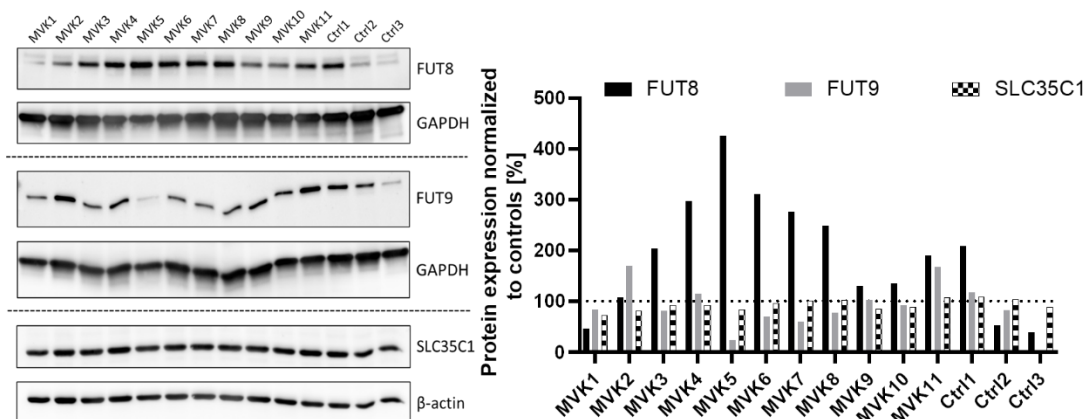


Figure 54 - Western blots of FUT8, FUT9 and SLC35C1. Depicted are the western blots and the quantification results to the corresponding loading controls. Ctrl3 was excluded for FUT9 analysis.

The enzymes DPY19L1 and DPY19L3 were analyzed to cover the C-mannosylation pathway (n=1). DPY19L1 was elevated in MVK patients except for MVK1, 10 and 11, which had normal levels. DPY19L3 levels were less expressed in MVK patients ranging from 21 % (MVK5) to 50 % (MVK6). Interestingly, MVK1 – MVK5 showed an increase in DPY19L3 amount.

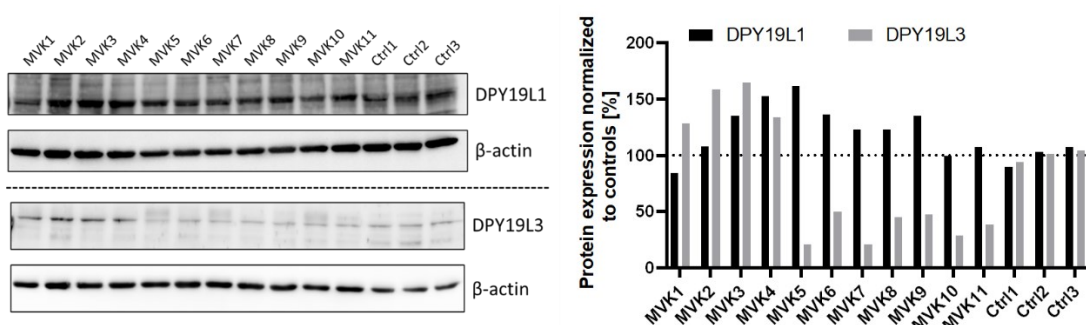


Figure 55 - Western blots of DPY19L1 and DPY19L3. Depicted are the western blots and the quantification results to the corresponding loading controls.

For analyzing the nucleotide activated sugar pathway, the amount of the proteins GMPPA, PMM2, PGM2, ALG5 and GALE were checked (n=1). As seen in the upper graph on the right side in Figure 56, the proteins GMPPA, PMM2 and PGM2 in MVK patients were decreased (GMPPA was slightly increased in MVK9). Interestingly PMM2 was in MVK5 downregulated to 46 %. ALG5 was slightly downregulated except for MVK 1, 3

and 9. The GALE expression was diverse. MVK1, 2, 3, 4, 5, 10 and 11 were downregulated. The others showed an increase whereby this is caused by a bubble, which can be seen on the loading control.

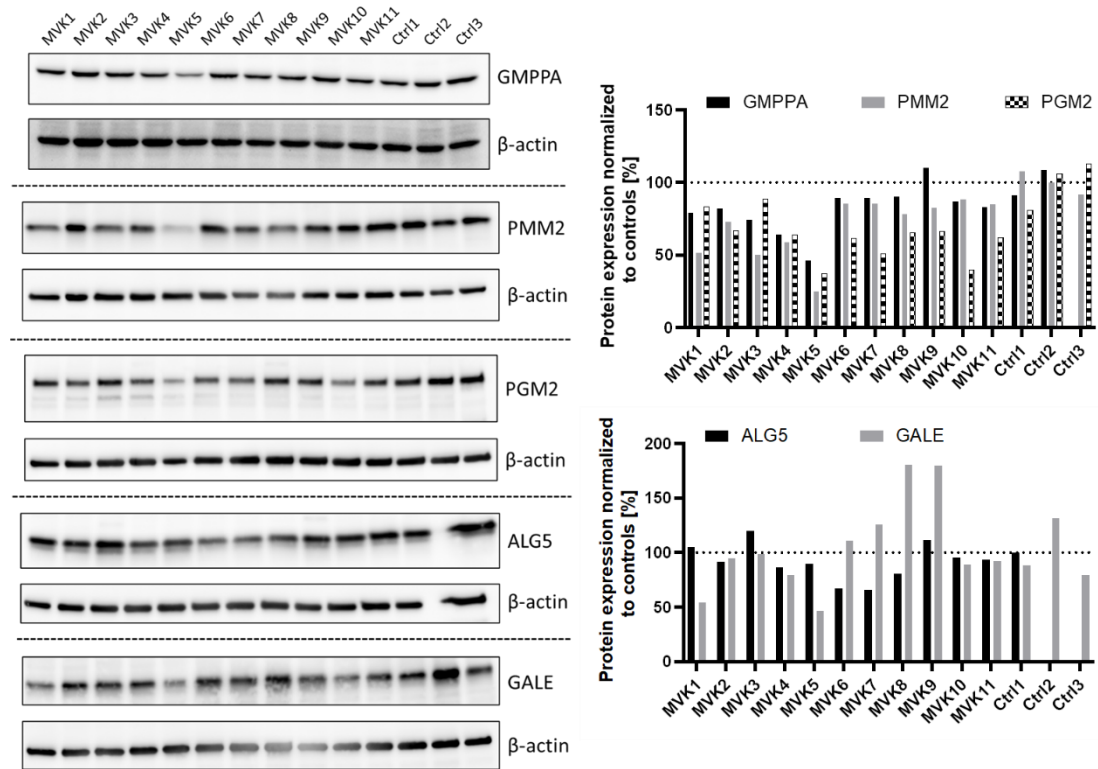


Figure 56 - Western blots of GMPPA, PMM2, PGM2, ALG5 and GALE. Depicted are the western blots and the quantification results to the corresponding loading controls. For ALG5 only Ctrl1 was used for quantification.

The N-glycosylation pathway was also intensively analyzed for protein expression abnormalities (n=1) and are depicted in Figure 57. The enzyme DPAGT1 was downregulated in MVK1 (42 %), MVK5 (10 %), MVK7 (79 %), MVK10 (80 %) and MVK11 (88 %). MVK8 had the highest upregulation with 203 % followed by MVK9 (141 %), MVK4 (124 %) and MVK2 (121 %). The levels of DPAGT1 in the controls were also quite diverse ranging from 180 % to 50 %, so results must be considered with caution. For ALG13 the protein expression is increased in MVK2 (144 %), MVK1 (138 %), MVK9 (122 %), MVK8 (121 %), MVK7 (116 %) and MVK6 (106 %). MVK5 demonstrated the lowest expression with 26 % followed by MVK10 (84 %), MVK3 (90 %) and MV11 (91 %). The expression of ALG9 was downregulated in MVK patients (except for MVK9, 108 %) ranging from 23 % (MVK5) to 67 % (MVK1).

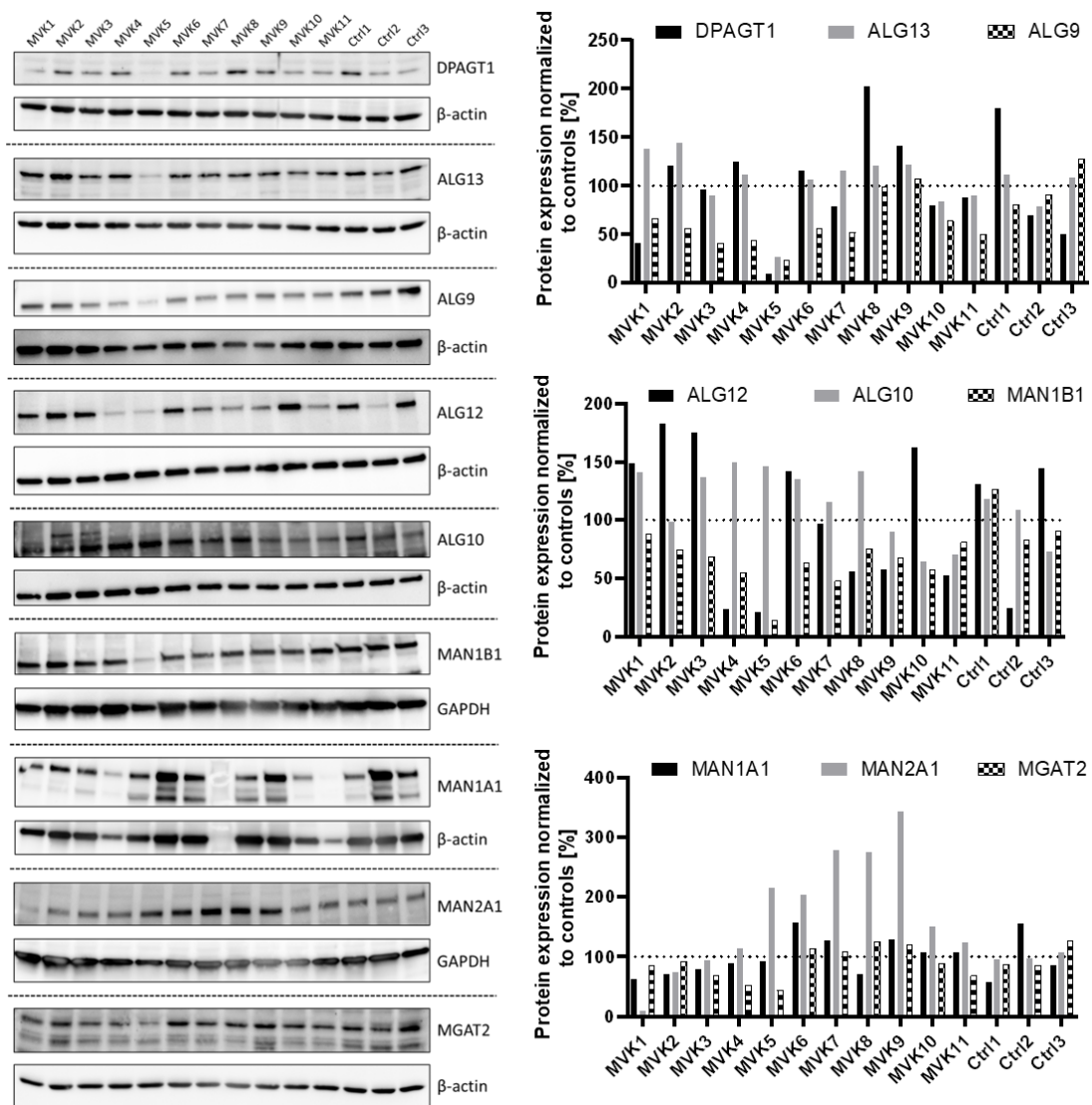


Figure 57 - Western blots of DPAGT1, ALG13, ALG9, ALG12, ALG10, MAN1B1, MAN1A1, MAN2A1 and MGAT2. Depicted are the western blots and the quantification results to the corresponding loading controls.

The ALG12 expression showed a diverse pattern in the MVK patients (183 % - 21 %) and in the controls (144 % - 25 %). For ALG10 most MVK patients showed an increase in expression. MVK4 presented the highest with 150 %, followed by MVK5 (146 %), MVK8 (142 %), MVK1 (141 %), MVK3 (137 %), MVK6 (135 %) and MVK7 (116 %). MVK2 (99 %) and MVK9 (90 %) were comparable to controls. MVK10 (65 %) and MVK11 (71 %) displayed a downregulation. The enzyme MAN1B1 was downregulated in all MVK patients ranging from 14 % (MVK5) to 88 % (MVK1).

The ALG12 expression showed a diverse pattern in the MVK patients (157 % - 62 %) and in the controls (156 % - 58 %). The protein expression of MAN2A1 was upregulated in most MVK patients. MVK9 showed the highest increase with 344 %. Results for MAN2A1 need to be treated with caution, as a bubble effect is visible on the loading

control GAPDH. MGAT2 expression was downregulated in most MVK patients, ranging from 44 % (MVK5) to 93 % (MVK2). MVK7 (109 %), MVK6 (112 %) MVK9 (121 %) and MVK8 (125%) showed an increase in protein expression.

The enzyme POMT2 was analyzed to cover the O-mannosylation pathway (n=1). MVK1 showed the highest increase in protein expression of 580 % followed by MVK8 with 343 %. MVK6 had the lowest expression with 27 %.

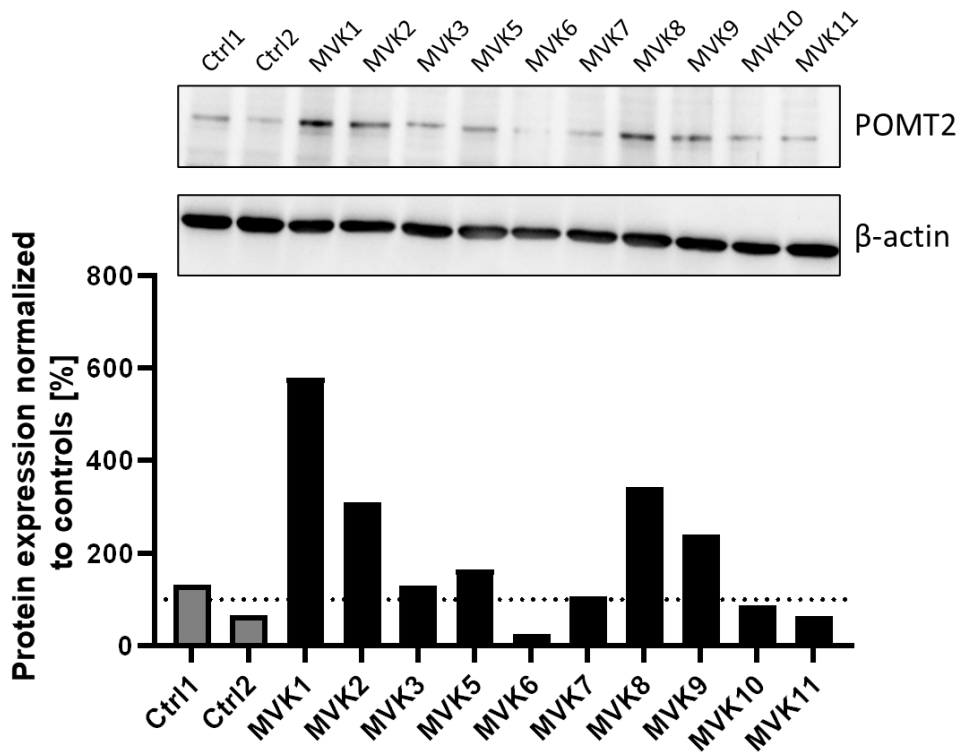


Figure 58 - Western blot of POMT2. Depicted are western blot and the quantification results to the corresponding loading control.

7.10 LLO analysis

For the analysis of short lipid-linked-oligosaccharides, MVK patients' cells were metabolically labeled for 30 min with [2-³H] mannose. Cells were extracted with chloroform/methanol and phase partitioned (3:2). The incorporation of [2-³H] mannose into Dol-P-Man glycans was analyzed by thin layer chromatography. The profiles of the MVK patients, control and Dol-P-Man standard can be seen in Figure 59. The Dol-P-Man standard runs at around 11 cm. The control only shows one peak at 11 cm, which is Dol-P-Man. All MVK patients show a Dol-P-Man peak, but all smaller compared to controls. MVK1 displays the smallest Dol-P-Man peak followed by MVK6 and MVK10. Noticeably, all MVK patients show a completely different profile with peaks before 11 cm which are short LLOs containing up to 5 mannose residues. This indicates the accumulation of short lipid-linked-oligosaccharides in MVK patients. MVK1 and MVK6 have the highest peaks at 3 – 4 cm, where it is assumed that Dol-P-Man₅ runs at that length.

Results

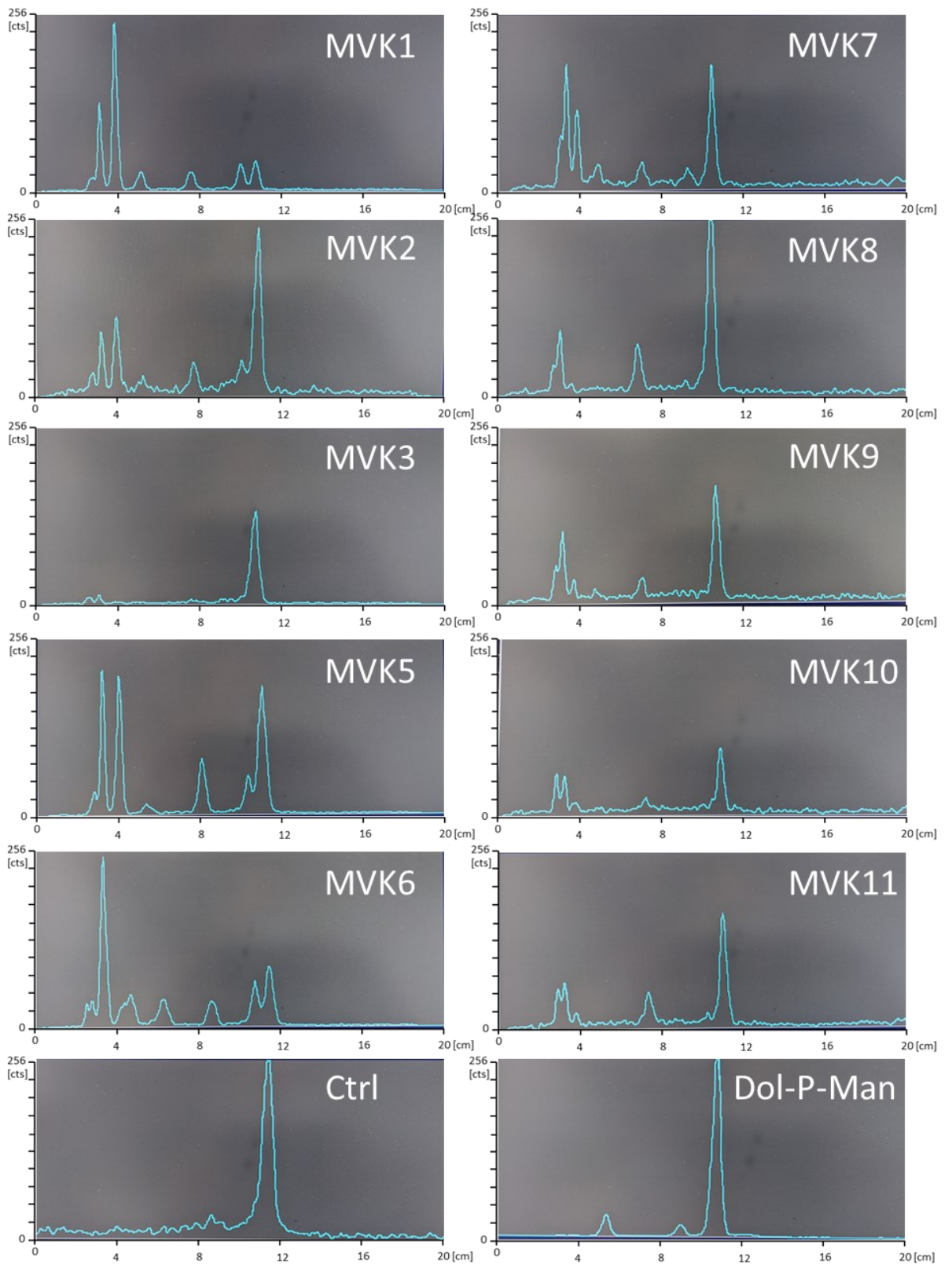


Figure 59 - Short LLO profiles of MVK patients and control.

7.11 Prime PCR analysis

For analysis of the impact of the MVK defect on other metabolic pathways, two PrimePCR pathway assays from BioRad were used to measure mRNA levels of specific genes by qPCR. MVK2, 8, 9 (most severe phenotype) and a control were analyzed and the predesigned human pathway plates *Glycolysis and Gluconeogenesis H96* and *Regulation of Lipid Metabolism Tier1 H96* were used. Samples were analyzed in triplicates (n=3) and the reference genes *TBP*, *GAPDH* and *HPRT1* were used for normalization.

The *Glycolysis and Gluconeogenesis H96* plate includes 24 targets and quality controls. Significant results are depicted in Figure 60 for MVK patients normalized to control.

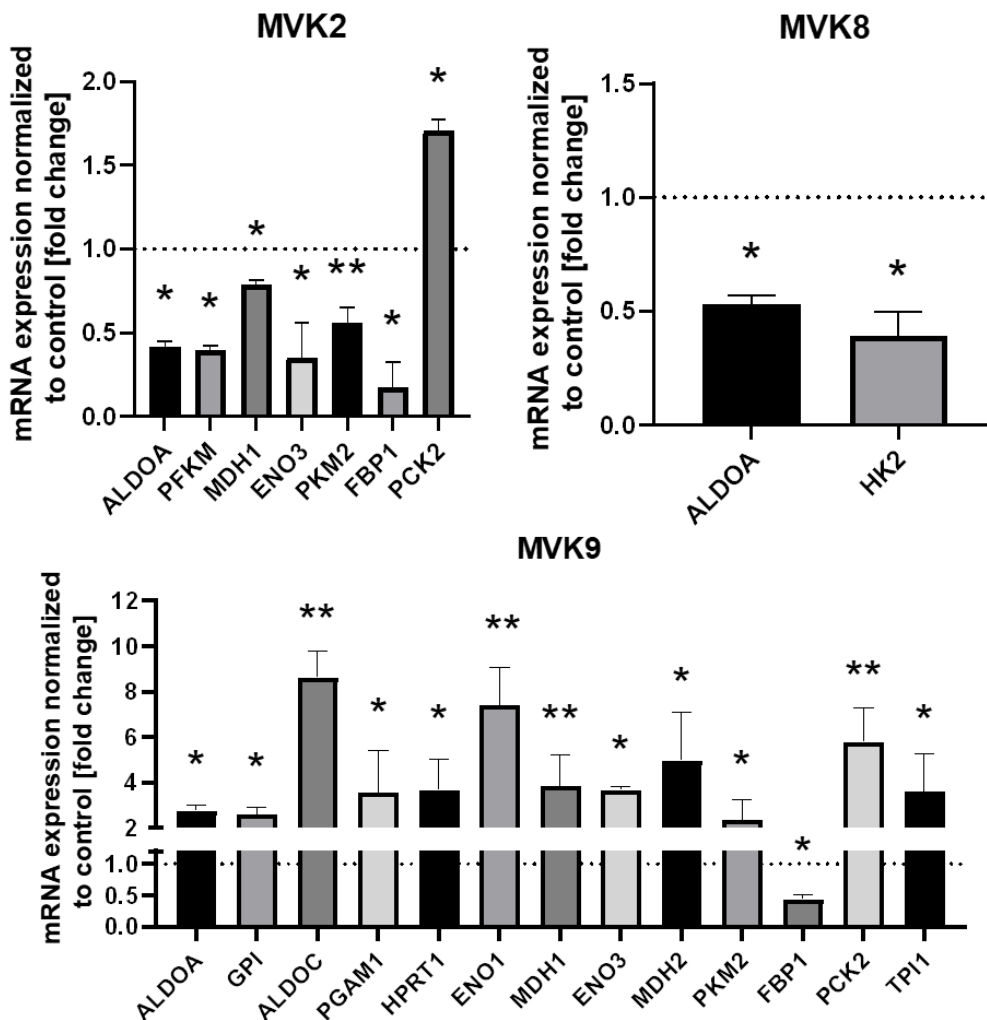


Figure 60 - PrimePCR glycolysis and gluconeogenesis results. Depicted are significant results of MVK2, 8 and 9 normalized to a control. Data are presented as biological replicates' mean \pm SD (n=3).

ALDOA (Aldolase, Fructose-Bisphosphate A) was downregulated in MVK2 (0.41 ± 0.04) and MVK8 (0.53 ± 0.04) by around 50 %. Whereas, in MVK9 (2.8 ± 0.2) it was increased nearly 3 times. Other downregulated transcripts in the MVK2 patient were *PFKM* (Phosphofructokinase) with 0.4 ± 0.03 , *MDH1* (Malate Dehydrogenase 1) with 0.8 ± 0.03 , *ENO3* (Enolase 3) with 0.4 ± 0.2 , *PKM2* (Pyruvate Kinase M2) with 0.6 ± 0.01 and *FBP1* (Fructose-Bisphosphatase 1) with 0.2 ± 0.2 . Also, in MVK9 a decrease of *FBP1* to 0.4 ± 0.06 was found. mRNA of the transcript *PCK2* (Phosphoenolpyruvate Carboxykinase 2) was highly upregulated in MVK2 (1.7 ± 0.15) and MVK9 (5.8 ± 1.5). In MVK9 are several other genes were upregulated. The highest upregulation was measured for *ALDOC* (Aldolase, Fructose-Bisphosphate A), *ENO1* (Enolase 1) and *MDH2* (Malate Dehydrogenase 2).

The *Regulation of Lipid Metabolism Tier1 H96* plate includes 88 targets and quality controls. Significant results are depicted in Figure 61 - Figure 63 for MVK patients normalized to control.

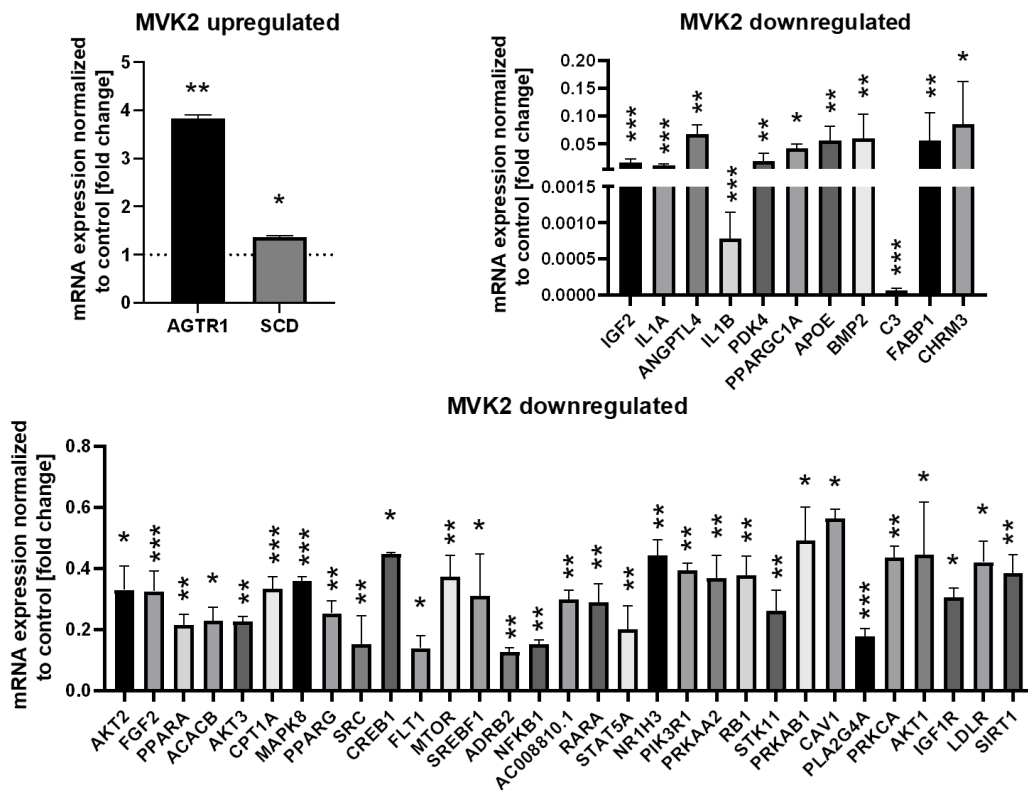


Figure 61 - Regulation of lipid metabolism Tier1 results of MVK2. Depicted are significant results of MVK2 normalized to control. Data are presented as biological replicates' mean \pm SD (n=3).

In patient MVK2, the transcript *AGTR1* (Angiotensin II Receptor Type 1) with 3.8 ± 0.01 and *SCD* (Stearoyl-CoA Desaturase) with 1.4 ± 0.03 were upregulated. But in total, 43 genes of the panel were downregulated in patient MVK2. In Figure 61 on the upper right graph 11 genes are depicted with the greatest downregulation compared to

control. *C3* (Complement Component 3) with 0.00007 ± 0.00003 and *IL1B* (Interleukin 1 Beta) with 0.0008 ± 0.0004 are the most downregulated genes compared to control.

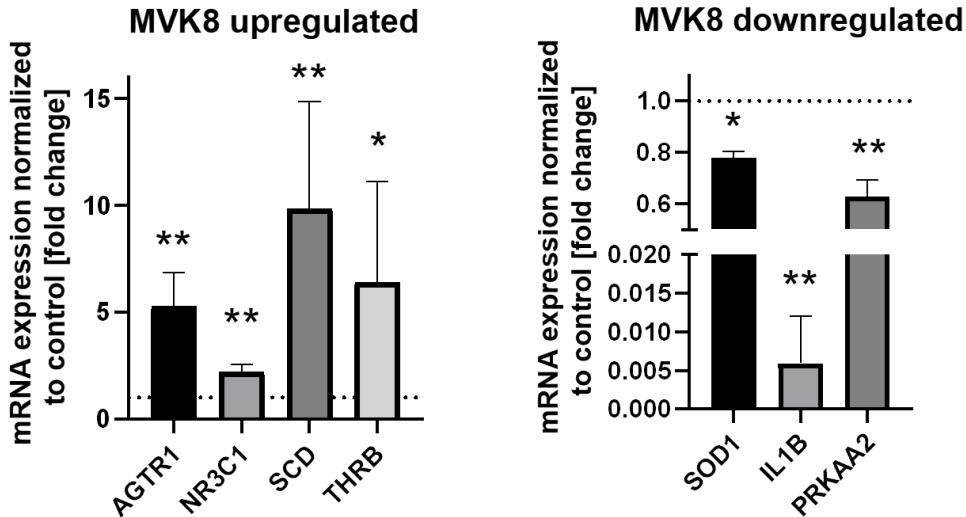


Figure 62 - Regulation of lipid metabolism Tier1 results of MVK8. Depicted are significant results of MVK8 normalized to control. Data are presented as biological replicates' mean \pm SD (n=3).

The significant results for patient MVK8 included 7 genes, 4 are upregulated and 3 downregulated. *AGTR1* (5.3 ± 1.6) and *SCD* (9.9 ± 5.0) were upregulated similar to MVK2. Additionally, *NR3C1* (Nuclear Receptor Subfamily 3 Group C Member 1) with 2.2 ± 0.4 and *THRβ* (Thyroid Hormone Receptor Beta) with 6.4 ± 4.7 were also upregulated. Downregulation of *SOD1* (Superoxide Dismutase 1) to 0.78 ± 0.03 , *IL1B* to 0.006 ± 0.006 and *PRKAA2* (Protein Kinase AMP-Activated Catalytic Subunit Alpha 2) to 0.63 ± 0.06 were measured by the assay.

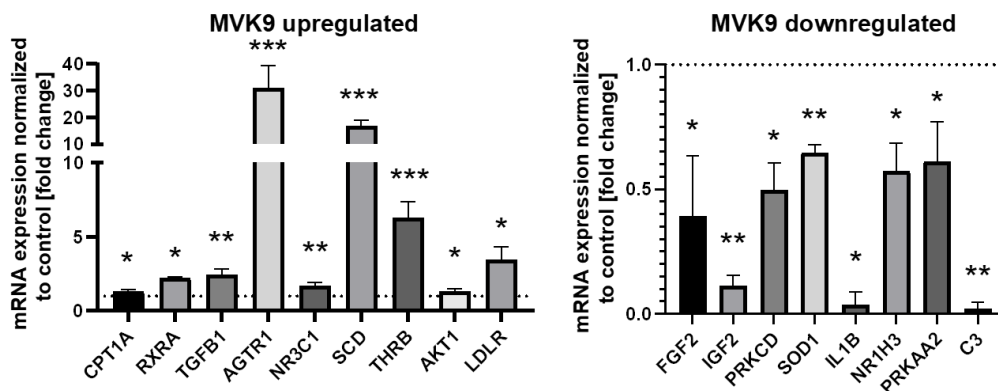


Figure 63 - Regulation of lipid metabolism Tier1 results of MVK9. Depicted are significant results of MVK9 normalized to control. Data are presented as biological replicates' mean \pm SD (n=3).

The significant results for patient MVK9 include 17 genes, 9 are upregulated and 8 downregulated. *AGTR1* (5.3 ± 1.6), *NR3C1* (1.7 ± 0.22), *SCD* (17.0 ± 2.1) and *THRβ* (6.3 ± 1.1) are upregulated in MVK9 like in MVK8. Analysis also revealed downregulation for

SOD1 (0.6 ± 0.03), *IL1B* (0.04 ± 0.05) and *PRKAA2* (0.6 ± 0.2) as in MVK8. Furthermore, *FGF2* (Fibroblast Growth Factor 2) to 0.4 ± 0.2 , *IGF2* (Insulin Like Growth Factor 2) to 0.1 ± 0.04 , *NR1H3* (Nuclear Receptor Subfamily 1 Group H Member 3) to 0.6 ± 0.1 and C3 to 0.02 ± 0.03 are downregulated, as in MVK2.

Comparing the three MVK patients (MVK2, 8 and 9), *AGTR1* and *SCD* are genes with the same upregulation trend, and the genes *SOD1*, *IL1B* and *PRKAA2* are downregulated in all three.

7.12 Energy metabolite analysis

In cooperation with the metabolomics core technology facility of the Heidelberg University, energy metabolites were measured by LC-FLR. The focus was on the metabolites adenosine monophosphate (AMP), adenosine diphosphate (ADP), adenosine triphosphate (ATP), methylthioadenosine (MTA), nicotinamide adenine dinucleotide (NAD/NADH), S-adenosyl-L-homocysteine (SAHC) and S-adenosylmethionine (SAM) which were analyzed in patients' fibroblast lysates and controls. Results (n=3) can be seen in Figure 64 and Figure 65. Values were normalized to cell number.

For AMP, MVK1, 2, 4, 5 and 7 show a significant increase ranging from 590 pmol/mio cells (MVK7) to 2,119 pmol/mio cells \pm 316 pmol/mio cells compared to the control with 383 pmol/mio cells \pm 104 pmol/mio cells. The energy metabolite ADP is only significantly elevated in MVK2 (6,483 pmol/mio cells \pm 1,346 pmol/mio cells), MVK4 (9,454 pmol/mio cells \pm 1017 pmol/mio cells) and MVK5 (6764 pmol/mio cells \pm 91 pmol/mio cells) compared to the control (3,311 pmol/mio cells \pm 655 pmol/mio cells). MVK3, 4, 5 and 10 display a significant increase in ATP and MTA (additional MVK7 and 11 for MTA).

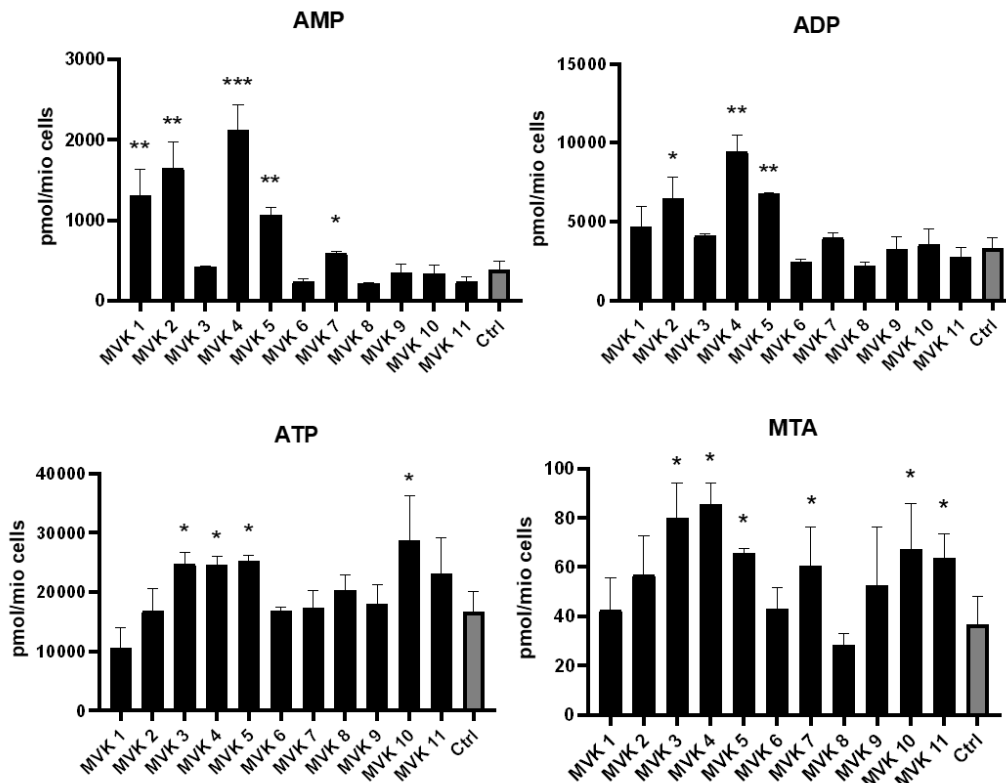


Figure 64 - Energy metabolite measurement in MVK patient fibroblast and control cells. Depicted is the detected energy metabolite in pmol/ mio cells in MVK patient fibroblast and in control cells. Data are presented as biological replicates' mean \pm SD (n=3).

ATP ranged from 24,572 pmol/mio cells \pm 1,429 pmol/mio cells (MVK4) to 28,787 pmol/mio cells \pm 7,482 pmol/mio cells (MVK10) compared to control with 16,608 pmol/mio cells \pm 3,527 pmol/mio cells. The range for MTA was from 64 pmol/mio cells \pm 10 pmol/mio cells (MVK11) to 86 pmol/mio cells \pm 8 pmol/mio cells (MVK4) compared to the control with 37 pmol/mio cells \pm 11 pmol/mio cells.

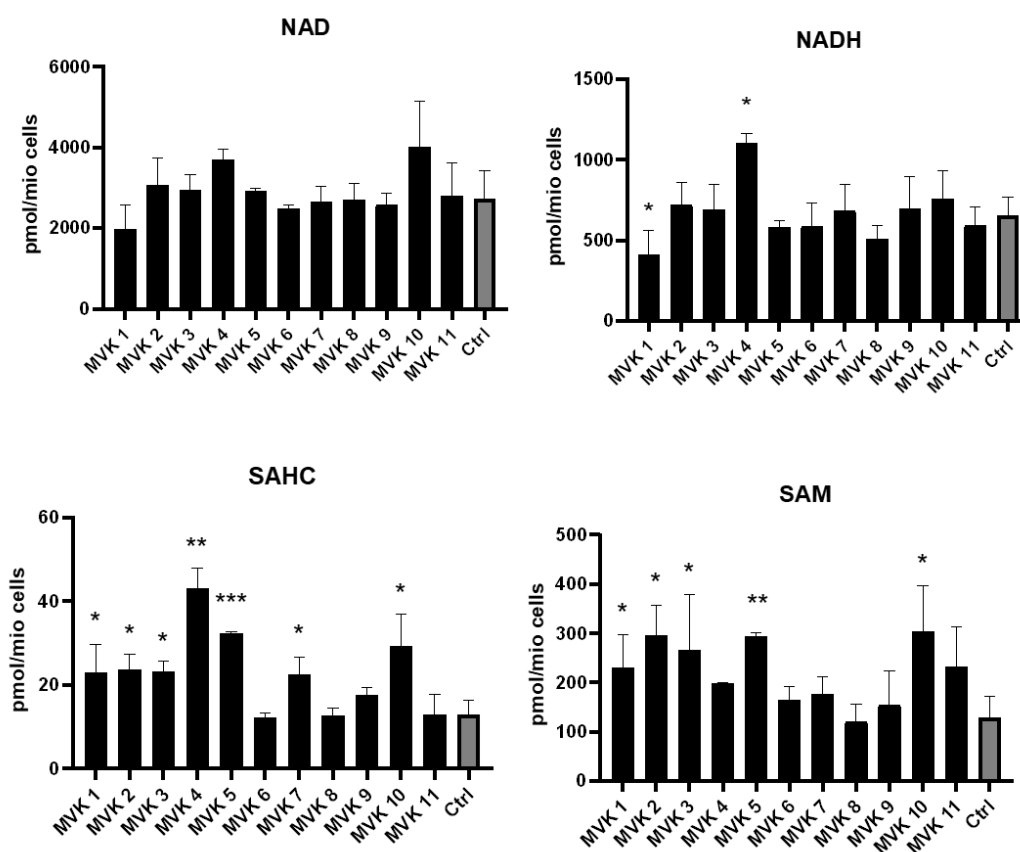


Figure 65 - Energy metabolites measurement in MVK patient fibroblast and control cells. Depicted is the detected energy metabolite in pmol/ mio cells in MVK patient fibroblast and in control cells. Data are presented as biological replicates' mean \pm SD (n=3).

NAD showed no changes in MVK patients and for NADH only MVK4 (28,787 pmol/mio cells \pm 7,482 pmol/mio cells) had a significant increase compared to the control (28,787 pmol/mio cells \pm 7,482 pmol/mio cells). MVK1 (28,787 pmol/mio cells \pm 7,482 pmol/mio cells) had a significant decrease in NADH. For SAHC, a significant increase in MVK1, 2, 3, 4, 5, 7 and 10 was found ranging from 23 pmol/mio cells \pm 4 pmol/mio cells (MVK7) to 43 pmol/mio cells \pm 5 pmol/mio cells (MVK4) compared to the control (13 pmol/mio cells \pm 3 pmol/mio cells). SAM displayed a general elevation in MVK patients with significant increase in MVK1, 2, 3, 5 and 10. The significant increase ranged from 231 pmol/mio cells \pm 66 pmol/mio cells (MVK1) to 305 pmol/mio cells \pm 92 pmol/mio cells (MVK10) compared to control with 129 pmol/mio cells \pm 43 pmol/mio cells.

7.13 Measurement of amino acids in cell lysates

As changes in for example cell growth can be related to a decompensated amino acid (AA) metabolism, it was decided to screen for abnormalities concerning amino acids. MVK patients' fibroblast lysates and controls (n=2) were analyzed in triplicates by ESI-MS/MS. Values were normalized to controls and protein amount and are displayed in Figure 66 - Figure 68.

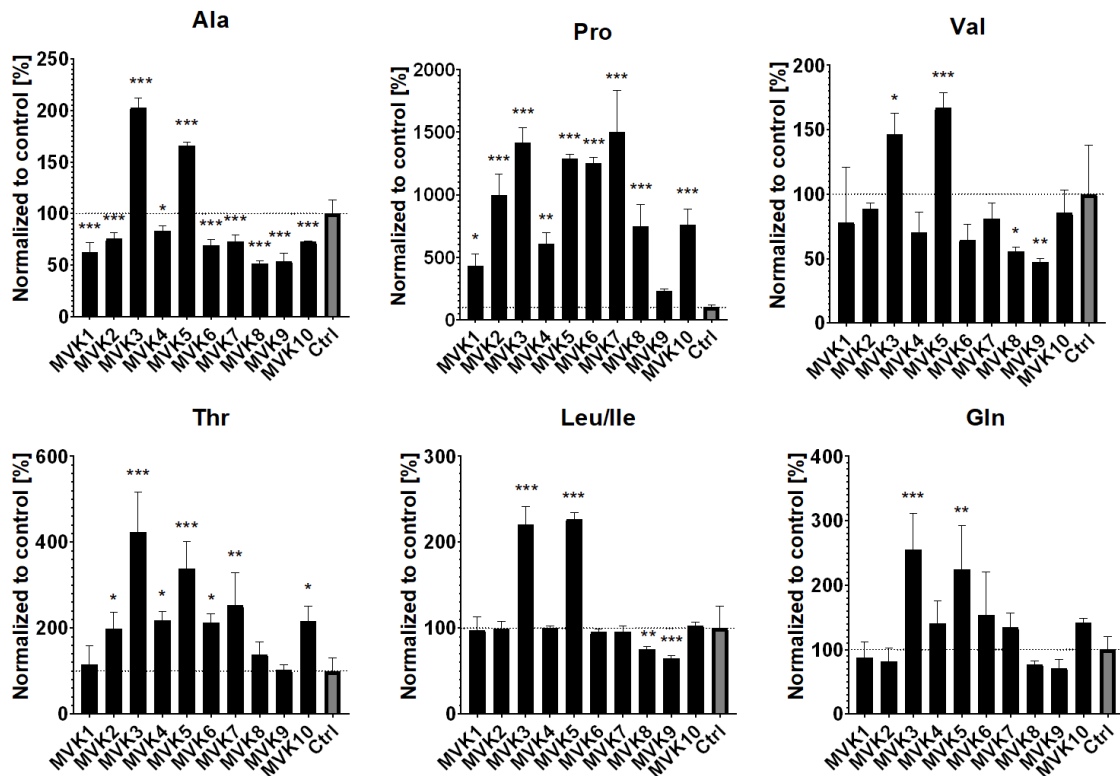


Figure 66 - Determination of amino acid levels in MVK patient fibroblast and control cells. Results of MVK patients were normalized to the controls (set to 100). Data are presented as biological replicates' mean \pm SD (n=2).

Alanine (Ala) was decreased in most MVK patients ranging from 52 % \pm 2.7 % (MVK8) to 83 % \pm 5.2 % (MVK4), except for MVK3 (203 % \pm 8.8 %) and MVK5 (166 % \pm 3.2 %). For proline (Pro) all MVK patients showed a (significant) increase ranging from 232 % \pm 16 % (MVK9) to 1498 % \pm 337 % (MVK7). For valine (Val) the general trend was a decrease, except for MVK3 and MVK5. Threonine was increased in MVK patients ranging from 102 % \pm 13 % (MVK9) to 424 % \pm 93 % (MVK3) compared to controls. The amino acids leucine (Leu), isoleucine (Ile) and glutamine (Gln) showed comparable amounts in patients and controls. Also, MVK3 and MVK5 are not considered for the following analysis as they did not follow the general trend.

Results

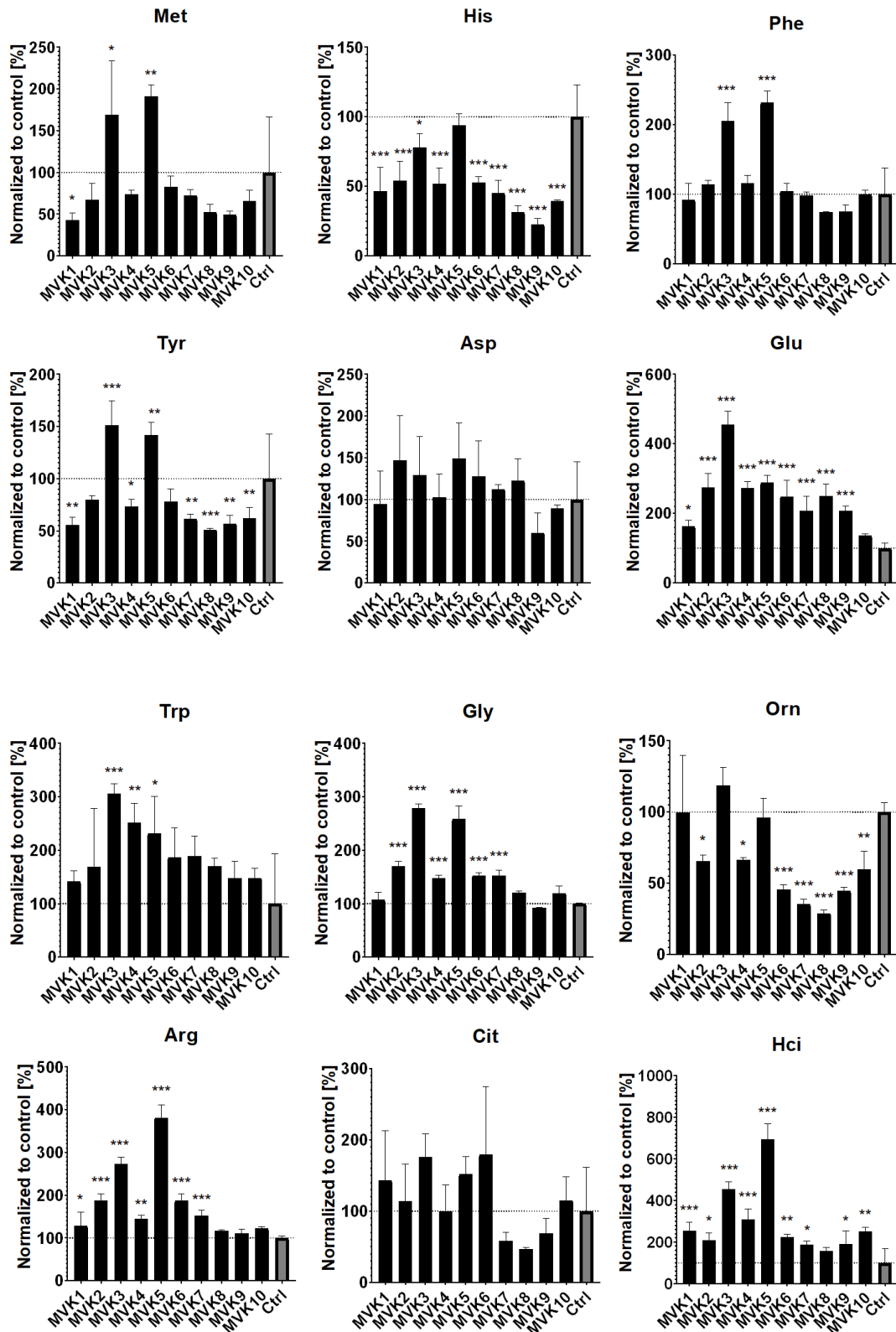


Figure 67 - Continuation of AA determination. Results of MVK patients were normalized to the controls (set to 100 %). Data are presented as biological replicates' mean \pm SD (n=2).

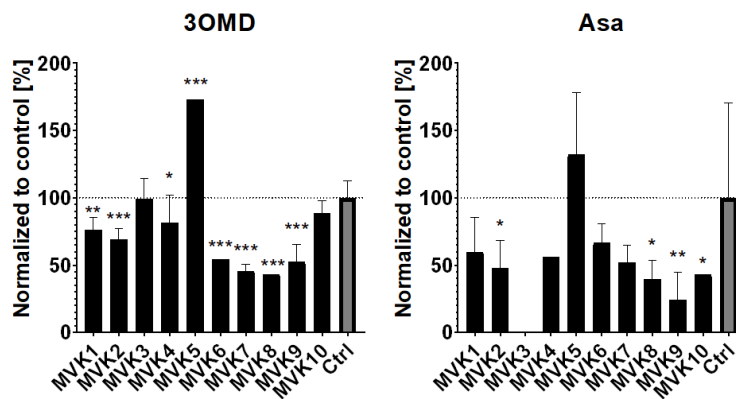


Figure 68 - Continuation of AA determination. Results of MVK patients were normalized to the controls (set to 100 %). Data are presented as biological replicates' mean \pm SD (n=2).

For methionine (Met), a general decrease in MVK patients could be seen and MVK1 had the lowest significant reduction of 42 % \pm 8 %. The amino acids histidine (His), tyrosine (Tyr), ornithine (Orn), 3-O-methyl-dopa (3OMD) and argininosuccinic acid (Asa) showed a significant downregulation. No changes were found for phenylalanine (Phe), aspartic acid (Asp), tryptophane (Trp) and citrulline (Cit). A general significant increase in glutamic acid (Glut), glycine (Gly), arginine (Arg) and homocitrulline (HCl) could be demonstrated in the analysis.

7.14 Lipid analysis

As the mevalonate pathway produces important substrates for the lipid cholesterol and other lipids, it was interesting to see if there is a general effect on the lipid metabolism.

7.14.1 Lipid Oil Red O analysis

To get an overall view on the lipid build up in patient cells compared to control cells, the staining compound Oil Red O was used to stain triglycerides. After fixation and staining the cells were viewed under a light microscope and then quantified (n=3) by destaining and measuring the extract in a photometer. As seen in Figure 69, there was a general increase of triglycerides in the MVK cells except for MVK2 and MVK11.

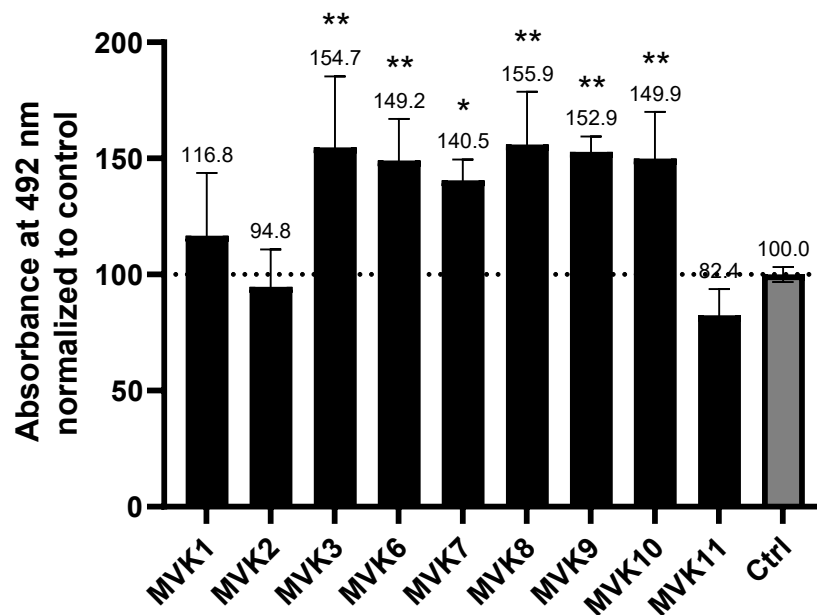


Figure 69 - Quantification of Oil Red O staining in MVK patients normalized to the control. Cells were grown in a 24 well plate (n=3), stain was extracted in 250 μ l isopropanol and 200 μ l were used to measure the Oil Red O stain in a 96 well plate reader at 492 nm.

7.14.2 Dolichol measurement

As dolichol is a direct product of the mevalonate pathway, it was especially interesting to see what effect the MVK defect has on it. In collaboration with Britta Brügger (BZH, Heidelberg) the total dolichyl phosphate (DoIP) levels were measured in cell lysates (n=2) by RP-LC-MS. Results can be seen in Figure 70. All 11 MVK patients showed at least $*$ ($p < 0,05$) a significant reduction in total dolichyl phosphate levels. Patient MVK8 (0.084 ± 0.001 DoIP [ng]/PC [nmol]) and MVK10 (0.081 ± 0.028 DoIP [ng]/PC [nmol]) had the lowest levels.

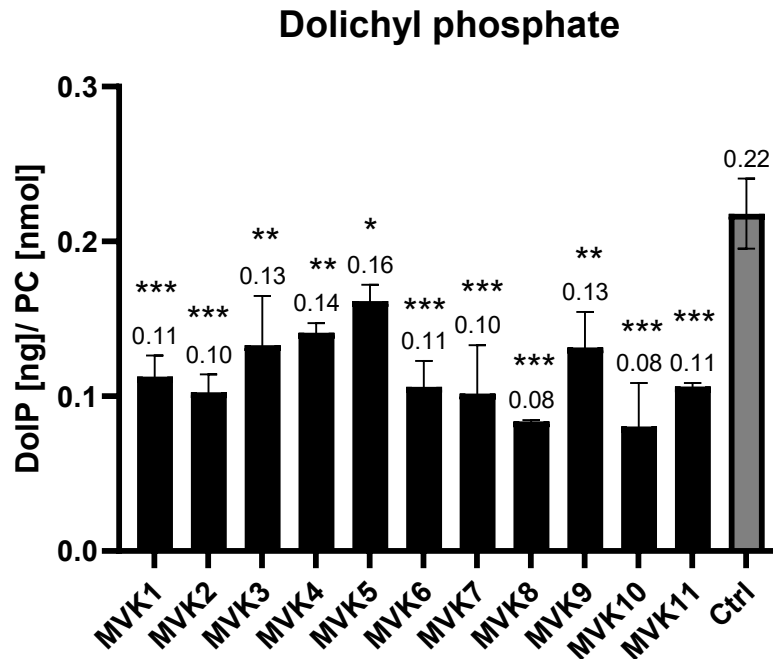


Figure 70 - Dolichyl phosphate levels in MVK patients' fibroblasts and controls. Total DoIP amounts were normalized to phosphatidylcholine (PC). Data are presented as biological replicates' mean \pm SD (n=2).

After the total amount of dolichyl phosphate was measured, the distribution of different dolichyl phosphate species ranging from C70 to C105 were determined. The different chain length dolichyl phosphates can be seen in Figure 71 and Figure 72.

Starting at C70 DoIP, all MVK patients showed an elevation ranging from 0.375 % \pm 0.035 % (MVK5) to 0.85 % \pm 0.057 % (MVK7) compared to the control (0.305 % \pm 0.021 %). MVK6 (0.53 % \pm 0.042 %), MVK7, MVK8 (0.59 % \pm 0.141 %) and MVK10 (0.51 % \pm 0.014 %) were significantly increased. For C75 DoIP only MVK7 (0.83 % \pm 0.057 %), MVK8 (0.655 % \pm 0.148 %) and MVK10 (0.62 % \pm 0.042 %) have a significant increase compared to the control (0.395 % \pm 0.021 %). Except for MVK5, the general trend was an elevation in this species. The result for species C80 DoIP was similar to C75 DoIP. For C85 DoIP all MVK patients, except MVK5, showed a significant elevation compared to the control (2.33 % \pm 0.042 %) ranging from 2.84 % \pm 0.014 % (MVK4) to 4.265 % \pm 0.46 % (MVK10). The C90 DoIP species were significantly (***, $p > 0.001$) elevated in all MVK patients, except MVK5, compared to the control (18.92 % \pm 0.205 %). They ranged from 21.94 % \pm 0.983 % (MVK4) to 31.38 % \pm 0.134 % (MVK10). For C95 DoIP MVK patients show a slight increase compared to the control (52.39 % \pm 0.247 %), except for MVK5 (52.2 % \pm 0.049 %). Significant elevation ranging from 53.10 % \pm 0.212 % (MVK9) to 65.43 % \pm 0.41 % (MVK11) were seen.

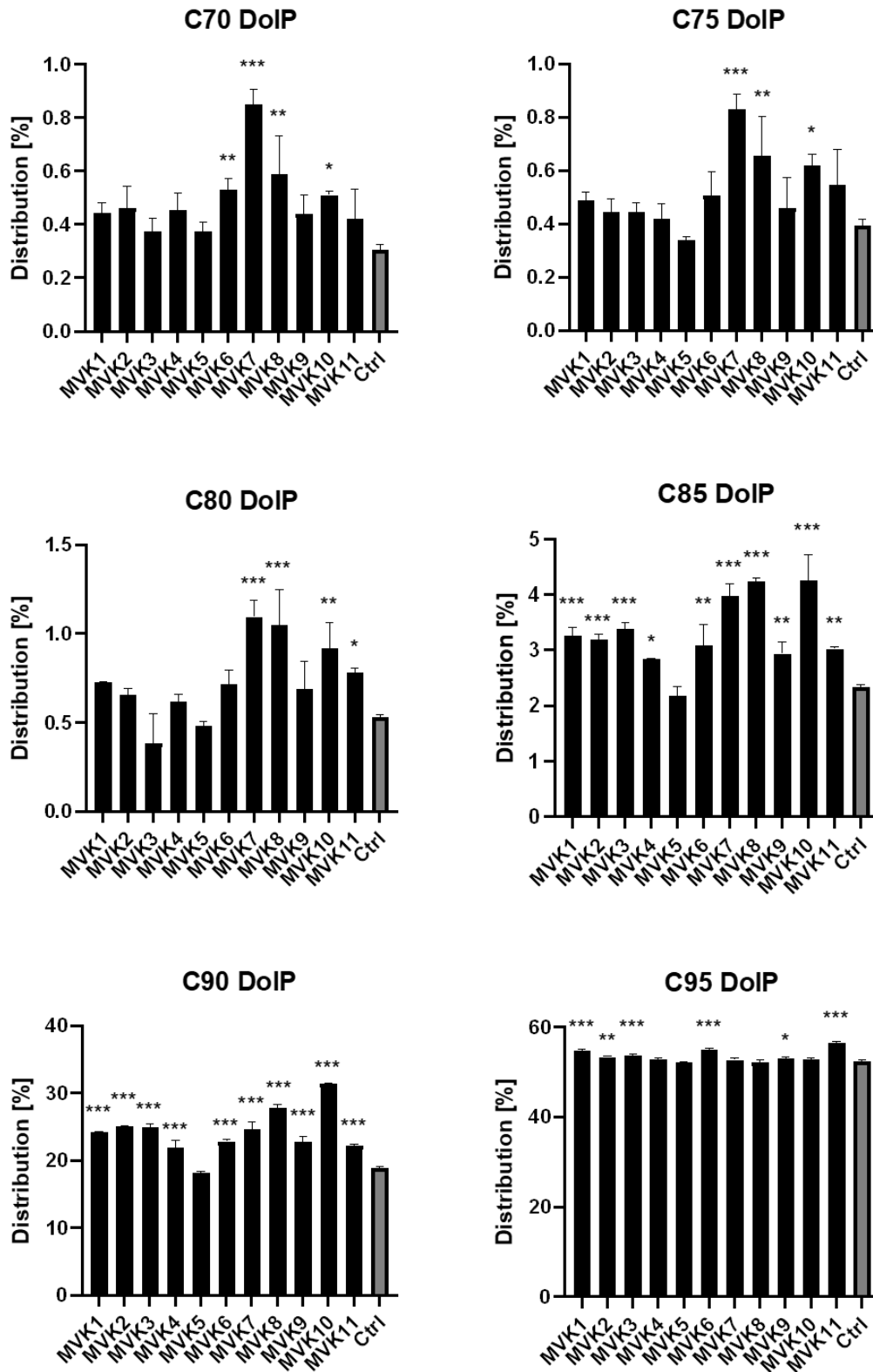


Figure 71 - DoIP species distribution in MVK patients and control. Distribution of DolPs ranging from C70 to C105 in MVK patient fibroblasts and control cells displayed as a percentage of all DoIP species. Data are presented as biological replicates' mean \pm SD (n=2).

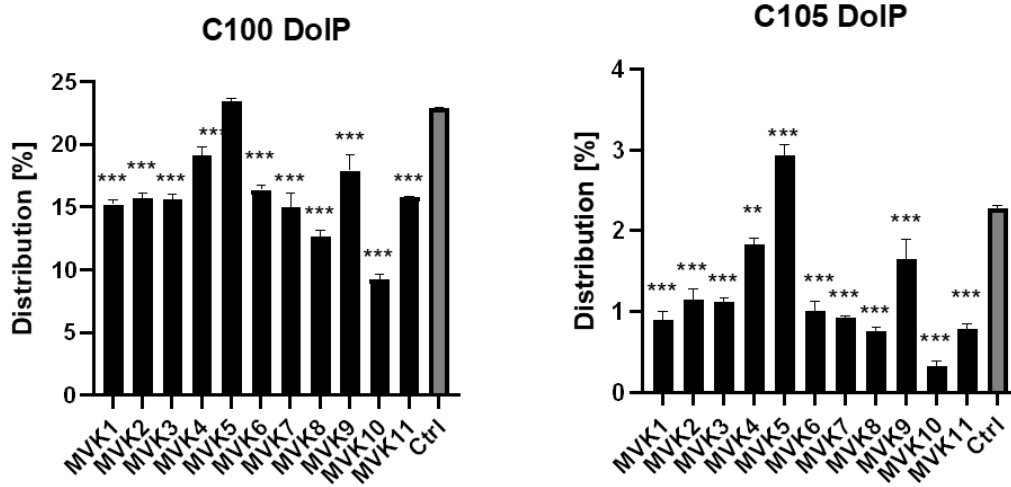


Figure 72 - Continuation of DoIP species distribution. Distribution of DoIPs ranging from C70 to C105 in MVK patient fibroblasts and control cells displayed as a percentage of all DoIP species. Data are presented as biological replicates' mean \pm SD (n=2).

For the DoIP species C100 and C105, the trend is different. All MVK patients (except MVK5) showed a significant decrease (***, $p > 0.001$) compared to the control. Levels of C100 DoIP ranged from 9.25 % \pm 0.39 % (MVK10) to 19.15 % \pm 0.67 % (MVK4) and for C105 DoIP from 0.79 % \pm 0.057 % (MVK10) to 1.84 % \pm 0.071 % (MVK4). The control levels were 22.87 % \pm 0.092 % and 2.28 % \pm 0.035 %, respectively. Interestingly, this time MVK 5 was elevated for C100 DoIP to 23.39 % \pm 0.24 % and for C105 DoIP up to 2.94 % \pm 0.14 %.

7.14.3 Lipidomics

As lipid abnormalities were seen in the MVK patients a lipidomic analysis with nano-electrospray ionization tandem mass spectrometry was performed in collaboration with Britta Brügger (BZH, Heidelberg). Lipids were measured in cell lysates from MVK patients (n=4) and controls (n=4).

The analysis of the steroids cholesterol (Chol) and cholesterol ester (CE) can be seen in Figure 73. The cholesterol levels were quite diverse in the MVK patients and ranged from 21.6 ± 0.3 Mol % (MVK3) to 31.5 ± 1.0 Mol % (MVK6) compared to the control with 26.3 ± 1.0 Mol %. Particularly striking were the cholesterol ester levels that were significantly (***) ($p > 0.001$) decreased in all MVK patients compared to the controls.

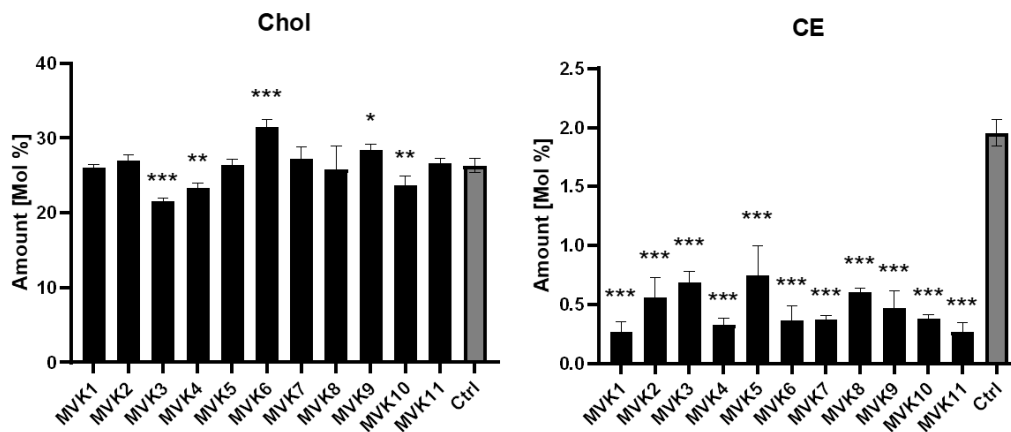


Figure 73 - Cholesterol and cholesterol ester measurement. Depicted is the detected lipid in Mol % in MVK patient fibroblast and in control cells. Data are presented as biological replicates' mean \pm SD (n=4).

The results of the sphingolipid measurements of ceramide and sphingomyelin are depicted in Figure 74. Ceramide was (significantly) increased in all MVK patients ranging from 0.286 ± 0.01 Mol % (MVK1) to 2.1 ± 0.16 Mol % (MVK10) compared to the control with 0.263 ± 0.003 Mol %. Also, for sphingomyelin an increase in MVK patients was visible ranging from 4.2 ± 0.06 Mol % (MVK3) to 7.7 ± 0.2 Mol % (MVK6) compared to the controls with 4.6 ± 0.2 Mol %.

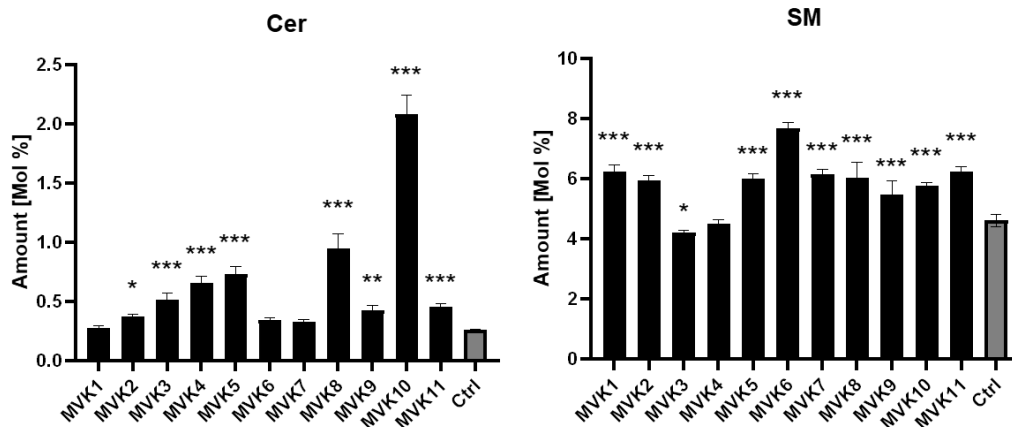


Figure 74 - Ceramide and sphingomyelin measurement. Depicted is the detected lipid in Mol % in MVK patient fibroblast and in control cells. Data are presented as biological replicates' mean \pm SD (n=4).

The ester linked glycerophospholipids phosphatidylethanolamines (PE) and phosphatidylserines (PS) were also measured, and results can be seen in Figure 75. Except for MVK3 (16.4 ± 1.5 Mol %), all MVK patients had a significant decrease in PE ranging from 10.3 ± 0.4 Mol % (MVK6) to 15.6 ± 0.5 Mol % (MVK4) compared to the control (16.7 ± 0.5 Mol %). The analysis of PS revealed an increase in MVK patients ranging from 5.26 ± 0.5 Mol % (MVK3) to 6.1 ± 0.3 Mol % (MVK1) compared to the controls (5.23 ± 0.1 Mol %). The increase was significant for MVK1, 4, 5, 7, 10 and 11.

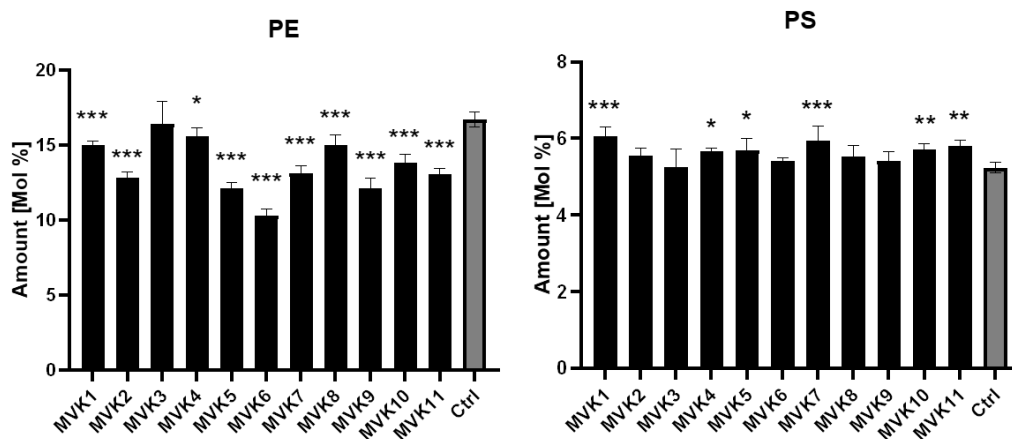


Figure 75 - Phosphatidylethanolamines and phosphatidylserines measurement. Depicted is the detected lipid in Mol % in MVK patient fibroblast and in control cells. Data are presented as biological replicates' mean \pm SD (n=4).

The results of the plasmalogens (ether linked glycerophospholipids) alkyl-phosphatidylcholines (PC O-), alkyl-phosphatidylserines (PS O-) and alkyl-phosphatidylinositols (PI O-) can be seen in Figure 76 and Figure 77. All MVK patients showed an increase in these ethers linked to glycerophospholipids compared to the controls. PC O- levels range from 3.93 ± 0.2 Mol % (MVK8) to 5.15 ± 0.1 Mol % (MVK5) compared to the controls (3.79 ± 0.09 Mol %). The plasmalogen PS O- was significantly increased (**, $p < 0.01$) in all MVK patients in the range of 0.405 ± 0.03 Mol % (MVK9) to

0.452 ± 0.027 Mol % (MVK6) compared to the controls (0.339 ± 0.02 Mol %). For PI O- also all MVK patients show a significant increase (**, p<0.01) compared to the controls (0.109 ± 0.008 Mol %), except for MVK1 (0.141 ± 0.025 Mol %).

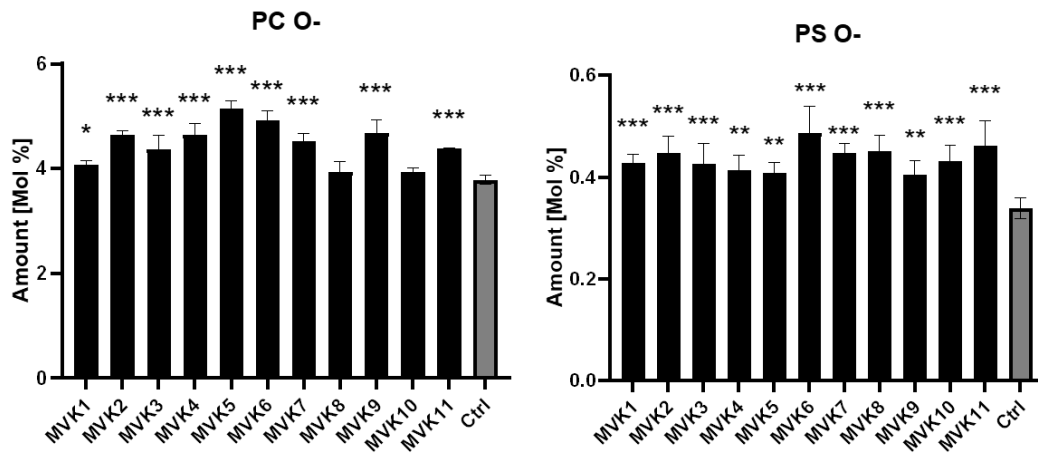


Figure 76 – Alkyl-phosphatidylcholines and alkyl-phosphatidylserines measurement. Depicted is the detected lipid in Mol % in MVK patient fibroblast and in control cells. Data are presented as biological replicates' mean ± SD (n=4).

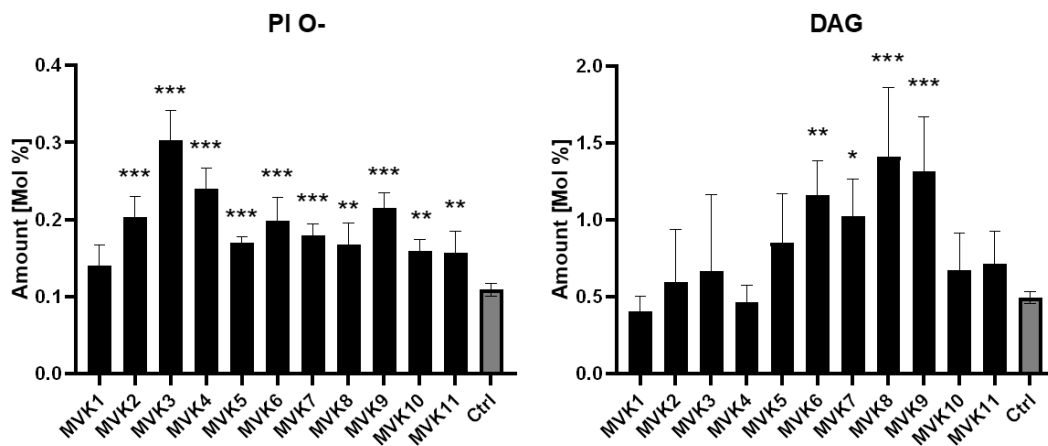


Figure 77 – Alkyl-phosphatidylinositols and diacylglycerol measurement. Depicted is the detected lipid in Mol % in MVK patient fibroblast and in control cells. Data are presented as biological replicates' mean ± SD (n=4).

The glycerolipid diacylglycerol (DAG) was also analyzed and results can be seen in Figure 77. Except for MVK1 and MVK4, the MVK patients showed an increase in DAG compared to the controls (0.497 ± 0.038 Mol %). MVK6(1.16 ± 0.2 Mol %), MVK7(1.03 ± 0.24 Mol %), MVK8 (1.41 ± 0.45 Mol %) and MVK9 (1.32 ± 0.35 Mol %) had a significant increase.

7.15 Proteomics analysis

Proteome profiling was supported by the Core Facility for Mass Spectrometry & Proteomics (CFMP) at the Center for Molecular Biology at University of Heidelberg (ZMBH). MVK patients (n=1) and five controls were measured by LC-ESI-MS. Several steps were performed for filtering and data manipulation. First contaminants were removed and then data log (2) transformed and normalized. Second, clustering in groups (healthy individuals, MVK defect) and phenotype (healthy, mild, severe) was performed (see Figure 78).

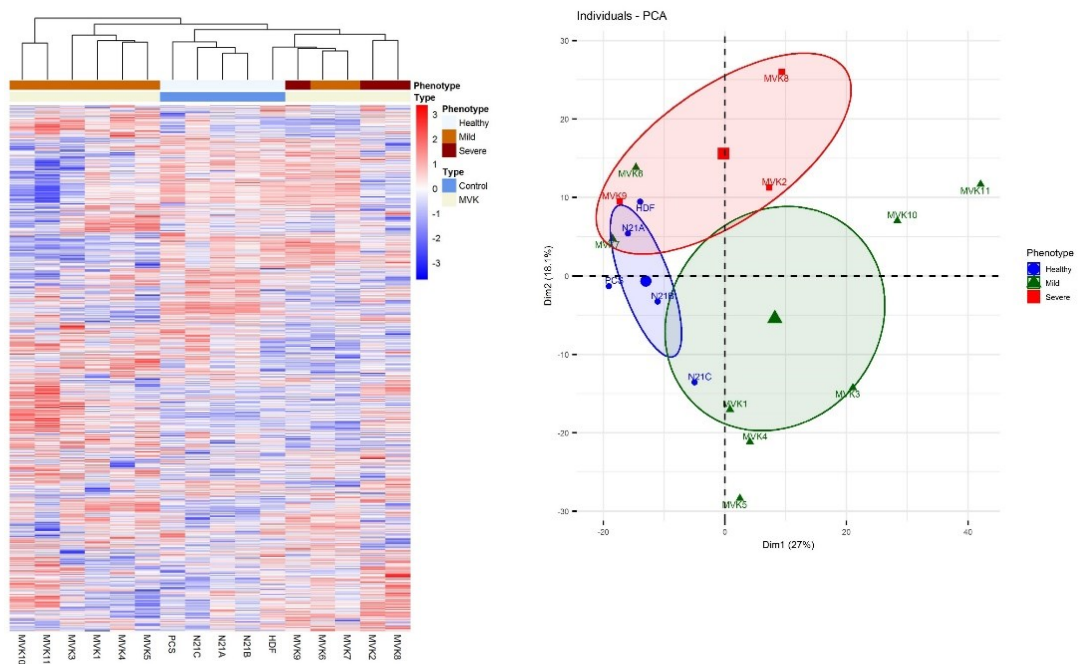


Figure 78 - Clustering in groups and PCA. Left side: Heatmap of MVK versus control. Right side: PCA blot of MVK versus control. Figure created by Marcin Luzarowski (ZMBH).

Based on the results of the clustering and PCA, three groups were defined: Healthy (controls), mild (MVK1, 3, 4, 5, 10, 11) and severe (MVK2, 6, 7, 8, 9). The data was annotated using the new groups (Figure 79) and one-way ANOVA (1 factor – phenotype) was used to test for significant changes (FDR/BH corrected $p \leq 0.05$) followed by TukeyHSD (pairwise comparison $p \leq 0.05$). Selected were:

- MVK affected: Control-mild $p \leq 0.05$ and Control-severe $p \leq 0.05$
- Severely affected: Control-severe $p \leq 0.05$ and Severe-mild $p \leq 0.05$
- Mildly affected: Control-mild $p \leq 0.05$ and Severe-mild $p \leq 0.05$

In the last step, enrichment (KEGG pathway) analysis was performed for significantly affected proteins.

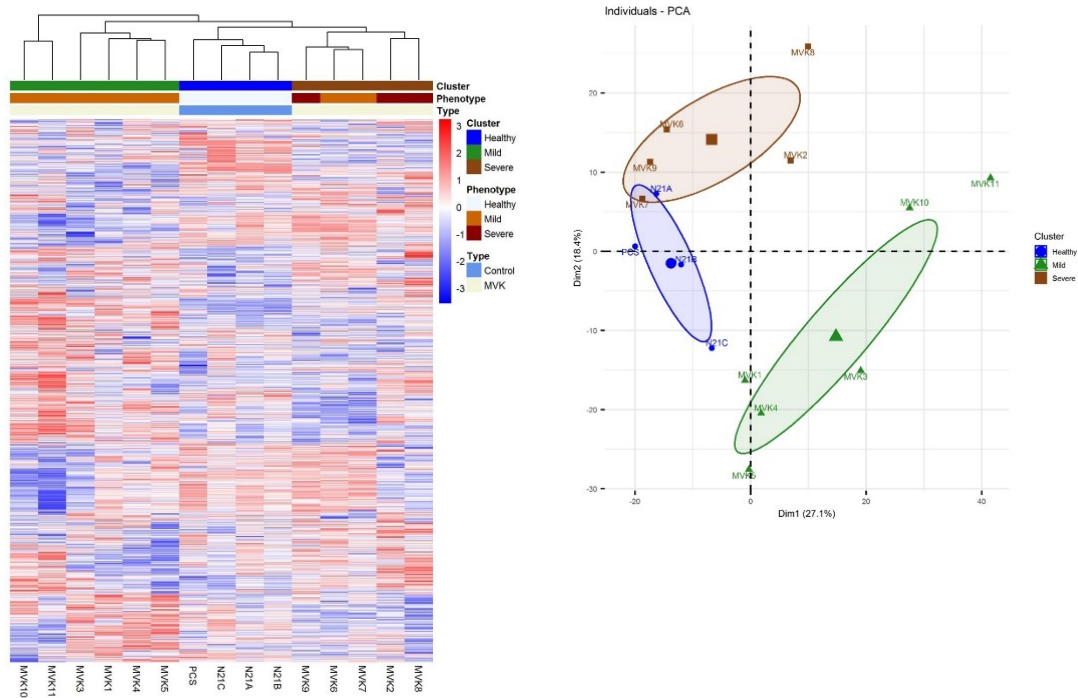


Figure 79 - New groups after clustering and PCA. Left side: Heatmap of MVK versus control after clustering. Right side: PCA blot of MVK versus control after clustering. Figure created by Marcin Luzarowski (ZMBH)

The results of the enrichment KEGG pathway analysis can be seen in Figure 80 - Figure 81 and four reference pathways were chosen with the highest coverage of affected genes for the group of all MVK patients, the severe phenotype and the mild phenotype. The arrows depict whether a gene is up- or down-regulated. A full list of all significant affected genes can be found in 10.6.

For the MVK affected group, 58 significantly affected proteins were found. The pathway with the highest coverage of affected genes of 0.14 is the pathway of the Epstein-Barr virus infection ($p=0.049$) followed by the antigen processing and presentation of 0.12 ($p=0.038$). The pathway of biosynthesis of nucleotide sugars ($p=0.049$) and the pathway of the 2-oxocarboxylic acid metabolism ($p=0.021$) had a coverage of 0.08.

For the severely affected group (MVK2, 6, 7, 8, 9), 36 significantly affected proteins were found. This low number made it not possible to perform a KEGG pathway analysis. A general pathway was found, and genes are depicted in Table 38.

For the mildly affected group (MVK1, 3, 4, 5, 10, 11), 115 significantly affected proteins were found. The pathway with the highest coverage of affected genes for the mild phenotype group (MVK1, 3, 4, 5, 10, 11) with 0.17 was the lysosome pathway ($p>0.001$) followed by the phagosome with 0.13 ($p>0.001$). The pathway of other glycan degradation had a coverage of 0.05 ($p=0.003$) and the pathway of the glycosphingolipid biosynthesis - ganglio series ($p>0.001$) had a coverage of 0.03.

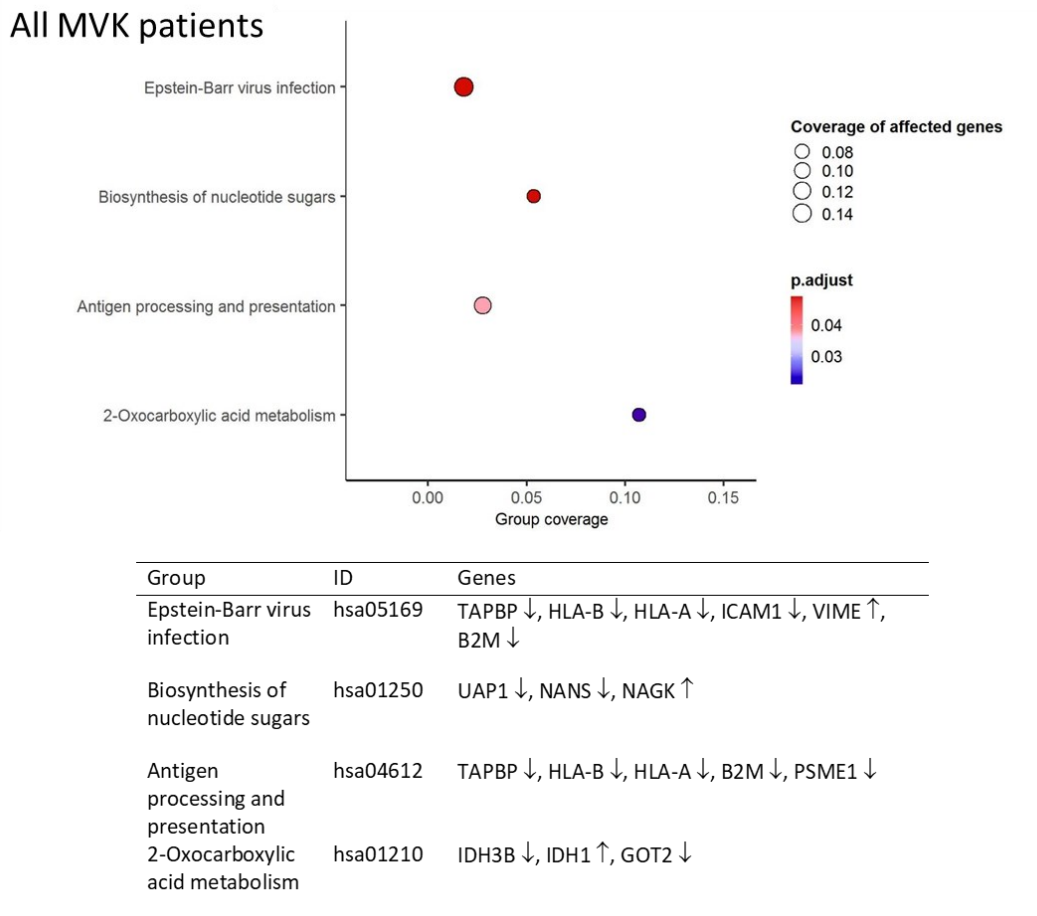


Figure 80 - KEGG pathway analysis of MVK affected. Depicted are the results of the KEGG pathway analysis with affected genes for all MVK patients.

Table 38 - KEGG pathway analysis of severely affected. Depicted are the results of the KEGG pathway analysis with affected genes for the severe phenotype of MVK.

| Severe phenotype | | |
|--------------------|----------|--|
| Group | ID | Genes |
| Metabolic pathways | Hsa01100 | HSD17B4 ↓, IDH2 ↓, ACLY ↑, PFKP ↑, PTGS1 ↓, UAP1 ↑, PAPSS1 ↑ |

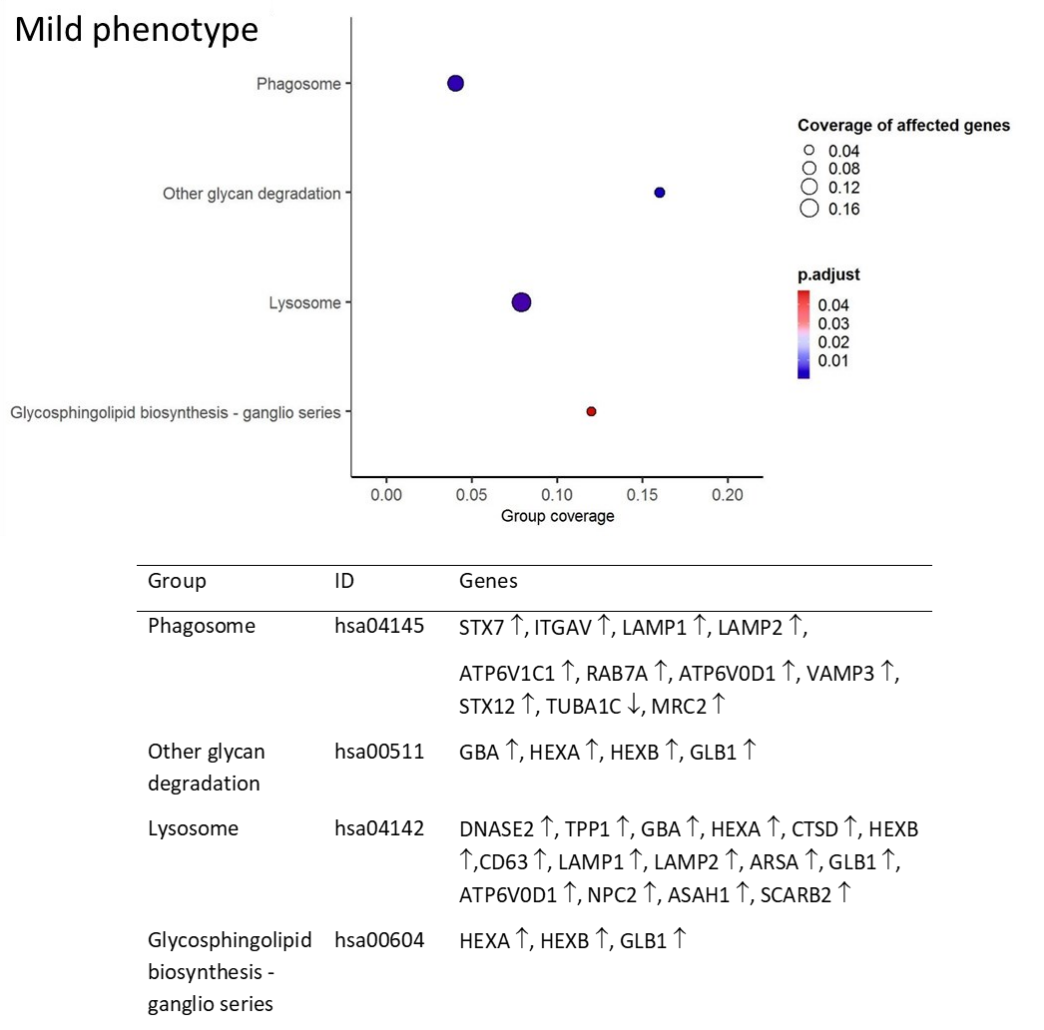


Figure 81 - KEGG pathway analysis of mildly affected. Depicted are the results of the KEGG pathway analysis with affected genes for the mild phenotype of MVK.

7.16 Complementation of fibroblasts with the MVK-wildtype gene

A viral complementation study with the *MVK* wildtype gene was performed. The listed mutations of the *MVK* patients (see Table 34) should be complemented with the *MVK* construct, which causes the phenotype observed in the primary fibroblast of the patients. The *MVK* wildtype cDNA was tagged to produce the *MVK_MYC* construct and to detect it specifically. The construct was cloned into the retroviral vector pLNCX2 as described in section 6.4. Patient cells and control cells were transfected with the pLNCX2_ *MVK_MYC*-tag plasmid or the empty pLNCX2 vector (mock). Cells were grown in 0.1 % neomycin to have a slight selection pressure and that cells won't lose the plasmid. Transfection for *MVK4* and *MVK8* did not succeed, as cells died in the selection phase.

7.16.1 Expression of *MVK_MYC*

The transfected cells were harvested as explained in section 6.1.3. To investigate the expression of the 43 kDa *MVK_Myc* construct, western blot analysis with anti-Myc and anti-MVK antibodies was performed. As seen in Figure 82, a clear signal with the anti-Myc antibody at 43 kDa was detected in the cells transfected with the pLNCX2_ *MVK_MYC*-tag vector. In comparison to the cells transfected with mock, an increase in signal intensity of 13120 % (*MVK1*) to 1145 % (*MVK5*) in patients was achieved. The control displays an increase of 1733 %. This shows that the transfection was successful and that the construct is expressed.

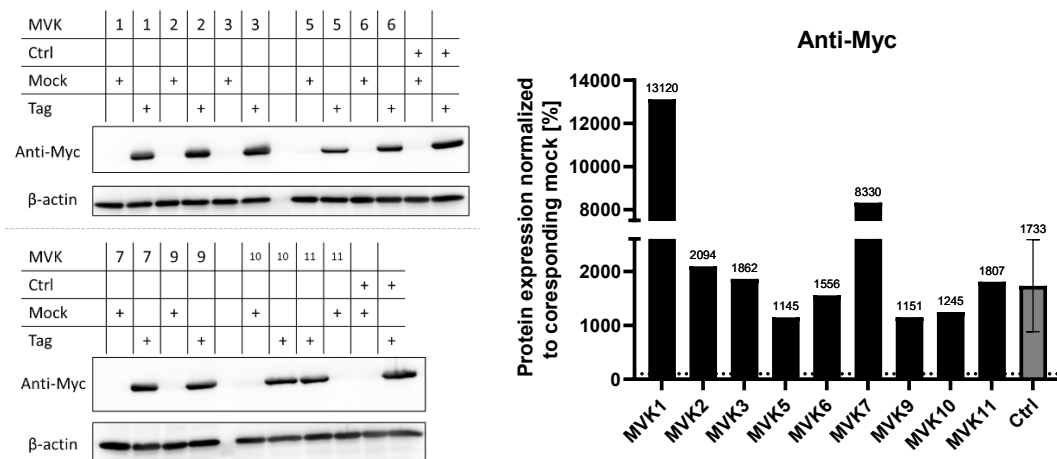


Figure 82 - Detection of *MVK Myc*-tag construct in lysates by anti-Myc of transfected cells. Left side: Western blots of *MVK* patient fibroblasts and control cells with anti-Myc detection. Right side: Quantification of western blot signal normalized to β-actin.

The analysis was repeated and the antibody anti-MVK was used (Figure 83). A clear overexpression of the MVK_Myc construct in all cells was detected. In comparison to the cells transfected with mock, an increase in signal intensity of 1194 % (MVK1) to 225 % (MVK6) was achieved in the patients. The control displayed the lowest increase of 185 %. The pattern of anti-MVK correlates with the one of anti-Myc. Patient MVK1 shows the highest overexpression followed by MVK7 and MVK2.

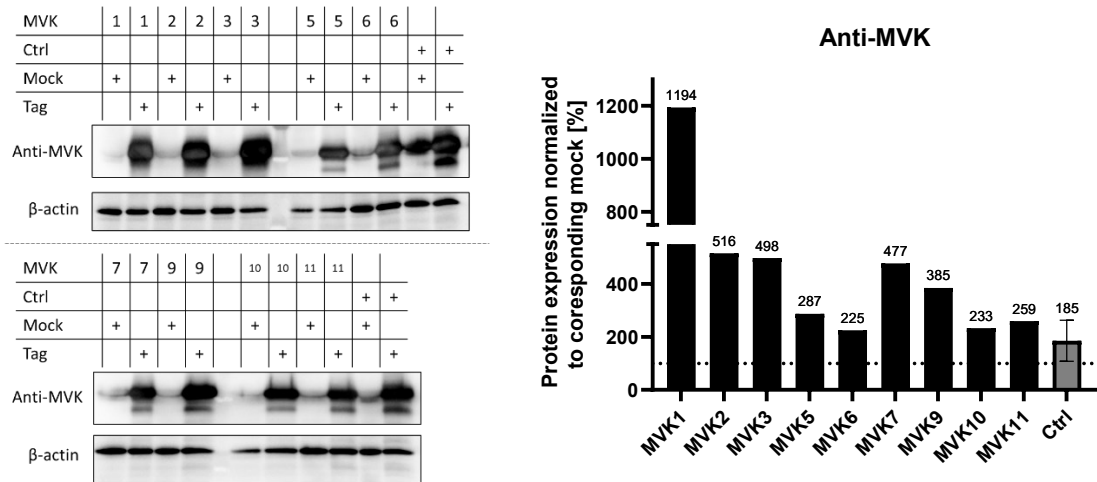


Figure 83 - Detection of MVK Myc-tag by construct anti-MVK in lysates of transfected cells. Left side: Western blots of MVK patient fibroblasts and control cells with anti-MVK detection. Right side: Quantification of western blot signal normalized to β -actin.

8 Discussion

The mevalonate kinase deficiency (MKD) is an inherited disorder of the cholesterol biosynthesis. This early-onset disease is caused by mutations in the *MVK* gene and was first described in the 1980s [78], [79]. MDK belongs to the ultra-rare diseases as only approximately 300 patients have been identified and have been reported to literature [83], [84]. There are two groups into which the *MVK* patients are divided. The mevalonate kinase deficiency (MKD)/ hyperimmunoglobulinemia D syndrome (HIDS) group and the mevalonic aciduria (MVA) group, which is the more severe end of the spectrum of symptoms. The clinical picture was summarized in Figure 11 and includes recurrent febrile crises, often accompanied by hepatosplenomegaly, lymphadenopathy, arthralgia, and skin rashes. The gold standard screening method to diagnose this disease is the proof of urinary mevalonic acid excretion by stable isotope dilution chromatographic-mass spectrometric analysis as patients have a massive permanent increase of mevalonic acid excretion in urine. The prognosis for patients with early onset multisystemic MVA is poor and half of them die in infancy or early childhood [83]. As diagnosis based on the multisystemic and variable symptoms is nearly impossible, a significant number of patients may remain undiagnosed and not treated efficiently [17]. This hypothesis is supported by the fact that most of the MKD patients have been found in Western Europe or other developed countries as screening for inborn errors of metabolism is here way more common [83], [84].

8.1 Disease causing mutations in the *MVK* gene

The new patient MVK9 displayed the typical symptoms of MVA patients and was diagnosed by the elevated mevalonate acid excretion in urine. During pregnancy the child presented with severe hypertrophic cardiomyopathy and developed severe respiratory distress and hypoxemia immediately after birth. The clinical examination revealed dysmorphic facial features, including prominent frontal bossing, hypertelorism, a triangular-shaped face with low-set ears, and macroglossia. Impaired cardiac function and ophthalmic features like bilateral cataracts and diffuse retinal hemorrhages were present. The patient also developed a skin rash several days after birth and unfortunately died at day 11 due to cardiac arrest. Genetic analysis confirmed the *MVK* deficiency by finding the homozygous mutation in exon 9 (c.[803T>C], p.[Ile268Thr]). To increase the cohort and to get a better understanding of the pathophysiology, ten diagnosed *MVK* patients were included in this work. Sanger sequencing of these patients revealed two new mutations, c.782T>C in *MVK10* and c.790dupC in *MVK3*, which are not in the NCBI ClinVar database yet. All 11 patients belong to the MVA group, whereby also differences in the severity of the phenotype were present. The variants and phenotype of all *MVK* patients characterized in this study are depicted in Table 34. MVK9 carries the same variant as patient MVK2. Both patients showed a severe phenotype with fatal outcome. The affected amino acid I²⁶⁸ and adjacent amino acids (S²⁶⁷, D²⁶⁹, A²⁷⁰, I²⁷¹) are highly conserved throughout different

species and even in species like *Xenopus tropicalis* and *Caenorhabditis elegans* this region is highly conserved (see Table 32). This indicates the importance of this protein part for functional and structural integrity.

In silico methods were used to predict whether the c.[803T>C] mutation in the *MVK* gene could have a pathogenic effect in the patient. The mutation leads to a change from Ile to Thr at position 268 in the protein. Six high-performance in-silico prediction meta scores were annotated using the dbNSFP database v4.2A and all scores predicted a pathogenic variant (Table 33). The DynaMut software was used to get an understanding of the impact of the mutation on the tertiary structure of the *MVK* protein. The prediction showed a destabilizing effect and an increase of flexibility in the molecule. All these results let assume a severe impact in the *MVK* proteins of patients MVK9 and MVK2.

8.2 MVK expression analysis

The analysis revealed a diminished *MVK* protein expression in all *MVK* patients ranging from 65 % (MVK11) to 4 % (MVK5) residual amount compared to controls as seen in Figure 17. The average protein expression of all *MVK* patients together was 27 %. Interestingly, all mutations in the patients lead to a reduced protein expression which was supported by the results of the immunofluorescence staining showing a diminished signal intensity compared to controls (see Figure 20). A cytosolic location was confirmed by the colocalization with the cytosolic PMM2 [105]. Notably, cell morphology of patients MVK 8 and MVK11 were different compared to all other cell lines presenting with more spread out growing and bigger cytosolic volume.

To elucidate whether the mutations already had an effect on mRNA stability, the *MVK* transcript levels were analyzed by qRT-PCR. As seen in Figure 18, all patients showed significant increased *MVK* mRNA levels except for patient MVK5 (0.69). MVK9 showed the highest transcript level of 4.11 compared to controls. The results let assume that the mutations (except MVK5) did not impact the stability of the *MVK* transcripts, and the reduced protein expression was the result of protein instability or degeneration. Only the homozygous mutation c.[60T>A] in MVK5 lead to decreased stability and/or degradation of the mRNA transcript. The elevated transcript level in most of the *MVK* patients is rated as compensatory effect of the cells to synthesize more *MVK* protein. In this course also the two genes *HMGCR* and *PMVK* were analyzed by qRT-PCR, as these are the ones before and after the mevalonate kinase in the polyisoprene pathway. The results showed that the mutations in the *MVK* gene leads to an increase in *HMGCR* transcript in the range of 1.8 (MVK10) to 3.9 (MVK9) which was assumed to allocate more *HMGCR* protein and hereby substrate for the *MVK*. No effect on *PMVK* transcript level was found (Figure 19).

8.3 Impaired cellular proliferation

Since during cultivation of the primary fibroblast of the MVK patients a slower growing was observed for some of the patient cells, an analysis on cell growth and proliferation was performed. For the starting seeding density of 1000 cells per well all MVK patients except MVK1 and MVK2 showed a significantly decreased specific growth rate. The new patient MVK9 had the lowest specific growth rate and the highest doubling time (Figure 22). For a seeding density of 2000 cells also MVK1 and MVK2 had a significantly decreased specific growth rate compared to controls. Interestingly, MVK patients often show a phenotype like skin rash and edema. An important product of the mevalonate pathway is vitamin D. It is known that vitamin D is very important for skin health [106], [107]. Unfortunately, no data on vitamin D levels in MVK patients were available, but low levels may be a reason for these skin phenotypes. Additionally, MVK patients can have low levels of coenzyme Q10 as seen in Table 34 as this is also a product of the mevalonate pathway. Coenzyme Q10 is antioxidant and protects cells against free radicals. Is also works together with vitamin E as Q10 regenerates it [108]. These two features may also have an impact on fibroblast growth and lead to the skin phenotype of the MVK patients. A common treatment regime for MVK patients is a combination of coenzyme Q10, vitamin E and vitamin C as is has been shown that it positively affects the disease course [17]. However, also vitamin D supplementation should be considered.

8.4 Impaired glycosylation status in MVA and the connection to CDG

Dolichol displays the lipid anchor in the lipid linked oligosaccharide synthesis and is also needed for the buildup of Dol-P-Man and Dol-P-Glc, all essential for the N-glycosylation machinery. Since one of the end products of the mevalonate pathway is dolichol, the hypothesis was made, that MKD patients might have a reduced amount of dolichol and thereby an impaired N-glycosylation. To address this question, lectin binding studies and expression analysis of N-glycosylation markers (ICAM1, LAMP1 and LAMP2) followed by total N-glycan analysis by xCGE-LIF with patients` fibroblasts protein extracts were carried out. Furthermore, a glycosphingolipid analysis by xCGE-LIF was performed.

The lectin NPA was used to detect α -mannose residues of attached glycans to proteins. The results show a significant increase in the NPA signal indicating a shift to more high-mannose type glycans in MVK patients (Figure 24). The mean of all MVK patients resulted in an increase to 140 % NPA signal compared to controls. This feature is supported by the results of the lectin ConA, which recognizes α -mannose and additional α -glucose residues. The mean of all MVK patients resulted in an increase to 206 % ConA signal compared to controls (Figure 25). The lectins GNA and LCH also belong to this category and the results showed an increase in signal in the MVK patients (Figure 26). LCH is also used as a core fucose binding lectin and data correlated with the results of AAL below (see below) [109]. The average of MVK patients together resulted

in an increase to 155 % for GNA and 173 % for LCH compared to controls. The lectin DSL was used for the detection of β 1-6-mannose-GlcNAc, β 1-2-mannose-GlcNAc and GlcNAc residues. All MVK patients displayed an elevated signal (177 %) compared to controls (Figure 27). To address the fucosylation status of the MVK patients the lectin AAL was used. The mean all MVK patients together resulted in an increase to 155 % of the AAL signal compared to controls (Figure 28). Sialylation was checked with MAL I. The results displayed an increase in MVK patients of 169 % compared to controls (Figure 29). The lectins SNA and WGA recognize sialic acids residues attached to terminal galactose and WGA additional N-acetyl-D-glucosamine. MVK patients showed a slight increase compared to controls whereby the increase was not significant as results were quite diverse (Figure 30). Last the lectin ECL for galactose residues was used. Five of the MVK patients (MVK1, 2, 6, 10, 11) showed an increase whereby the other ones showed a decrease in signal (Figure 31). Lectin analysis with ConA, SNA and WGA were not performed for MVK10 and MVK11.

As the lectin binding studies revealed a general disturbance on the protein N-glycosylation in MVK patients, the glycosylation and expression status of the glycosylation markers ICAM1, LAMP1 and LAMP2 were examined next. These proteins are modified with multiple N-glycans and are therefore used as marker proteins for glycosylation [110], [111]. Western blot analysis of the MVK patients' fibroblasts revealed hypoglycosylated forms of ICAM1 which is shown by the significantly reduced ratio of glycosylated to non-glycosylated ICAM1 in all MVK patients (Figure 33). Since ICAM1 is a cell adhesion molecule that belongs to the immunoglobulin superfamily, the cell proliferation phenotype observed in the patients' fibroblast might be correlated to the hypoglycosylation of ICAM1. The growth in cell culture at a certain confluency is dependent on the cell-cell interaction as proliferation signals are exchanged between the cells. If the cell-cell interaction is impaired due to hypoglycosylated receptor structures, proliferation is affected subsequently. It has been shown that loss or blockade of functional ICAM1 reduced cell proliferation in tight skin mice [112]. Combining this with the other findings, glycosylation of ICAM1 might be necessary for the functionality of the protein [113]. Due to insufficient glycosylation ICAM1 is dysfunctional and proliferation signaling at higher cell densities is attenuated. ICAM1 might only be one protein for which this context is true. The relationship between hypoglycosylated ICAM1 and reduced proliferation might be directly correlated with the phenotype of the MVK patients presenting with microcephaly and failure to thrive. Reduced glycosylation of ICAM1 was reported by He *et al.* in ALG1-, MPI- and PMM2-CDG [114].

For LAMP1 a significant elevated expression in MVK1, 2, 3, 7, 8, 9, 10 and 11 was found. Also, a broader band than for the controls was found, that indicated the presence of hypoglycosylated LAMP1 forms. An overexpression of LAMP1 is found in several cancer types [115]–[118] and an abnormal glycosylation may play a role in the Nieman-Pick disease [119]. For LAMP2 the effect of the broader protein band was even more

prominent in the MVK patients than for controls. As for LAMP1 the broader band in LAMP2 indicates hypoglycosylation protein forms which have been found also in other CDG types as ALG3-CDG [120] and STT3A-CDG [121]. Interestingly in MVK1, 3, 5, 6 and 10 LAMP2 was significantly more expressed compared to controls. Damaghi *et al.* showed in their study, that chronic acidosis in the tumor microenvironment leads to an enhanced expression in LAMP2 [122]. As MVK patients have a state of chronic acidosis because of high levels of mevalonic acid in the body this finding can be a reason for this. In conclusion it could be shown that MVK deficiency leads to a hypoglycosylation of the analyzed marker proteins.

As lectin and western blot studies pointed to a deregulation of N-glycosylation machinery, a quantitative total N-glycan analysis by xCGE-LIF was performed. Therefore, the focus was put on the patients MVK2, 8 and 9 presenting with the most severe phenotype of the patient cohort. In total, 29 N-glycans have been measured and compared to the controls. The analysis revealed a significant increase in high mannose structures in patient MVK2 and MVK9 and supports the result of the lectin binding studies (NPA, ConA). N-glycans are distinguished in complex types, high mannose types and hybrid types. As depicted in Figure 37, a reduction in complex type glycans was seen in all MVK patients. The results for high mannose and hybrid types were diverse. MVK2 and MVK9 (significant) had an increase in high mannose type glycans and MVK8 had a decrease. Vice versa is it for hybrid type glycans, as MVK2 and MVK9 had comparable control levels, but MVK8 a significant increase. To get a better general picture in MVK patients the analysis should be repeated with the missing MVK patients. Notably, in several CDG-I defects (ALG3-, ALG9-, ALG11-, ALG12-, RFT1-, SRD5A3-, DOLK-, DPM1-, DPM3-, MPDU1-, and ALG13-CD) an increase of high mannose structures bound to whole serum glycoproteins was recently reported [123]. This feature was also shown for PGM1-CDG in serum and patient-derived fibroblasts by Zang *et al.* and Wong *et al.* [124], [125]. In more detail, a markedly increase of the Man2 and Man3 was detected in the MVK patients. This overlaps with the Man3 findings in ALG3-CDG, MPDU1-CDG, DPM1-CDG, DPM3-CDG, SRD5A3-CDG, DOLK-CDG, RFT1-CDG, ALG11-CDG, ALG13-CDG, HFI, [123] and also PMM2-CDG plus MPI [126].

All three MVK patients showed an increase in the core fucosylated structure FMan3 which correlates with the results for lectin AAL and especially LCH. Whether these markedly altered sugar structures might serve as diagnostic marker for MKD needs to be determined. To find out, more patients have to be analyzed for abnormalities in the total N-glycans, especially in serum or plasma samples as this is the optimal material for rapid CDG diagnostics. In conclusion it could be shown by lectin studies combined with total N-glycan analysis by xCGE-LIF that MVK deficiency leads to a general disturbance on the protein N-glycosylation.

The new MVK9 patients was also analyzed for abnormalities in glycosphingolipids (Figure 39) and revealed four significantly altered sugar structures. The ganglioside GD3

was present to 19 % in MVK9, whereas it was completely absent in controls. GD3 is a minor ganglioside in most normal tissue and belongs to the acidic glycosphingolipids [127]. GD3 synthase (or sialyltransferase II) catalyzes the addition of a second sialic acid residue to the one of its immediate precursor GM3. GM3 was decreased in MVK9. It is known that GD3 is highly expressed during development and in pathological conditions e.g., in atherosclerosis [128] and in a variety of tumors like central nervous system tumors [129]. Malisan *et al.* proposed that GD3 induces mitochondrial damage and apoptosis [130]. The ganglioside GM2 was also significantly increased in MVK9. Accumulation of GM2 is known to cause neuroinflammation in a mouse model [131] and tumors [129]. Therefore, deregulation of GM2 and GM3 might be an explanation for the brain and CNS phenotype in MVK phenotype. A significant decrease in the ganglioside disialyl Lc4 was also found in MVK9. Recent studies found that disialyl Lc4 is a marker for prostate cancer and increased levels correlate with severity [132]. The feature of a reduced level is uncertain. The fucosylated GSL fucosyl Gm1a and Lex penta were significantly increased in MVK9 which supports the earlier findings of a general hyperfucosylation seen in MVK patients. Notably, elevated expression of GM1a was found in activation of immune cells [133] which supports the hyperinflammatory state MVK patients present. Lex penta plays a role in cell-cell adhesion and communication and is also associated with tumor progression [134], [135]. This finding could also be a reason for the growth and development retardation seen in the MVK phenotype and MVK fibroblasts. Whether these four significantly altered sugar structures and especially GD3 might serve as diagnostic marker for MKD needs to be determined. To find out, more patients have to be analyzed for abnormalities in the glycosphingolipids.

8.5 nCounter expression analysis revealed dysregulation of multiple glycosylation pathways

Although the focus of the study was on N-glycosylation, the transcript nCounter analysis revealed dysregulation of other important cellular pathways as well. The cellular stress genes *ACOX3*, *HiF1alpha* and *SGK1* are upregulated in the MVK patients. *ACOX3* catalyzes the reaction in the peroxisomal β -oxidation where it desaturates acyl-CoA activated fatty acids [136]. It is involved in the degradation of branched-chain fatty acids and is a marker for peroxisomal stress resulting in increased β -oxidation [137]. The protein HiF1alpha is involved in mitochondrial metabolism and has a role in regulating immune cell effector functions [138], [139]. The hyperinflammation state of MVK patients can be a reason for this. An increase can also stimulate some glycolysis-associated genes and regulate the ATP and ROS production. Interestingly, an increase of ATP in the MVK patients' fibroblast was found (see below). In this group *SGK1* had the highest upregulation and contributes to the regulation of inflammation, cell proliferation and apoptosis by activating certain potassium, sodium and chloride channels [140]. An increase displays an important hint for overall cellular stress being present. The transcript reduction of *mTOR* can be explained by the upregulation of *HiF1alpha* as HiF1alpha associated metabolism inhibits the activity of mTOR [139]. The

myopathy phenotype of MVK patients can be explained by this finding as mTOR is a key regulator in maintaining skeletal muscle mass [141]. mTor dysregulation is also connected to neurodegenerative diseases and inflammatory conditions, which is both seen in MVK patients [142]. Concerning the N-glycosylation pathway, the analysis revealed a general upregulation trend in MVK patients. The highest upregulation was seen in *B4GALT1* (1 order of logarithmic magnitude), *MAN1A1* (1.5 order of logarithmic magnitude) and *MAN2A1* (1 order of logarithmic magnitude). The Golgi *B4GALT1* catalyzes the reaction of adding galactose to N-acetylglucosamine on a variety of N-glycans as well as O-glycans. The mannosidases *MAN1A1* and *MAN2A1* also reside in the Golgi lumen and are responsible for the trimming of mannose residues of the N-glycan tree. Also, *MAN1B1* which catalyzes the same reaction, but is mostly located in the ER, was increased. The transcript levels of *MGAT2* and *MGAT3*, which are involved in the N-glycan processing and synthesis of complex- and hybrid type glycans by adding N-acetylglucosamine in the Golgi apparatus [143], were upregulated in the MVK patients. For *FUT8* (MVK1, 6, 7, 8, 10) and *FUT9* a slight upregulation in transcript levels were visible. *FUT9* catalyzes the transfer of fucose from GDP-fucose to GlcNAc-residues of a distal lactosamine unit of a glycoprotein. The upregulation of fucosylation in MVK patients proven by lectin stainings and xCGE-LIF of N-glycans (see above) correlate with this result. Taken all results of the upregulation of the above-mentioned glycosidases and glycosyltransferases together, a profound dysregulation of the N-glycosylation pathway in MVK patients seemed to be present. Interestingly, *FUT9* is also involved in the biosynthesis of Lewis X (LeX) antigen [144]. This correlates with the finding of increased Lex penta found in the new MVK9 patient by the glycosphingolipid analysis. In the group for Nucleotide activated sugars a reduced expression for *GALE* (-1.2 order of logarithmic magnitude), *GMPPA*, *PGM2* (-1.2 order of logarithmic magnitude) and *UAP1* was found. *GALE* catalyzes the epimerization of UDP-glucose to UDP-galactose, and the epimerization of UDP-N-acetylglucosamine to UDP-N-acetylgalactosamine. The enzyme *GMPPA* is involved in the synthesis of GDP-mannose whereas *PGM2* and *UAP1* allocate UDP-N-acetylglucosamine. In addition, an upregulation of *GFPT1* transcripts was visible which pointed to disturbance of the synthesis of GlcNAc-6-P from Fructose-6-P. Also, *PGM1* transcripts were elevated. *PGM1* is an important enzyme for the production of UDP-Gal and UDP-Glc. These results indicate an impairment of essential enzymes in the nucleotide activated sugar synthesis and thereby key sugar donor substrates which is assumed to contribute to the general hypoglycosylation and disturbance on the protein N-glycosylation found in MVK patients. In the O-Glycosylation group are *B3GalNAcT2* and *OGT* both increased in MVK patients. *B3GalNAcT2* is responsible for the attachment of GalNAc-beta-1-3GlcNAc to O-glycans and to some extent to N-glycans. The enzyme *OGT* catalyzes the transfer of a single N-acetylglucosamine in an O-linked manner. These results indicate an impairment in O-glycosylation in MVK patients, which is e.g., important for sorting and secretion of glycoproteins. Mucin-type O-glycopeptides play several roles in cell adhesion and immunological processes and may also contribute to the MVK phenotype

[145]. Interestingly, in the group of dolichol synthesis, which includes the six genes *DHDDS*, *DOLK*, *DPM1*, *DPM2*, *DPM3*, and *SRD5A3*, only *DPM2* was significantly affected and showed a slight downregulation. The MVK mutations seem not to have a significant impact on this pathway. C-mannosylation transcripts are upregulated in MVK patients as an increase *DPY19L1*, *DPY19L3* and *DPY19L4* was present. These enzymes mediate the specific C-mannosylation of tryptophan residues. The upregulation might be a compensatory mechanism by the cells due to reduced availability of Dol-P-Man as donor sugar substrate. These findings indicate that C-mannosylation might be impaired in the MVK patients. For *DPY19L2* a downregulation was found. This enzyme is known to be required for sperm head elongation and acrosome formation during spermatogenesis [146], whereas its role in fibroblasts still needs to be elucidated. However, since its transcript level was downregulated in MVK patients' fibroblast, one can assume that its role in maintaining the cellular metabolism is considered less important than that of the other DPY enzymes. Nevertheless, it could be shown here for the first time, that *DPY19L2* is transcribed in human fibroblasts indicating an alternative and unknown role for the enzyme in this cell type. A group of transcripts including *POMT1* and *POMT2* involved in the O-mannosylation were significantly upregulated. These enzymes are necessary to generate the O-mannose-glycan core structures found on alpha-dystroglycan which is connected to muscular dystrophy as Walker-Warburg syndrome, Muscle Eye Brain disease and limb-girdle muscular dystrophy type 2K [50], [51], [147], [148]. Regrettably, due to the poor growing of patient fibroblasts, only reduced amounts of cell material for all analyses could be received. Thereby, the glycosylation status of alpha-dystroglycan was not analyzed in this work but is considered for future experiments. A clinical feature of MVK patients is muscular weakness and could be caused by impaired O-mannosylation [149]. For all MVK patients together no significant deregulation on *POMGnT1* and *POMGnT2* was found, but in some individual patients they were affected. *POMGnT1* is affected in MVK1, 7 and 11 and *POMGnT2* downregulated in MVK2, 4, 5 and 8. The last group was the Transporter group in which the transporters provide the sugar substrates for N-glycan processing in the Golgi apparatus. The transporter for UDP-galactose (*SLC35A2*) and for GDP-fucose (*SCL35C1*) were both downregulated. Lectin blots revealed an increase in fucosylation so this could be a compensatory mechanism. The same could be applied to the upregulation of the CMP-sialic acid transporter *SLC35A1*.

8.5.1 Analysis of nCounter hits on protein level

To verify if the abnormalities found on transcript level have an effect on the respective proteins as well, western Blot analyses were conducted. The two enzymes *DHDDS* and *SRD5A3* are involved in the dolichol synthesis and were analyzed on protein level. As seen in Figure 52 only MVK1 showed an increase in protein amount for *DHDDS* while for the other MVK patients a decrease was visible. On transcript level only for MVK1 a significant decrease was found, and this does not correlate with protein results. Furthermore, for MVK3, 4, 5, and 10 was a minor increase in transcript level detected

and does also not correlate with protein data. For the other MVK patients the data correlates. For SRD5A3 the results on both levels do correlate except for MVK3 and 8. The MVK defect resulted in general in lower protein expression of DHDDS and SRD5A3 caused probably by low levels of substrate. OGT protein levels in most MVK patients were comparable to controls, whereby MVK1 demonstrated an increase (Figure 53). The increase in transcripts did not have an impact on protein level. For FUT8, responsible for core fucosylation, an increase in protein amount was detected by western blot analysis (Figure 54). Transcript increase was seen for MVK1, 6, 7, 8 and 10. The upregulation of fucosylation in MVK patients proven by lectin stainings and xCGE-LIF of N-glycans (see above) correlate with this result. The general level of FUT9 in the MVK patients was comparable to the controls. The increase in FUT9 protein seen in MVK2 was also detected on transcript level. SCL35C1 in MVK patients had comparable amounts to controls, while on transcript level an increase for all MVK patients was detected. For DPY19L1 protein data and transcript data correlates and for DPY19L3 only for MVK1 and 3 (Figure 55). Unfortunately, DPY19L2 antibody was not available due to manufacture problems at the time when experiments were performed but is considered for future experiments. Nonetheless it could be shown, that the C-mannosylation might be impaired in MVK patients. For the proteins GMPPA, PMM2 and PGM2 a reduction in protein expression (Figure 56) was detected which correlates with the transcript level of *GMPAA* and *PGM2*. PMM2 data only overlapped for MVK2, 6, 8 and 10. The protein amount for ALG5 was decreased in MVK2, 4, 5, 6, 7, 8 and for the others MVK patients was comparable to controls. Transcript data showed a decrease in MVK2, 3, 4 and 5. Western blot analysis for GALE demonstrated for most MVK patients reduced protein amount and this correlates with reduced transcript levels. The increase found in MVK6, 7, 8 and 9 were presumably caused by a bubble in the lane of the loading control and analysis should be repeated. These results indicate an impairment of essential enzymes in the nucleotide activated sugar synthesis and thereby key sugar donor substrates which is assumed to contribute to the general disturbance on the protein N-glycosylation found in MVK patients. The protein amount for DPAGT1 was reduced in MVK1, 5, 7, 10 and 11 and in the other patients comparable to controls, whereby the three controls had high differences in themselves ranging from 200 % to 50 % (Figure 57). Transcript levels for MVK2, 3, 4, 6 and 10 correlate. For ALG13 protein levels in MVK patients comparable to controls (except MVK5) were found. This was also seen for the transcript level. The downregulation in protein amount for ALG9 did not correlate with results of the mRNA analysis where a slight increase was detected. For the protein ALG12 an increase in both the protein amount and transcript level was found. Interestingly, control2 showed a really low protein amount in ALG12. Furthermore, MVK patients showed an increase in ALG10 protein expression. For MAN1B1 a general downregulation was visible in MVK patients while the transcript levels were significantly increased compared to control. Next, MAN1A1 and MGAT2 protein amounts were comparable to controls. This does not correlate with the transcript levels, which were significantly increased in MVK patients. The results for MAN2A1 protein amounts must

be considered with caution, as here a presumable bubble effect for MVK6 – MVK9 in the lane for the loading control was visible. In conclusion, these results indicate an impairment of essential enzymes in the N-glycosylation pathway which is assumed to contribute to the general disturbance on the protein N-glycosylation found in MVK patients. POMT2 western blot analysis revealed a general increase in protein expression and increase on transcript levels was also found (Figure 58). This finding further strengthens the hypothesis that O-mannosylation might be impaired in MVK patients which will be analyzed based on the glycosylation status of alpha-dystroglycan in the near future.

It needs to be mentioned, that the western blot analysis was performed time only once and the cell pellets for this analysis were not the same as for the nCounter analysis. Additionally, results should be considered with caution as antibody specificity is sometimes not sufficient. Nonetheless changes on protein level were visible in MVK patients and this showed an impact of the MVK defect on these proteins. Furthermore, it is known, that transcript data and protein expression data must not correlate so the differing results do not have to be wrong [150]. For future experiments a repetition with at least three replicates is considered.

8.6 LLO analysis

Lipid-linked Oligosaccharides (LLO) are sugar structures that are build up on the lipid carrier dolichol and display the precursors for N-glycans. LLO are synthesized on the cytosolic side of the ER membrane followed by reaction steps taking place in the lumen of the ER. After extraction of the radiolabeled oligosaccharides, these were separated by HPLC and incorporated radioactivity was measured by liquid scintillation counting of the HPLC fractions. Hereby no differences of MVK patients and controls were detected. In contrast, in an alternative approach to analyze shorter LLO from Dol-P-Man₁ to Dol-P-Man₅ conducted by thin layer chromatography (TLC) under hydrophobic conditions abnormal profiles for short LLOs were found in MVK patients (Figure 59). This analysis revealed a variety of accumulations of structures running at the positions of Dol-P-Man₂ to Dol-P-Man₅ in MVK patients. Furthermore, a reduction of Dol-P-Man levels was found. PMM2-CDG accumulation of the same species were found by Körner *et al.* [151]. Concerning the direct measurement of Dol-P-Man please see below. Since no differences in the HPLC studies (in which the sugar moieties are directly approached) were found, it is speculated that the variations found by TLC analysis in the MVK patients were due to an abnormal composition of the lipid anchor dolichol and not caused by an altered sugar structure.

8.7 PrimePCR analysis revealed impact on the metabolism

The PrimePCR analysis revealed dysregulation of glycolysis, gluconeogenesis, and lipid metabolism in MVK2, MVK8 and MVK9 patient. Transcript of *ALDOA* was in MVK2 and MVK8 around 50 % downregulated while in MVK9 a nearly 3 times increase was

seen (Figure 60). ALDOA catalyzes the reversible conversion of fructose-1,6-bisphosphate to glyceraldehyde 3-phosphate and dihydroxyacetone phosphate. Mutations in this gene have been associated with Glycogen Storage Disease XII and results in myopathies, which is also seen in MVK patients [152]. Furthermore, this gene is related to the progression of multiple types of cancer [153]. The transcript *FBP1* was downregulated in MVK2 and MVK9. Fructose-1,6-diphosphatase deficiency is associated with hypoglycemia and metabolic acidosis [154]. For *PCK2* significant upregulation was found in MVK2 and MVK9. It is a mitochondrial enzyme that catalyzes the conversion of oxaloacetate to phosphoenolpyruvate. A recent study by Dong *et al.* reveals a novel function as overexpression of *PCK2* resulted in upregulation of inflammatory response in mice and Kupffer cells [155]. The hyperinflammation state of MVK patients could be related to this finding. The overall results of the glycolysis and gluconeogenesis revealed an impaired metabolism in MVK patients.

The results for the regulation of lipid metabolism showed a severe deregulation in the MVK patients MVK2, 8 and 9. The following genes were in all three patients affected. The transcript *AGTR1* was upregulated which is an important regulator of blood pressure and volume in the cardiovascular system [156]. The role in MVK patients remains unclear. Another task is the primary regulation of the aldosterone secretion. Aldosterone is a steroid hormone, which is produced from cholesterol [157]. As cholesterol levels are affected in MVK patients this could be a compensatory mechanism. *SCD* was also upregulated, which encodes an enzyme located in the ER membrane and involved in fatty acid biosynthesis. It contributes to cell growth, survival, differentiation and metabolic regulation [158]. The impaired cell growth and differentiation seen in MVK patients could be caused by it. For *SOD1*, *IL1B* and *PRKAA2* a significant downregulation was found. The enzyme *SOD1* encodes an enzyme for catalyzing superoxide breakdown and is so an antioxidant. Studies have indicated that *SOD1* dysfunction may have a pathogenic role in neurodegenerative disorders like amyotrophic lateral sclerosis (ALS) [159]. This feature could be involved in the brain phenotype seen in MVK patients. *IL1B* is a member of the interleukin 1 cytokine family and an important mediator of inflammatory response. It is also involved in cell proliferation, differentiation, and apoptosis. A recent meta-analysis on *IL1B* gene polymorphism by Harati-Sadegh *et al.* revealed a connection to eye disorders which is also seen in MVK patients' phenotype [160]. The transcript *PRKAA2* encodes a protein of a catalytic subunit of the AMP-activated protein kinase (AMPK), which is an important energy-sensing enzyme monitoring the cellular energy status. AMPK gets activated in response to cellular stresses and inactivates acetyl-CoA carboxylase (ACC) and beta-hydroxy beta-methylglutaryl-CoA reductase (HMGCR), which are enzymes of the isoprenoid pathway. As described above, an increase in *HMGCR* transcripts was found in MVK patients and this correlates with the downregulation of *PRKAA2*. Furthermore, it was shown that in mammalian cells the Dol-P-Man synthase (DPM) activity is regulated by AMPK via phosphorylation. DPM is one of the regulator factors in the LLO biosynthesis [161], [162].

8.8 Energy metabolites homeostasis is impaired

The deregulations found by PrimePCR analysis in MVK patients gave a reason to analyze the energy metabolites in cell lysates of the patients. For AMP, ADP and ATP and upregulation trend was found in MVK patients' fibroblasts. The cellular stress of the cells demands more energy and results showed an impaired energy homeostasis in the MVK patients. The increase of ATP can also be explained by the HIF1alpha increase, as this leads to an increase in ATP production [139]. Also, a slight increase in NAD and NADH showed a disruption in the energy metabolism. Furthermore, SAHC and SAM was upregulated. This is probably caused by the increased levels of the amino acid threonine, which will be discussed in the next paragraph.

8.9 Amino acid profile indicates abnormalities

The amino acids biosynthesis is coupled to the isoprenoid pathway via the molecule acetyl-CoA. As changes e.g., in cell growth can be related to a decompensated amino acid metabolism, a screening for abnormalities concerning amino acids in cell lysates was performed. Additionally, Proline was found to be highly upregulated compared to controls. Recent studies suggest that proline biosynthesis and catabolism are essential processes in disease as it has a significant role in redox homeostasis. Increased proline levels may result in increased hydroxyproline levels, and this feature is associated with hepatic fibrosis [163]. The hepatomegaly phenotype seen in MVK patients might be associated with this finding. Furthermore, the decreased ornithine levels can be explained by the use to synthesize proline via glutamate-5-semialdehyde and 1-pyrroline-5-carboxylate. It is also known that alanine and proline are surrogate parameters for mitochondrial dysfunction. Shyh-Chang *et al.* showed in their studies that threonine and SAM metabolism are coupled in pluripotent stem cells [164]. The increased level on threonine can explain the increased levels of SAM found by the energy metabolite analysis. The essential amino acids (EAAs) methionine and histidine were significantly reduced in MVK patients. In general, EAAs are important for cell growth and differentiation, and this could play a role in the MVK phenotype [165]. Glutamine is coupled to the energy homeostasis and the significant increase correlates with the result of energy metabolites, which showed an impairment.

8.10 Impaired lipid homeostasis

The abnormal results of the LLO analysis identified by TLC in combination with the potential deregulations in genes needed for the lipid metabolism found by PrimePCR analysis in MVK patients gave reason to analyze the MVK patient fibroblasts concerning lipid abnormalities. Lipids are ubiquitous distributed in the cells and play important roles in signal transduction, cellular components e.g. membrane lipids and energy metabolites as lipid droplets, which are storage for triglycerides and cholesterol esters [166], [167]. To get an overall view on the lipid build up in MVK patient cells compared to control cells, the staining compound Oil Red O was used to stain triglycerides. The

analysis revealed a significant accumulation of lipid droplets in MVK patients' cells (Figure 69). Furthermore, as dolichyl phosphate is a direct product of the mevalonate pathway it was especially interesting to see what effect an MVK defect has. As seen in Figure 70 a significant decrease of around 50 % in dolichyl phosphate levels in MVK patient fibroblasts was visible. This is to the current knowledge the first time that MVK patients were analyzed for dolichyl phosphate levels. In the past it was revealed by Hoffman et al. that MKD patient lymphoblasts presented low levels of dolichol by estimating quantities and assumed dolichyl phosphate should also be decreased [168]. There are several downstream proteins of MVK, where it already had been shown, that defects in these enzymes as DHDDS, SRD5A3 and DOLK cause lower levels of dolichol and therefore result in congenital disorder of glycosylation [169]. To this class of inborn metabolic diseases, the dolichol biosynthesis defects, the MVK defect can now be added. CDG patients present with a multisystemic phenotype with a lot of clinical features that matches the ones of MVA patients. Overlapping symptoms are mental retardation, ocular symptoms, psychomotor retardation, skin lesions, cardiomyopathy, hypotonia and facial dysmorphism [63]. The febrile attacks of MVA patients are not seen in CDG patients and is unique. It is believed to be caused by insufficient levels of anti-inflammatory isoprenylated proteins. The low levels of geranylgeranyl-PP cause caspase-1 activation and IL-1 β secretion [170], [171]. After the total amount of dolichyl phosphate was measured, the distribution of different dolichyl phosphate species ranging from C70 to C105 were determined (Figure 71 and Figure 72). This analysis revealed a markedly impairment in DolP species in MVK patients. A marked increase in the shorter DolPs, ranging from C70 to C95, and a significant decrease of the longer DolPs, C100 and C105, was observed. This shows a shift towards shorter DolP species in MVK patients as a result of the impaired isoprenoid pathway caused by mutations in the MVK gene. The hypothesis is that the general decrease in DolP levels and to some extent the shift to shorter DolP species are the main factors for the MVK phenotype. The glycosyltransferases, which are DolP dependent in N-glycosylation and C- and O-mannosylation, are highly specific and their function is affected by lower total DolP levels and shorter DolP species [172], [173]. In several experiments it has been shown that the level of DolP in the ER is one important rate-controlling factor [174], [175]. Patients with mutations in the DHDDS gene, which is downstream of the mevalonate kinase and also responsible for dolichol synthesis, showed also aberrant dolichol chain lengths which is in line with presented findings [176]. The eye phenotype of DHDDS patients and MVK patients correlate. Additionally, lower total DolP levels and shorter DolP species were found in one of our SRD5A3 patients in a recent study (Analytical Chemistry - Manuscript ID ac-2022-03623a). Furthermore, a lipidomics analysis with nano-electrospray ionization tandem mass spectrometry was initiated to get a broader view of the lipid homeostasis in the fibroblast. The cholesterol levels in the MVK patients were diverse and comparable to control. This result matches earlier results from Brennstuhl *et al.* who reported cholesterol levels from MVK patients to be within the normal range [17]. So, the clinical phenotype is not the cause of a dysfunctional

cholesterol biosynthesis. Interestingly, significantly decreased amounts of cholesterol esters in the presented MVK patient cohort were found. Cholesterol esters are a group of lipids where cholesterol is bound to a fatty acid. Excess cholesterol is normally bound in insoluble cholesterol esters for storage. MVK patients probably do not have excess cholesterol levels so there is no need for storage. The results of the sphingolipids ceramide and sphingomyelin showed a significant increase in MVK patients. Ceramide is an important molecule for cellular differentiation and signal transduction. Furthermore, it's the main lipid in the stratum corneum (horny layer of the skin) and responsible for protecting the skin against dryness [177]. Excessive ceramide could be responsible for excessive fluid retention and therefore cause of edema present in MVK patients. Increase of ceramide as a result of stress response is also a possibility [178]. The sphingolipid sphingomyelin is an important membrane component and increase can be, to some extent, the cause of liver and CNS phenotype of MVK patients as this is also seen in the Nieman-Pick disease group [179]. Phosphatidylethanolamines (PE) are the second most abundant phospholipids in mammalian cells and were significantly decreased in MVK patients. They play an important role in vital mitochondria function and in neurological development [180]. The decreased level mimic mitochondrial dysfunction and the brain retardation in MVK patients can also be associated with this finding. PE are synthesized by decarboxylation of phosphatidylserines (PS) by the phosphatidylserine decarboxylase (PSD) in the mitochondria. Interestingly, a significant increase of PS in MVK patients' fibroblast was found, which again shows a dysfunction of mitochondria in MVK patients. The importance of PE synthesis was shown in a mice experiment where deleting both copies of PSD resulted in embryonic lethality [181]. PE are also important for membrane fusion and play a pivotal role in cell division by mediating a coordinate movement between the contractile ring and plasma membrane [182]. This finding is another possible connection with the impairment in cell growth seen in MVK patients' fibroblasts. Furthermore, PE are key substrates for GPI anchor synthesis, which are glycolipids that are posttranslationally conjugated to the C-terminus of some proteins. This modification enables the protein to be tethered to the outer leaflet of the plasma membrane and reduction in PE leads to impairment of GPI anchors [183]. GPI anchors were not analyzed in the MVK patients but should be considered for future experiments. PS are also components of the eukaryotic membranes and the most abundant negatively charged phospholipid class [184]. These results showed that in general the lipid composition of the membrane is altered in MVK patients, and this will contribute to the MVK phenotype. In this context Fu *et al.* showed that lipid disequilibrium in the ER membranes can also activate the unfolded protein response (UPR) [185]. Vice versa is the lipid equilibrium affected by upregulated UPR caused by impairment of glycosylation, which have been mentioned above to be present in the MVK patients. ER stress by UPR is thought to contribute to liver disease, neurodegeneration and metabolic disease [186]–[188]. In the plasmalogen group (ether linked lipids) a significant increase of phosphatidylcholines (PC O-), phosphatidylserines (PS O-) and phosphatidylinositols (PI O-) was found. Plasmalogens are peroxisome-

derived glycerophospholipids and make up 15 -20 % of the phospholipids found in cell membranes. The synthesis starts in the peroxisomes and continues in the ER. The functions are connected to membrane fluidity, cell differentiation, signal transduction and antioxidation [189], [190]. This dysregulation of the plasmalogens indicates a defect in the peroxisomes in fibroblast of the MVK patients. The glycerolipid diacylglycerol (DAG) presented an increase in the MVK patients. DAGs are intermediates of the triglyceride biosynthesis and this result correlated with the increase of triglycerides seen by the lipid Oil Red O staining discussed earlier. In conclusion, the results have shown, that the lipid homeostasis is impaired in the MVK patients.

8.11 Proteomics measurement

Protein profiling was performed for all MVK patients by LC-ESI-MS. Patients were divided into two groups, the severely affected (MVK2, 6, 7, 8, 9) and the mildly affected (MVK1, 3, 4, 5, 10, 11) one. This was done to find deregulated proteins which are specific for the severely or mildly affected patients. The analysis revealed 58 significantly deregulated proteins in all MVK patients. This approach was used to get a general overview for the MVK patients and only the main results will be discussed. The KEGG pathway analysis resulted in the following four pathways with the highest coverage (Figure 80). Interestingly, the pathway with the highest coverage was the Epstein-Barr virus infection pathway. However, as almost all humans get infected with this virus during their lifetime, this finding was not surprising [191]. A downregulation of ICAM1 was found in and this correlates with the results of the western blots. Furthermore, the pathway of nucleotide sugars was affected which again correlates with the former results of the nCounter and western blot analysis. The antigen processing and presentation pathway was also affected in MVK patients which might be linked to the hyperinflammatory state of the MVK patients. The last pathway was the 2-oxocarboxylic acid metabolism. This finding correlates with the impairment found in the amino acids metabolism and strengthens these results. For the severe phenotype group 36 significantly deregulated proteins were found. This low number made it impossible to perform a KEGG pathway analysis. Nonetheless, a decreased protein amount for IDH2, responsible for the oxidative decarboxylation of isocitrate to 2-oxoglutarate, and an increase for UAP1, predicted to be involved in UDP-N-acetylglucosamine biosynthetic process, was found. The UAP1 dysregulation was also seen in the nCounter expression analysis earlier described. Furthermore, an increase in the protein amount of ACLY, responsible for the synthesis of cytosolic acetyl-CoA, the linker of the mevalonate and amino acid biosynthesis (see above), and PFKF, key role in glycolysis regulation, was present. In the mild affected group, 115 significantly deregulated proteins were detected. The pathway with the highest coverage of affected genes for this group was the phagosome pathway. Here LAMP1 and LAMP2 expression was found to be increased. This correlates with the results of the western blot analysis. The pathway for other glycan degradation was also affected and support the findings for the impaired glycan synthesis. The hits in the lysosome pathway can be the result of an increase of

the unfolded protein response as a consequence of deficient glycosylation of proteins. The finding in the “glycosphingolipid biosynthesis – ganglio series” pathway, where an increase in proteins was detected, correlates with GSL analysis earlier discussed.

All these data support the above presented findings by the other performed analyses. In conclusion it needs to be mentioned, that only one sample per MVK patient was analyzed and should be repeated at least in triplicates. Also, this shotgun proteomics approach is not suitable to detect all changes in protein levels as sensitivity is not sufficient for low abundant and membrane proteins [192]. Especially enzymes involved in the glycosylation machinery are mostly low abundant membrane proteins. For future experiments a more suitable methodology with differential centrifugation to resolve the complex protein extracts will be considered [193]. The separation of membrane fractions from the soluble one will drastically increase the sensitivity to detect these proteins involved in glycosylation.

8.12 Conclusion

Taken all data together, this is the first metabolic study concerning MVK deficiency which was performed in patients' fibroblasts. For all patients presented in this work pathogenic variants were identified by sanger sequencing, revealing two new mutations, c.782T>C in MVK10 and c.790dupC in MVK3, which are not listed in the NCBI ClinVar database yet. The new patient MVK9 was successfully diagnosed and characterized to belong to the severe spectrum of the MVK disease. To the current knowledge this is the first time that a systematic analysis of glycosylation in MVA was performed. Lectin binding studies combined with analysis of glycoprotein markers revealed an immense impairment in the N-glycosylation pathway. This could be attributed to deregulations of the expression of important glycosylation genes and proteins on transcript and protein level conducted by nCounter and western blot studies. Profound analysis of total N-glycans further revealed a reduction of complex type N-glycans and abnormalities within the group of high mannose type glycans which is also known from diverse CDG-I types. Furthermore, it could be shown for the first time that MVK deficiency led to low levels of dolichyl phosphate normally needed for the synthesis of Dol-P-Man and Dol-P-Gluc, the essential donor sugar substrates for N-glycosylation, O-mannosylation, C-mannosylation and GPI anchor synthesis which is ascribed to be the main mechanism for the observed hypoglycosylation. The impairment in lipid homeostasis is also directly caused by the MVK defect. Additionally, secondary effects on energy metabolism and amino acids metabolism could be revealed.

In summary, it was demonstrated here for the first time that a defect in the MVK leads to a global glycosylation deficiency in patients. The MVK defect therefore belongs to the disease group of congenital disorders of glycosylation. It is proposed to name this new defect 'MVK-CDG'. Since it can be assumed that the enzymes following MVK also lead to a glycosylation defect, these should be included in the list of suspected CDG genes in the context of genetic patient diagnostics.

8.13 Future perspective

The complementation of the MVK patients' cells with the wildtype gene tagged with Myc (MVK_MYC) was successful as proven by western blot analysis (Figure 82 and Figure 83). The next step would be to test if the expressed protein has an activity by enzymatic assays. If this is the case, these cell models open the door to further elucidate the MDK defect. It will be interesting to repeat the analysis, performed in this work, to see if the phenotype of these cells is rescued. Another interesting approach would be to mimic the patient mutations via a CRISPR/Cas approach in different cell types e.g. HepG2 cells. This could also be done for the downstream enzymes of MVK. The performed analyses in this work transferred to these cells and cell culture supernatants would further help to elucidate the glycosylation defect. Furthermore, this work showed that there are several key findings in MVK patients which could be used as potential diagnostic

markers. Analysis of N-glycans derived from whole serum or plasma glycoproteins and studies concerning urinary dolichol profiles should be performed to improve the diagnostic procedure of new patients. Further, the O-glycan synthesis and especially alpha-dystroglycan glycosylation should be analyzed. This applies also to the GPI anchor synthesis, as it is also dependent on Dol-P-Man. Additionally, therapeutic approaches for MVA with this new knowledge can be tested. One strategy could be to replenish the missing substrates dolichol and DolP. Unfortunately, it already has been shown in cell models that external contribution of dolichol to the cellular pool for glycosylation reactions seem to be very limited [169]. Nonetheless, dietary supplementation of spinach and oils, which contain high amounts of long chain polyisoprenoids could be considered.

9 Literature

- [1] S. A. Holstein and R. J. Hohl, "Isoprenoids: remarkable diversity of form and function," *Lipids*, vol. 39, no. 4, pp. 293–309, Apr. 2004, doi: 10.1007/S11745-004-1233-3.
- [2] J. L. Goldstein and M. S. Brown, "Regulation of the mevalonate pathway," *Nature*, vol. 343, no. 6257, pp. 425–430, 1990, doi: 10.1038/343425A0.
- [3] I. Buhaescu and H. Izzedine, "Mevalonate pathway: A review of clinical and therapeutical implications," *Clinical Biochemistry*, vol. 40, no. 9–10, pp. 575–584, Jun. 2007. doi: 10.1016/j.clinbiochem.2007.03.016.
- [4] N. Dellas, S. T. Thomas, G. Manning, and J. P. Noel, "Discovery of a metabolic alternative to the classical mevalonate pathway," *Elife*, vol. 2013, no. 2, Dec. 2013, doi: 10.7554/ELIFE.00672.001.
- [5] J. M. Vinokur, T. P. Korman, Z. Cao, and J. U. Bowie, "Evidence of a Novel Mevalonate Pathway in Archaea," *Biochemistry*, vol. 53, no. 25, p. 4161, Jul. 2014, doi: 10.1021/BI500566Q.
- [6] Y. Azami, A. Hattori, H. Nishimura, H. Kawaide, T. Yoshimura, and H. Hemmi, "(R)-Mevalonate 3-Phosphate Is an Intermediate of the Mevalonate Pathway in Thermoplasma acidophilum," *J Biol Chem*, vol. 289, no. 23, p. 15957, Jun. 2014, doi: 10.1074/JBC.M114.562686.
- [7] U. Schweizer, S. Bohleber, and N. Fradejas-Villar, "The modified base isopentenyladenosine and its derivatives in tRNA," <https://doi.org/10.1080/15476286.2017.1294309>, vol. 14, no. 9, pp. 1197–1208, Sep. 2017, doi: 10.1080/15476286.2017.1294309.
- [8] G. Popják and W. S. Agnew, "Squalene synthetase," *Mol Cell Biochem*, vol. 27, no. 2, pp. 97–116, Oct. 1979, doi: 10.1007/BF00218354.
- [9] D. S. Schade, L. Shey, and R. P. Eaton, "Cholesterol review: A metabolically important molecule," *Endocrine Practice*, vol. 26, no. 12, pp. 1514–1523, Dec. 2020, doi: 10.4158/EP-2020-0347.
- [10] A. A. Kandutsch, H. Paulus, E. Levin, and K. Bloch, "Purification of Geranylgeranyl Pyrophosphate Synthetase from *Micrococcus Zysodeikticus**," *Journal of Biological Chemistry*, vol. 239, no. 8, pp. 2507–2515, 1964, doi: 10.1016/S0021-9258(18)93880-9.
- [11] J. F. Moomaw and P. J. Casey, "Mammalian protein geranylgeranyltransferase. Subunit composition and metal requirements.," *Journal of Biological Chemistry*, vol. 267, no. 24, pp. 17438–17443, Oct. 1992, doi: 10.1016/S0021-9258(18)41945-X.
- [12] Y. Reiss, J. L. Goldstein, M. C. Seabra, P. J. Casey, and M. S. Brown, "Inhibition of purified p21ras farnesyl:protein transferase by Cys-AAX tetrapeptides," *Cell*, vol. 62, no. 1, pp. 81–88, Jul. 1990, doi: 10.1016/0092-8674(90)90242-7.
- [13] H. Teclebrhan, J. Olsson, E. Swiezewska, and G. Dallner, "Biosynthesis of the side chain of ubiquinone:trans-prenyltransferase in rat liver microsomes.," *Journal of Biological Chemistry*, vol. 268, no. 31, pp. 23081–23086, Nov. 1993, doi: 10.1016/S0021-9258(19)49428-3.
- [14] K. Grabińska and G. Palamarczyk, "Dolichol biosynthesis in the yeast *Saccharomyces cerevisiae*: an insight into the regulatory role of farnesyl diphosphate synthase," *FEMS Yeast Res*, vol. 2, no. 3, pp. 259–265, Aug. 2002, doi: 10.1111/J.1567-1364.2002.TB00093.X.
- [15] K. K. Carroll, N. Guthrie, and K. Ravi, "Dolichol: function, metabolism, and accumulation in human tissues," *BIOCHEM. CELL BIOL.*, vol. 70, 1992, [Online]. Available: www.nrcresearchpress.com
- [16] F. W. Hemming, "Dolichol: a curriculum cognitionis," *Biochemistry and Cell Biology*, vol. 70, no. 6, pp. 377–381, 2011, doi: 10.1139/O92-058.

- [17] H. Brennenstuhl *et al.*, "Phenotypic diversity, disease progression, and pathogenicity of MVK missense variants in mevalonic aciduria," *J Inherit Metab Dis*, vol. 44, no. 5, pp. 1272–1287, Sep. 2021, doi: 10.1002/JIMD.12412.
- [18] A. Dell, A. Galadari, F. Sastre, and P. Hitchen, "Similarities and differences in the glycosylation mechanisms in prokaryotes and eukaryotes," *Int J Microbiol*, 2010, doi: 10.1155/2010/148178.
- [19] I. Braakman and D. N. Hebert, "Protein folding in the endoplasmic reticulum," *Cold Spring Harb Perspect Biol*, vol. 5, no. 5, 2013, doi: 10.1101/CSHPERSPECT.A013201.
- [20] M. Aebi, "N-linked protein glycosylation in the ER," *Biochimica et Biophysica Acta (BBA) - Molecular Cell Research*, vol. 1833, no. 11, pp. 2430–2437, Nov. 2013, doi: 10.1016/J.BBAMCR.2013.04.001.
- [21] A. Alavi and J. S. Axford, "Sweet and sour: the impact of sugars on disease," *Rheumatology (Oxford)*, vol. 47, no. 6, pp. 760–770, Jun. 2008, doi: 10.1093/RHEUMATOLOGY/KEN081.
- [22] G. Lauc, M. Pezer, I. Rudan, and H. Campbell, "Mechanisms of disease: The human N-glycome," *Biochimica et Biophysica Acta (BBA) - General Subjects*, vol. 1860, no. 8, pp. 1574–1582, Aug. 2016, doi: 10.1016/J.BBAGEN.2015.10.016.
- [23] G. A. Khoury, R. C. Baliban, and C. A. Floudas, "Proteome-wide post-translational modification statistics: frequency analysis and curation of the swiss-prot database," *Scientific Reports 2011 1:1*, vol. 1, no. 1, pp. 1–5, Sep. 2011, doi: 10.1038/srep00090.
- [24] R. Apweiler, H. Hermjakob, and N. Sharon, "On the frequency of protein glycosylation, as deduced from analysis of the SWISS-PROT database," *Biochim Biophys Acta*, vol. 1473, no. 1, pp. 4–8, Dec. 1999, doi: 10.1016/S0304-4165(99)00165-8.
- [25] R. G. Spiro, "Protein glycosylation: nature, distribution, enzymatic formation, and disease implications of glycopeptide bonds," *Glycobiology*, vol. 12, no. 4, pp. 43R-56R, Apr. 2002, doi: 10.1093/GLYCOB/12.4.43R.
- [26] V. A *et al.*, "Essentials of Glycobiology," *Cold Spring Harbor (NY)*, vol. 039, pp. 2015–2017, 2009, Accessed: Feb. 04, 2022. [Online]. Available: <https://pubmed.ncbi.nlm.nih.gov/20301239/>
- [27] K. F. Medzihradsky, "Characterization of site-specific N-glycosylation," *Methods Mol Biol*, vol. 446, pp. 293–316, Mar. 2008, doi: 10.1007/978-1-60327-084-7_21.
- [28] T. Pitti, C. T. Chen, H. N. Lin, W. K. Choong, W. L. Hsu, and T. Y. Sung, "N-GlyDE: a two-stage N-linked glycosylation site prediction incorporating gapped dipeptides and pattern-based encoding," *Scientific Reports 2019 9:1*, vol. 9, no. 1, pp. 1–11, Nov. 2019, doi: 10.1038/s41598-019-52341-z.
- [29] M. L. Medus *et al.*, "N-glycosylation Triggers a Dual Selection Pressure in Eukaryotic Secretory Proteins," *Sci Rep*, vol. 7, no. 1, Dec. 2017, doi: 10.1038/S41598-017-09173-6.
- [30] C. Reily, T. J. Stewart, M. B. Renfrow, and J. Novak, "Glycosylation in health and disease," *Nature Reviews Nephrology 2019 15:6*, vol. 15, no. 6, pp. 346–366, Mar. 2019, doi: 10.1038/s41581-019-0129-4.
- [31] A. C. R. D. ; E. J. D. ; F. H. H. ; S. P. ; B. C. R. ; H. G. W. ; E. M. Varki and E., *Essentials of Glycobiology, 3rd edition*. Cold Spring Harbor (NY): Cold Spring Harbor Laboratory Press, 2015. Accessed: Sep. 14, 2020. [Online]. Available: <http://www.ncbi.nlm.nih.gov/pubmed/27010055><https://www.ncbi.nlm.nih.gov/books/NBK310274/>
- [32] P. Burda and M. Aebi, "The dolichol pathway of N-linked glycosylation," *Biochimica et Biophysica Acta (BBA) - General Subjects*, vol. 1426, no. 2, pp. 239–257, Jan. 1999, doi: 10.1016/S0304-4165(98)00127-5.

- [33] J. Helenius and M. Aebi, "Transmembrane movement of dolichol linked carbohydrates during N-glycoprotein biosynthesis in the endoplasmic reticulum," *Semin Cell Dev Biol*, vol. 13, no. 3, pp. 171–178, 2002, doi: 10.1016/S1084-9521(02)00045-9.
- [34] R. Knauer and L. Lehle, "The oligosaccharyltransferase complex from yeast," *Biochim Biophys Acta*, vol. 1426, no. 2, pp. 259–273, Jan. 1999, doi: 10.1016/S0304-4165(98)00128-7.
- [35] C. Abeijon and C. B. Hirschberg, "Topography of glycosylation reactions in the endoplasmic reticulum," *Trends Biochem Sci*, vol. 17, no. 1, pp. 32–36, 1992, doi: 10.1016/0968-0004(92)90424-8.
- [36] A. Varki, "Biological roles of oligosaccharides: all of the theories are correct," *Glycobiology*, vol. 3, no. 2, p. 97, Apr. 1993, doi: 10.1093/GLYCOB/3.2.97.
- [37] D. Rymen *et al.*, "MAN1B1 Deficiency: An Unexpected CDG-II," *PLoS Genet*, vol. 9, no. 12, 2013, doi: 10.1371/JOURNAL.PGEN.1003989.
- [38] B. B. Allan and W. E. Balch, "In vitro analysis of endoplasmic-reticulum-to-golgi transport in mammalian cells," *Curr Protoc Cell Biol*, vol. Chapter 11, no. 1, Oct. 2001, doi: 10.1002/0471143030.CB1103S00.
- [39] H. H. Freeze and C. Kranz, "Endoglycosidase and glycoamidase release of N-linked glycans," *Curr Protoc Immunol*, vol. Chapter 8, no. SUPPL. 83, 2008, doi: 10.1002/0471142735.IM0815S83.
- [40] G. P. Bhide and K. J. Colley, "Sialylation of N-glycans: mechanism, cellular compartmentalization and function," *Histochem Cell Biol*, vol. 147, no. 2, p. 149, Feb. 2017, doi: 10.1007/S00418-016-1520-X.
- [41] C. Liao *et al.*, "FUT8 and Protein Core Fucosylation in Tumours: From Diagnosis to Treatment," *J Cancer*, vol. 12, no. 13, p. 4109, 2021, doi: 10.7150/JCA.58268.
- [42] M. Schneider, E. Al-Shareffi, and R. S. Haltiwanger, "Biological functions of fucose in mammals," *Glycobiology*, vol. 27, no. 7, pp. 601–618, Jul. 2017, doi: 10.1093/GLYCOB/CWX034.
- [43] R. Kornfeld and S. Kornfeld, "ASSEMBLY OF ASPARAGINE-LINKED OLIGOSACCHARIDES," <https://doi.org/10.1146/annurev.bi.54.070185.003215>, vol. VOL. 54, pp. 631–664, Nov. 2003, doi: 10.1146/ANNUREV.BI.54.070185.003215.
- [44] R. S. Haltiwanger, L. Wells, H. H. Freeze, and P. Stanley, "Other Classes of Eukaryotic Glycans," *Essentials of Glycobiology, 3rd edition*, vol. 013, p. Chapter 13, 2017, doi: 10.1101/GLYCOBIOLOGY.3E.013.
- [45] P. H. Jensen, D. Kolarich, and N. H. Packer, "Mucin-type O-glycosylation – putting the pieces together," *FEBS J*, vol. 277, no. 1, pp. 81–94, Jan. 2010, doi: 10.1111/J.1742-4658.2009.07429.X.
- [46] H. bin Ruan, J. P. Singh, M. D. Li, J. Wu, and X. Yang, "Cracking the O-GlcNAc Code in Metabolism," *Trends Endocrinol Metab*, vol. 24, no. 6, p. 301, Jun. 2013, doi: 10.1016/J.TEM.2013.02.002.
- [47] S. Strahl-Bolsinger, M. Gentzsch, and W. Tanner, "Protein O-mannosylation," *Biochimica et Biophysica Acta (BBA) - General Subjects*, vol. 1426, no. 2, pp. 297–307, Jan. 1999, doi: 10.1016/S0304-4165(98)00131-7.
- [48] M. Lommel and S. Strahl, "Protein O-mannosylation: Conserved from bacteria to humans," *Glycobiology*, vol. 19, no. 8, pp. 816–828, Aug. 2009, doi: 10.1093/GLYCOB/CWP066.
- [49] M. Loibl and S. Strahl, "Protein O-mannosylation: What we have learned from baker's yeast," *Biochimica et Biophysica Acta (BBA) - Molecular Cell Research*, vol. 1833, no. 11, pp. 2438–2446, Nov. 2013, doi: 10.1016/J.BBAMCR.2013.02.008.

- [50] J. Vajsar and H. Schachter, "Walker-Warburg syndrome," *Orphanet J Rare Dis*, vol. 1, no. 1, p. 29, 2006, doi: 10.1186/1750-1172-1-29.
- [51] A. M. Shenoy, J. A. Markowitz, C. G. Bonnemann, K. Krishnamoorthy, A. D. Bossler, and B. S. Tseng, "Muscle-Eye-Brain Disease," *J Clin Neuromuscul Dis*, vol. 11, no. 3, p. 124, Mar. 2010, doi: 10.1097/CND.0B013E3181C5054D.
- [52] F. F. R. Buettner, A. Ashikov, B. Tiemann, L. Lehle, and H. Bakker, "C. elegans DPY-19 Is a C-Mannosyltransferase Glycosylating Thrombospondin Repeats," *Mol Cell*, vol. 50, no. 2, pp. 295–302, Apr. 2013, doi: 10.1016/J.MOLCEL.2013.03.003/ATTACHMENT/311F8DAC-DE0D-4F3E-9785-7A8203F60628/MMC1.PDF.
- [53] A. Shcherbakova, B. Tiemann, F. F. R. Buettner, and H. Bakker, "Distinct C-mannosylation of netrin receptor thrombospondin type 1 repeats by mammalian DPY19L1 and DPY19L3," *Proc Natl Acad Sci U S A*, vol. 114, no. 10, pp. 2574–2579, Mar. 2017, doi: 10.1073/PNAS.1613165114/-/DCSUPPLEMENTAL.
- [54] M. A. Doucey, D. Hess, R. Cacan, and J. Hofsteenge, "Protein C-Mannosylation Is Enzyme-catalysed and Uses Dolichyl-Phosphate-Mannose as a Precursor," *Mol Biol Cell*, vol. 9, no. 2, p. 291, 1998, doi: 10.1091/MBC.9.2.291.
- [55] J. Hofsteenge, D. R. Müller, T. de Beer, A. Löffler, W. J. Richter, and J. F. G. Vliegthart, "New type of linkage between a carbohydrate and a protein: C-glycosylation of a specific tryptophan residue in human RNase Us," *Biochemistry*, vol. 33, no. 46, pp. 13524–13530, Nov. 1994, doi: 10.1021/BI00250A003.
- [56] K. Julenius, "NetCGlyc 1.0: prediction of mammalian C-mannosylation sites," *Glycobiology*, vol. 17, no. 8, pp. 868–876, Aug. 2007, doi: 10.1093/GLYCOB/CWM050.
- [57] A. Regina Todeschini and S. itiroh Hakomori, "Functional role of glycosphingolipids and gangliosides in control of cell adhesion, motility, and growth, through glycosynaptic microdomains," *Biochim Biophys Acta*, vol. 1780, no. 3, p. 421, Mar. 2008, doi: 10.1016/J.BBAGEN.2007.10.008.
- [58] A. H. Merrill, "Sphingolipid and Glycosphingolipid Metabolic Pathways in the Era of Sphingolipidomics," *Chem Rev*, vol. 111, no. 10, p. 6387, Oct. 2011, doi: 10.1021/CR2002917.
- [59] G. D'Angelo, S. Capasso, L. Sticco, and D. Russo, "Glycosphingolipids: synthesis and functions," *FEBS J*, vol. 280, no. 24, pp. 6338–6353, Dec. 2013, doi: 10.1111/FEBS.12559.
- [60] G. van Meer, D. R. Voelker, and G. W. Feigenson, "Membrane lipids: where they are and how they behave," *Nat Rev Mol Cell Biol*, vol. 9, no. 2, p. 112, Feb. 2008, doi: 10.1038/NRM2330.
- [61] K. Kitatani, J. Idkowiak-Baldys, and Y. A. Hannun, "The sphingolipid salvage pathway in ceramide metabolism and signaling," *Cell Signal*, vol. 20, no. 6, p. 1010, Jun. 2008, doi: 10.1016/J.CELLSIG.2007.12.006.
- [62] J. Jaeken *et al.*, "Familial psychomotor retardation with markedly fluctuating serum prolactin, FSH and GH levels, partial TBG-deficiency, increased serum arylsulphatase A and increased CSF protein: a new syndrome?: 90," *Pediatric Research 1980 14:2*, vol. 14, no. 2, pp. 179–179, Feb. 1980, doi: 10.1203/00006450-198002000-00117.
- [63] R. Péanne *et al.*, "Congenital disorders of glycosylation (CDG): Quo vadis?," *Eur J Med Genet*, vol. 61, no. 11, pp. 643–663, Nov. 2018, doi: 10.1016/J.EJMG.2017.10.012.
- [64] B. G. Ng and H. H. Freeze, "Perspectives on Glycosylation and its Congenital Disorders," *Trends Genet*, vol. 34, no. 6, p. 466, Jun. 2018, doi: 10.1016/J.TIG.2018.03.002.
- [65] J. Jaeken, T. Hennet, G. Matthijs, and H. H. Freeze, "CDG nomenclature: Time for a change!," *Biochim Biophys Acta*, vol. 1792, no. 9, p. 825, Sep. 2009, doi: 10.1016/J.BBADIS.2009.08.005.

- [66] K. Mention *et al.*, "Development of liver disease despite mannose treatment in two patients with CDG-Ib," *Mol Genet Metab*, vol. 93, no. 1, pp. 40–43, Jan. 2008, doi: 10.1016/J.YMGME.2007.08.126.
- [67] H. K. Harms, K. P. Zimmer, K. Kurnik, R. M. Bertele-Harms, S. Weidinger, and K. Reiter, "Oral mannose therapy persistently corrects the severe clinical symptoms and biochemical abnormalities of phosphomannose isomerase deficiency," *Acta Paediatr*, vol. 91, no. 10, pp. 1065–1072, 2002, doi: 10.1080/080352502760311566.
- [68] E. Schrapers *et al.*, "News on Clinical Details and Treatment in PGM1-CDG," *JIMD Rep*, vol. 26, p. 77, 2016, doi: 10.1007/8904_2015_471.
- [69] R. G. Feichtinger *et al.*, "A spoonful of L-fucose—an efficient therapy for GFUS-CDG, a new glycosylation disorder," *EMBO Mol Med*, vol. 13, no. 9, p. e14332, Sep. 2021, doi: 10.15252/EMMM.202114332.
- [70] T. Marquardt, K. Lühn, G. Srikrishna, H. H. Freeze, E. Harms, and D. Vestweber, "Correction of Leukocyte Adhesion Deficiency Type II With Oral Fucose," *Blood*, vol. 94, no. 12, pp. 3976–3985, Dec. 1999, doi: 10.1182/BLOOD.V94.12.3976.
- [71] E. Morava, "Galactose supplementation in phosphoglucomutase-1 deficiency; review and outlook for a novel treatable CDG," *Mol Genet Metab*, vol. 112, no. 4, p. 275, 2014, doi: 10.1016/J.YMGME.2014.06.002.
- [72] K. Dörre *et al.*, "A new case of UDP-galactose transporter deficiency (SLC35A2-CDG): molecular basis, clinical phenotype, and therapeutic approach," *J Inherit Metab Dis*, vol. 38, no. 5, pp. 931–940, Sep. 2015, doi: 10.1007/S10545-015-9828-6.
- [73] Z. Durin *et al.*, "Differential Effects of D-Galactose Supplementation on Golgi Glycosylation Defects in TMEM165 Deficiency," *Front Cell Dev Biol*, vol. 10, p. 1, May 2022, doi: 10.3389/FCCELL.2022.903953.
- [74] J. Jaeken and R. Péanne, "What is new in CDG?," *J Inherit Metab Dis*, vol. 40, no. 4, pp. 569–586, Jul. 2017, doi: 10.1007/s10545-017-0050-6.
- [75] J. Jaeken, "Congenital disorders of glycosylation," *Ann N Y Acad Sci*, vol. 1214, no. 1, pp. 190–198, 2010, doi: 10.1111/J.1749-6632.2010.05840.X.
- [76] K. M. Gibson, G. F. Hoffmann, R. D. Tanaka, R. W. Bishop, and K. L. Chambliss, "Mevalonate kinase Map position 12q24," *Chromosome Research*, vol. 5, no. 2, p. 150, 1997, doi: 10.1023/A:1018430527386.
- [77] S. Hogenboom, J. J. M. Tuyp, M. Espeel, J. Koster, R. J. A. Wanders, and H. R. Watersham, "Mevalonate kinase is a cytosolic enzyme in humans," *J Cell Sci*, vol. 117, no. 4, pp. 631–639, Feb. 2004, doi: 10.1242/JCS.00910.
- [78] G. Hoffmann, K. M. Gibson, I. K. Brandt, P. I. Bader, R. S. Wappner, and L. Sweetman, "Mevalonic Aciduria — An Inborn Error of Cholesterol and Nonsterol Isoprene Biosynthesis," *The new england journal of medicine*, vol. 314, no. 25, pp. 1610–1614, Nov. 1986, doi: 10.1056/NEJM198606193142504.
- [79] R. Berger, G. P. A. Smit, H. Schierbeek, K. Bijsterveld, and R. le Coultre, "Mevalonic aciduria: an inborn error of cholesterol biosynthesis?," *Clinica Chimica Acta*, vol. 152, no. 1–2, pp. 219–222, Oct. 1985, doi: 10.1016/0009-8981(85)90195-0.
- [80] D. Haas and G. F. Hoffmann, "Mevalonate kinase deficiencies: from mevalonic aciduria to hyperimmunoglobulinemia D syndrome," *Orphanet J Rare Dis*, vol. 1, no. 1, p. 13, 2006, doi: 10.1186/1750-1172-1-13.
- [81] A. Simon *et al.*, "Simvastatin Treatment for Inflammatory Attacks of the Hyperimmunoglobulinemia D and Periodic Fever Syndrome," *Clin Pharmacol Ther*, vol. 75, no. 5, pp. 476–483, May 2004, doi: 10.1016/J.CLPT.2004.01.012.

- [82] A. Simon *et al.*, "Mevalonate kinase deficiency," *Neurology*, vol. 62, no. 6, pp. 994–997, Mar. 2004, doi: 10.1212/01.WNL.0000115390.33405.F7.
- [83] G. F. Hoffmann *et al.*, "Clinical and Biochemical Phenotype in 11 Patients With Mevalonic Aciduria," *Pediatrics*, vol. 91, no. 5, 1993.
- [84] V. Prietsch *et al.*, "Mevalonate Kinase Deficiency: Enlarging the Clinical and Biochemical Spectrum," *Pediatrics*, vol. 111, no. 2, pp. 258–261, Feb. 2003, doi: 10.1542/PEDS.111.2.258.
- [85] G. F. Hoffmann *et al.*, "Facts and artefacts in mevalonic aciduria: development of a stable isotope dilution GCMS assay for mevalonic acid and its application to physiological fluids, tissue samples, prenatal diagnosis and carrier detection," *Clinica Chimica Acta*, vol. 198, no. 3, pp. 209–227, 1991, doi: 10.1016/0009-8981(91)90355-G.
- [86] E. Jellum, T. Kluge, H. C. Børresen, O. Stokke, and L. Eldjarn, "Pyroglutamic aciduria--a new inborn error of metabolism," *Scand J Clin Lab Invest*, vol. 26, no. 4, pp. 327–335, 1970, doi: 10.3109/00365517009046241.
- [87] O H LOWRY, N J ROSEBROUGH, A L FARR, and R J RANDALL, "Protein measurement with the Folin phenol reagent," *J Biol Chem*, 1951, Accessed: Feb. 21, 2022. [Online]. Available: <https://pubmed.ncbi.nlm.nih.gov/14907713/>
- [88] U. K. Laemmli, "Cleavage of Structural Proteins during the Assembly of the Head of Bacteriophage T4," *Nature* 1970 227:5259, vol. 227, no. 5259, pp. 680–685, 1970, doi: 10.1038/227680a0.
- [89] R. Hennig, E. Rapp, R. Kottler, S. Cajic, M. Borowiak, and U. Reichl, "N-Glycosylation Fingerprinting of Viral Glycoproteins by xCGE-LIF," *Methods Mol Biol*, vol. 1331, pp. 123–143, Jan. 2015, doi: 10.1007/978-1-4939-2874-3_8.
- [90] C. Rossdam *et al.*, "Approach for Profiling of Glycosphingolipid Glycosylation by Multiplexed Capillary Gel Electrophoresis Coupled to Laser-Induced Fluorescence Detection to Identify Cell-Surface Markers of Human Pluripotent Stem Cells and Derived Cardiomyocytes," *Anal Chem*, vol. 91, no. 10, pp. 6413–6418, May 2019, doi: 10.1021/ACS.ANALCHEM.9B01114/ASSET/IMAGES/LARGE/AC-2019-01114R_0002.JPEG.
- [91] C. Thiel *et al.*, "Improved diagnostics lead to identification of three new patients with congenital disorder of glycosylation-Ip," *Hum Mutat*, vol. 33, no. 3, pp. 485–487, Mar. 2012, doi: 10.1002/humu.22019.
- [92] C. Körner, L. Lehle, and K. von Figura, "Abnormal synthesis of mannose 1-phosphate derived carbohydrates in carbohydrate-deficient glycoprotein syndrome type I fibroblasts with phosphomannomutase deficiency," *Glycobiology*, vol. 8, no. 2, pp. 165–171, Feb. 1998, doi: 10.1093/GLYCOB/8.2.165.
- [93] C. Korner, R. Knauer, U. Holzbach, F. Hanefeld, L. Lehle, and K. von Figura, "Carbohydrate-Deficient Glycoprotein Syndrome Type V: Deficiency of dolichyl-P-Glc:Man 9 GlcNAc 2-PP-dolichyl Glucosyltransferase," 1998.
- [94] L. LEHLE, "Biosynthesis of the Core Region of Yeast Mannoproteins: Formation of a Glucosylated Dolichol-Bound Oligosaccharide Precursor, Its Transfer to Protein and Subsequent Modification," *Eur J Biochem*, vol. 109, no. 2, pp. 589–601, 1980, doi: 10.1111/J.1432-1033.1980.TB04832.X.
- [95] S. W. Sauer *et al.*, "Intracerebral accumulation of glutaric and 3-hydroxyglutaric acids secondary to limited flux across the blood–brain barrier constitute a biochemical risk factor for neurodegeneration in glutaryl-CoA dehydrogenase deficiency," *J Neurochem*, vol. 97, no. 3, pp. 899–910, May 2006, doi: 10.1111/J.1471-4159.2006.03813.X.
- [96] K. Bürstenbinder, G. Rzewuski, M. Wirtz, R. Hell, and M. Sauter, "The role of methionine recycling for ethylene synthesis in Arabidopsis," *The Plant Journal*, vol. 49, no. 2, pp. 238–249, Jan. 2007, doi: 10.1111/J.1365-313X.2006.02942.X.

- [97] B. D. Weger *et al.*, "Extensive Regulation of Diurnal Transcription and Metabolism by Glucocorticoids," *PLoS Genet*, vol. 12, no. 12, p. e1006512, Dec. 2016, doi: 10.1371/JOURNAL.PGEN.1006512.
- [98] G. Liebisch, M. Binder, R. Schifferer, T. Langmann, B. Schulz, and G. Schmitz, "High throughput quantification of cholesterol and cholesteryl ester by electrospray ionization tandem mass spectrometry (ESI-MS/MS)," *Biochim Biophys Acta Mol Cell Biol Lipids*, vol. 1761, no. 1, pp. 121–128, Jan. 2006, doi: 10.1016/j.bbalip.2005.12.007.
- [99] C. Özbalci, T. Sachsenheimer, and B. Brügger, "Quantitative analysis of cellular lipids by nano-electrospray ionization mass spectrometry," *Methods in Molecular Biology*, vol. 1033, pp. 3–20, 2013, doi: 10.1007/978-1-62703-487-6_1.
- [100] R. Heidasch *et al.*, "Intramembrane protease SPP defines a cholesterol-regulated switch of the mevalonate pathway," *bioRxiv*, p. 2021.07.19.452877, Jan. 2022, doi: 10.1101/2021.07.19.452877.
- [101] D. Wessel and U. I. Flügge, "A method for the quantitative recovery of protein in dilute solution in the presence of detergents and lipids," *Anal Biochem*, vol. 138, no. 1, pp. 141–143, Apr. 1984, doi: 10.1016/0003-2697(84)90782-6.
- [102] J. Rappsilber, M. Mann, and Y. Ishihama, "Protocol for micro-purification, enrichment, pre-fractionation and storage of peptides for proteomics using StageTips," *Nature Protocols* 2007 2:8, vol. 2, no. 8, pp. 1896–1906, Aug. 2007, doi: 10.1038/nprot.2007.261.
- [103] X. Liu, C. Li, C. Mou, Y. Dong, and Y. Tu, "dbNSFP v4: a comprehensive database of transcript-specific functional predictions and annotations for human nonsynonymous and splice-site SNVs," *Genome Med*, vol. 12, no. 1, pp. 1–8, Dec. 2020, doi: 10.1186/S13073-020-00803-9/FIGURES/4.
- [104] X. Liu, X. Jian, and E. Boerwinkle, "dbNSFP: A Lightweight Database of Human Nonsynonymous SNPs and Their Functional Predictions," *Hum Mutat*, vol. 32, no. 8, p. 894, Aug. 2011, doi: 10.1002/HUMU.21517.
- [105] J. Jaeken, "Congenital disorders of glycosylation," *Handb Clin Neurol*, vol. 113, pp. 1737–1743, Jan. 2013, doi: 10.1016/B978-0-444-59565-2.00044-7.
- [106] L. A. Plum and H. F. Deluca, "Vitamin D, disease and therapeutic opportunities," *Nature Reviews Drug Discovery*, vol. 9, no. 12, pp. 941–955, Dec. 2010, doi: 10.1038/nrd3318.
- [107] M. F. Holick, "Sunlight and vitamin D for bone health and prevention of autoimmune diseases, cancers, and cardiovascular disease," *Am J Clin Nutr*, vol. 80, no. 6, pp. 1678S–1688S, Dec. 2004, doi: 10.1093/AJCN/80.6.1678S.
- [108] N. Puizina-Ivić, "Skin aging," *Acta Dermatovenerol Alp Pannonica Adriat*, vol. 17, no. 2, pp. 47–54, Jun. 2008, doi: 10.5124/jkma.2000.43.5.448.
- [109] H. Tateno, S. Nakamura-Tsuruta, and J. Hirabayashi, "Comparative analysis of core-fucose-binding lectins from *Lens culinaris* and *Pisum sativum* using frontal affinity chromatography," *Glycobiology*, vol. 19, no. 5, pp. 527–536, May 2009, doi: 10.1093/GLYCOB/CWP016.
- [110] Y. Yang *et al.*, "Structural Basis for Dimerization of ICAM-1 on the Cell Surface," *Mol Cell*, vol. 14, no. 2, pp. 269–276, Apr. 2004, doi: 10.1016/S1097-2765(04)00204-7.
- [111] N. Andrejewski *et al.*, "Normal Lysosomal Morphology and Function in LAMP-1-deficient Mice *," *Journal of Biological Chemistry*, vol. 274, no. 18, pp. 12692–12701, Apr. 1999, doi: 10.1074/JBC.274.18.12692.
- [112] Y. Matsushita *et al.*, "Intercellular Adhesion Molecule-1 Deficiency Attenuates the Development of Skin Fibrosis in Tight-Skin Mice," *The Journal of Immunology*, vol. 179, no. 1, pp. 698–707, Jul. 2007, doi: 10.4049/JIMMUNOL.179.1.698.

- [113] T. N. Ramos, D. C. Bullard, and S. R. Barnum, "ICAM-1: Isoforms and Phenotypes," *The Journal of Immunology*, vol. 192, no. 10, pp. 4469–4474, May 2014, doi: 10.4049/JIMMUNOL.1400135.
- [114] P. He, B. G. Ng, M. E. Losfeld, W. Zhu, and H. H. Freeze, "Identification of Intercellular Cell Adhesion Molecule 1 (ICAM-1) as a Hypoglycosylation Marker in Congenital Disorders of Glycosylation Cells," *J Biol Chem*, vol. 287, no. 22, p. 18210, May 2012, doi: 10.1074/JBC.M112.355677.
- [115] Q. Dang *et al.*, "LAMP1 Overexpression Predicts for Poor Prognosis in Diffuse Large B-cell Lymphoma," *Clin Lymphoma Myeloma Leuk*, vol. 18, no. 11, pp. 749–754, Nov. 2018, doi: 10.1016/J.CLML.2018.07.288.
- [116] Q. Wang *et al.*, "LAMP1 expression is associated with poor prognosis in breast cancer," *Oncol Lett*, vol. 14, no. 4, p. 4729, 2017, doi: 10.3892/OL.2017.6757.
- [117] Y. Xu, X. Cao, S. Zhang, Y. Zhang, and Z. Shen, "High expression of LAMP1 as a prognostic marker in patients with epithelial ovarian cancer," *Int J Clin Exp Pathol*, vol. 10, no. 8, p. 9104, 2017, Accessed: Aug. 01, 2022. [Online]. Available: /pmc/articles/PMC6965383/
- [118] M. Lu *et al.*, "LAMP1 expression is associated with malignant behaviours and predicts unfavourable prognosis in laryngeal squamous cell carcinoma," *Pathology*, vol. 48, no. 7, pp. 684–690, Dec. 2016, doi: 10.1016/J.PATHOL.2016.08.001.
- [119] N. X. Cawley *et al.*, "Abnormal LAMP1 glycosylation may play a role in Niemann-Pick disease, type C pathology," *PLoS One*, vol. 15, no. 1, p. e0227829, Jan. 2020, doi: 10.1371/JOURNAL.PONE.0227829.
- [120] A. Ferrer *et al.*, "Fetal glycosylation defect due to ALG3 and COG5 variants detected via amniocentesis: Complex glycosylation defect with embryonic lethal phenotype," *Mol Genet Metab*, vol. 131, no. 4, pp. 424–429, Dec. 2020, doi: 10.1016/J.YMGME.2020.11.003.
- [121] M. P. Wilson *et al.*, "Active site variants in STT3A cause a dominant type I congenital disorder of glycosylation with neuromusculoskeletal findings," *The American Journal of Human Genetics*, vol. 108, no. 11, pp. 2130–2144, Nov. 2021, doi: 10.1016/J.AJHG.2021.09.012.
- [122] M. Damaghi *et al.*, "Chronic acidosis in the tumour microenvironment selects for overexpression of LAMP2 in the plasma membrane," *Nat Commun*, vol. 6, Dec. 2015, doi: 10.1038/NCOMMS9752.
- [123] N. Abu Bakar *et al.*, "Synergistic use of glycomics and single-molecule molecular inversion probes for identification of congenital disorders of glycosylation type-1," *J Inherit Metab Dis*, vol. 45, no. 4, pp. 769–781, Jul. 2022, doi: 10.1002/JIMD.12496.
- [124] N. Abu Bakar *et al.*, "Intact transferrin and total plasma glycoprofiling for diagnosis and therapy monitoring in phosphoglucomutase-I deficiency," *Transl Res*, vol. 199, p. 62, Sep. 2018, doi: 10.1016/J.TRSL.2018.04.008.
- [125] S. Y. W. Wong *et al.*, "ORAL D-GALACTOSE SUPPLEMENTATION IN PGM1-CDG," *Genet Med*, vol. 19, no. 11, p. 1226, Nov. 2017, doi: 10.1038/GIM.2017.41.
- [126] W. Zhang *et al.*, "A Novel N-Tetrasaccharide in Patients with Congenital Disorders of Glycosylation Including Asparagine-Linked Glycosylation Protein 1, Phosphomannomutase 2, and Phosphomannose Isomerase Deficiencies," *Clin Chem*, vol. 62, no. 1, p. 208, Jan. 2016, doi: 10.1373/CLINCHEM.2015.243279.
- [127] E. v. Dyatlovitskaya and L. D. Bergelson, "Glycosphingolipids and antitumor immunity," *Biochim Biophys Acta*, vol. 907, no. 2, pp. 125–143, Jul. 1987, doi: 10.1016/0304-419X(87)90002-3.
- [128] N. v. Prokazova and L. D. Bergelson, "Gangliosides and atherosclerosis," *Lipids*, vol. 29, no. 1, pp. 1–5, Jan. 1994, doi: 10.1007/BF02537083.

- [129] C. J. Wikstrand, P. Fredman, L. Svennerholm, and D. D. Bigner, "Detection of glioma-associated gangliosides GM2, GD2, GD3, 3'-isoLM1 3',6'-isoLD1 in central nervous system tumors in vitro and in vivo using epitope-defined monoclonal antibodies," *Prog Brain Res*, vol. 101, no. C, pp. 213–223, Jan. 1994, doi: 10.1016/S0079-6123(08)61951-2.
- [130] F. Malisan and R. Testi, "GD3 ganglioside and apoptosis," *Biochimica et Biophysica Acta (BBA) - Molecular and Cell Biology of Lipids*, vol. 1585, no. 2–3, pp. 179–187, Dec. 2002, doi: 10.1016/S1388-1981(02)00339-6.
- [131] S. A. Demir, Z. K. Timur, N. Ateş, L. A. Martínez, and V. Seyrantepe, "GM2 ganglioside accumulation causes neuroinflammation and behavioral alterations in a mouse model of early onset Tay-Sachs disease," *J Neuroinflammation*, vol. 17, no. 1, pp. 1–18, Sep. 2020, doi: 10.1186/S12974-020-01947-6/FIGURES/9.
- [132] S. Saito *et al.*, "RM2 antigen (β 1,4-GalNAc-disialyl-Lc4) as a new marker for prostate cancer," *Int J Cancer*, vol. 115, no. 1, pp. 105–113, May 2005, doi: 10.1002/IJC.20868.
- [133] T. Zhang, A. A. de Waard, M. Wuhrer, and R. M. Spaapen, "The role of glycosphingolipids in immune cell functions," *Front Immunol*, vol. 10, no. JAN, p. 90, 2019, doi: 10.3389/FIMMU.2019.00090/BIBTEX.
- [134] Y. Luo *et al.*, "Cellular interaction through LewisX cluster: theoretical studies," *J Mol Model*, vol. 14, no. 10, pp. 901–910, 2008, doi: 10.1007/S00894-008-0325-9.
- [135] S. itiroh Hakomori, "Functional role of glycosphingolipids in tumor progression," *Tohoku J Exp Med*, vol. 168, no. 2, pp. 211–222, 1992, doi: 10.1620/TJEM.168.211.
- [136] Y. Poirier, V. D. Antonenkov, T. Glumoff, and J. K. Hiltunen, "Peroxisomal β -oxidation—A metabolic pathway with multiple functions," *Biochimica et Biophysica Acta (BBA) - Molecular Cell Research*, vol. 1763, no. 12, pp. 1413–1426, Dec. 2006, doi: 10.1016/J.BBAMCR.2006.08.034.
- [137] S. Ferdinandusse *et al.*, "A novel case of ACOX2 deficiency leads to recognition of a third human peroxisomal acyl-CoA oxidase," *Biochimica et Biophysica Acta (BBA) - Molecular Basis of Disease*, vol. 1864, no. 3, pp. 952–958, Mar. 2018, doi: 10.1016/J.BBADIS.2017.12.032.
- [138] S. E. Corcoran and L. A. J. O'Neill, "HIF1 α and metabolic reprogramming in inflammation," *J Clin Invest*, vol. 126, no. 10, p. 3699, Oct. 2016, doi: 10.1172/JCI84431.
- [139] Q. Yu, L. Dong, Y. Li, and G. Liu, "SIRT1 and HIF1 α signaling in metabolism and immune responses," *Cancer Lett*, vol. 418, pp. 20–26, Apr. 2018, doi: 10.1016/J.CANLET.2017.12.035.
- [140] V. Vallon *et al.*, "Role of Sgk1 in salt and potassium homeostasis," *Am J Physiol Regul Integr Comp Physiol*, vol. 288, no. 1 57-1, pp. 4–10, Jan. 2005, doi: 10.1152/AJPREGU.00369.2004/ASSET/IMAGES/LARGE/ZH60120424430002.JPEG.
- [141] M. S. Yoon, "mTOR as a Key Regulator in Maintaining Skeletal Muscle Mass," *Front Physiol*, vol. 8, no. OCT, p. 788, Oct. 2017, doi: 10.3389/FPHYS.2017.00788.
- [142] Y. el Hiani, E. E. A. Egom, and X. P. Dong, "mTOR signalling: jack-of-all-trades1," <https://doi.org/10.1139/bcb-2018-0004>, vol. 97, no. 1, pp. 58–67, 2018, doi: 10.1139/BCB-2018-0004.
- [143] A. Varki *et al.*, "Essentials of Glycobiology," *Essentials of Glycobiology*, 2022, doi: 10.1101/9781621824213.
- [144] H. Kashiwazaki, M. Kakizaki, Y. Ikehara, A. Togayachi, H. Narimatsu, and R. Watanabe, "Mice lacking α 1,3-fucosyltransferase 9 exhibit modulation of in vivo immune responses against pathogens," *Pathol Int*, vol. 64, no. 5, pp. 199–208, 2014, doi: 10.1111/PIN.12159/SUPPINFO.
- [145] F. G. Hanisch, "O-glycosylation of the mucin type," *Biol Chem*, vol. 382, no. 2, pp. 143–149, Feb. 2001, doi: 10.1515/BC.2001.022/MACHINEREADABLECITATION/RIS.

- [146] Y. L. Shang *et al.*, "Novel DPY19L2 variants in globozoospermic patients and the overcoming this male infertility," *Asian J Androl*, vol. 21, no. 2, p. 183, Mar. 2019, doi: 10.4103/AJA.AJA_79_18.
- [147] Y. Hara *et al.*, "A Dystroglycan Mutation Associated with Limb-Girdle Muscular Dystrophy," *N Engl J Med*, vol. 364, no. 10, p. 939, Mar. 2011, doi: 10.1056/NEJMOA1006939.
- [148] Y. Hara *et al.*, "A Dystroglycan Mutation Associated with Limb-Girdle Muscular Dystrophy," *N Engl J Med*, vol. 364, no. 10, p. 939, Mar. 2011, doi: 10.1056/NEJMOA1006939.
- [149] C. M. Dobson, S. J. Hempel, S. H. Stalnaker, R. Stuart, and L. Wells, "O-Mannosylation and Human Disease," *Cell Mol Life Sci*, vol. 70, no. 16, p. 2849, Aug. 2013, doi: 10.1007/S00018-012-1193-0.
- [150] Y. Fukao, "Discordance between protein and transcript levels detected by selected reaction monitoring," *Plant Signal Behav*, vol. 10, no. 5, pp. 1–6, 2015, doi: 10.1080/15592324.2015.1017697.
- [151] C. Körner, L. Lehle, and K. von Figura, "Carbohydrate-deficient glycoprotein syndrome type 1: correction of the glycosylation defect by deprivation of glucose or supplementation of mannose," *Glycoconjugate Journal* 1998 15:5, vol. 15, no. 5, pp. 499–505, 1998, doi: 10.1023/A:1006939104442.
- [152] M. A. Tarnopolsky, "Myopathies Related to Glycogen Metabolism Disorders," *Neurotherapeutics*, vol. 15, no. 4, p. 915, Oct. 2018, doi: 10.1007/S13311-018-00684-2.
- [153] G. Lu, W. Shi, and Y. Zhang, "Prognostic Implications and Immune Infiltration Analysis of ALDOA in Lung Adenocarcinoma," *Front Genet*, vol. 12, p. 721021, Dec. 2021, doi: 10.3389/FGENE.2021.721021/FULL.
- [154] S. Bijarnia-Mahay, S. Bhatia, and V. Arora, "Fructose-1,6-Bisphosphatase Deficiency," *GeneReviews*[®], Dec. 2019, Accessed: Aug. 09, 2022. [Online]. Available: <https://www.ncbi.nlm.nih.gov/books/NBK550349/>
- [155] H. Dong *et al.*, "A Novel Function of Mitochondrial Phosphoenolpyruvate Carboxykinase as a Regulator of Inflammatory Response in Kupffer Cells," *Front Cell Dev Biol*, vol. 9, Dec. 2021, doi: 10.3389/FCELL.2021.726931/FULL.
- [156] M. M. Semianiv *et al.*, "Association of AGTR1 (rs5186), VDR (rs2228570) genes polymorphism with blood pressure elevation in patients with essential arterial hypertension," *J Med Life*, vol. 14, no. 6, p. 782, Nov. 2021, doi: 10.25122/JML-2021-0018.
- [157] K. K. Gaddam, E. Pimenta, S. Husain, and D. A. Calhoun, "Aldosterone and Cardiovascular Disease," *Curr Probl Cardiol*, vol. 34, no. 2, pp. 51–84, Feb. 2009, doi: 10.1016/J.CPCARDIOL.2008.10.002.
- [158] K. Kikuchi and H. Tsukamoto, "Stearoyl-CoA Desaturase and Tumorigenesis," *Chem Biol Interact*, vol. 316, p. 108917, Jan. 2020, doi: 10.1016/J.CBI.2019.108917.
- [159] E. Abati, N. Bresolin, G. Comi, and S. Corti, "Silence superoxide dismutase 1 (SOD1): a promising therapeutic target for amyotrophic lateral sclerosis (ALS)," *Expert Opin Ther Targets*, vol. 24, no. 4, pp. 295–310, Apr. 2020, doi: 10.1080/14728222.2020.1738390.
- [160] M. Harati-Sadegh *et al.*, "IL1A and IL1B gene polymorphisms and keratoconus susceptibility: evidence from an updated meta-analysis," <https://doi.org/10.1080/13816810.2021.1925926>, vol. 42, no. 5, pp. 503–513, 2021, doi: 10.1080/13816810.2021.1925926.
- [161] K. Baksi, J. Tavarez-Pagan, J. Martinez, and D. Banerjee, "Unique structural motif supports mannosylphospho dolichol synthase: an important angiogenesis regulator," *Curr Drug Targets*, vol. 9, no. 4, pp. 262–271, Mar. 2008, doi: 10.2174/138945008783954916.

- [162] J. A. Martínez, J. J. Tavárez, C. M. Oliveira, and D. K. Banerjee, "Potentiation of angiogenic switch in capillary endothelial cells by cAMP: A cross-talk between up-regulated LLO biosynthesis and the HSP-70 expression," *Glycoconjugate Journal* 2006 23:3, vol. 23, no. 3, pp. 209–220, May 2006, doi: 10.1007/S10719-006-7926-2.
- [163] L. A. Vettore, R. L. Westbrook, and D. A. Tennant, "Proline metabolism and redox; maintaining a balance in health and disease," *Amino Acids*, vol. 53, no. 12, p. 1779, Dec. 2021, doi: 10.1007/S00726-021-03051-2.
- [164] N. Shyh-Chang *et al.*, "Influence of threonine metabolism on S-adenosylmethionine and histone methylation," *Science*, vol. 339, no. 6116, pp. 222–226, Jan. 2013, doi: 10.1126/SCIENCE.1226603.
- [165] J. Moro, D. Tomé, P. Schmidely, T. C. Demersay, and D. Azzout-Marniche, "Histidine: A Systematic Review on Metabolism and Physiological Effects in Human and Different Animal Species," *Nutrients* 2020, Vol. 12, Page 1414, vol. 12, no. 5, p. 1414, May 2020, doi: 10.3390/NU12051414.
- [166] M. A. Welte and A. P. Gould, "Lipid droplet functions beyond energy storage," *Biochim Biophys Acta*, vol. 1862, no. 10 Pt B, p. 1260, Oct. 2017, doi: 10.1016/J.BBALIP.2017.07.006.
- [167] S. Xu, X. Zhang, and P. Liu, "Lipid droplet proteins and metabolic diseases," *Biochimica et Biophysica Acta (BBA) - Molecular Basis of Disease*, vol. 1864, no. 5, pp. 1968–1983, May 2018, doi: 10.1016/J.BBADIS.2017.07.019.
- [168] G. F. Hoffmann, U. N. Wiesmann, S. Brendel, R. Kennedy Keller, and K. Michael Gibson, "Regulatory Adaptation of Isoprenoid Biosynthesis and the LDL Receptor Pathway in Fibroblasts from Patients with Mevalonate Kinase Deficiency," *Pediatric Research* 1997 41:4, vol. 41, no. 4, pp. 541–546, 1997, doi: 10.1203/00006450-199704000-00014.
- [169] V. Cantagrel and D. J. Lefeber, "From glycosylation disorders to dolichol biosynthesis defects: A new class of metabolic diseases," *Journal of Inherited Metabolic Disease*, vol. 34, no. 4, J Inherit Metab Dis, pp. 859–867, Aug. 2011. doi: 10.1007/s10545-011-9301-0.
- [170] S. H. L. Mandey, L. M. Kuijk, J. Frenkel, and H. R. Waterham, "A role for geranylgeranylation in interleukin-1 β secretion," *Arthritis Rheum*, vol. 54, no. 11, pp. 3690–3695, Nov. 2006, doi: 10.1002/ART.22194.
- [171] L. M. Kuijk *et al.*, "Statin synergizes with LPS to induce IL-1 β release by THP-1 cells through activation of caspase-1," *Mol Immunol*, vol. 45, no. 8, pp. 2158–2165, Apr. 2008, doi: 10.1016/J.MOLIMM.2007.12.008.
- [172] L. Jaenicke, K. van Leyen, and H. U. Siegmund, "Dolichyl phosphate-dependent glycosyltransferases utilize truncated cofactors," *Biol Chem Hoppe Seyler*, vol. 372, no. 11, pp. 1021–1026, 1991, doi: 10.1515/BCHM3.1991.372.2.1021.
- [173] B. Schenk, F. Fernandez, and C. J. Waechter, "The ins(ide) and outs(ide) of dolichyl phosphate biosynthesis and recycling in the endoplasmic reticulum," *Glycobiology*, vol. 11, no. 5, pp. 61R–70R, May 2001, doi: 10.1093/GLYCOB/11.5.61R.
- [174] M. J. Spiro, R. G. Spirol, and E. P. Joslin, "Control of N-Linked Carbohydrate Unit Synthesis in Thyroid Endoplasmic Reticulum by Membrane Organization and Dolichyl Phosphate Availability*," *J Biol Chem*, vol. 261, no. 31, pp. 14725–14732, 1986, doi: 10.1016/S0021-9258(18)66931-5.
- [175] A. G. Rosenwald, J. Stoll, and S. S. Krag, "Regulation of glycosylation. Three enzymes compete for a common pool of dolichyl phosphate in vivo.," *Journal of Biological Chemistry*, vol. 265, no. 24, pp. 14544–14553, Aug. 1990, doi: 10.1016/S0021-9258(18)77337-7.
- [176] S. Ramachandra Rao *et al.*, "Retinal Degeneration Caused by Rod-Specific Dhdds Ablation Occurs without Concomitant Inhibition of Protein N-Glycosylation," *iScience*, vol. 23, no. 6, p. 101198, Jun. 2020, doi: 10.1016/j.isci.2020.101198.

- [177] B. L. Lew, Y. Cho, J. Kim, W. Y. Sim, and N. I. Kim, "Ceramide and Cell Signaling Molecules in Psoriatic Epidermis: Reduced Levels of Ceramides, PKC- α , and JNK," *J Korean Med Sci*, vol. 21, no. 1, p. 95, 2006, doi: 10.3346/JKMS.2006.21.1.95.
- [178] M. N. Nikolova-Karakashian and K. A. Rozenova, "Ceramide in Stress Response," *Sphingolipids as Signaling and Regulatory Molecules*, vol. 688, p. 86, 2010, doi: 10.1007/978-1-4419-6741-1_6.
- [179] S. Wheeler and D. J. Sillence, "Niemann–Pick type C disease: cellular pathology and pharmacotherapy," *J Neurochem*, vol. 153, no. 6, pp. 674–692, Jun. 2020, doi: 10.1111/JNC.14895.
- [180] D. Patel and S. N. Witt, "Ethanolamine and Phosphatidylethanolamine: Partners in Health and Disease," *Oxid Med Cell Longev*, vol. 2017, 2017, doi: 10.1155/2017/4829180.
- [181] R. Steenbergen, T. S. Nanowski, A. Beigneux, A. Kulinski, S. G. Young, and J. E. Vance, "Disruption of the Phosphatidylserine Decarboxylase Gene in Mice Causes Embryonic Lethality and Mitochondrial Defects," *J Biol Chem*, vol. 280, no. 48, p. 40032, Dec. 2005, doi: 10.1074/JBC.M506510200.
- [182] K. Emoto *et al.*, "Redistribution of phosphatidylethanolamine at the cleavage furrow of dividing cells during cytokinesis," *Proc Natl Acad Sci U S A*, vol. 93, no. 23, p. 12867, Nov. 1996, doi: 10.1073/PNAS.93.23.12867.
- [183] M. G. Paulick and C. R. Bertozzi, "The Glycosylphosphatidylinositol Anchor: A Complex Membrane-Anchoring Structure for Proteins," *Biochemistry*, vol. 47, no. 27, p. 6991, Jul. 2008, doi: 10.1021/B18006324.
- [184] P. A. Leventis and S. Grinstein, "The Distribution and Function of Phosphatidylserine in Cellular Membranes," <http://dx.doi.org/10.1146/annurev.biophys.093008.131234>, vol. 39, no. 1, pp. 407–427, May 2010, doi: 10.1146/ANNUREV.BIOPHYS.093008.131234.
- [185] S. Fu, S. M. Watkins, and G. S. Hotamisligil, "The Role of Endoplasmic Reticulum in Hepatic Lipid Homeostasis and Stress Signaling," *Cell Metab*, vol. 15, no. 5, pp. 623–634, May 2012, doi: 10.1016/J.CMET.2012.03.007.
- [186] H. Malhi and R. J. Kaufman, "Endoplasmic reticulum stress in liver disease," *J Hepatol*, vol. 54, no. 4, pp. 795–809, Apr. 2011, doi: 10.1016/J.JHEP.2010.11.005.
- [187] M. Halliday and G. R. Mallucci, "Targeting the unfolded protein response in neurodegeneration: A new approach to therapy," *Neuropharmacology*, vol. 76 Pt A, no. PART A, pp. 169–174, 2014, doi: 10.1016/J.NEUROPHARM.2013.08.034.
- [188] U. Özcan *et al.*, "Endoplasmic reticulum stress links obesity, insulin action, and type 2 diabetes," *Science*, vol. 306, no. 5695, pp. 457–461, Oct. 2004, doi: 10.1126/SCIENCE.1103160.
- [189] N. E. Braverman and A. B. Moser, "Functions of plasmalogen lipids in health and disease," *Biochimica et Biophysica Acta (BBA) - Molecular Basis of Disease*, vol. 1822, no. 9, pp. 1442–1452, Sep. 2012, doi: 10.1016/J.BBADIS.2012.05.008.
- [190] J. M. Dean and I. J. Lodhi, "Structural and functional roles of ether lipids," *Protein Cell*, vol. 9, no. 2, p. 196, Feb. 2018, doi: 10.1007/S13238-017-0423-5.
- [191] J. R. Kerr, "Epstein-Barr virus (EBV) reactivation and therapeutic inhibitors," *J Clin Pathol*, vol. 72, no. 10, pp. 651–658, Oct. 2019, doi: 10.1136/JCLINPATH-2019-205822.
- [192] C. D. L. Nguyen *et al.*, "A sensitive and simple targeted proteomics approach to quantify transcription factor and membrane proteins of the unfolded protein response pathway in glioblastoma cells," *Sci Rep*, vol. 9, no. 1, Dec. 2019, doi: 10.1038/S41598-019-45237-5.
- [193] S. Matallana-Surget, B. Leroy, and R. Wattiez, "Shotgun proteomics: concept, key points and data mining," <https://doi.org/10.1586/epr.09.101>, vol. 7, no. 1, pp. 5–7, Feb. 2014, doi: 10.1586/EPR.09.101.

10 Appendix

10.1 Nucleotide- and protein sequence

10.1.1 MVK (NM_000431.4) mRNA

Nucleotides in green show the coding sequence of the MVK mRNA. CDS is in total 1191 bb.

```

1      gctctggggtt gtgggagttg gggagctgct ccggcttcgg cgcggagggg cggcggccgg
61      ggaggcggcg gcggcggcag gattcccagg AGCCATGTTG TCAGAAGTCC TACTGGTGTC
121     TGCTCCGGGG AAAGTCATCC TTCATGGAGA ACATGCCGTG GTACATGGCA AGGTAGCACT
181     GGCTGTATCC TTGAACTGA GAACATTCCT CCGGCTTCAA CCCCACAGCA ATGGGAAAAGT
241     GGACCTCAGC TTACCCAACA TTGGTATCAA GCGGGCCTGG GATGTGGCCA GGCTTCAGTC
301     ACTGGACACA AGCTTTCTGG AGCAAGGTGA TGTCACAACA CCCACCTCAG AGCAAGTGGA
361     GAAGCTAAAG GAGGTTGCAG GCTTGCCCTGA CACTGTGCT GTCACCGAGC GCCTGGCTGT
421     GCTGGCCTTT CTTTACTTAT ACCTGTCCAT CTGCCGGAAG CAGAGGGCCC TGCCGAGCCT
481     GGATATCGTA GTGTGGTCGG AGCTGCCCCC CGGGGCGGGC TTGGGCTCCA GCGCCGCTA
541     CTCGGTGTGT CTGGCAGCAG CCCTCCTGAC TGTGTGCGAG GAGATCCCAA ACCCGCTGAA
601     GGACGGGGAT TGCCTCAACA GGTGGACCAA GGAGGATTTG GAGCTAATTA ACAAGTGGGC
661     CTTCCAAGGG GAGAGAATGA TTCACGGGAA CCCCTCCGGA GTGGACAATG CTGTACAGCAG
721     CTGGGGAGGA GCCCTCCGAT ACCATCAAGG GAAGATTTC A CCTTAAAGA GGTCCGACAG
781     TCTCCAGATC CTGCTGACCA ACACAAAAGT CCCTCGCAAT ACCAGGGCCC TTGTGGCTGG
841     CGTCAGAAAC AGGCTGCTCA AGTTCACAGA GATCGTGGCC CCCCTCCTGA CCTCAATAGA
901     TGCCATCTCC CTGGAGTGTG AGCGCGTGCT GGGAGAGATG GGGGAAGCCC CAGCCCCGGA
961     GCAGTACCTC GTGCTGGAAG AGCTCATTGA CATGAACCAG CACCATCTGA ATGCCCTCGG
1021    CGTGGGCCAC GCCTCTCTGG ACCAGCTCTG CCAGGTGACC AGGGCCCGCG GACTTCACAG
1081    CAAGCTGACT GGCGCAGGCG GTGGTGGCTG TGGCATCACA CTCCTCAAGC CAGGGCTGGA
1141    GCAGCCAGAA GTGGAGGCCA CGAAGCAGGC CCTGACCAGC TGTGGCTTTG ACTGCTTGA
1201    AACCAGCATC GGTGCCCCCG GCGTCTCCAT CCACTCAGCC ACCTCCCTGG ACAGCCGAGT
1261    CCAGCAAGCC CTGGATGGCC TCTGAgagga gccacgaca ctgcagcccc acccagatgc
1321    ccctttctgg attattctgg gggctgcagt tcgactctgt gctggccagc gagcggcccag
1381    ctcttgacac tgctggagag gccccagccg cttggcgatg ccagccaagc tctgcagtcc

```

Appendix

1441 cagcgggtggg acctagggag gcatggtctg ccctctgcat cctctggagc cagccgagca
1501 ggaggcctag gagggtcctc tgagactcca gacctgaggc gagaagggct gcttccctga
1561 agctcccaca gtcccatctg cttcaggccc ccgccttggc ctgtgttctt cctggccgcc
1621 tgggtccaat gctcaggtgc tggggcctgg ttcccggaga agtgtgcctt ctctctccct
1681 tttcagggac cgccccctgt ctctcagggc caggcctctc cctcctccag gaagccttcc
1741 cctaccctt gtcgccctc cctcccagag cacctgctgt ctgggtggct cactcagcac
1801 ttggtgtggc cttcccttct acctagcggg atggggctcc cccaggggct gtcccggagg
1861 cgggtggcct ggttaaataa ggcagggttt atatgcactt tcttccgac tgtacctgag
1921 aggtttgtgg aaaagatggc aaatgggaa taaaagatt ttgtgtcaac agtagagact
1981 ccaggccacc agcacctccc tctgtccctg tcccctctcc agctgtttcc tccatggagc
2041 tcttcagcaa tggagggaaa tagggtttg ggtcactttg ttgtgctgt tggggatgag
2101 gtggcttttc ccagatggc cttgctggag agggactggg acacggctct cagtccatca
2161 gcacaactct aggctgctgc tgcggagggga gaagttgagc ttctagctc cagaatcaca
2221 agcaccacag agagcacaga cctgtgtaag acaggaaagc agaacctgcc atcgctcctg
2281 gggcgcgcct tcctttctga aatgaactgg ctggatggag aaaacagact caaatgttct
2341 ggccccggtg cctggcactc cccacccccg cccccaccg gccctatttg aactttatat
2401 tgcagtcagc ttggtgcttt ccgaaatgcc attagccatc aggaaacct tgtagtgggt
2461 gccttgccag ccagaacctc tgggaccac ggacctgcaa agaggccgag tggaaagggt
2521 ggggccggcg cagggatttc aggatgaggt gaaagcgatt cagtgcgcgt ctgcccttgg
2581 ccactagggg gcagctggcg gccttccctg ctgttgtctt cctgcagggt gagaggagca
2641 ggagccgagc tccacccccca cgccagcctt gggccccggc tgggatcact gctgggaaag
2701 tgagagtgaa gggaggacgc ctacccagc ttaacttgta gaaatggccc cagatcactg
2761 atggctgttc cctgccctt ccctcaaaa cacaacgcat aaagcagtaa tactaattaa
2821 tactgaacgc tca

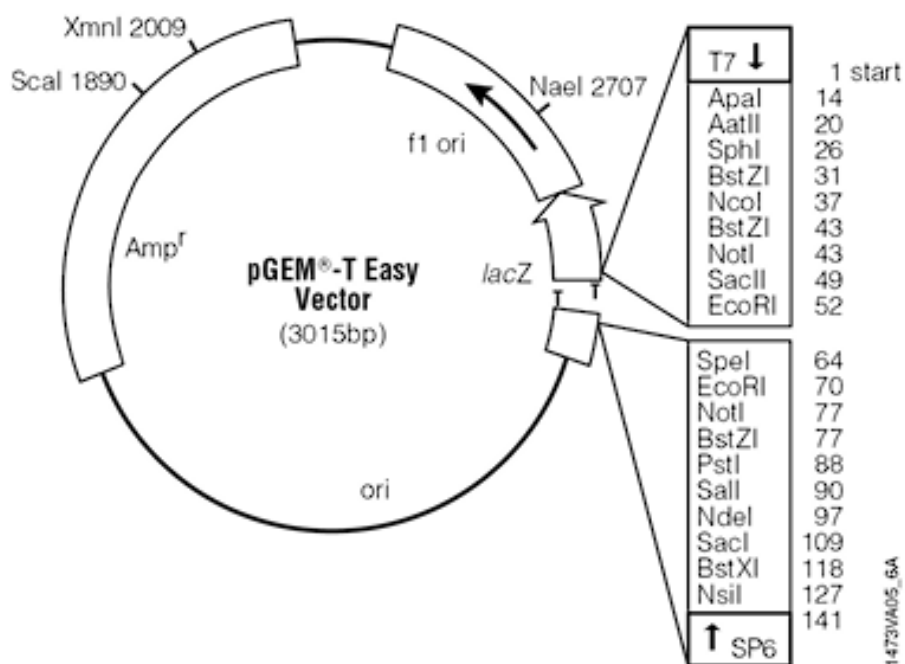
10.1.2 Amino acids sequence of MVK

```

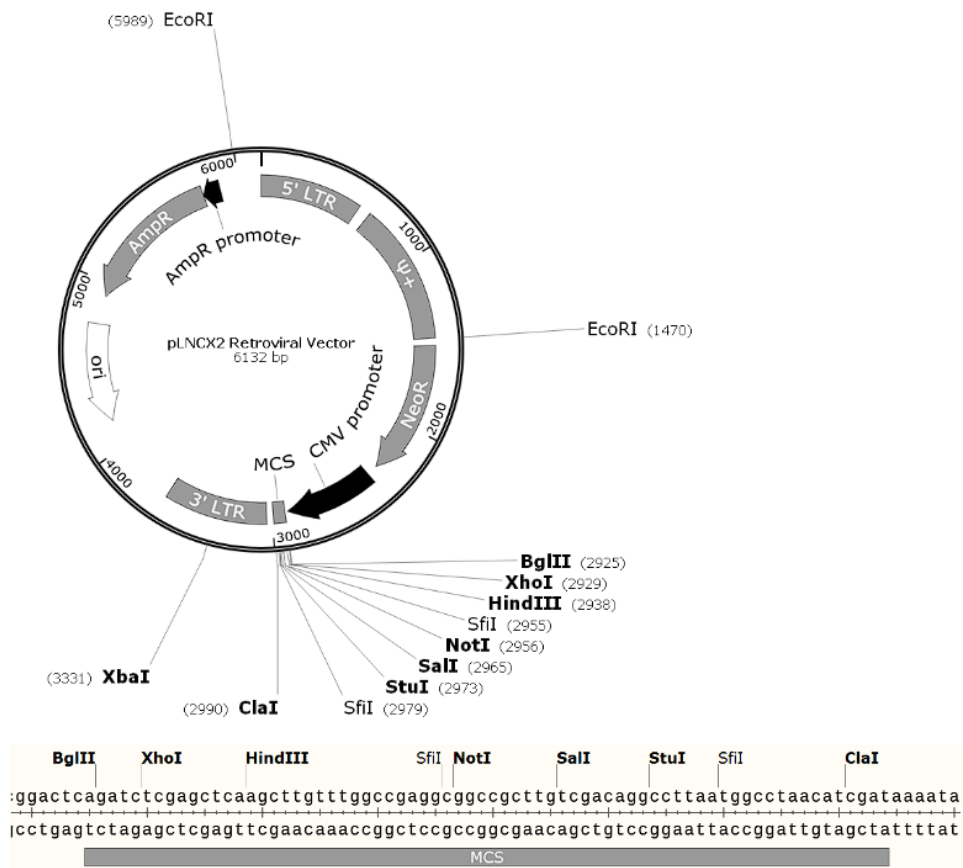
1      MLSEVLLVSA PGKVILHGEH AVVHGKVALA VSLNLRRTFLR LQPHSNGKVD
51     LSLPNIGIKR AWDVARLQSL DTSFLEQGDV TTPTSEQVEK LKEVAGLPDD
101    CAVTERLAVL AFLYLYLSIC RKQRALPSLD IVVWSELPPG AGLGSSAAYS
151    VCLAAALLTV CEEIPNPLKD GDCVNRWTK E DLELINKWAF QGERMIHGPN
201    SGVDNAVSTW GGALRYHQGK ISSLKRSPAL QILLTNTKVP RNTRALVAGV
251    RNRLKFPEI VAPLLTSIDA ISLECERVLG EMGEAPAPEQ YLVLEELIDM
301    NQHHLNALGV GHASLDQLCQ VTRARGLHSK LTGAGGGGCG ITLLKPGLEQ
351    PEVEATKQAL TSCGFDCLET SIGAPGVSIIH SATSLDSRVQ QALDGL
    
```

10.2 Vector maps

10.2.1 pGEM-T Easy Vector



10.2.2 pLNCX2 Vector



10.3 ΔC_t -values of gene expression

MVK

| | Mean | SD |
|---------|--------|-------|
| MVK1 | 10.907 | 0.807 |
| MVK2 | 10.677 | 1.025 |
| MVK3 | 11.732 | 0.707 |
| MVK4 | 11.029 | 0.850 |
| MVK5 | 12.715 | 0.845 |
| MVK6 | 11.018 | 0.987 |
| MVK7 | 11.594 | 0.675 |
| MVK8 | 10.676 | 0.951 |
| MVK9 | 10.117 | 0.650 |
| MVK10 | 11.203 | 0.750 |
| MVK11 | 11.127 | 0.824 |
| Control | 12.175 | 0.823 |

HMGCR

HMGCR

| | Mean | SD |
|---------|--------|-------|
| MVK1 | 14.015 | 0.666 |
| MVK2 | 13.945 | 1.446 |
| MVK3 | 13.315 | 0.174 |
| MVK4 | 13.482 | 1.419 |
| MVK5 | 13.864 | 0.429 |
| MVK6 | 14.057 | 1.397 |
| MVK7 | 14.290 | 1.304 |
| MVK8 | 14.138 | 1.072 |
| MVK9 | 13.734 | 2.210 |
| MVK10 | 14.366 | 0.804 |
| MVK11 | 13.751 | 0.764 |
| Control | 15.118 | 0.805 |

PMVK

| | Mean | SD |
|---------|--------|-------|
| MVK1 | 17.101 | 0.409 |
| MVK2 | 17.407 | 0.729 |
| MVK3 | 16.942 | 0.132 |
| MVK4 | 17.214 | 0.496 |
| MVK5 | 17.401 | 0.260 |
| MVK6 | 17.068 | 0.701 |
| MVK7 | 17.602 | 1.065 |
| MVK8 | 17.395 | 0.270 |
| MVK9 | 17.257 | 0.729 |
| MVK10 | 17.210 | 0.383 |
| MVK11 | 16.881 | 0.132 |
| Control | 17.575 | 0.589 |

10.4 nCounter ratios

| Probe Name | MVK1 | MVK2 | MVK3 | MVK4 | MVK5 | MVK6 | MVK7 | MVK8 | MVK9 | MVK10 | MVK11 |
|------------|-------|-------|-------|-------|-------|-------|-------|-------|-------|-------|-------|
| ACADL | 1.03 | -1.01 | -1.01 | 2.07 | 1.05 | 1.17 | -1.01 | 1.02 | 1.07 | 1.12 | 1.07 |
| ACOX3 | 1.44 | 1.08 | 1.16 | 1.39 | 1.51 | 1.28 | 1.06 | 1.12 | -1.07 | 1.01 | 1.10 |
| ACTB | 1.03 | -1.00 | 1.12 | 1.02 | 1.30 | -1.10 | -1.07 | -1.08 | 1.02 | -1.30 | 1.05 |
| ALG1 | 1.22 | 1.12 | 1.07 | -1.03 | 1.14 | 1.07 | 1.08 | -1.09 | -1.00 | 1.02 | -1.01 |
| ALG10 | -5.44 | -5.67 | -5.67 | -5.37 | -5.34 | -4.78 | -4.49 | -5.52 | 1.92 | 1.83 | 2.03 |
| ALG11 | 1.17 | -1.18 | 1.06 | -1.01 | -1.06 | -1.10 | -1.01 | 1.03 | -1.13 | 1.08 | 1.18 |
| ALG12 | 1.22 | 1.15 | 1.03 | 1.11 | 1.12 | 1.42 | 1.33 | 1.58 | 1.31 | 1.45 | 1.65 |
| ALG13 | 1.34 | 1.09 | -1.04 | 1.04 | 1.09 | 1.11 | 1.07 | -1.03 | 1.12 | 1.13 | 1.02 |
| ALG14 | 1.19 | 1.16 | -1.18 | 1.04 | 1.08 | 1.06 | 1.01 | 1.13 | -1.08 | 1.18 | 1.44 |
| ALG2 | 1.31 | -1.05 | 1.02 | 1.08 | -1.04 | 1.07 | 1.28 | 1.19 | 1.08 | 1.15 | 1.05 |
| ALG3 | -1.09 | -1.30 | -1.01 | -1.22 | -1.31 | -1.27 | -1.17 | -1.30 | -1.17 | -1.12 | -1.30 |
| ALG5 | 1.15 | -1.13 | -1.02 | -1.16 | -1.03 | 1.04 | 1.24 | 1.02 | 1.03 | 1.09 | 1.10 |
| ALG6 | 5.11 | 1.35 | 1.75 | 3.01 | 1.08 | 3.68 | 3.65 | 2.98 | 1.93 | 1.83 | 3.06 |
| ALG8 | -1.00 | -1.05 | 1.08 | -1.07 | 1.00 | -1.02 | 1.12 | -1.09 | 1.01 | 1.09 | 1.03 |
| ALG9 | 1.07 | 1.02 | 1.07 | -1.00 | 1.09 | 1.05 | 1.14 | 1.09 | 1.04 | 1.08 | 1.20 |
| B3GalNAct2 | 1.53 | 1.22 | 1.19 | 1.23 | 1.42 | 1.60 | 1.77 | 1.13 | 1.34 | 1.58 | 1.35 |
| B4GALT1 | 2.48 | 1.87 | 1.51 | 2.50 | 3.64 | 1.58 | 2.19 | 1.62 | 2.01 | 1.88 | 1.05 |
| C1orf43 | 1.14 | 1.00 | -1.16 | -1.03 | -1.16 | 1.09 | 1.04 | 1.08 | 1.09 | 1.29 | 1.14 |
| DHDDS | -1.29 | -1.11 | 1.09 | 1.14 | 1.16 | -1.02 | -1.11 | -1.33 | -1.08 | 1.08 | -1.12 |
| DOLK | 1.12 | 1.03 | 1.10 | -1.04 | -1.02 | 1.15 | 1.06 | 1.19 | -1.04 | 1.27 | 1.14 |
| DPAGT1 | 1.09 | 1.01 | 1.19 | 1.09 | -1.02 | 1.09 | 1.22 | -1.02 | -1.12 | 1.30 | 1.03 |
| DPM1 | 1.01 | -1.09 | -1.03 | 1.05 | 1.11 | 1.01 | -1.01 | -1.08 | 1.01 | 1.05 | -1.17 |
| DPM2 | -1.17 | -1.05 | -1.06 | -1.18 | -1.08 | 1.04 | 1.02 | -1.17 | 1.03 | -1.15 | -1.06 |
| DPM3 | -1.27 | -1.09 | -1.48 | -1.40 | -1.30 | -1.04 | -1.15 | -1.08 | -1.23 | 1.09 | 1.09 |
| DPY19L1 | 1.49 | 1.15 | 1.26 | 1.02 | 1.09 | 1.35 | 1.32 | 1.55 | 1.42 | 1.29 | 1.36 |
| DPY19L2 | -2.02 | -1.51 | 1.01 | -1.94 | -6.68 | -1.52 | -1.55 | -1.04 | -4.01 | -3.85 | 1.18 |
| DPY19L3 | 1.48 | -1.14 | 1.16 | -1.10 | 1.28 | 1.46 | 1.49 | 1.14 | 1.38 | 1.43 | 1.54 |
| DPY19L4 | 1.54 | 1.50 | 1.25 | 1.29 | 1.25 | 1.73 | 1.79 | 1.89 | 1.44 | 1.78 | 1.53 |
| FUT8 | 1.65 | -1.26 | -1.17 | -1.79 | -1.21 | 1.43 | 1.77 | 1.70 | -1.30 | 1.67 | -1.02 |
| FUT9 | 1.03 | 1.69 | -1.01 | 1.04 | 1.05 | 1.17 | -1.01 | 1.02 | 1.07 | 1.77 | 1.07 |
| GALE | -5.63 | -2.24 | -1.37 | -2.41 | -2.06 | -3.14 | -2.52 | -3.01 | -1.94 | -3.41 | -1.75 |
| GANAB | 1.39 | 1.28 | 1.28 | 1.15 | 1.34 | 1.42 | 1.36 | 1.03 | 1.47 | 1.28 | 1.23 |
| GAPDH | -1.37 | -1.07 | 1.08 | 1.05 | -1.16 | -1.06 | -1.09 | 1.01 | 1.19 | -1.12 | -1.05 |
| GFPT1 | 1.30 | -1.13 | 1.34 | 1.35 | 1.42 | -1.10 | 1.08 | -1.26 | 1.07 | 1.10 | 1.19 |
| GMPPA | -1.31 | -1.32 | -1.10 | -1.26 | -1.06 | -1.19 | -1.17 | -1.32 | -1.08 | -1.26 | -1.39 |
| GMPPB | -1.29 | -1.24 | -1.13 | -1.23 | 1.15 | -1.27 | -1.17 | -1.65 | -1.02 | -1.30 | -1.09 |
| GNE | 1.24 | 1.12 | -1.02 | 1.04 | 1.18 | 1.31 | 1.20 | 1.23 | 1.17 | 1.05 | 1.38 |
| HSPA5 | -1.34 | -1.66 | -1.16 | -1.45 | -1.36 | 1.27 | 1.12 | -1.11 | 1.05 | -1.36 | -1.08 |
| HiF1alpha | 1.95 | 1.62 | 1.78 | 1.82 | 1.65 | 1.60 | 2.07 | 1.50 | 2.14 | 1.78 | 1.21 |
| MAN1A1 | 3.14 | 2.26 | 2.69 | 1.95 | 2.36 | 5.68 | 4.47 | 6.67 | 3.08 | 4.94 | 2.37 |
| MAN1B1 | 1.51 | 1.34 | 1.52 | 1.60 | 1.54 | 1.58 | 1.58 | 1.21 | 1.47 | 1.40 | 1.59 |
| MAN2A1 | 2.99 | 1.95 | 1.69 | 1.68 | 1.73 | 2.65 | 2.43 | 1.38 | 2.28 | 1.80 | 2.29 |
| MGAT1 | -1.07 | -1.20 | -1.27 | -1.51 | -1.37 | -1.21 | -1.26 | 1.01 | -1.31 | -1.11 | -1.08 |
| MGAT2 | 1.10 | 1.17 | 1.22 | 1.11 | 1.23 | 1.26 | 1.21 | 1.03 | 1.10 | 1.13 | 1.13 |
| MGAT3 | 1.03 | -1.01 | -1.01 | 1.04 | 1.05 | 1.17 | -1.01 | 1.02 | 1.07 | 1.12 | 1.07 |
| MGAT5 | -1.35 | 1.41 | 1.16 | -1.29 | 1.10 | -1.08 | -1.28 | -1.03 | 1.22 | -1.32 | 1.24 |
| MOGS | -1.01 | -1.19 | 1.10 | 1.11 | 1.20 | -1.03 | 1.03 | -1.02 | 1.03 | -1.08 | -1.07 |
| MPDU1 | -1.05 | -1.04 | -1.19 | -1.13 | -1.13 | -1.17 | -1.23 | -1.18 | -1.18 | -1.02 | 1.00 |
| MPI | 1.14 | -1.08 | 1.10 | 1.05 | -1.38 | 1.17 | 1.16 | -1.00 | 1.24 | 1.07 | -1.09 |
| OGT | 1.73 | 1.22 | 1.19 | 1.61 | 1.28 | 1.52 | 1.37 | 1.34 | 1.24 | 1.63 | 1.27 |
| PGM1 | 1.99 | 1.41 | 2.02 | 2.01 | 1.40 | 1.51 | 1.52 | 1.32 | 1.47 | 2.05 | 1.72 |
| PGM2 | -2.04 | -2.81 | -1.11 | -2.11 | -1.63 | -2.38 | -2.69 | -3.13 | -2.05 | -3.57 | -2.45 |
| PMM1 | -1.02 | 1.23 | 1.06 | 1.00 | 1.09 | 1.24 | 1.05 | 1.03 | -1.07 | 1.08 | 1.16 |
| PMM2 | 1.14 | -1.06 | 1.14 | 1.02 | 1.06 | -1.08 | 1.00 | -1.32 | 1.10 | -1.05 | 1.01 |
| POLR2A | -1.01 | 1.03 | -1.09 | -1.14 | 1.02 | 1.07 | -1.06 | 1.13 | -1.08 | -1.01 | 1.10 |
| POMGnT1 | -1.25 | -1.18 | -1.07 | -1.13 | -1.29 | -1.16 | -1.52 | -1.14 | -1.53 | 1.04 | 1.41 |
| POMGnT2 | -1.44 | -1.37 | -1.32 | -1.48 | -1.60 | -1.03 | -1.13 | -1.87 | -1.05 | 1.07 | -1.04 |
| POMT1 | 1.03 | 1.02 | 1.08 | 1.01 | 1.06 | 1.13 | 1.08 | 1.11 | -1.05 | 1.28 | 1.52 |
| POMT2 | 1.99 | 1.20 | 1.56 | 1.65 | 1.30 | 1.33 | 1.48 | 1.23 | 1.44 | 1.45 | 1.45 |
| RAB7A | 1.07 | 1.02 | 1.10 | 1.15 | 1.06 | 1.17 | 1.15 | 1.07 | -1.15 | 1.22 | 1.05 |
| RFT1 | 1.28 | 1.00 | -1.05 | -1.08 | 1.15 | -1.02 | 1.19 | -1.00 | 1.09 | -1.06 | -1.09 |
| SGK1 | 3.76 | 1.51 | 2.88 | 2.19 | 3.94 | 2.54 | 3.23 | 2.30 | 1.78 | 3.10 | -1.36 |
| SLC35A1 | 1.44 | 1.21 | 1.29 | 1.23 | -1.12 | 1.29 | 1.45 | 1.40 | 1.11 | 1.64 | 1.24 |
| SLC35A2 | -1.07 | -1.12 | -1.08 | -1.20 | -1.01 | -1.36 | -1.29 | -1.32 | -1.06 | -1.33 | -1.04 |
| SLC35A3 | 1.17 | -1.10 | -1.02 | 1.07 | 1.20 | -1.14 | -1.17 | -1.08 | -1.16 | 1.12 | 1.01 |
| SLC35C1 | -1.36 | -1.66 | -1.50 | -1.40 | -1.45 | -1.65 | -1.50 | -1.36 | -1.53 | -1.53 | -1.22 |
| SNRPD3 | 1.09 | 1.05 | -1.14 | -1.19 | -1.03 | -1.09 | -1.02 | -1.08 | -1.16 | -1.08 | -1.19 |
| SRD5A3 | -1.17 | -1.53 | 1.24 | -1.03 | 1.01 | 1.06 | 1.30 | -1.04 | -1.24 | -1.27 | 1.12 |
| ST3GAL3 | -1.01 | -1.09 | -1.22 | -1.19 | -1.44 | 1.03 | -1.09 | -1.04 | -1.09 | -1.10 | 1.22 |
| ST6GAL1 | 1.64 | -6.47 | -1.62 | 1.16 | -2.56 | -1.75 | -1.45 | -4.54 | 1.74 | -2.95 | -7.80 |
| UAP1 | -1.58 | -1.19 | 1.10 | 1.09 | -1.12 | -1.30 | -1.29 | -2.08 | -1.26 | -1.52 | -1.70 |
| mTOR | -1.20 | -1.21 | -1.21 | -1.24 | -1.25 | -1.24 | -1.28 | -1.25 | -1.35 | -1.04 | 1.05 |

10.5 PrimePCR ΔC_t -values*Glycolysis and Gluconeogenesis H96*

| | Ctrl | | MVK2 | | MVK8 | | MVK9 | |
|--------------|--------|-------|--------|-------|--------|-------|--------|-------|
| | Mean | SD | Mean | SD | Mean | SD | Mean | SD |
| <i>ALDOA</i> | 0.259 | 0.389 | 1.542 | 0.102 | 1.183 | 0.094 | -1.055 | 0.043 |
| <i>PFKM</i> | 3.576 | 0.539 | 4.925 | 0.090 | 4.385 | 0.173 | 2.830 | 0.158 |
| <i>GPI</i> | 2.853 | 0.359 | 3.408 | 0.389 | 3.306 | 0.259 | 1.485 | 0.113 |
| <i>ALDOC</i> | 6.433 | 0.391 | 7.252 | 0.242 | 6.373 | 0.169 | 3.330 | 0.138 |
| <i>PGAM1</i> | 0.386 | 0.326 | 0.612 | 0.318 | 0.652 | 0.130 | -1.340 | 0.558 |
| <i>HPRT1</i> | 2.536 | 0.287 | 2.218 | 0.182 | 2.380 | 0.247 | 0.705 | 0.373 |
| <i>ENO1</i> | 0.243 | 0.247 | 0.688 | 0.181 | -0.047 | 0.786 | -2.625 | 0.233 |
| <i>HK2</i> | 2.986 | 0.383 | 3.102 | 0.232 | 4.375 | 0.349 | 2.640 | 0.018 |
| <i>MDH1</i> | 1.026 | 0.129 | 1.372 | 0.044 | 1.215 | 0.100 | -0.865 | 0.373 |
| <i>ENO3</i> | 9.533 | 0.433 | 11.195 | 0.673 | 9.638 | 0.462 | 7.655 | 0.033 |
| <i>MDH2</i> | 0.293 | 0.241 | 0.255 | 0.155 | 0.442 | 0.236 | -1.955 | 0.443 |
| <i>PKM2</i> | -1.674 | 0.150 | -0.818 | 0.190 | -1.366 | 0.612 | -2.845 | 0.393 |
| <i>FBP1</i> | 10.413 | 0.338 | 13.315 | 1.063 | | | 11.590 | 0.148 |
| <i>PCK2</i> | 6.799 | 0.274 | 6.028 | 0.046 | 7.415 | 0.449 | 4.290 | 0.268 |
| <i>TPI1</i> | -1.071 | 0.135 | -1.135 | 0.219 | -0.863 | 0.064 | -2.845 | 0.482 |

Regulation of Lipid Metabolism Tier1 H96

| | Ctrl | | MVK2 | | MVK8 | | MVK9 | |
|----------------|--------|-------|--------|-------|--------|-------|--------|-------|
| | Mean | SD | Mean | SD | Mean | SD | Mean | SD |
| <i>AKT2</i> | 2.354 | 0.604 | 3.978 | 0.265 | 2.508 | 0.592 | 2.018 | 0.147 |
| <i>FGF2</i> | -1.786 | 0.132 | -0.149 | 0.225 | -0.552 | 0.712 | -0.269 | 0.684 |
| <i>IGF2</i> | 5.398 | 0.780 | 11.371 | 0.499 | 11.452 | 1.788 | 8.614 | 0.469 |
| <i>PPARA</i> | 3.508 | 0.600 | 5.734 | 0.193 | 3.981 | 0.453 | 4.011 | 0.108 |
| <i>PRKCD</i> | 7.721 | 0.196 | 10.284 | 0.217 | 8.188 | 0.336 | 8.748 | 0.268 |
| <i>SOD1</i> | -1.919 | 0.114 | -2.012 | 0.299 | -1.559 | 0.039 | -1.292 | 0.057 |
| <i>ACACB</i> | 7.874 | 0.691 | 10.018 | 0.223 | 7.121 | 1.029 | 7.744 | 0.298 |
| <i>AKT3</i> | 1.644 | 0.418 | 3.784 | 0.080 | 2.158 | 0.805 | 1.668 | 0.449 |
| <i>CPT1A</i> | 2.208 | 0.075 | 3.794 | 0.135 | 2.328 | 0.702 | 1.814 | 0.119 |
| <i>IL1A</i> | 5.454 | 0.692 | 11.818 | 0.173 | 9.463 | 0.000 | 7.817 | 0.000 |
| <i>MAPK8</i> | 1.944 | 0.091 | 3.418 | 0.046 | 2.394 | 0.671 | 2.251 | 0.574 |
| <i>PPARG</i> | 2.834 | 0.554 | 4.828 | 0.192 | 2.054 | 0.515 | 1.788 | 0.246 |
| <i>SRC</i> | 3.191 | 0.573 | 6.058 | 0.647 | 4.021 | 0.961 | 3.951 | 0.090 |
| <i>ANGPTL4</i> | 7.231 | 0.900 | 11.141 | 0.282 | 9.774 | 2.079 | 7.631 | 0.133 |
| <i>CREB1</i> | 2.208 | 0.407 | 3.368 | 0.012 | 1.998 | 0.699 | 1.491 | 0.207 |
| <i>FLT1</i> | 3.844 | 1.209 | 6.728 | 0.365 | 5.908 | 0.821 | 5.014 | 0.449 |
| <i>IL1B</i> | 0.738 | 0.503 | 11.151 | 0.505 | 9.214 | 2.173 | 6.518 | 1.731 |
| <i>MTOR</i> | 2.774 | 0.135 | 4.214 | 0.215 | 2.644 | 0.810 | 2.831 | 0.402 |

Appendix

| | | | | | | | | |
|------------|--------|-------|--------|-------|--------|-------|--------|-------|
| PKD4 | 7.314 | 0.788 | 13.418 | 1.208 | 8.917 | 3.283 | 9.803 | 0.750 |
| PPARGC1A | 6.228 | 1.628 | 10.821 | 0.246 | 8.758 | 2.927 | 6.801 | 0.945 |
| SREBF1 | 4.918 | 0.395 | 6.691 | 0.483 | 3.704 | 0.803 | 2.978 | 0.079 |
| ADRB2 | 7.308 | 0.667 | 10.288 | 0.123 | 6.504 | 1.022 | 7.454 | 1.622 |
| APOE | 8.744 | 0.760 | 13.021 | 0.568 | 9.258 | 0.863 | 9.964 | 0.589 |
| NFKB1 | 0.898 | 0.475 | 3.611 | 0.104 | 1.298 | 0.897 | 1.518 | 0.662 |
| AC008810.1 | 0.828 | 0.419 | 2.571 | 0.121 | 1.384 | 0.356 | 1.218 | 0.114 |
| RARA | 4.551 | 0.456 | 6.354 | 0.228 | 4.768 | 0.704 | 3.948 | 0.249 |
| STAT5A | 4.934 | 0.458 | 7.318 | 0.438 | 5.644 | 1.030 | 5.024 | 0.150 |
| BMP2 | 7.458 | 0.684 | 11.764 | 0.834 | 8.184 | 1.381 | 8.504 | 0.557 |
| NR1H3 | 3.731 | 0.308 | 4.911 | 0.137 | 4.498 | 0.950 | 4.554 | 0.222 |
| PIK3R1 | 1.351 | 0.274 | 2.694 | 0.068 | 0.674 | 0.629 | 1.714 | 0.127 |
| PRKAA2 | 5.198 | 0.098 | 6.658 | 0.250 | 5.871 | 0.116 | 5.938 | 0.299 |
| RB1 | 1.851 | 0.172 | 3.271 | 0.208 | 2.041 | 0.584 | 2.244 | 0.386 |
| STK11 | 1.578 | 0.389 | 3.538 | 0.281 | 1.698 | 0.897 | 1.231 | 0.240 |
| C3 | -0.299 | 0.676 | 13.684 | 0.611 | 4.102 | 5.468 | 6.311 | 1.715 |
| FABP1 | 9.561 | 0.448 | 14.088 | 1.028 | 10.144 | 2.204 | 9.188 | 0.747 |
| PRKAB1 | 4.374 | 0.395 | 5.424 | 0.261 | 3.891 | 0.680 | 3.754 | 0.438 |
| RXRA | 3.551 | 0.389 | 3.904 | 0.156 | 3.098 | 0.504 | 2.398 | 0.055 |
| TGFB1 | 1.871 | 0.167 | 2.481 | 0.295 | 1.718 | 0.675 | 0.574 | 0.178 |
| AGTR1 | 7.471 | 0.575 | 5.534 | 0.022 | 5.111 | 0.344 | 2.554 | 0.321 |
| CAV1 | -3.349 | 0.294 | -2.519 | 0.062 | -3.129 | 0.846 | -2.839 | 0.600 |
| NR3C1 | 2.344 | 0.113 | 2.324 | 0.262 | 1.224 | 0.209 | 1.601 | 0.160 |
| PLA2G4A | 6.318 | 0.302 | 8.818 | 0.174 | 5.784 | 0.922 | 5.521 | 0.363 |
| PRKCA | 0.931 | 0.202 | 2.128 | 0.097 | 0.918 | 0.477 | 1.204 | 0.241 |
| SCD | 2.774 | 0.139 | 2.318 | 0.026 | -0.412 | 0.558 | -1.302 | 0.149 |
| THRB | 5.231 | 0.248 | 5.208 | 0.063 | 2.921 | 1.130 | 2.591 | 0.196 |
| AKT1 | 0.824 | 0.085 | 2.058 | 0.426 | 0.731 | 0.423 | 0.394 | 0.128 |
| CHRM3 | 6.714 | 0.697 | 10.701 | 1.136 | 7.711 | 2.203 | 6.331 | 0.866 |
| IGF1R | 1.764 | 0.850 | 3.474 | 0.109 | 1.828 | 0.845 | 1.484 | 0.349 |
| LDLR | 2.284 | 0.512 | 3.544 | 0.186 | 1.164 | 0.745 | 0.524 | 0.287 |
| SIRT1 | 2.634 | 0.335 | 4.024 | 0.192 | 2.461 | 0.697 | 2.171 | 0.293 |

10.6 Proteomics measurement

| MVk affected | Severe affected | Mild affected | |
|--------------|-----------------|---------------|---------|
| ACTC1 | ACLY | ANXA2 | ITGAV |
| AHNAK2 | CARHSP1 | AP2B1 | KTN1 |
| AKR1B1 | CD109 | ARL6IP5 | LAMP1 |
| ALDH1A1 | CNN2 | ARSA | LAMP2 |
| ATL3 | CNPY3 | ASAH1 | LAMTOR1 |
| ATP2B1 | CNTNAP1 | ATP6V0D1 | LRP1 |
| B2M | FKBP2 | ATP6V1C1 | LRPAP1 |
| CAPG | FSCN1 | ATXN10 | MCM3 |
| CD109 | HNRNPH2 | CAPRIN1 | MGST3 |
| CDC42 | HSD17B4 | CBR3 | MRC2 |
| CEMIP | IDH2 | CD109 | MXRA7 |
| CPD | IPO5 | CD59 | MYOF |
| DPYSL3 | KPNB1 | CD63 | NACA |
| EPB41L2 | LRP1 | CNN3 | NCSTN |
| FBLIM1 | MACROH2A1 | COMT | NNT |
| FGF2 | MICOS13 | COTL1 | NPC2 |
| FHL1 | MME | CRABP2 | NRDC |
| FN1 | MYLK | CSE1L | NUDC |
| GBE1 | NAP1L4 | CTSD | PA2G4 |
| GOT2 | NEXN | CYB5R3 | PABPC1 |
| HCCS | PAPSS1 | DDRKG1 | PAICS |
| HLA-A | PFKP | DNASE2 | PAWR |
| HLA-B | PSME1 | EEF1A1 | PCBP1 |
| ICAM1 | PTGS1 | EEF1A2 | PCNA |
| IDH1 | RAI14 | EEF2 | PCYOX1 |
| IDH3B | RANGAP1 | EGFR | PGRMC2 |
| LGALS3 | RECK | EIF3A | PLBD2 |
| LOXL2 | RIC8A | EIF3E | PPIC |
| LRP1 | SEC62 | EIF3F | PSMA4 |
| LRPPRC | STOM | EIF3I | PSME1 |
| MT2A | TGM2 | EIF3L | PSME2 |
| NAGK | TGOLN2 | EIF4A1 | PTGS1 |
| NAMPT | THY1 | EIF6 | QARS1 |
| NANS | UAP1 | EPHX1 | RAB7A |
| NES | VIM | ERP29 | RAN |
| PAPSS2 | YWHAQ | FARSB | RANBP1 |
| PLS3 | | FAS | RANGAP1 |
| PSME1 | | FKBP93 | RAP1B |
| PTGS1 | | FLNA | RPL10 |
| PYGB | | FTH1 | RPL22 |
| RAB10 | | FUS TLS | RPL23 |
| RAB14 | | G3BP1 | RPL3 |
| RAD23B | | GBA | RPS21 |
| RANGAP1 | | GLB1 | SAMHD1 |
| SARS1 | | GLO1 | SCARB2 |
| SH3BGRL | | GLS | SPTAN1 |
| SLC25A5 | | GNAI2 | STMN1 |
| SNX3 | | GNAI3 | STX12 |
| SOD2 | | GNB2 | STX7 |
| SQSTM1 | | GNG12 | TGM2 |
| SRI | | GPC1 | TMEM43 |
| ST13 | | GPNMB | TPP1 |
| TAPBP | | HADHB | TUBA1C |
| TGM2 | | HEXA | UAP1 |
| UAP1 | | HEXB | UROD |
| VIM | | HPRT1 | VAMP3 |
| VPS35 | | HSP90AB1 | VIM |
| YKT6 | | HSPB1 | |

10.7 Publications

Novel variants and clinical symptoms in four new ALG3-CDG patients, review of the literature and identification of AAGRP-ALG3 as a novel ALG3 variant with an alanine and glycine rich N-terminus.

Himmelreich N, Dimitrov B, Geiger V, Zielonka M, Hutter AM, Beedgen L, Hüllen A, Breuer M, Peters V, Thiemann KC, Hoffmann GF, Sinning I, Dupré T, Vuillaumier-Barrot S, Barrey C, Denecke J, Kölfen W, Düker G, Ganschow R, Lentze MJ, Moore S, Seta N, Ziegler A, Thiel C.

Human Mutation, 2019

Fatal outcome after heart surgery in PMM2-CDG due to a rare homozygous gene variant with double effects

Görlacher M, Panagiotou E, Himmelreich N, Hüllen A, Beedgen L, Dimitrov B, Geiger V, Zielonka M, Peters V, Strahl S, Vázquez-Jiménez J, Kerst G, Thiel C.

Molecular Genetics and Metabolism Reports, 2020

A patient-based medaka alg2 mutant as a model for hypo-N-glycosylation.

Gücüm S, Sakson R, Hoffmann M, Grote V, Becker C, Pakari K, Beedgen L, Thiel C, Rapp E, Ruppert T, Thumberger T, Wittbrodt J.

Development, 2021

Phenotypic diversity, disease progression, and pathogenicity of MVK missense variants in mevalonic aciduria.

Brennenstuhl H, Nashawi M, Schröter J, Baronio F, Beedgen L, Gleich F, Jeltsch K, von Landenberg C, Martini S, Simon A, Thiel C, Tsiakas K, Opladen T, Kölker S, Hoffmann GF, Haas D.

Inherited Metabolic Disorders, 2021

A rapid and simple procedure for the isolation and cultivation of fibroblast-like cells from medaka and zebrafish embryos and fin clip biopsies.

Beedgen L, Hüllen A, Gücüm S, Thumberger T, Wittbrodt J, Thiel C.

Laboratory Animals, 2021

10.8 Conference attendance

11. May 2018: Glycokids Annual Meeting, Hübingen, Germany

1- – 2. July 2018: IZN Neuroscience Retreat, Schöntal, Germany - **Poster presentation**

15. – 16. November 2018: 1st Annual Meeting FOR2509 DFG, Hoechst, Germany - **Poster presentation**

28. – 30. January 2019: GlycoBioTec 2019, Berlin, Germany - **Poster presentation**

13. – 15. March 2019: APS Annual Meeting, Fulda, Germany - **Poster presentation**

20. – 21. March 2019: Euro-CDG Meeting, Paris, France

2. July 2019: Teaching Workshop on Protein Glycosylation, Heidelberg, Germany

14. – 17. July 2019: IZN Neuroscience Retreat, Schöntal, Germany - **Poster presentation**

26. – 27. September 2019: 2nd Annual Meeting FOR2509 DFG, Obernkirchen, Germany - **Poster presentation**

27. – 29. October 2019: 30th Joint Glycobiology Meeting, Lille, France - **Poster presentation**

22. – 24. January 2020: Proteomics Workshop, Heidelberg, Germany

11 Declaration

As per § 8(3) b) and c) of the doctoral degree regulations:

1. I hereby declare that I have written the submitted dissertation myself and, in this process, have used no other sources or materials than those expressly indicated.
2. I hereby declare that I have not applied to be examined at any other institution, nor have I used the dissertation in this or any other form at any other institution as an examination paper nor submitted it to any other faculty as a dissertation.

Heidelberg,

Lars Beedgen

12 Acknowledgment

First and foremost, I would like to thank my research supervisor, Priv.-Doz. Dr. Christian Thiel for giving me the opportunity for my doctoral research and being a tremendous mentor for me. I would like to thank you for encouraging my research and for allowing me to grow as a research scientist. It has been a great pleasure to have been part of his group for the past few years and I will definitely miss our conference attendances.

Also, I would like to express my sincere gratitude to my primary doctoral supervisor Prof. Dr. Britta Brügger who supported me with her extensive knowledge and the great ideas she gave me in my TAC-meeting discussions. Additionally, I would like to thank my referees Prof. Dr. Matthias Mack and Dr. Mirko Völkers for being part of my examination committee. My corporation partners Dr. Erdmann Rapp and Dr. Thomas Ruppert need to be mentioned here for their scientific support as well.

My sincere thanks and gratitude goes to Virginia Geiger for her excellent technical assistance in the lab and to Bianca Dimitrov for proofreading my work. You both made lab life so much better, and I really enjoyed our private activities like the folk festival Wasen and so on. Furthermore, I want to thank my PhD student colleagues Andreas Hüllen and Kristina Falkenstein as I cannot imagine having done this without your mental support. We had so many good times in our “castle” office and shopping addiction is one of our connections.

A special thanks goes to the whole team of the metabolic laboratory for the support and help during my research: Nastassja Himmelreich, Andreas Hecker, Simone Hengst, Dorothea Messner-Schmitt, Tanja Lunczer, and Kathrin Schwarz. You made my lab life a whole lot easier and enjoyable. In this context I also want to mention PD Dr. Jürgen Okun, who gave me the opportunity to conduct my bachelor and master thesis in his lab and supported me throughout the years. I also want to thank all the students we had over the years in our lab and especially Lukas Hoeren with whom I established the Apache Friday music session.

Moreover, I want to thank my friends Tim, Jan, Maurice, Jonas, Martin, and Kai who had my back in every life situation and for the great moments we had and will have.

Finally, I would like to express my very profound gratitude to my parents Claudia and Bernd and to my grandmother Maria for providing me with unfailing support and continuous encouragement throughout my years of study and through the process of researching and writing this dissertation. This accomplishment would not have been possible without you. In this context I also want to thank my two siblings Franziska and Jonas for everything. My sincere gratitude also goes to my girlfriend Caroline who supported me tremendously in the final steps of my work. Thank you all!